DOE/SNF/REP-073
Rev. 0

United States Department of Energy

National Spent Nuclear Fuel Program

Review of DOE Spent Nuclear Fuel Release Rate Test Results

August 2003

U.S. Department of Energy
Assistant Secretary for Environmental Management
Office of Nuclear Material and Spent Fuel

DOE/SNF/REP-073
Rev. 0

Review of DOE Spent Nuclear Fuel Release Rate Test Results

August 2003

WBS# C.1.07.02.01.02.03

Idaho National Engineering and Environmental Laboratory
Idaho Falls, Idaho 83415

Prepared for the
U.S. Department of Energy
Assistant Secretary for Environmental Management
Under DOE Idaho Operations Office
Contract DE-AC07-99ID13727

REVISION LOG

Revision	DAR No.	Issue Date
0	NSNF-386	August 2003

Review of DOE Spent Nuclear Fuel Release Rate Test Results

August 2003

Colleen Shelton-Davis (Signature) **Date:** 8-6-03

National Spent Nuclear Fuel Program
Document Preparer

Henry Loo (Signature) **Date:** 8-6-03

National Spent Nuclear Fuel Program
Technical Lead

Neal Mackay (Signature) **Date:** 8/6/03

National Spent Nuclear Fuel Program
Program Support Organization Quality Engineer

Philip Wheatley (Signature) **Date:** 8.6.03

National Spent Nuclear Fuel Program
Program Support Organization Manager

ABSTRACT

The National Spent Nuclear Fuel Program has been tasked with providing all necessary documentation, performing research and analyses, and addressing packaging issues to ensure DOE-owned spent nuclear fuel is accepted for disposal at a monitored geological repository (currently expected to be located at Yucca Mountain, Nevada). One aspect of these requirements is a laboratory study on the release characteristics of spent nuclear fuel over time in the repository environment. The release rate test program evaluated four fuel types (uranium metal, aluminum based, mixed oxide, and graphite) using several experimental methods. Flow through tests were completed for aluminum-based fuel, uranium metal, and mixed oxide fuels. Drip tests and colloidal analyses were performed with all but the graphite fuel. Batch tests were completed with uranium metal fuel and mixed oxide fuel. Some colloid experiments with uranium metal fuel and mixed oxide fuel were done. The test program was designed to be similar to the commercial fuel program for comparison purposes.

Results from the mixed oxide tests indicate release rates comparable to the commercial uranium dioxide fuel tests. Plutonium content is higher with the mixed oxide fuel and thus the release is greater, but the fraction of sample content that is reacting is similar. Uranium metal fuel reacts relatively quickly to form a variety of uranium oxyhydroxide products. Monitoring changes in these products over time may have more bearing on actual releases in the repository than the initial fuel dissolution. Aluminum based fuel, specifically uranium aluminide, degrades at rates somewhat comparable to commercial fuel. It may not be a congruent rate, however, and different reaction products are formed due to the high aluminum content. Radionuclides released as colloids may be significant from a transport viewpoint. Colloid generation from fuel degradation is initially very high with uranium metal fuel, but appears to drop significantly after a few months.

SUMMARY

Current U. S. Department of Energy (DOE) policy is that DOE-owned spent nuclear fuel will be disposed of in a geological repository proposed at the Yucca Mountain Project site in Nevada. In support of the performance assessment, experiments were performed to evaluate the potential for radionuclides to be released to the environment during fuel degradation. The project was terminated prematurely because of funding constraints, but several years worth of results were generated. In parallel to the laboratory research, a review of literature data that could be applied to specific DOE fuel types was completed. A general model that encompassed all relevant published data was generated. Finally, a comparison between the literature model and the experimental results was presented with recommendations for describing the expected fuel performance in a repository.

The release rate test project included three fuel groups (uranium metal, aluminum-based, and mixed oxide) used in three experimental methods. Graphite fuel was originally planned for study, but the project was terminated prior to any experimentation. Flow through tests were designed to evaluate the forward dissolution rate with no back reactions. Results should give the maximum release rate and the dependence on individual solution components. Unsaturated drip tests simulated the expected repository conditions to more closely estimate the actual release rates. An evaluation of alteration product generation and composition could also be made from these tests. Static batch tests were originally developed to accelerate the drip test conditions and to provide information on the solution composition at the fuel surface. This test method was also used to support the anoxic/oxic studies with uranium metal fuel. In addition, some colloid generation and stability tests were performed with each fuel type, though they were the most extensive with uranium metal fuel.

Uranium metal fuel reacted rapidly in water and produced a variety of alteration products. Nearly all the plutonium and some of the uranium released were colloid-sized particles. However, they appear to agglomerate over time producing larger particles that may precipitate out of solution. Uranium release rates ranged between 4 and 44,000 $mg/m^2/d$, depending on the environmental conditions. Data from the literature review were used to derive an Arrhenius equation describing uranium degradation. The expression was based on an anoxic environment, which is more conservative than an oxic atmosphere. All experimental data were enveloped by this expression, and thus it is the recommended model for a conservative estimate of uranium metal fuel degradation in the repository.

Aluminum-based fuel was generally more resistant to degradation than uranium metal fuel. Uranium release rates ranged from 0.1 to 420 $mg/m^2/d$, depending on the material and the environmental conditions. Preferential attack in the form of pitting was found in some experiments, and others had an aluminum oxide gel on the surface that controlled releases. The literature review reported a different expression for each type of aluminum-based fuel, and the one for aluminum alloy fuels was selected for comparison with the experimental data. Model values were at about the median of the test results. The Yucca Mountain Project prepared an analysis and model report to predict aluminum fuel

degradation and used specific values rather than an equation. The conservative numbers bounded most of the experimental results, but not all. New values are presented that encompass all the test data.

Mixed oxide fuel is quite resistant to degradation in water systems, more resistant than commercial UO_2 fuels. Release rates of uranium were about 0.1 $mg/m^2/d$ or less, depending on the test method. No literature data were available on mixed oxides, so information from individual oxides (uranium and plutonium) was used for comparison. The plutonium dissolution rate is more conservative than uranium and describes little of the data generated by the release rate experiments. However, the UO_2 model adopted by the Yucca Mountain Project bounds the mixed oxide fuel degradation quite well. Particle size may be a concern because of the redistribution of radionuclides during irradiation. Fragments will expose the grain boundaries where certain elements may have accumulated.

Peach Bottom fuel elements were retrieved from storage for inclusion in the release rate test project. Initial characterization was completed to ensure proper identification of the compacts, and samples were selected. Prior to test preparations or shipping of the samples to the experimental laboratories, the project was terminated. Therefore, all samples were returned to storage.

The release rate test project was terminated before all the anticipated data could be collected. However, some information is available, and a reasonable comparison to published data was made. The literature-derived equation for uranium metal fuel is adequate to bound the expected uranium release rates. A similar expression for aluminum-based fuel may be acceptable as a best estimate but is not conservative. Specific numerical values for an upper bound were presented based on the experimental results.

ACKNOWLEDGMENTS

The information in this report is a compilation of knowledge from several contributors. Below is a list of those people from whom information was received for this document. (Listed in alphabetical order.)

John Abrefah, Pacific Northwest National Laboratory

Terri S. Bray, Argonne National Laboratory - East

Pat A. Finn, Argonne National Laboratory - East

Jeff A. Fortner, Argonne National Laboratory - East

Margaret M. Goldberg, Argonne National Laboratory - East

Natraj Iyer, Savannah River Site

Michael D. Kaminski, Argonne National Laboratory - East

Macintyre Louthan, Savannah River Site

Carol J. Mertz, Argonne National Laboratory - East

Robert V. Strain, Argonne National Laboratory - East

CONTENTS

FIGURES

TABLES

ACRONYMS

ACRR	Annular Core Research Reactor
ANL-E	Argonne National Laboratory – East
ANL-W	Argonne National Laboratory – West
CFR	Code of Federal Regulations
DOE	U.S. Department of Energy
EDS	Energy Dispersive Spectroscopy
FFTF	Fast Flux Test Facility
FRR	foreign research reactor
HWCTR	Heavy Water Components Test Reactor
ICP-MS	inductively coupled plasma – mass spectrometry
INEEL	Idaho National Engineering and Environmental Laboratory
LLNL	Lawrence Livermore National Laboratory
LWBR	light water breeder reactor
LWR	light water reactor
MGR	monitored geological repository
MOX	mixed oxide
MTHM	metric tons of heavy metal
NNPP	Naval Nuclear Propulsion Program
NSNFP	National Spent Nuclear Fuel Program
ORNL	Oak Ridge National Laboratory
PNNL	Pacific Northwest National Laboratory
QARD	Quality Assurance Requirements Document
SEM	Scanning Electron Microscopy
SNF	spent nuclear fuel
SRS	Savannah River Site

TEM	Transmission Electron Microscopy
TRIGA	Training Research Isotopes-General Atomics
WASRD	Waste Acceptance System Requirements Document
YMP	Yucca Mountain Project

Review of DOE Spent Nuclear Fuel Release Rate Test Results

1. INTRODUCTION

The U.S. Department of Energy (DOE) has produced over 200 nuclear fuel types from various projects during the last 50 years. In 1992, a decision was made to discontinue reprocessing of spent nuclear fuel (SNF) for uranium recovery and instead direct dispose of the SNF in a monitored geological repository (MGR). The Yucca Mountain Project (YMP) in Nevada is the current proposed repository site. The most likely mechanism for release of radionuclides from an MGR into the biosphere is slow dissolution and transport by groundwater and the use of groundwater in various farming activities. It must be shown through laboratory experimentation and computer modeling that the cumulative release of specific radionuclides to the accessible environment for 10,000 years after disposal is within specified limits. The details of these requirements are stated in the Code of Federal Regulations (10 CFR 63,[1] and 40 CFR 197[2]).

DOE implemented a release rate test project under the National Spent Nuclear Fuel Program (NSNFP), located at the Idaho National Engineering and Environmental Laboratory (INEEL), to evaluate the SNF radionuclide release characteristics. Dearien[3] summarized the preliminary requirements for acceptance of DOE-owned SNF at a repository and provided recommendations on how to meet the requirements. With respect to SNF leachability (the initial step in release of radionuclides), he suggested existing data, bounding or sensitivity studies, and grouping of similar fuel types, be used as much as possible. A team of experts was assembled to evaluate the data requirements, fuel types, and their potential impact on the overall repository performance, and possible methods of collecting information (including existing data). Their results are discussed in Section 2.

American Society for Testing and Materials (ASTM) C 1174-91, "Standard Practice for Prediction of the Long-Term Behavior of Waste Package Materials Including Waste Forms Used in the Geologic Disposal of High-Level Nuclear Waste"[4] was used as a guide during development of the project. This practice describes the iterative process of developing predictive models using a number of different types of laboratory testing. Initial models were selected from literature reviews and from the data generated in studying radioactive releases from commercial spent fuel. Exchange of information between experimenters and modelers have been conducted through periodic status meetings and summary reports and will be complete through this final report and data transfer.

Six test methods are described in this ASTM:

1. *Attribute tests*—tests designed to define the inherent properties of the material such as chemical composition and radionuclide content.
2. *Characterization tests*—tests used to assist in understanding reaction mechanisms such as anodic polarization tests and X-ray diffraction of reaction products.
3. *Accelerated tests*—tests with more aggressive than actual conditions in order to predict long-term behavior in a shorter timeframe.
4. *Service condition test*—in situ tests designed to simulate actual expected conditions as much as possible.
5. *Analog tests*—analyses of existing analog materials that can be used to predict or confirm expected reactions in a repository.

6. *Confirmatory tests*—tests designed to confirm the model predictions (preferably in situ).

The first three types of tests were included in the release rate test project (see further discussion in Section 2.2). A limited review of analog studies was performed by the performance assessment organization of the NSNFP and is linked to the research in this project. Service condition and confirmatory tests could be performed at a future date, if required. The ASTM sections on modeling and prediction are not within the scope of this project.

1.1 Scope and Objectives

The release rate test project was created to experimentally evaluate the degradation rates and mechanisms of selected fuel. Data from the experiments will be fed into models to predict the release of radionuclides to the environment, ultimately estimating the dose rate over time at the repository site boundary. The primary objective of the project is to provide experimental confirmation that radionuclide releases from SNF over the 10,000-year regulatory period have been conservatively modeled. In order to meet this goal, several aspects of research have been implemented. Review of available data on degradation of nuclear fuel (spent or unirradiated) or similar materials has been initiated by several organizations that are discussed in later sections. NSNFP is preparing a document to summarize all the results.

A significant effort was made to reduce the amount of experiments that would be required and still meet the expected needs of the regulation. Based on predicted release rates from YMP preliminary models and information of fuel composition and volume, four fuel types were selected for study. Six experimental methods were chosen, primarily based on work in progress with commercial fuels. Laboratory tests were initiated to evaluate SNF behavior in a wide variety of conditions (temperature, solution chemistry, and oxygen content). Results provide information on dissolution rates, radionuclide release rates, reaction mechanisms, gas generation, reaction product composition, form and type of reaction products, and solution chemistry changes. Because of funding changes in the overall NSNFP, experiments were discontinued prior to completion of the entire planned matrix. This report outlines the experimental strategy planned, describes the tests that were completed with results, and discusses the consequences of work that was eliminated. Although data generated by the release rate project feed into predictive models and the performance assessment, only the experimental work and resulting documentation are within the scope of the project. However, personnel have interfaced closely with the modelers, the performance assessment personnel, and those at the YMP repository to ensure the research meets the data needs and technology risks are minimized.

1.2 References

1. 10 CFR 63, "Disposal of High-Level Radioactive Wastes in a Proposed Geological Repository at Yucca Mountain, Nevada," *Code of Federal Regulations*, Office of Federal Register, November 2001.

2. 40 CFR 197, "Public Health and Environmental Radiation Protection Standard for Yucca Mountain Nevada," *Code of Federal Regulations*, Office of Federal Register, June 2001.

3. J. A. Dearien, "Guidelines for Meeting Repository Requirements for Disposal of U.S. Department of Energy Spent Nuclear Fuel (Draft)," DOE/SNF/REP-009, September 1997.

4. ASTM C 1174-91, "Standard Practice for Prediction of the Long-Term Behavior of Waste Package Materials Including Waste Forms Used in the Geologic Disposal of High-Level Nuclear Waste," 1997.

2. PROGRAM DESCRIPTION

A team of experts was established early in the project from each DOE site that has an interest in the project results. Included are the primary fuel storage sites (Hanford, INEEL, and Savannah River Site), laboratories with experimental capabilities (Argonne National Laboratory-East [ANL-E], ANL-West [ANL-W], Lawrence Livermore National Laboratory, and Pacific Northwest National Laboratory [PNNL]), YMP, and the Naval Reactor Program (Bettis Atomic Power Laboratory). Oak Ridge National Laboratory was included at a later date because of their expertise with Peach Bottom fuel. Team members met approximately every 6 months to discuss the experimental progress and any issues with the project direction. In the first few discussions, a program plan was developed to define fuel selection, experimental methods, and quality assurance requirements.[1]

The program plan describes the criteria for fuel selection and presents an initial list of recommendations. Once data from preliminary predictive models were available, the selection list was reviewed, and a few changes were recommended. Four experimental methods were chosen based on the ASTM definitions and the experiments performed with commercial fuel. Sections 2.1 and 2.2 discuss the selection processes and results in detail. Quality assurance requirements are outlined in the program plan, and all experimental activities are required to comply with the *Quality Assurance Requirements and Description* (QARD).[2] Each test site was responsible for implementing a quality assurance program that is approved by the NSNFP Quality Assurance organization.

2.1 Fuel Selection

In order to simplify the laboratory testing required to study the release rate characteristics of DOE-owned SNF, a grouping of similar fuel types was completed. Table 2-1 lists the resulting eleven groups based on characteristics expected to be important to radionuclide releases (primarily fuel matrix, although cladding and enrichment were considered). A brief description of each group is below.[3]

Group 1 Classified. This group is entirely Naval fuel, and the Naval Nuclear Propulsion Program is responsible for providing any information required for disposal acceptance. It will not be addressed in the balance of this document.

Table 2-1. Fuel groups for release rate testing.

Group Number	Group Title
Group 1	Classified
Group 2	Plutonium/Uranium Alloy (Pu/U alloy)
Group 3	Plutonium/Uranium Carbide (Pu/U carbide)
Group 4	Mixed Oxide (MOX)
Group 5	Uranium/Thorium Carbide (U/Th carbide)
Group 6	Uranium/Thorium Oxide (U/Th oxide)
Group 7	Uranium Metal (U metal)
Group 8	Uranium Oxide (U oxide)
Group 9	Aluminum-Based Fuel (Al-based)
Group 10	Miscellaneous Fuel
Group 11	Uranium Zirconium Hydride Fuel (U-Zr-Hx)

Group 2 Plutonium/uranium alloy fuels. Center sections of the Fermi driver fuel subassembly (uranium-molybdenum alloy with stainless steel cladding) compose over 40% (based on metric tonnes of heavy metal [MTHM]) of this group with an enrichment of about 25% ^{235}U. Additional fuel types included in Group 2 are the Heavy Water Components Test Reactor driver assemblies and the Annular Core Research Reactor fuels. Heavy Water Components Test Reactor assemblies are a uranium thorium alloy with an enrichment of 80% ^{235}U composing about 24% of the Group 2 inventory. Annular Core Research Reactor fuels are uranium zirconium alloys with an enrichment of 12% ^{235}U and make up about 26% of the inventory. Alloying the plutonium and uranium can cause a significant change in the degradation properties of the material. Preferential attack at grain boundaries is more likely in an alloy and may cause incongruent releases. Conversely, the alloying element may stabilize the uranium reducing its susceptibility to dissolution, which is fairly rapid in the unalloyed form.

Group 3 Plutonium/uranium carbide fuel. Most of this group is fuel from the Fast Flux Test Facility. The fuel consists of uranium carbide pellets or spheres with a helium or sodium bond between the fuel and the nongraphite cladding. Effective enrichments range from 10 to 18% ^{235}U. Very little is known about the expected degradation properties of these particles.

Group 4 Mixed oxide fuel. Mixed oxide (MOX) fuels are a mixture of uranium and plutonium oxides with an effective enrichment over 15% ^{235}U. Fast Flux Test Facility driver and test fuel assemblies compose the majority of this group. Cladding materials vary. Although the uranium oxide is expected to react in a similar fashion as the commercial fuel (uranium oxide), the high plutonium content adds an unknown factor.

Group 5 Uranium/thorium carbide fuel. Fort St. Vrain and Peach Bottom fuels compose the bulk of Group 5, with a small amount from the General Atomic Gas Cooled Reactor. Fissile (thorium with 93% enriched ^{235}U) and fertile (only thorium) carbide particles with pyrolytic carbon coatings are the unique characteristic of these fuels. Peach Bottom Core 1 fuel particles have one coating; Peach Bottom Core 2 particles have two coatings; and the Fort St. Vrain particles have a silicon carbide layer over two pyrolytic coatings, making it particularly robust. The particles are bonded together by a carbonaceous matrix material with no cladding. Fort St. Vrain and Peach Bottom Core 2 fuels are generally in excellent condition (with some exceptions where Core 2 fuels have seen long exposures to groundwater), but it is estimated that about 60% of the Core 1 particles have been breached. Expected releases from the damaged fuel could be very significant.

Group 6 Uranium/thorium oxide fuel. Shippingport light water breeder reactor fuels make up most of the uranium/thorium oxide group. Reactor tests were used to demonstrate production of fissile ^{233}U from thorium. Uranium oxide, up to 98% enriched ^{233}U, mixed with thorium oxide was made into cylindrically shaped ceramic pellets and placed into Zircaloy-4 tubes. The ceramic is expected to react differently than standard uranium oxide, but in an unknown manner.

Group 7 Uranium metal fuel. Most of the fuel in this group is zirconium clad N-reactor fuel, but also includes some aluminum clad Single Pass Reactor fuel. Enrichments are less than 2% ^{235}U and typically have low burnups. A fair amount of information is available on uranium metal chemistry and degradation, which is different than uranium alloys or uranium oxides.

Group 8 Uranium oxide fuel. Uranium oxide fuels are from commercial reactors (particularly debris from the Three Mile Island reactor accident) or are fuels similar to commercial spent fuel. Enrichment of commercial fuel is typically 1–2% ^{235}U. However, High Flux Isotope Reactor and Shippingport Pressurized Water Reactor fuels are included in this group and have enrichments up to 93% ^{235}U. Stainless steel is the primary cladding material, but most of the material in this group is damaged.

Research has been continuing with commercial fuel for a number of years, and thus, a great deal of information is available about uranium oxide fuel.

Group 9 Aluminum-based fuel. Fuel types included in Group 9 are uranium aluminide, uranium silicide, and uranium oxide dispersed in a continuous aluminum phase with aluminum cladding. Over 36% of the fuel inventory are from foreign research reactors. Enrichments vary between 11 and 93% ^{235}U, with the silicide fuels having less than 20% ^{235}U. Some work has been done with aluminum and silicide fuels, and the reactions are different than other uranium metal or alloy fuels.

Group 10 Miscellaneous fuel. DOE owns some fuels that have miscellaneous matrices that do not fit into any of the other groups. This small group will be modeled as uranium metal fuel as a bounding condition. No further consideration is given to this category because it contains a small amount (0.03 MTHM) and examining each fuel element is not practical.

Group 11 Uranium zirconium hydride fuel. The majority of this fuel group is from the Training Research Isotopes General Atomics (TRIGA) reactor. Uranium particles are dispersed in a zirconium hydride matrix and are clad with aluminum, stainless steel, or Incoloy-800. Enrichments vary widely. The unique matrix is expected to provide some resistance to degradation over other metallic fuels.

Each of these groups (except Groups 1 and 10) was prioritized by the release rate test team according to the need for laboratory data based on mass of material, fissile content, selected fission product content, expected release rates, uniqueness, and availability. Final selection criteria and results are reported in "Selection of Fuel Types for Release Rate Testing."[4] Table 2-2 lists the specific data on volume, fissile content, and amount of technetium and neptunium for each of the fuel categories (initial modeling efforts indicate technetium and neptunium are the most likely to exceed regulatory limits). Fissile material is based on the sum of the fissionable radioisotopes (^{233}U, ^{235}U, ^{237}Np, ^{238}Pu, ^{239}Pu, ^{240}Pu, ^{241}Pu, ^{242}Pu, ^{241}Am, ^{243}Am, and ^{244}Cm) listed in "Performance Assessment of Direct Disposal in Unsaturated TUFF of Spent Nuclear Fuel and High-Level Waste Owned by U.S. Department of Energy."[5]

Table 2-2. Selected data for DOE-owned fuel groups.

Group Number	Group Name	Mass (MTHM)	Fissile Content (Ci)	^{99}Tc (Ci)	^{237}Np (Ci)
2	Pu/U alloy	9.1	95,372	330	5.54
3	Pu/U carbide	0.1	9,926	1	0.02
4	MOX	12.4	1,329,113	125	3.86
5	Th/U carbide	26.3	53,689	400	8.90
6	Th/U oxide	50.4	150,702	213	2.81
7	U metal	2,127.2	2,785,425	3,541	78.82
8	U oxide	178.1	2,231,742	1,533	39.38
9	Al-based	20.9	173,779	1,273	11.03
11	U-Zr-Hx	1.6	28,733	44	0.56

Note: These data were used for planning purposes only; they have not been qualified per the Yucca Mountain Project quality assurance document *Quality Assurance Requirements and Description*, DOE/RW-0333P (see Reference 2).

Preliminary modeling at the time of the selection process indicated only five fuel groups had a potential for making a significant impact on the repository: Groups 4 (MOX), 5 (Th/U carbide), 7 (uranium metal), 8 (uranium oxide), and 9 (aluminum-based). Uranium metal and aluminum-based fuels made the largest impact. Uniqueness was also considered as a selection criterion. Although each group is, by definition, a collection of similar fuel types unique from other groups, a uniqueness factor was added to the carbide fuel groups (3 and 5). These fuels are different enough from metal, alloy, and oxide fuels that standard test methods could prove ineffective. The last criterion used in the analysis is availability. Samples of SNF had to be accessible within a reasonable cost and timeframe to be considered for testing, preferably one representative or bounding of the entire group. Four fuel types were immediately available: N-reactor fuel from Group 7, MOX fuel from Group 4, and several fuel types from Group 9 (Al-based). Peach Bottom fuel (Group 5) was scheduled for repackaging and thus, samples could be collected at that time.

Uranium metal fuel (Group 7) has the most mass based on MTHM, the most fissile material, the most ^{99}Tc and ^{237}Np, is expected to have a significant impact on the repository, and samples are available. Thus, it was chosen as the highest priority for testing. Group 8, uranium oxide, should be the second priority based on MTHM, fissile material, and ^{99}Tc and ^{237}Np content. However, a great deal of information is available (compared to other fuel groups) on similar fuels because of the extensive testing with commercial fuel. Data from those experiments will be used when modeling Group 8 fuels rather than duplicating the effort. Even though the mass of aluminum based fuel (Group 9) is not particularly high, it was chosen second in priority due to the high fissile material, ^{99}Tc, and ^{237}Np content and the modeling results (high potential for a significant impact on repository performance). Samples are also available for testing. MOX fuel (Group 4) contains a large amount of fissile material, even though it is low in mass and ^{99}Tc and ^{237}Np content. It was shown to have a potential for causing a significant impact to the repository dose, and samples are available, so it was chosen as the third priority. Group 5, Th/U carbide, was also shown to potentially have an impact on the repository dose, and its release characteristics could be very unique. For these reasons, it was chosen for testing (samples could be retrieved) even though the fissile material, ^{99}Tc, and ^{237}Np content and mass were not particularly high. The remaining groups, 2 (Pu/U alloy), 3 (Pu/U carbide), 6 (Th/U oxide), and 11 (U-Zr-Hx) will not be tested experimentally. Their mass, fissile material, ^{99}Tc, and ^{237}Np content were generally low, samples would be difficult to retrieve, and initial models showed an insignificant impact to the overall repository performance. Their release characteristics will be estimated using literature data, experimental results with other fuel, or estimates of values that would conservatively bound the group. Table 2-3 summarizes the results of the fuel selection process. Only the four highest priority groups were scheduled for experimental analysis (see Reference 4).

Table 2-3. Fuel group testing priorities.

Ranking	Group Number	Group Name	Testing Recommended?
1	7	U metal	Yes
2	9	Al-based	Yes
3	4	MOX	Yes
4	5	Th/U Carbide	Yes
5	11	U-Zr-Hx	No
6	6	Th/U Oxide	No
7	2	Pu/U alloy	No
8	3	Pu/U carbide	No
9	8	U oxide	No

2.2 Experimental Methods

In addition to selecting the fuel materials that would be evaluated, the experimental methods for performing the evaluations had to be chosen. A decision was made to focus more on depth with a few fuel types (using only the four defined in Section 2.1) rather than a limited amount of tests with a larger range of materials (see Reference 4). Information that would be useful for understanding and predicting long-term degradation of SNF in a repository environment includes:

- Initial physical and chemical characteristics
- Changes in physical and chemical characteristics over time
- Forward reaction rate
- Release rates of various radionuclides over time
- Chemical and physical form of released radionuclides
- Potential for generation and stability of colloids
- Degradation mechanisms and rates
- Characterization of reaction products
- Paragenesis
- Degradation dependence on temperature and solution composition
- Changes in solution chemistry over time
- Gas generation rates and composition.

Five test methods were selected to address these technical needs. Characterization of the fuel is necessary as a baseline for comparison during the experimental progression and will address the first item above. This may include physical condition, microstructure, and isotopic composition and distribution. The amount of characterization required for each fuel type will depend on the information already available. Forward reaction rates and the effects of temperature and solution chemistry are the primary purpose of flow through tests. However, some information on mechanisms, reaction products, and releases over time can also be gleaned. Unsaturated drip tests provide some information on nearly all areas with the exception of initial conditions, forward reaction rate, and effects of temperature and solution composition. Static batch tests are designed to study the changes in solution chemistry over time, but can also provide information on releases, mechanisms, reaction products, and gas generation. An evaluation of colloid generation is included in the drip and batch tests, but a separate experimental task is in place for detailed studies on size, composition, and stability. Additional tests could be performed to define or clarify certain aspects of the fuel degradation. For example, galvanic tests could be performed to evaluate potential fuel/container interactions, and gap inventory analyses are done to determine the amount of volatile radionuclides available for immediate release. Each of these test methods is described in more detail in the following sections.

2.2.1 Characterization

Certain information is required about the fuel samples prior to any testing in order to have an initial point of reference. Characterization of a sample similar to the ones used in the experiments provides this baseline. This group of tests corresponds to the ASTM categories of attribute and characterization tests.[6] A number of different techniques are available to study the various characteristics of a fuel sample. The methods used depend on the information already known, the capabilities of the method, and the needs of the experimenter. Visual examination and optical metallography provide information on the integrity of the sample (physical damage) and the structure (phase distribution, grain size and shape, etc.) Inductively coupled plasma—mass spectrometry (ICP-MS) provides data on isotopic content. Electron microscopy (transmission, scanning, and microprobe) results in fission product identification and distribution within the sample. The specific methods used for each fuel type are discussed in the section for that particular fuel.

2.2.2 Flow Through Dissolution Tests

Flow through dissolution tests, a form of accelerated tests per ASTM C-1174, (see Reference 6) are performed by contacting a fuel sample with a relatively large volume of flowing water. By increasing the flow rate until a steady state dissolution rate is achieved, the forward reaction rate (the dissolution rate when no back reactions occur between the dissolved components and the sample) can be found. The forward reaction rate is equivalent to the intrinsic rate at a particular temperature and solution composition. Because these tests are relatively short term (typically less than 1 year), a matrix of various environmental conditions can be completed within a reasonable timeframe. Thus, the dependence of the dissolution rate on temperature and solution chemistry can be found. Flow through tests can also be used to identify any preferential leaching of particular elements, such as cesium and technetium. This work is being performed at PNNL.

Figure 2-1 is a schematic of the flow through test apparatus. The solution is fed from the feedwater container to the specimen cell with a controlled flow pump. Flow is in an upward fashion to ensure continuous immersion. Specimen cells are about 5 cm long, are made of 316 stainless steel, and are capped at both ends using 316 stainless steel frits with openings of about 2 μm. Samples are taken from the exit solution and the off-gas for analyses. Temperature, solution chemistry, pH, and oxygen content (by sparging the feed solution with selected gases) are varied in the test matrices.[7]

2.2.3 Unsaturated Drip Tests

Unsaturated drip dissolution tests are designed to simulate expected repository conditions. These are also a type of accelerated test according to ASTM C-1174 due to the small size samples and simulation in a laboratory. Groundwater from the YMP site is equilibrated with Topopah Spring tuff and then slowly dripped onto the fuel particles and allowed to drain through a mesh on the sample holder bottom. Tests are also performed with only water vapor. The SNF surface area to solution volume is kept high to maximize the feedback effects (in contrast to the flow through test where back reactions were minimized). Analyses of the sample, solution, and gas provide information on fuel degradation rates, radionuclide release rates, chemical and physical form of released products, secondary phase formation, paragenesis, solution chemistry changes, and reaction mechanisms. Because drip tests are designed to simulate actual repository conditions, the longer the test is run, the better the data produced (they typically continue for a number of years). These experiments are conducted at ANL-E.

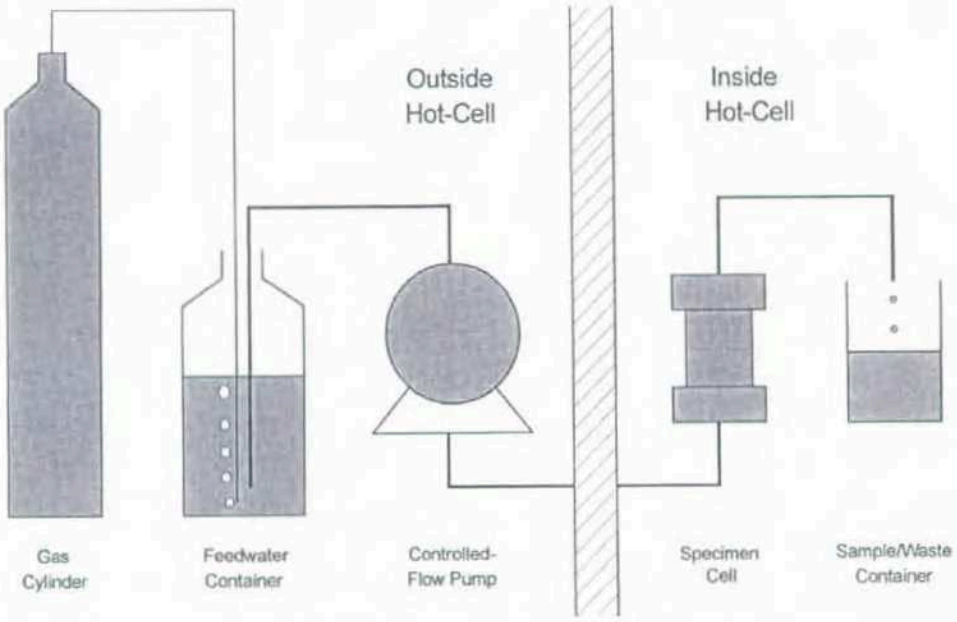

Figure 2-1. Schematic of flow through test experimental equipment.

Figure 2-2 illustrates the test equipment currently used in unsaturated drip tests with uranium metal and aluminum-based fuels. Early versions of the equipment used a one stage fuel holder, with 10 µm laser drilled holes in the bottom (still used with the MOX fuel). However, the more reactive fuels (uranium metal, in particular) plugged the holes very quickly and prevented the solution from passing through (discussed in Section 3.3). The current version requires fuel samples be placed on the first of a three-stage fuel holder. The top stage has a gold mesh bottom with openings of 0.6 mm; the second stage also has a gold mesh bottom with 0.25-mm openings. Zircaloy-4 with laser-drilled 10-µm holes is used in the bottom chamber. Solution is injected in either 0.75-mL (high drip rate) or 0.075-mL (low drip rate) increments approximately every 3.5 days. A stainless steel test vessel collects the solution and any particulate material that passes through the three stages. All tests are performed at a constant 90°C. Samples can be taken of the solution or solids from any stage or from the test vessel. Pressure in the spent fuel holder is also monitored, and gas samples can be removed for analyses.[8]

2.2.4 Static Batch Tests

Static batch dissolution tests, also performed at ANL-E, are a third type of accelerated test according to ASTM C-1174. Crushed fuel samples are placed in a holder with just enough liquid to form a constant thin film on the surface. The fuel surface area to solution volume is larger than in the drip tests, but still much less than the flow through tests. Thus, compositional changes in the solution can be more closely monitored as the water reacts with the fuel. Detailed information on the reaction phases formed during degradation can be collected in typically less than 2 years (depending on the fuel type).

Particles of spent fuel are placed on the gold mesh sample holder and lowered into the stainless steel test vessel. The vessel is then sealed and placed in an oven at 90°C. (See Figure 2-3 for a photograph of the test equipment.) Enough solution is added for a fuel surface area to solution volume ratio of about 3,000 to 5,000 m^{-1}. After a specified length of time, the vessel is opened, and solution and solid samples are taken for analyses. Each test continues for a different duration, providing reaction sequence information over time.[9]

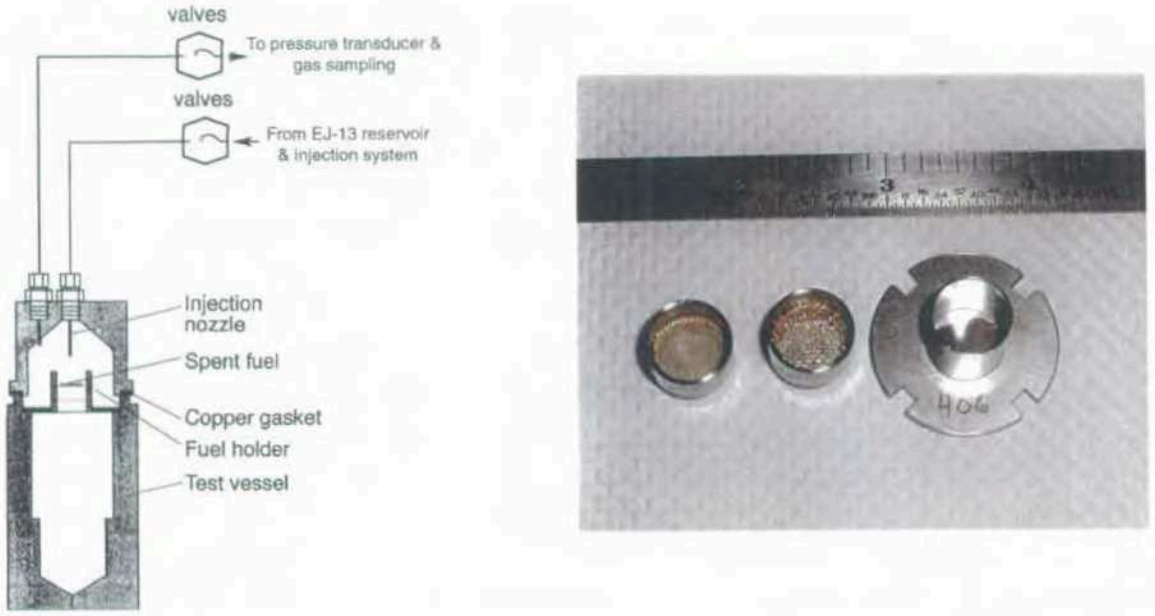

Figure 2-2. Schematic of unsaturated drip test vessel (left) and photo of three-stage fuel holder (right).

Figure 2-3. Photograph of static batch test equipment.

2.2.5 Colloid Tests

Colloids are small particles between 1 and 1,000 nm in size that can remain suspended in a liquid, depending on specific conditions. Larger particles will precipitate and settle out of solution. Smaller particles are considered dissolved in solution and are subject to solubility limits. Colloids pose a unique problem with respect to a repository environment in that the concentration of a particular radionuclide can exceed its solubility limit and remain suspended in solution. Depending on the amount and stability, the presence of colloids can alter the release values of certain radionuclides. Sparingly, soluble radionuclides associated with colloids can be present in solution at concentrations that substantially exceed the solubility of the radionuclide and can be mobilized greater distances than predicted based on solubility in groundwater. Transport of radionuclide contaminants at numerous waste sites have been underestimated by models when compared to the field data.[10] Previous work with high-level waste glasses indicate that significant quantities of actinide-bearing colloids may be generated during degradation.[11] Therefore, a study of the generation and characteristics of potential colloids from DOE SNF was included in the release rate test project.[12]

For the purposes of this project, three types of colloids are of interest: real, pseudo, and waste form colloids. Real colloids are formed from the hydrolysis and polymerization of actinide ions dissolved in solution. The formation of real colloids is solubility limited based on solution chemistry, preventing significant introduction to the environment. Radionuclides adsorbing onto preexisting groundwater colloids can be transported via pseudo-colloids. This mechanism will allow radionuclides to be released and transported in groundwater above the solubility limit. Even more significant is the generation of waste form colloids. As the waste form (SNF in this project) degrades, it forms alteration phases on the surface. Colloid-sized particles of the alteration phase, including radionuclides, spall from the surface into solution. Figure 2-4 depicts the three types of colloids examined by this project (see Reference 12).

A series of experiments were designed to evaluate the generation, stability, and characterization of colloids from degradation of DOE-owned SNF. Analysis of the corrosion products from unsaturated drip tests and static batch tests provide some information. Additional controlled batch tests allow constant monitoring of the degradation process without interference from other processes. These latter tests can also be used to evaluate the interaction of radionuclides with specific ions that may be present in the groundwater (see Reference 12).

Several analytical techniques are available that provide different types of characterization information about colloids. Changes in solution chemistry will be determined by measuring pH, conductivity (ionic strength), and potentiometry (Eh). Dynamic light scattering (DLS) is used to determine the particle size distribution and bulk colloid concentration in solution. It is based on the fluctuations of light scattered by the constant motion of the suspended colloids. This method can be performed in situ and is applicable to the test sequences specifically designed for colloid studies.

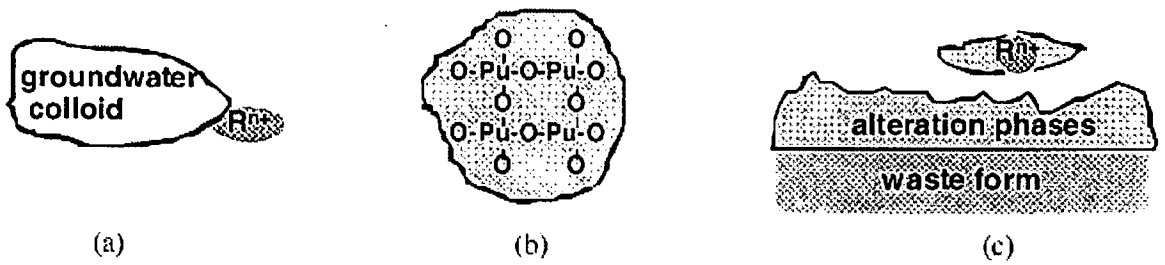

Figure 2-4. Three types of radionuclide bearing colloids: a) pseudo-colloid, b) real colloid, and c) waste form colloid.

Sequential filtration involves separating colloids in a solution into designated size fractions. ICP-MS and nuclear spectroscopy of the filtrates provide data on the elemental composition and activity of radionuclides associated with a particular size fraction. Samples from unsaturated drip and static batch tests are well suited for this technique. Transmission electron microscopy (TEM) will be used to determine the morphology, structure, and elemental composition of the colloids by energy dispersive x-ray spectroscopy (EDS), electron diffraction, and electron energy loss spectroscopy. X-ray diffraction may also be used to determine mineral form of reaction products. A relatively new technique, size exclusion chromatography—ICP-MS, is a highly sensitive method of quantifying actinides at very low concentrations. It will be used to identify and quantify radionuclides associated with colloids in a specific size fraction. Lastly, electrophoretic measurements will be made to determine the surface charge of the colloids, which is used to understand stability and transport properties (see Reference 12).

2.3 Simulated Groundwater

Several wells have been drilled and sampled near the potential repository site at Yucca Mountain, Nevada. The groundwater retrieved from a well designated as J-13 most closely simulates the pore fluid found in the proposed disposal site. Thus, its composition, and variations thereof, are often used as a representative of the solution expected in the repository. Many of the release rate experiments described in this document have test solutions based on the composition of J-13 well water.

PNNL prepares simulated J-13 well water using deionized water and laboratory chemicals according to a specified formulation. The following compounds are used to make the solution: CaSO4, $CaCl_2 \bullet 2H_2O$, $Mg(NO_3)_2 \bullet 6H_2O$, NaF, $NaHCO_3$, $KHCO_3$, and silicic acid. Samples of the resulting solutions are analyzed for verification of a reasonable duplication. The bicarbonates and silicic acid must be completely dissolved before the other chemicals are added to ensure the correct final composition and prevent precipitation. Column 2 of Table 2-4 shows the composition PNNL is trying to achieve. Variations are made to the composition so specific conditions can be evaluated experimentally. For example, increasing the nitrate or bicarbonate concentration is used to change the pH (see Reference 7).

ANL-E has a supply of actual J-13 well water; thus, they do not need to prepare the solution with chemicals. The water is subsequently equilibrated with Topopah Spring tuff (also from the Yucca Mountain area) at 90°C according to a defined procedure, making it a good approximation of expected repository groundwater. A new designation, EJ-13, is used to describe the modified solution. Column 3 in Table 2-4 lists the expected range of composition for EJ-13 (see Reference 8).

Other solutions are used in specific tests at both PNNL and ANL-E. For instance, bicarbonate and nitric acid solutions are evaluated in flow through tests to isolate the effects to those constituents. Deionized water tests are performed in cases where a baseline reaction is needed. Silicon and iron solutions are used to evaluate their effects on the stability of colloids. Each of these specific solutions will be discussed in sections where they apply.

Table 2-4. Nominal composition of simulated J-13 and EJ-13 well water.

Ions	J-13 Concentration (mg/liter)	EJ-13 Concentration (mg/liter)
pH	~8.5	~8.1
Al	NA	0.3–2.0
B	NA	0.1–1.5
Ca	13	4–12
Cl	7.1	5–100
F	2.3	1.5–5.0
K	5.3	NA
Mg	1.9	0.05–4.0
Na	44	40–60
Si	33	30–90
NO_3	8.1	5–100
SO_4	18	12–100
HCO_3	120	60–140

2.4 References

1. National Spent Nuclear Fuel Program, "NSNFP Release Rate Test Program Plan," DOE/SNF/PP-011, Rev. 0, March 1998.

2. U.S. Department of Energy Office of Civilian Radioactive Waste Management, *Quality Assurance Requirements and Description,* DOE/RW/0333P, Rev. 8, June 5, 1998.

3. U.S. Department of Energy Environmental Management, *DOE Spent Nuclear Fuel Information in Support of TSPA – SR,* DOE/SNF/REP-0047, Rev. 0, August 1999.

4. U.S. Department of Energy Environmental Management, *Selection of Fuel Types for Release Rate Testing*, DOE/SNF/REP-045, Rev. 0, March 1999.

5. U.S. Department of Energy Office of Civilian Radioactive Waste Management, "Performance Assessment of Direct Disposal in Unsaturated TUFF of Spent Nuclear Fuel and High-Level Waste Owned by U.S. Department of Energy," SAND94-2563/3, Volume 3, Appendix B.

6. ASTM C 1174-91, "Standard Practice for Prediction of the Long-Term Behavior of Waste Package Materials Including Waste Forms Used in the Geologic Disposal of High-Level Nuclear Waste," 1997.

7. W. J. Gray and R. E. Einziger, *Initial Results from Dissolution Rate Testing of N-Reactor Spent Fuel Over a Range of Potential Geologic Repository Aqueous Conditions*, DOE/SNF/REP-022, PNNL-11894, UC-802, Revised April 1998.

8. Argonne National Laboratory, "Test Plan for Reactions Between Irradiated Uranium-Aluminum Fuel and J-13 Well Water Under Unsaturated Conditions," SNF-3A-087, Revision 0, January 27, 2000.

9. Argonne National Laboratory, "Test Plan for Batch Testing of Irradiated MOX Fuel," SNF-3A-002, Revision 0, April 8, 1998.

10. J. F. McCarthy and C. Degueldre, "Sampling and Characterization of Colloids and Particles in Groundwater for Studying Their Role in Contaminant Transport," *Environmental Particles*, Vol. 2, pp. 247-315, J. Buffle and H. P. van Leeuwen, editors, Boca Raton, Florida: Lewis Publishers, 1993.

11. E. C. Buck and J. K. Bates, "Microanalysis of Colloids and Suspended Particles from Nuclear Waste Glass Alteration," *Applied Geochemistry*, 14, pp. 635–653.

12. Argonne National Laboratory, "Test Plan for the Characterization of Spent Nuclear Fuel Colloids," SNF-3A-121, Revision 0, March 6, 2000.

3. URANIUM METAL FUEL

Uranium metal fuel makes up 85% of the total DOE SNF inventory based on metric tons of heavy metal and primarily consists of zirconium clad N-reactor fuel. An estimated 50% of this fuel has been damaged mechanically through handling processes or from subsequent corrosion of mechanically damaged regions from underwater storage. Because of the large amount of fuel in this group, it also represents the most fissile material and the highest technetium and neptunium content in the DOE inventory. The degraded condition increases the risk of radionuclide release, and uranium is known for its susceptibility to corrosion in water environments. An activity plan[1] was prepared to discuss the planned test requirements to predict uranium metal fuel behavior. Some flow through experiments had been completed prior to the preparation of the activity plan, and those results indicated additional testing was needed. Experimental plans included additional flow through tests, some characterization, static batch tests, and unsaturated drip tests. Colloid tests were added after the activity plan was issued because early results indicated that colloids were produced during dissolution, which could have a negative effect on the performance assessment. Quality assurance requirements were also defined in the activity plan. Test method details are discussed in Section 2.2. The characterization, static batch tests, most of the flow through tests, some unsaturated drip tests, and initial colloid tests were completed prior to the termination of the project.

Three N-reactor fuel elements were sectioned for potential experimental evaluation based primarily on physical condition. Some material was used for other testing in support of drying operations. All three elements are Mark IV fuel, uranium metal fuel meat coextruded with Zircaloy-2 cladding with a preirradiation U^{235} enrichment of 0.947%. N-reactor fuel consists of two concentric tubes and all samples were taken from the outer tube, with an outer diameter of 6.2 cm and an inner diameter of 4.3 cm. Elements #SFEC5,4378 and #SFEC5,4366 were stored in the K West basin, where fuel is stored in water-filled sealed canisters. K East basin contains fuel stored in open canisters, and element #SFEC5,2540 was removed from that facility. Sections from element #SFEC5,4378 were used for characterization, batch, and drip tests; and element #SFEC5,4366 was sectioned for flow through tests (see References 1 and 2).

3.1 Characterization

Characterization of element #SFEC5,4378 was performed at PNNL and at ANL-E. One end of the element was damaged, probably from reactor discharge operations, extending about 2 inches down the element length. Sections were removed from the damaged end, the edge of the damaged area, and from the intact center area. One-inch wide rings were cut from the outer element tube and then sectioned circumferentially into 16 samples (see Figure 3-1). PNNL performed a metallographic analysis of the intact and damage edge sections, and ANL-E examined the damaged section.[3,4]

A transverse and longitudinal face from the intact area of the fuel element was examined optically at PNNL. The samples were mounted and polished prior to the initial examination. Subsequent attack polishing and heat tinting (15 minutes under a halogen lamp) causes a light halo (partial oxidation) around the dark uranium hydride inclusions. Figure 3-2 shows the microstructure of the central intact sample, transverse view. The white, blocky features are uranium carbide inclusions, and the dark spots with a light halo are the uranium hydride inclusions. Distribution appears to be random throughout the surface with no obvious concentration gradient on both the transverse and longitudinal samples. Dark areas without the halo are considered pits, from particle pull-out or fuel matrix pits. No degradation between the cladding and the fuel matrix was seen (see Reference 3).

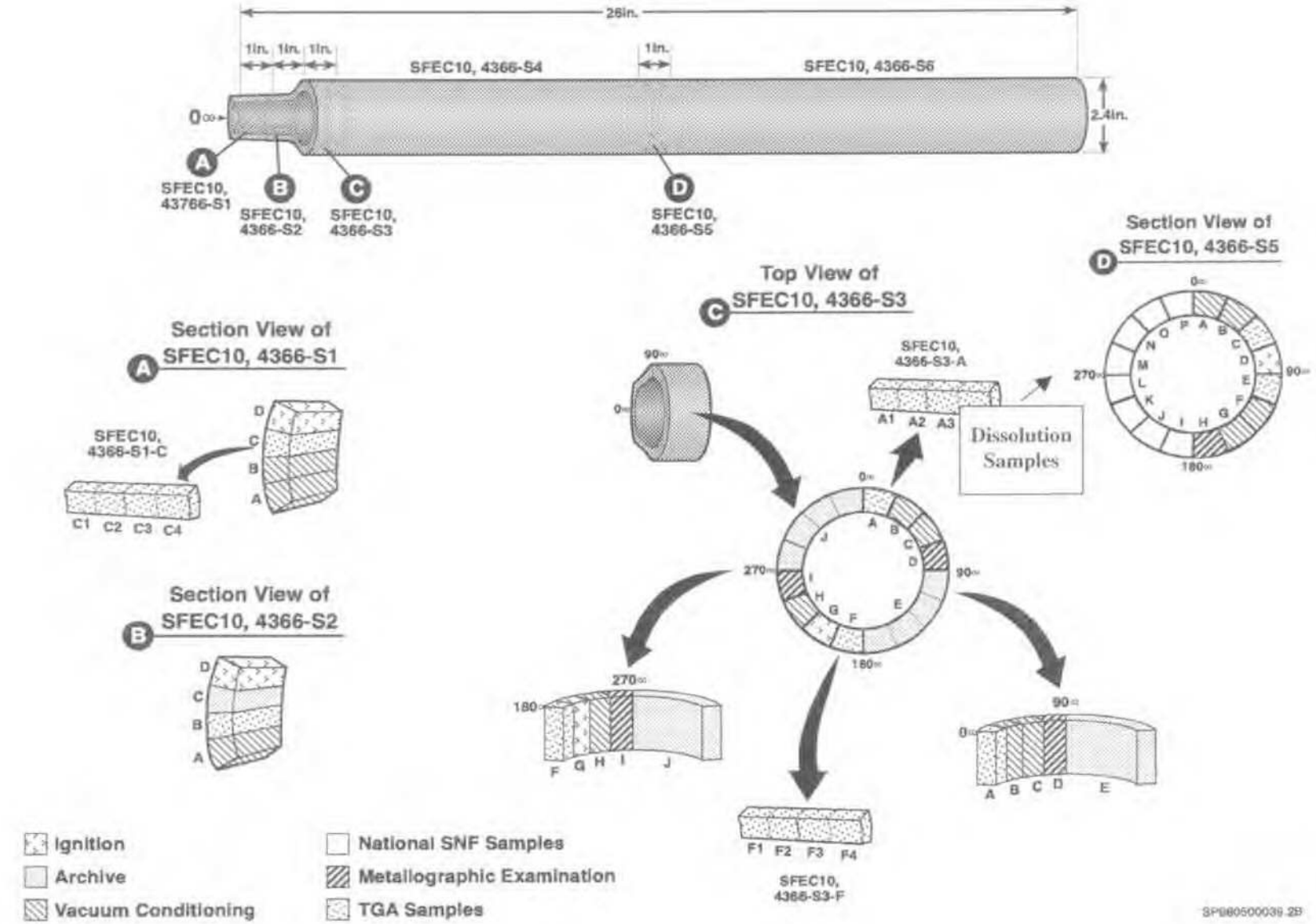

Figure 3-1. Sectioning diagram of N-reactor fuel element for release rate tests.

Figure 3-2. Microstructure of an intact N-reactor fuel section, longitudinal view, showing carbide and hydride inclusions, minor fuel pull-out, and pitting (see Reference 3).

In the sample at the damaged end, two major cracks were visible in the matrix. One was located at the inside surface, the other at the outer surface, and both originated at the breached end of the sample. The cracks branched down and across the fuel, as shown in Figure 3-3, forming a network of cracks. Portions of the crack branches penetrated into the cladding, also visible in Figure 3-3 (left). Heat tinting resulted in a halo around sections of the cracks, indicating hydrogen had migrated into the crack forming uranium hydrides. Other than the surface corrosion and subsequent cracking and hydriding within the cracks, the damaged section was very similar to the intact fuel sample, shown in Figure 3-2. Inclusions of uranium hydride and carbide are randomly located on the surface. The cladding-fuel matrix bond was not preferentially degraded and does not appear to be a pathway for hydrogen migration (see Reference 3).

Samples from the damaged end were examined at ANL-E using visual, metallography, and electron microprobe analyses (EMPA).[5] Visual inspection revealed that extensive cracking extending in all directions within the fuel meat was present in most samples (Figure 3-4). Dark areas near the cracks were visible on some samples, possibly regions of oxidized fuel. The bond between the fuel meat and cladding appeared intact even where cutting damage (burrs) was apparent (see Reference 5).

Both transverse and longitudinal orientations were investigated with metallographic and EMPA examinations. Cracking near the cladding/fuel interface was seen extending from the fuel towards and in some cases into, the cladding. The maximum cladding penetration was approximately 67 μm (Figure 3-5). Uranium carbide inclusions were seen uniformly throughout the sample surface and are shown as lighter blocks in Figure 3-5. An etching process, rather than the heat tint method used at PNNL, was used to reveal uranium hydrides. Although confirmation of the hydride composition was not made, the results were similar to those found at PNNL (distributed throughout the fuel). Some cracks displayed oxidation of the fuel along the crack surface, as shown in Figure 3-6 (see Reference 5).

Figure 3-3. N-reactor fuel sample at the damaged end showing crack network from the cladding through the fuel matrix (see Reference 3).

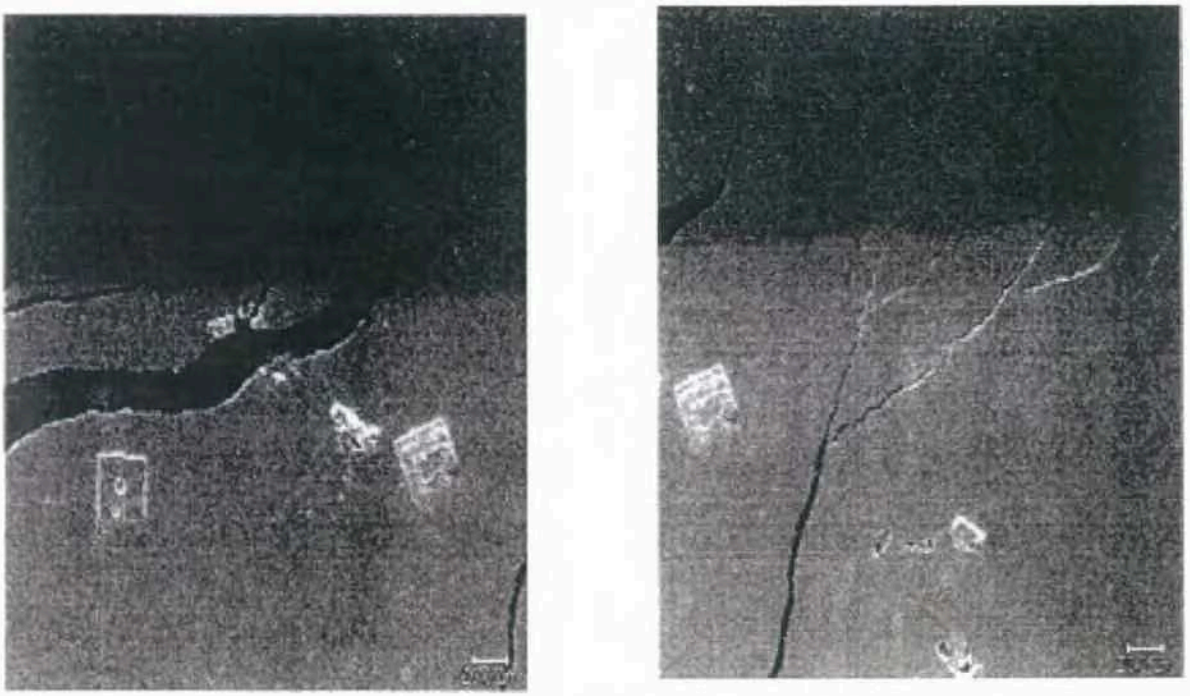

Figure 3-4. Uranium metal fuel sample showing extensive cracking (see Reference 5).

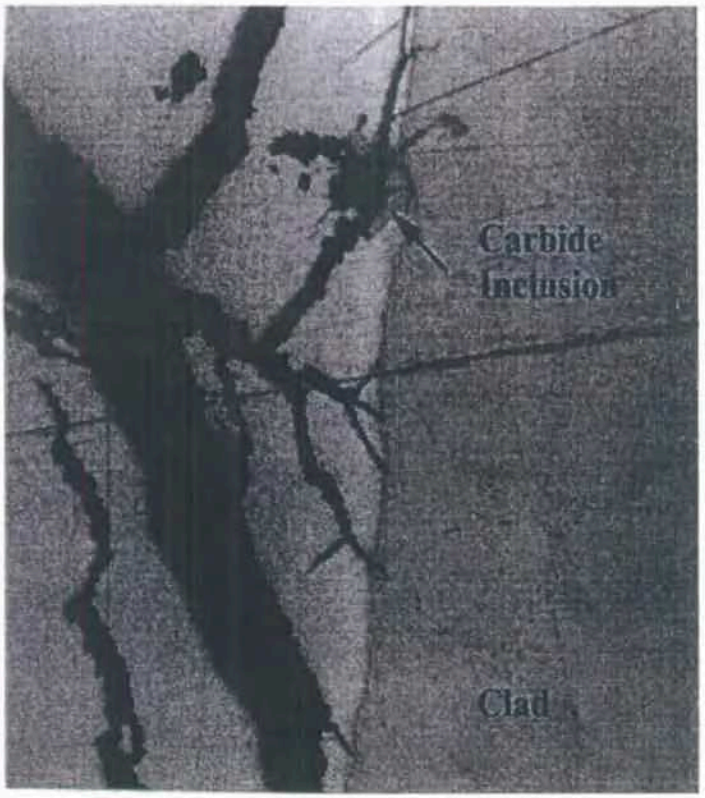

Figure 3-5. Uranium metal fuel scanning electron microscopy image showing crack extending into cladding (see Reference 5).

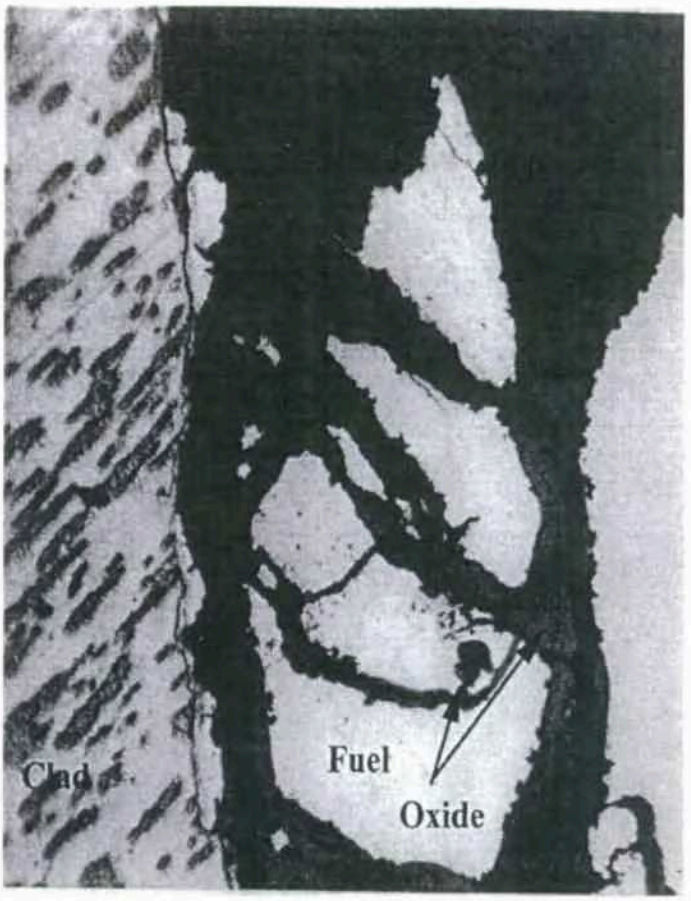

Figure 3-6. Uranium metal fuel sample indicating oxidation of fuel along crack surface (see Reference 5).

EMPA examination revealed a significant amount of interdiffusion between the cladding and fuel had occurred. Zirconium, the cladding material, had diffused into the fuel about 15 μm. An opposite gradient of uranium was found, decreasing as the zirconium increased into the cladding (see Figure 3-7). Scanning across a crack indicated that corrosion products were present, confirming the visual and metallographic examinations. No fission products were detected because the concentrations were below detection limits (see Reference 5).

3.2 Flow Through Dissolution Tests

Flow through dissolution tests with uranium metal fuel were performed at PNNL following the same methodology as was used with commercial light water reactor (LWR) fuel. Descriptions of the test method and equipment are found in Section 2.2.2. Temperature, pH, and solution chemistry were varied to evaluate the forward reaction rate under different environmental conditions. Samples of the effluent were removed one to three times per week and analyzed for uranium. Selected samples were also analyzed for americium, strontium, cesium, technetium, and plutonium. A direct comparison between the steady state results from the LWR experiments and the uranium metal fuel tests was anticipated. However, significant variations in the N-reactor fuel tests were found, and thus, additional tests were planned to identify the source of the irregularities.[6,7]

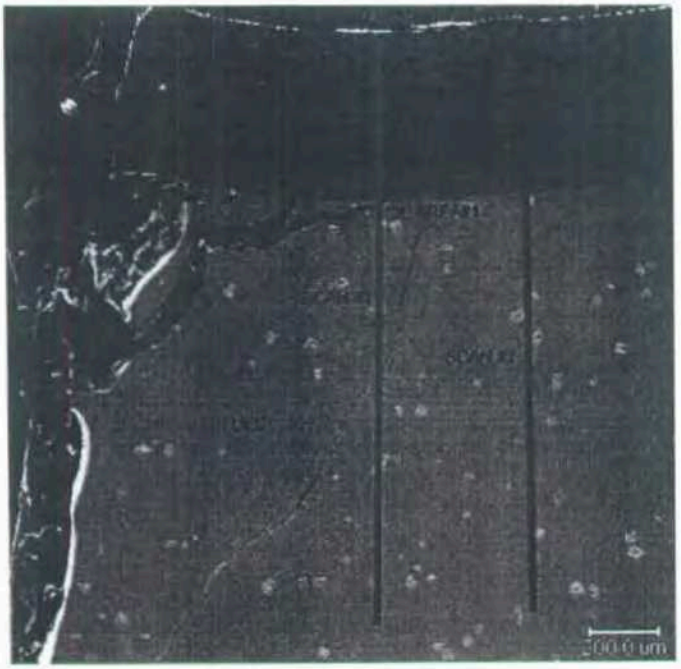

Figure 3-7. Uranium metal fuel electron microprobe analysis line scan across cladding and fuel meat indicating interdiffusion (see Reference 5).

3.2.1 Test Matrix

Ten dissolution experiments were originally planned with the uranium metal fuel at different conditions; five of which could be used as a direct comparison with LWR fuel. Solutions evaluated include simulated J-13 well water, bicarbonate solution, and nitric acid with pH ranges between 3 and 10. Feed initially flowed downward in the tests to effectively close the system and keep gases, primarily O_2 and CO_2, trapped in the solution. However, large irregularities were seen compared to LWR test results, probably caused by air pockets in the test cell. Thus, the initial six tests (1, 2, 3, 4, 9, and 10) were inverted so water flowed upward for the balance of the experiments. Temperatures were varied between 25 and 75°C. Table 3-1 lists the initial experimental conditions.

Some of the coupons were reused in subsequent experiments. Justification for reuse was based on the assumption that a visibly uncorroded coupon would not compromise the results in the following test. Because microscopic alterations to the material are possible that could change the release characteristics, this may be a contributing factor to the irregularity in test results (see Section 3.2.3). Column 2 in Table 3-1 shows the coupon used in each test and the exposure sequence (first, second, etc.) in parentheses. For example, sample K was used first in test matrix 1, then in test matrix 5, followed by test matrix 7, and finally in test 3A. Tests 3, 3A, and 3B have equivalent conditions but use different coupons for replication. It is important to ensure that irradiation of the fuel does not alter the reaction process. Thus, conditions shown for test numbers 1, 8, and 9 were duplicated with unirradiated uranium metal fuel to evaluate the effect of burnup and serve as a reference (see References 6 and 7).

Quartz liners were placed in the test cells to prevent any galvanic interaction in these tests (see Reference 7).

Table 3-1. Uranium metal fuel flow through dissolution test matrix.

Test	Specimen ID (exposure)	Temperature (°C)	Solution Chemistry	pH
1	K (1)	25	2×10^{-2} M carbonate	8
2	L (1)	75	2×10^{-2} M carbonate	10
3	M (1)	75	2×10^{-4} M carbonate	8
3A	K (4)	75	2×10^{-4} M carbonate	8
3B	N (3)	75	2×10^{-4} M carbonate	8
4	N (1)	25	2×10^{-4} M carbonate	10
5	K (2)	25	2×10^{-2} M carbonate	5
6	L (2)	75	2×10^{-4} M carbonate	5
7	K (3)	25	1×10^{-5} M nitric acid	5
8	N (2)	25	1×10^{-3} M nitric acid	3
9	O (1)	25	J-13 well water	8.5
10	P (1)	75	J-13 well water	8.5

Once the experiments described above were completed, questions about variability in the results were identified. Thus, additional tests were performed to evaluate two possible causes: galvanic corrosion and oxic vs. anoxic conditions. Electrochemical and flow through tests were designed to evaluate potential galvanic interactions between the uranium metal and the zircaloy cladding or stainless steel specimen cell. Open circuit measurements of the different metals versus a reference electrode provide a baseline of each material's potential. Subsequent corrosion rate measurements of uranium, isolated and galvanically connected to zircaloy and stainless steel, provide short-term estimates of the potential for galvanically enhanced corrosion. Flow through tests were also planned to provide specific dissolution rates with and without a galvanic connection. Below are the three flow through test configurations planned with 2×10^{-4} M carbonate at 75°C and pH of 10 (conditions that produced the highest dissolution rate in the original tests) (see Reference 7):

- Uranium metal SNF sample with cladding attached; ensure electrical connection between uranium and stainless steel specimen cell to create galvanic interaction.
- Uranium metal SNF sample with cladding attached; glass liner in specimen cell to prevent galvanic interaction.
- Uranium metal SNF sample with cladding removed; glass liner in specimen cell to prevent galvanic interaction.

Flow through tests were planned to evaluate the effect of oxic versus anoxic conditions. Unirradiated uranium metal would be exposed to deionized water at 25°C with an air sparge in the feed container. An effluent separator and hydrogen monitor were added to the exit stream to monitor the hydrogen production. After a period of time, the sparge gas would be changed to argon, providing an anoxic condition. Once the results appeared fairly stable, the feed would again be sparged with air.

Additional tests could then be performed with varying amounts of oxygen and possibly defining the point of transition between Stage 1 and Stage 2 corrosion (see Reference 7).

3.2.2 Sample and Solution Preparation

Uranium SNF samples for the flow through dissolution tests were taken from the 16 wedge segments described in Section 3.1. Selected segments were subsequently cut to remove the outer cladding and to reduce the sample size. The inner cladding layer was left intact. All the samples were tested in the as-cut condition except one. A passivation treatment of sample P was performed by exposing the coupon to 2% oxygen/98% argon at 250°C for 4 hours to evaluate the effects of a UO_2 oxide film (see Reference 6).

Unirradiated coupons were prepared by cutting uranium metal to the appropriate size and then grinding the surfaces to a 600-grit finish. Electrochemical coupons were prepared by cutting metal stock material to the desired size and shape (typically about $1/2 \times 1 \times 1/8$ inch). The zircaloy and stainless steel coupons were tested in the as-cut condition, but the cut surfaces of uranium metal were ground to a 600-grit finish (see Reference 7).

Surface area is a crucial element of the test analysis. Dissolution rates must be normalized to the surface area prior to performing any meaningful comparisons between different samples. The surface area of all the coupons described in this project were determined by geometric measurements of each sample. No roughness factor was applied because they had relatively smooth surfaces. However, the LWR specimens were small particles (1 to 5 mm fragments) and grain size powder. Surface area of the fragments was estimated by measuring the size distribution and calculating the total geometric surface area assuming a cubical geometry for each fragment. A roughness factor of three was then applied to account for the irregularities. The BET (Brunauer, Emmett, and Teller) method based on gas adsorption was used to predict the surface area of the powder (see Reference 6).

Five solutions were evaluated in the flow through tests. Simulated J-13 well water was prepared according to the description in Section 2.3. Sodium bicarbonate was diluted to 2×10^{-2} and 2×10^{-4} molar; a factor of ten above and below the nominal 2×10^{-3} carbonate content of J-13 well water. Air with the appropriate CO_2 concentration was sparged into the feed to maintain the desired pH. Nitric acid concentrated to a pH of 3, the calculated lower limit expected in the proposed repository, was maintained by sparging with CO_2-free air (see Reference 6). Deionized water was used with unirradiated uranium metal as a baseline and to investigate possible oxygen effects (see Reference 7).

3.2.3 Irradiated SNF Test Results

Dissolution rates from the flow through tests were calculated using isotopic analyses of the effluent samples and initial fuel composition, flow rate, sample mass, and surface area. Below is the formula for dissolution rate. Calculated rates for each sample were then graphed with respect to sampling time. Uranium concentration was analyzed in every sample, but other isotopes (Am, Pu, Cs, Tc, and Sr) were analyzed at various intervals (see Reference 6).

$$R_i = \frac{C_i F}{M A f_i} \qquad (3\text{-}1)$$

where

R_i = dissolution rate based on component i ($mg/m^2/d$)

C_i = concentration of component i in effluent (mg/mL or Bq/mL)

F = flow rate (mL/d)

M = mass of test specimen (mg)

A = surface area of test specimen (m^2/mg)

f_i = concentration of component i in test specimen (mg/mg or Bq/mg).

Once the graphs of dissolution rate versus time were completed, the average rate was calculated. With the variability of the data, choosing the timeframe to average is somewhat subjective. In general, the areas where data points are within ±30% are included in the averaging calculation. In most cases the data used in the average are noted on the graphs.

3.2.3.1 Uranium Dissolution Rates. Table 3-2 shows the average uranium dissolution rates calculated for each test condition described in Table 3-1 with the associated error band. Flow direction is listed for each test; "Both" indicates those tests where the flow was changed from downward to upward after a period of time. Because the test conditions (temperature, pH, or solution chemistry) were changed for those SNF samples that showed no degradation, the subsequent test number is also shown. It does not appear this practice caused any significant affects on the dissolution rates. The range of dissolution rates presented in Table 3-2 is at least two orders of magnitude with no obvious trends based on any conditions. Average rates were not calculated for four tests (test numbers 3, 3A, 9, and 10) due to the onset of Stage 2 corrosion, discussed below. Results for test 3B and 6 were taken from the initial Stage 1 region, before Stage 2 was initiated (see Reference 6).

Data from all the tests were plotted on a graph of dissolution rate versus time, although only a select few have been incorporated into this document. Average rates shown in Table 3-2 are also shown, as well as any data points of other elements. Figure 3-8 is a good example of the type of graph expected

Table 3-2. Uranium metal SNF dissolution test results.

Test Number	Flow Direction	Subsequent Test Number	Extent of Corrosion	Data Range for Rate Calculation (days)	U Dissolution Rate ($mg/m^2/d$)	Error on Dissolution Rate
1	Both	5	NA	64–137	155	±26
2	Both	6	NA	95–137	2,030	±220
3	Both	None	Extensive	—[a]	—[a]	NA
3A	Down	None	NA	—[a]	—[a]	NA
3B	Up	None	None	1–33	150	±16
4	Both	8	Slight	96–145	50	±4
5	Up	7	None	1–74	63	±11
6	Up	None	None	18–61	199	±50
7	Up	3A	Moderate	4–36	38	±4
8	Up	3B	Moderate	32–113	127	±14
9	Both	None	Extensive	—[a]	—[a]	NA
10	Both	None	Extensive	—[a]	—[a]	NA

a. No rate was calculated because stability was not achieved.

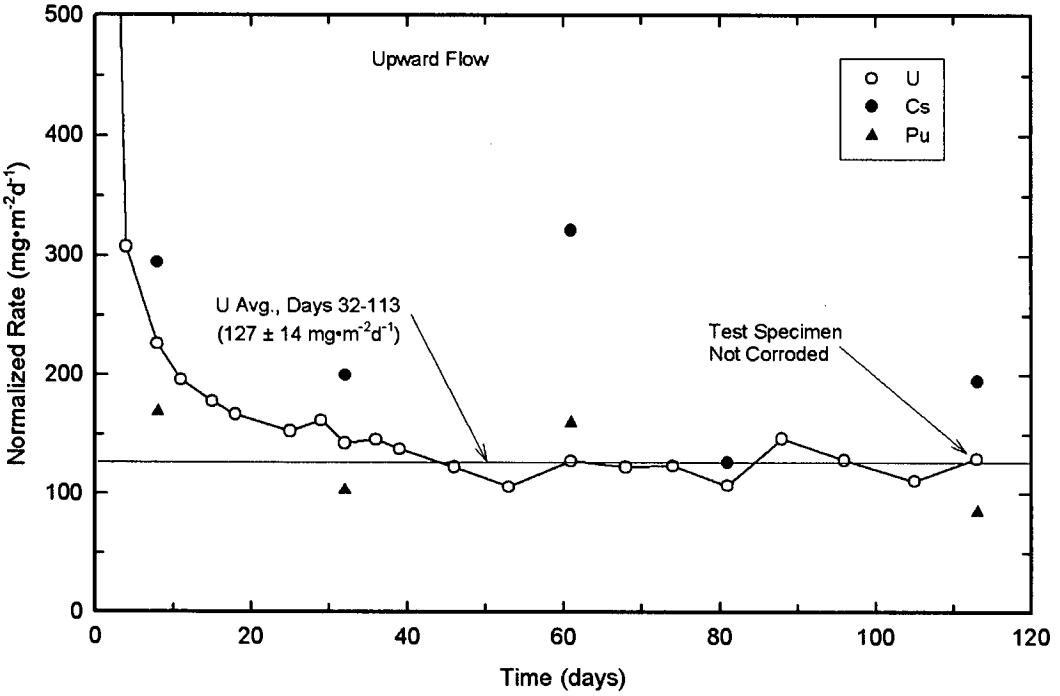

Figure 3-8. Dissolution rates of uranium metal SNF in dilute nitric acid, pH of 3, and 25°C (test 8).

from a flow through test. An initial high corrosion rate is common, and it was apparent in most of the flow through tests. After the first few weeks, the system stabilized and a consistent, average rate was calculated. At the conclusion of the test, the specimen did not appear corroded (though some discoloration is normal). Unfortunately, not all the test results were this uniform. Test 8 was performed in 2×10^{-3} M nitric acid with a pH of 3 at 25°C (see Reference 6).

Two SNF specimens were weighed before and after testing and the weight loss was compared to the calculated loss based on dissolution rate. Sample K (used in test 1, 5, 7, and 3B) was weighed before test 1 and after test 7 resulting in a loss of 21.8 mg. Integrating the area under the curves of uranium dissolution rate versus time for tests 1, 5, and 7 gave a weight loss of 19.4 mg. Using the same method with sample N from tests 4 and 8 resulted in a 23.4 mg loss by weight measurements and 20.0 mg from dissolution calculations. Less than 15% variation was seen with both samples, indicating dissolution rates are reasonably accurate (see Reference 6).

Changing the flow direction from downward to upward during the experiment resulted in an increase in dissolution rate in all six tests. Test 1 displayed this increase very clearly with a dissolution rate of about 25 mg/m^2/d prior to the flow direction change and about 200 mg/m^2/d afterwards, shown in Figure 3-9. It is possible that the sample material was not completely immersed during the upward flow period, exposing some surface to the atmosphere rather than liquid. The only experiment that did not show a distinct increase in dissolution rate when the flow direction was changed was test 9 (Figure 3-10), but all the data were highly variable. Test 10 results demonstrated a trend similar to test 3, but at much higher rates. Shown in Figure 3-11, dissolution increased from about 250 mg/m^2/d to about 2,000 mg/m^2/d. Note the passivation treatment did not appear to alter the test results. Average values shown in Table 3-2 were calculated from data collected during the upward flow regime in all the tests except number 3A (see Reference 6).

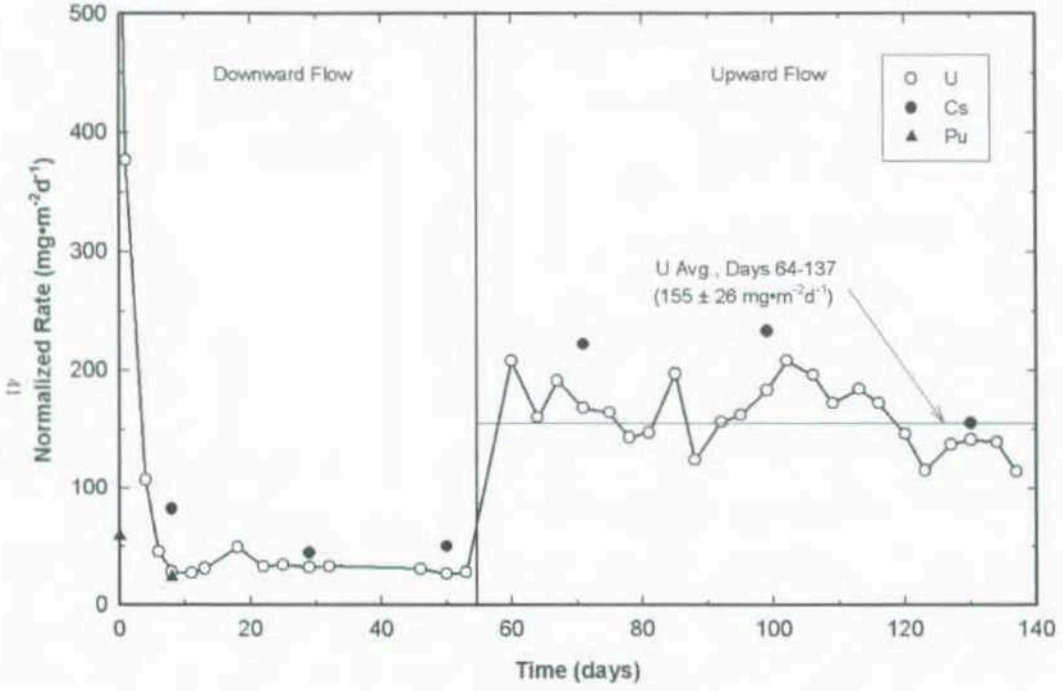

Figure 3-9. Dissolution rate of uranium spent nuclear fuel in 2×10^{-2} M carbonate, pH = 8, at 25°C (test 1) showing change in flow direction.

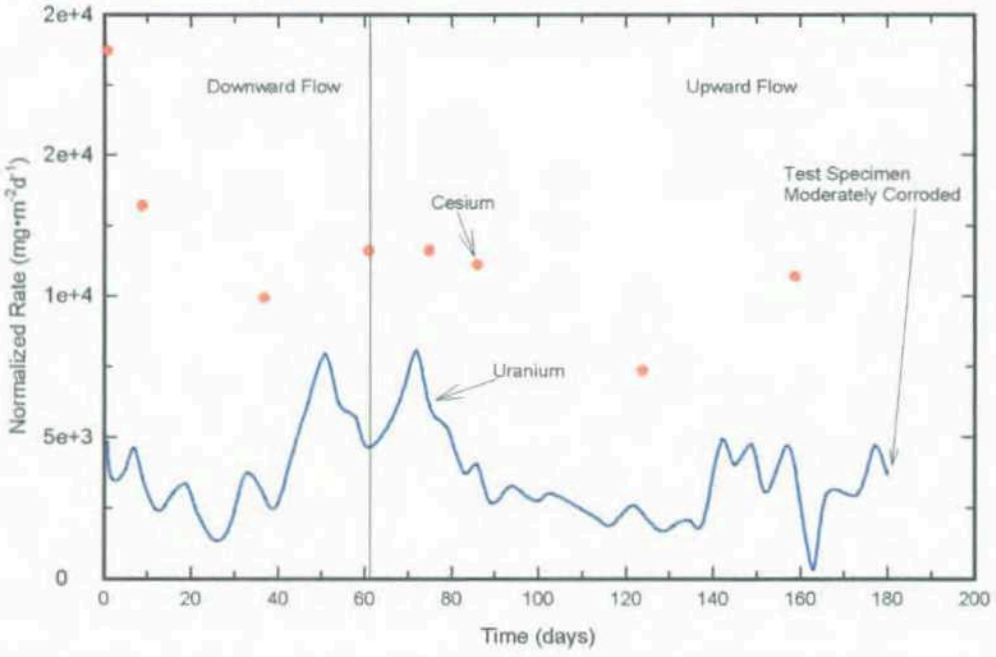

Figure 3-10. Dissolution rate of uranium spent nuclear fuel in simulated J-13 well water (test 9) at 25°C.

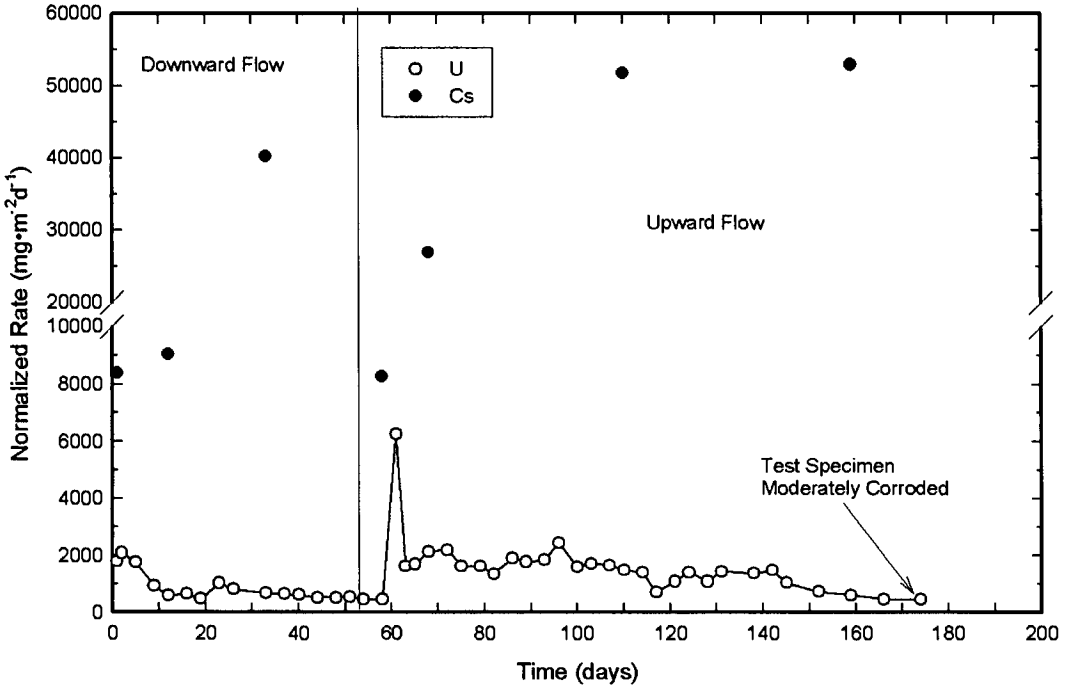

Figure 3-11. Dissolution rate of uranium spent nuclear fuel (passivated) in simulated J-13 well water (test 10) at 75°C.

3.2.3.2 Stage 2 Corrosion. After about 120 days from test initiation (20 days from changing the flow direction), the uranium concentration in the effluent from test 3 began to decrease significantly. The test cell was opened, and the sample was examined. Large quantities of black, sludge-like, corrosion products were found, and the sample was badly corroded. Thus, a forward reaction rate cannot be derived from these data. Specimens in the concurrent experiments were also examined. Tests 5, 6, and 8 specimens showed no visible corrosion, and testing was resumed. However, the fuel samples in tests 9 and 10 did show excessive attack and were terminated. Shortly after test 6 was restarted, the uranium concentration in the effluent began to rise significantly. It is not clear if the visual examination caused the increase (for example, by disrupting a protective film) or if it was coincidental. At the end of this test, the specimen was slightly corroded, and cesium concentrations were beginning to increase (see Reference 6).

The conditions of test 3 were repeated with two additional samples, labeled tests 3A and 3B. Flow direction was the only variable in the duplicate tests; fluid was dripping downward in test 3A, flow was upward in test 3B, and the flow was changed from downward to upward at about 100 days in test 3. Corrosion rates in all three experiments were generally between 100 and 400 $mg/m^2/d$. However, after about 150 days, the uranium concentration in the effluent dropped to detection limits. Visual inspection showed excessively degraded material, indicating the reacting uranium is retained in the corrosion products rather than being released to the environment. Because the initial few data points (through sample day 31) in test 3B are relatively stable (within the $\pm$30% range) and the specimen showed little to no attack during that time, they were used to calculate an average dissolution rate. Figure 3-12 shows the data points with time and the progression of visible degradation for test 3B (see Reference 6).

Gray and Einziger classified the two corrosion regimes as Stage 1 and Stage 2. Stage 1 was characterized by a relatively steady release of uranium into solution with no visible corrosion products. Uranium is assumed to be entirely in the +6 state and thus soluble. During Stage 2, uranium concentration in the effluent drops to below detection limits, cesium concentration increases dramatically, and large amounts of fine, black corrosion products are visible. In this case, uranium is assumed to form uranium

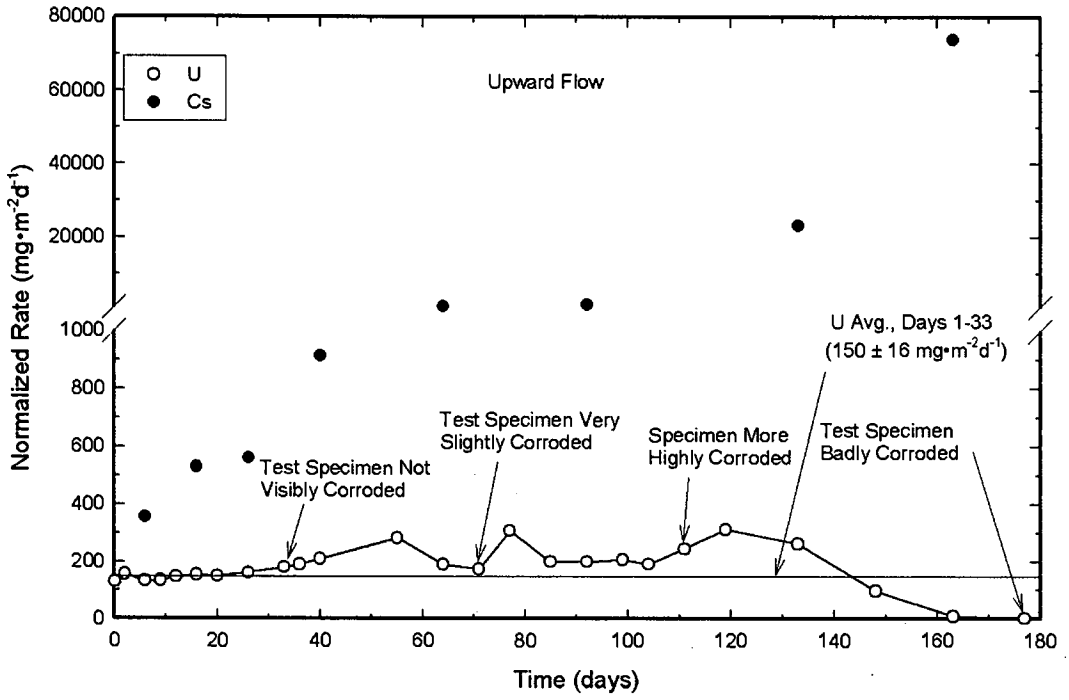

Figure 3-12. Dissolution rate of uranium spent nuclear fuel in 2×10^{-4} M carbonate, pH = 8, at 75°C (test 3B).

oxide in the +4 state, resulting in solid precipitates. Thus, no uranium was detected in the effluent. Increases in cesium concentration indicate the overall corrosion rate of the fuel is increasing, even though the uranium in solution is decreasing. The increased reaction rate may be depleting the available oxygen, suggesting an anoxic environment and inhibiting the oxidation of U(IV) to U(VI) (see Reference 6).

Defining at what point a reaction changes from Stage 1 to Stage 2 is somewhat subjective. Increases in the cesium concentration or decreases in the uranium concentration may be a clue, but the presence of corrosion products is the primary determining factor. Figure 3-12 (test 3B) shows some visible corrosion at about 70 days and a decrease in uranium dissolution rate at about 130 days. The cesium dissolution rate increased continually throughout the test. Tests 3 and 3A also had a decrease in uranium concentration beginning at 120 to 130 days and a fairly steady increase in cesium concentration. Tests 9 (Figure 3-10) and 10 (Figure 3-11) were moderately corroded at test termination and could also be classified as Stage 2 corrosion. Test 10 data followed a trend similar to tests 3, 3A, and 3B (decrease in uranium concentration and a steady increase in cesium concentration). However, test 9 results did not demonstrate either one of these trends. Several potential causes of Stage 2 corrosion have been proposed. Galvanic effects between the uranium metal and the zircaloy cladding or the stainless steel test cell could accelerate the corrosion. As the reaction proceeds, oxygen could be depleted from the solution resulting in an anoxic rather than oxic condition. Anoxic reactions with uranium are known to be more aggressive.[8] Another possibility involves the buildup of a protective oxide layer that subsequently cracks, resulting in alternating protective/reactive surfaces (see Reference 8). These theories are explored more thoroughly in the following sections.

3.2.3.3 Characterization of Corrosion Products. The fine, black corrosion products (sludge) from tests 3, 9, and 10 were dried and analyzed. X-ray diffraction (XRD) of the material from tests 9 and 10 (which used simulated J-13 well water) indicated only the presence of U_4O_9 (or uraninite). Analysis of the test 3 solids, however, indicated both uraninite and schoepite ($UO_3 \cdot 2H_2O$) were formed.

No uranium hydride or other compounds were seen in any of the three samples. The higher oxidation state was associated with the more heavily reacted sample (see Reference 6).

Measurements of particle size distribution with two of the sludge samples were completed. Size distribution of the corrosion products from test 3 (which used 10^{-4} M carbonate solution) is shown in Figure 3-13. For comparison, the sludge from test 10 (with simulated J-13 well water) is shown in Figure 3-14. Very few particles from test 10 are within the colloid range (1 nm to 1 μm), but about 10% of test 3 particles are colloidal. Notice also that test 3 appears to have a bimodal distribution, with peaks at about 11 microns and 600 microns. Test 10 had one peak at about 40 microns. Differences between the two tests include the solution chemistry, the rate, and extent of reaction (test 3 was more severely corroded than the test 10 sample after 170 days); and the sample in test 10 was passivated (see Reference 6). (The passivation treatment consisted of exposing the sample to a gas stream of argon with 2% oxygen at 250°C for 4 hours, creating an oxide layer on the surface.)

Portions of the sludge were dissolved and analyzed for isotopic content. Replicates were used to verify no undissolved material was present to skew the results. These data were compared to the original fuel sample composition calculated using an ORIGEN model and measured using fuel specimen L (from tests 2 and 6) in a series of nitric acid dissolution steps. An additional sample from the end of the same fuel element was completely dissolved and analyzed for the same elements. Table 3-3 lists the estimated SNF composition based on the three methods. Similar results were found with the ORIGEN calculation and the end sample, but test specimen L had consistently lower values (except uranium). These differences are attributed to the wide distribution of isotopes through a fuel element. The average concentration from sample L was used for comparison with the sludge composition (see Reference 6).

Isotopic composition of the sludge from tests 3, 9, and 10 were analyzed for the same elements as seen in Table 3-3. The fraction of each element retained in the sludge was calculated based on the sample L composition and normalized to the uranium retention. Equation (3-2) was used to calculate the percent

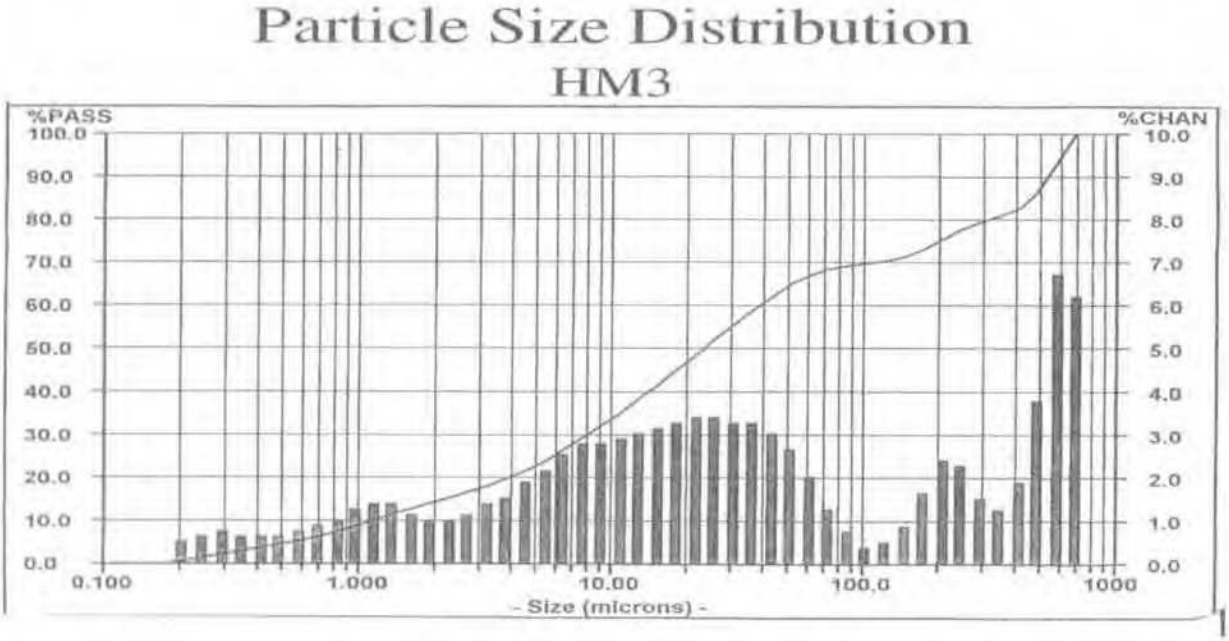

Figure 3-13. Particle size distribution of corrosion products from test 3, dilute carbonate solution with a pH of 8 at 75°C.

Particle Size Distribution

HP-10

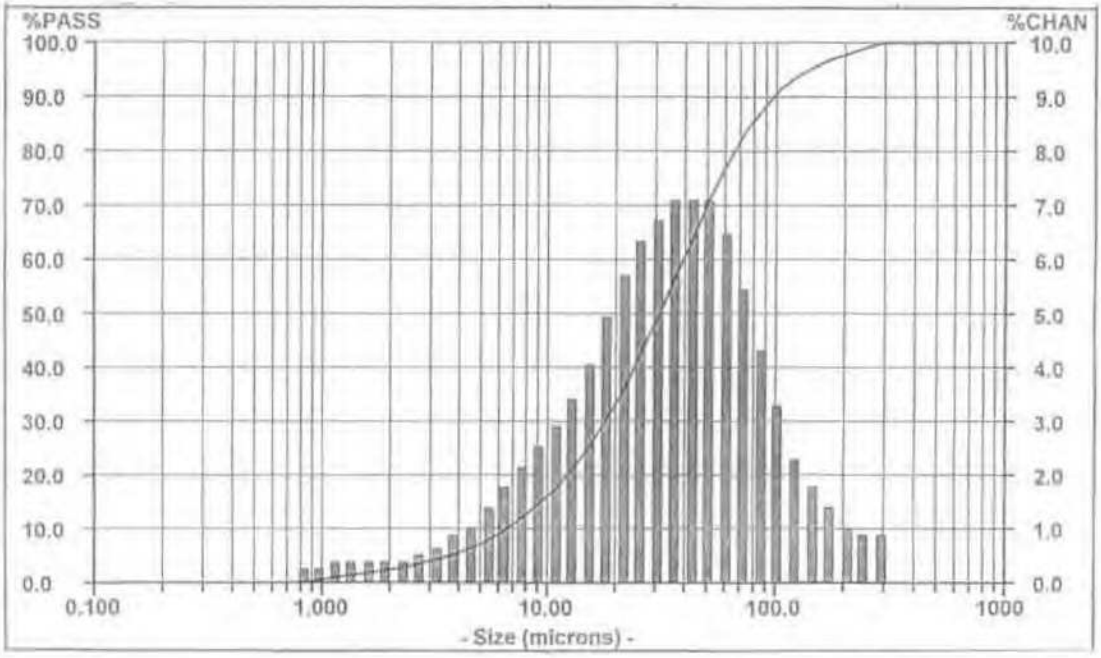

Figure 3-14. Particle size distribution of corrosion products from test 10, simulated J-13 well water at 75°C.

Table 3-3. Estimated isotopic inventory of uranium metal fuel samples.

Sample Source	Uranium (mg/g)	^{241}Am (µCi/g)	$^{239/240}$Pu (µCi/g)	^{238}Pu (µCi/g)	^{137}Cs (µCi/g)	^{99}Tc (µCi/g)	^{90}Sr (µCi/g)
End	945	12.5	70.8	4.31	2,490	0.620	2,160
ORIGEN	NL	10.8	70.4	7.12	2,790	NL	2,390
L (1)	1,010	2.48	38.4	1.38	1,450	0.451	1,110
L (2)	993	3.55	40.6	1.46	1,520	0.420	1,150
L (3)	996	2.78	38.9	1.52	1,460	0.499	1,200
L (avg)	1,000	3.10	39.3	1.45	1,480	0.457	1,150

NL—not listed with results

retained in the sludge. Replicate samples of each sludge were analyzed to detect homogeneity or sampling errors. Table 3-4 lists the results of the analysis and the percent of each element retained in the sludge sample (see Reference 6).

$$R\ (\%) = 100 * I_{test\ i}\ (\mu Ci/g) / ([U_{test\ i}\ (\mu Ci/g)/U_{sample\ L}\ (\mu Ci/g)] / I_{sample\ L} \qquad (3\text{-}2)$$

where

R = percent retention of isotope I in the sludge

$I_{test\ i}$ = composition of isotope I in test sample i

$I_{sample\ L}$ = average composition of isotope I in sample L

$U_{test\ i}$ = composition of uranium in test sample i

$U_{sample\ L}$ = average composition of uranium in sample L

Replicate analyses were similar, so the results were assumed to be representative of the actual reactions. Americium and plutonium were completely retained in the corrosion products. In several cases the value was above 100%, probably a reflection of the analytical and sampling errors. About half the technetium was retained in the sludge and half was released into the solution. Cesium and strontium retention was dependent on the test conditions. Test 3 used a carbonate solution, which resulted in about a third of the cesium and nearly all of the strontium being retained in the corrosion products. The sample in this test was also highly corroded and the sludge composition was different (uraninite and schoepite). Simulated J-13 well water was used in both tests 9 and 10, and they had similar results. Very little cesium (10–15%) and only about a third or less of strontium remained in the sludge. In actual repository conditions (with groundwater similar to J-13 water), most of the cesium and strontium and about half the technetium reacted from the fuel could be released to the environment based on these tests alone (see Reference 6).

Table 3-4. Isotopic composition and percent retention in the sludge from tests 3, 9, and 10.

Test Number	Uranium (mg/g)	^{241}Am		Pu[a]		^{137}Cs		^{99}Tc		^{90}Sr	
		(μCi/g)	(%)	(μCi/g)	(%)	(μCi/g)	(%)	(μCi/g)	(%)	(μCi/g)	(%)
3	897	4.0	144	1.4	91	515	38	0.04	55	82	79
3	823	2.7	105	1.7	115	449	37	0.03	58	142	107
3	863	4.3	160	1.7	111	578	37	0.04	56	113	89
3 (avg)			136		106		37		56		91
9	753	1.9	80	0.4	101	113	10	0.02	57	24	21
9	737	2.3	99	0.7	133	131	12	0.02	52	39	25
9 (avg)			89		117		11		55		23
10	779	2.5	104	0.5	117	130	11	0.02	51	45	34
10	661	2.6	125	0.7	121	137	14	0.03	51	48	34
10 (avg)			114		118		13		51		34

a. Average of $^{239/240}$Pu and ^{238}Pu.

Additional characterization of the sludge and the reacted samples was planned. Optical microscopy of the sample cross sections would provide information on possible cracking, pitting, hydriding, and preferential attack at the fuel/cladding interface. However, this work will not be done due to the premature conclusion of the release rate test project.

3.2.3.4 Comparison with LWR Fuel. Degradation mechanisms and rates of uranium metal fuel were compared to test results with commercial LWR (UO_2) fuel. It has been suggested that once the uranium metal begins to oxidize to UO_2, the reactions would be the same. However, the data do not support this assumption. No indications of Stage 2 corrosion were seen with the commercial LWR fuel experiments. Table 3-5 shows the average dissolution rate from the LWR tests with the same conditions as the uranium metal fuel tests. Only five conditions were duplicated in both test series (LWR and DOE-owned SNF). Because the uranium metal fuel in test 9 conditions (simulated J-13 at 25°C) indicated Stage 2 corrosion characteristics, no dissolution rate was reported. The rate varied between 2,000 and 5,000 $mg/m^2/d$ during the more stable region (see Figure 3-10). Uranium metal SNF had significantly higher dissolution rates than LWR fuel in every case, generally by a factor between 10 and 100. Based on these results, it is clear that uranium metal fuel does not behave in the same manner as UO_2 fuel, and predictions of releases must be based on a different model (see Reference 6).

3.2.4 Unirradiated Fuel Test Results

Experiments with unirradiated uranium metal fuel were performed to evaluate the effect of irradiation and to investigate two possible causes of Stage 2 corrosion. Irradiation effects were examined by repeating three test conditions listed in Table 3-1 (tests 1, 8, and 9) with unirradiated fuel specimens. Galvanic interaction with the stainless steel test cell or the zircaloy cladding could cause an increase in the uranium dissolution and thus may initiate Stage 2 corrosion. Electrochemical and flow through tests were designed to investigate any galvanic reactions. Another potential cause of Stage 2 corrosion is the absence of oxygen. Anoxic conditions have been reported to increase the dissolution of uranium. Flow through tests were also planned to examine the effects of oxygen content (see Reference 7).

3.2.4.1 Unirradiated Fuel Dissolution Tests. Three test conditions from Table 3-1 were duplicated with unirradiated uranium fuel samples: nitric acid solution at 25°C and pH of 5 (test 8 on Table 3-1), 2×10^{-2} M carbonate solution at 25°C and a pH of 8 (test 1), and simulated J-13 well water at 25°C (test 9). Dissolution calculations were performed as described in Section 3.3 for irradiated fuel and were graphed in a similar manner. Figures 3-15, 3-16, and 3-17 present the results for direct comparison with the irradiated fuel tests (Figures 3-8, 3-9, and 3-10, respectively).

Table 3-5. Comparison of uranium metal SNF and LWR dissolution rates.

Test Number	Temperature (°C)	pH	Carbonate (M)	LWR Dissolution ($mg/m^2/d$)	U metal SNF Dissolution ($mg/m^2/d$)
1	25	8	2×10^{-2}	4.1	155
2	75	10	2×10^{-2}	14	2,030
3B	75	8	2×10^{-4}	10	150
4	25	10	2×10^{-4}	0.49	50
9	25	8.5	J-13	3.0	—[a]

a. No value due to potential Stage 2 corrosion.

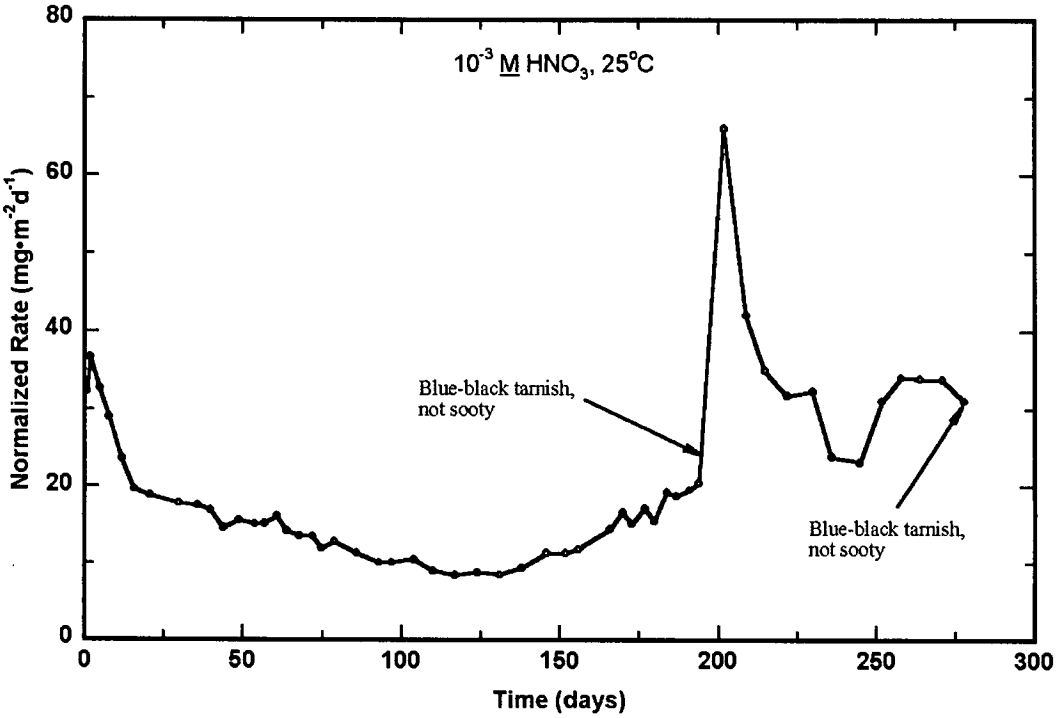

Figure 3-15. Dissolution rate of unirradiated uranium metal fuel in dilute nitric acid, pH of 5, and 25°C (test 8).

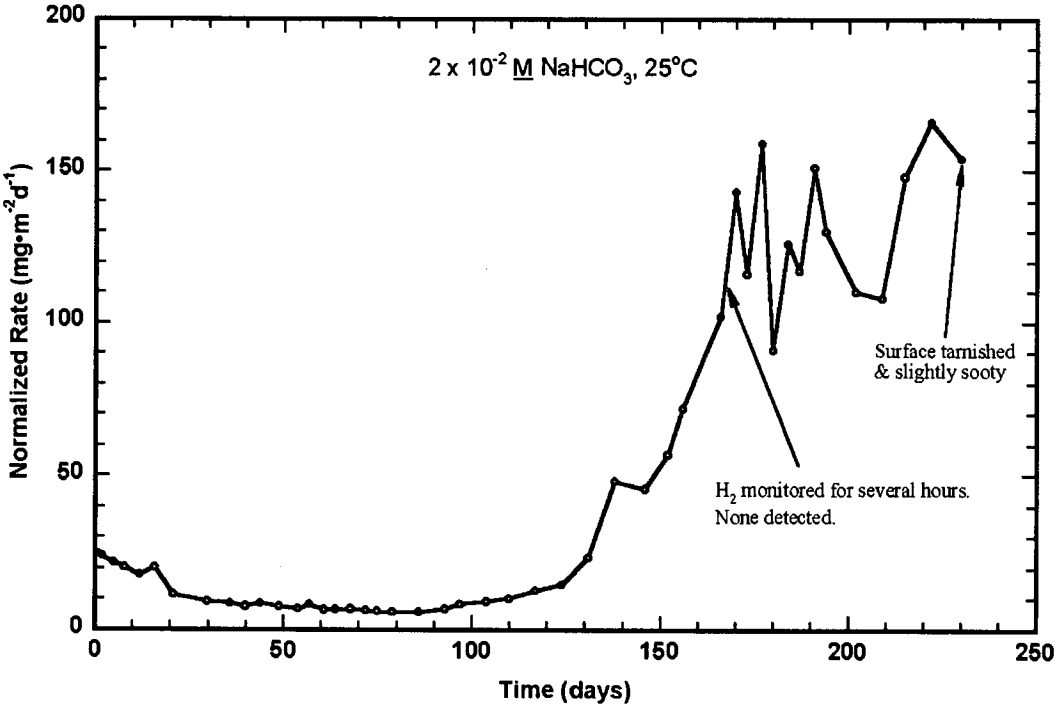

Figure 3-16. Dissolution rate of unirradiated uranium metal fuel in 0.02 M carbonate solution, pH of 8, and 25°C (test 1).

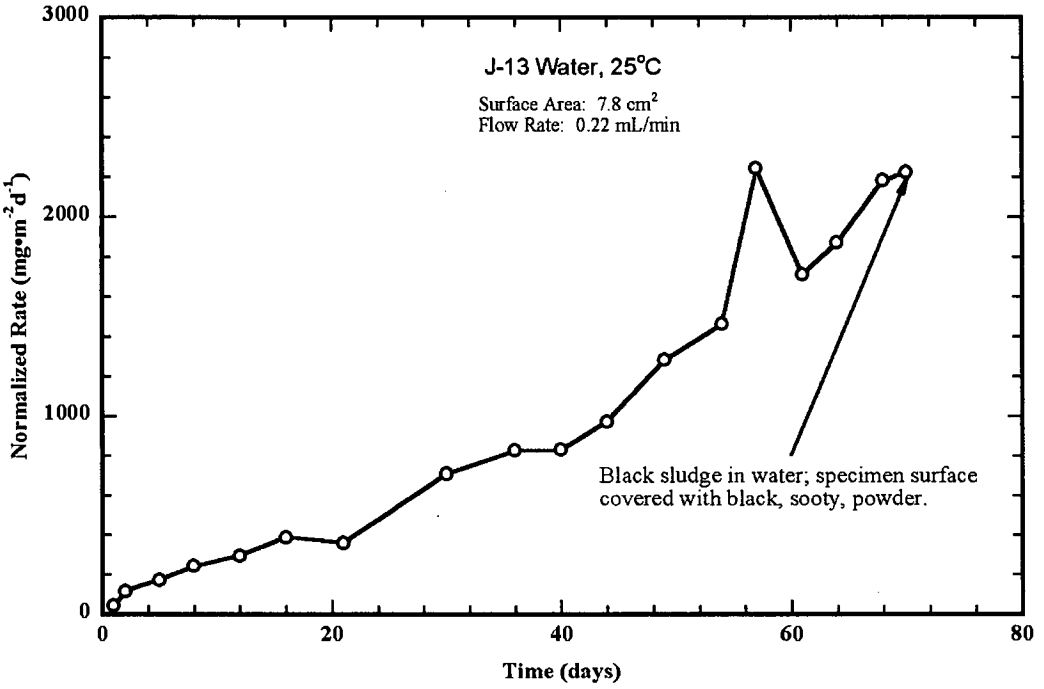

Figure 3-17. Dissolution rate of unirradiated uranium metal fuel in simulated J-13 well water at 25°C (test 9).

The nitric acid test with unirradiated fuel (Figure 3-15) shows a gentle decrease in the dissolution rate until about 125 days and then a slow increase. At about day 200, a spike was seen in the rate. This corresponds to an interruption in the test and an examination of the specimen. No corrosion products were visible. Subsequent results were more erratic and significantly higher. Similar results were seen with SNF (Figure 3-8) with respect to an initial stable period. However, this test was only run for about 110 days, and it was not interrupted. As such, no subsequent irregular period is seen. The SNF specimen also showed no signs of degradation at the end of the test. Dissolution rates were higher with the irradiated fuel, an average of about 130 mg/m^2/d compared to about 10 mg/m^2/d for the initial 200 days with unirradiated fuel.

Dissolution rates of unirradiated fuel in carbonate solution were quite stable for approximately the initial 100 days (Figure 3-16). At day 125, the rate began to rise rapidly and became very erratic. The test was terminated after 230 days, and the specimen was tarnished and showed indications of black, sooty corrosion products, possibly indicating the onset of Stage 2 corrosion. Other than a large change when the test conditions were changed from downward flow to upward flow, the carbonate test with the spent fuel (Figure 3-9) produced a fairly stable dissolution rate throughout the 130 day test. No indication of Stage 2 was seen with the irradiated samples. SNF test results indicated a much higher dissolution rate than the unirradiated fuel; an average of 155 mg/m^2/d versus 7 mg/m^2/d for unirradiated fuel in the initial stable region.

Figure 3-17 displays the dissolution rate over time of unirradiated uranium metal fuel in simulated J-13 well water. The rate increased in a near linear fashion continuously from test initiation until it was terminated at about 70 days. The final rate measured was about 2,300 mg/m^2/d; however, steady state had not been reached. Very different results were seen with irradiated SNF (Figure 3-10). Dissolution rates were very irregular and ranged as high as 8,000 mg/m^2/d and averaged about 3,000 mg/m^2/d, but no upward trends were seen. Both specimens were obviously corroded, and black corrosion products were visible, indicating Stage 2 corrosion.

A second test with unirradiated fuel in simulated J-13 water was performed with a faster flow rate (increased by a factor of six) and smaller sample size (decreased by about half). These conditions will increase the oxygen supply, which may prevent anoxic conditions. (Anoxic corrosion rates have been reported as larger than oxic corrosion rates for uranium metal (see Reference 8.) Results with the increased oxygen supply are shown in Figure 3-18. The dissolution rate was low (~3 mg/m^2/d) and fairly stable between days 10 and 25, followed by a rapid increase and then another stable but high region (~6,000 mg/m^2/d). Black corrosion products were visible at the conclusion of the test, as seen in the previous test. It appears that increasing the oxygen supply to the sample delayed the onset of Stage 2 corrosion, but did not eliminate it. One measurement of hydrogen in the off-gas was made, and the resulting dissolution rate was lower by about a factor of six than the rate calculated using uranium concentration. Anoxic corrosion is discussed in more detail in Section 3.2.4.3.

A summary of the dissolution rates measured with SNF and unirradiated uranium fuel are shown in Table 3-6. SNF had higher rates in every case. Irradiation may make the material more susceptible to degradation. However, surface preparation may also be a factor. The SNF specimens were tested in the as-cut condition, whereas the unirradiated samples were ground to a 120-grit finish. Some experiments with uranium metal have shown surface roughness influences the corrosion rate in oxygen (see Reference 8). Significant changes to the sample surface occur during the dissolution process. Increases in the roughness result in larger surface areas, which cause dissolution rate calculations to appear artificially high (see Equation (3-1)). Uranium metal SNF specimens were sectioned with either a slow-speed wafering saw or a milling machine, and thus, the original surface was relatively smooth. Figure 3-19 is a photograph of an SNF specimen after exposure to test 3A showing obvious surface roughness. Additional tests were planned to identify the cause of the increase in dissolution rate. Flow through experiments with SNF samples that are polished to a 600-grit finish were planned in the place of the galvanic tests (discussed in Section 3.2.4.2).[9] However, those experiments will not be performed due to the cancellation of the release rate test project.

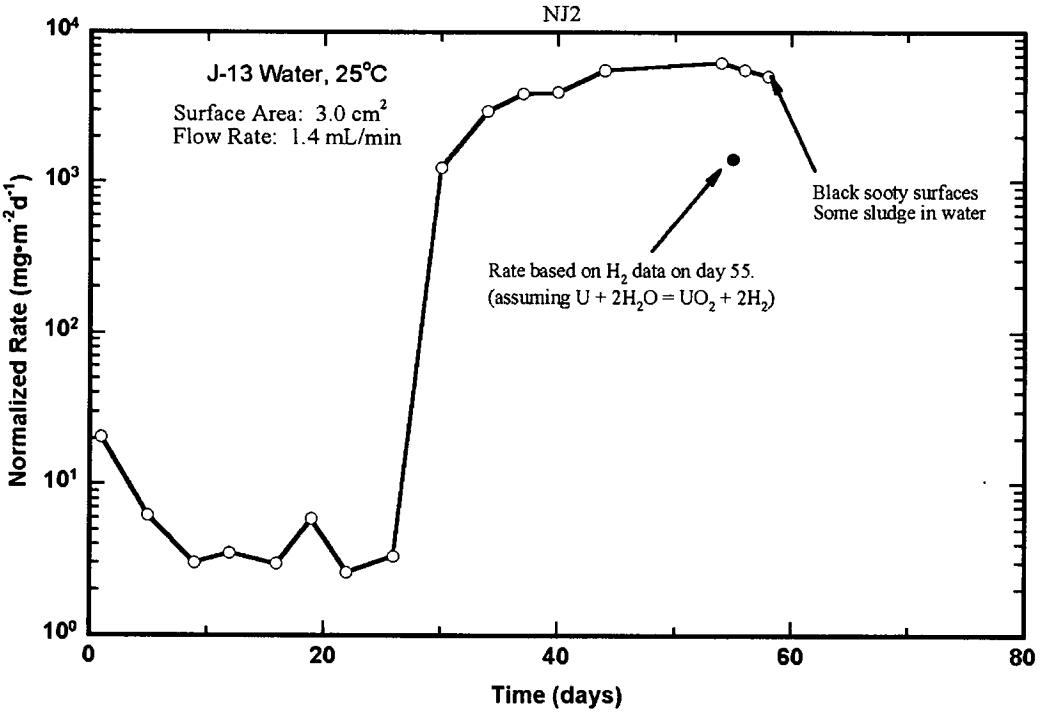

Figure 3-18. Dissolution rate of unirradiated uranium metal fuel in simulated J-13 well water at 25°C at increased flow rate.

Table 3-6. Dissolution rates of uranium metal SNF and unirradiated fuel in selected flow through tests.

Test Number	Temperature (°C)	Solution	pH	SNF ($mg/m^2/d$)	Unirradiated Fuel ($mg/m^2/d$)
1	25	0.02 M carbonate	8	155	10
8	25	0.001 M nitric acid	3	127	7
9	25	J-13	~8	~3,000	~2,300
9[a]	25	J-13	~8		4

a. Higher flow rate test, not performed with SNF.

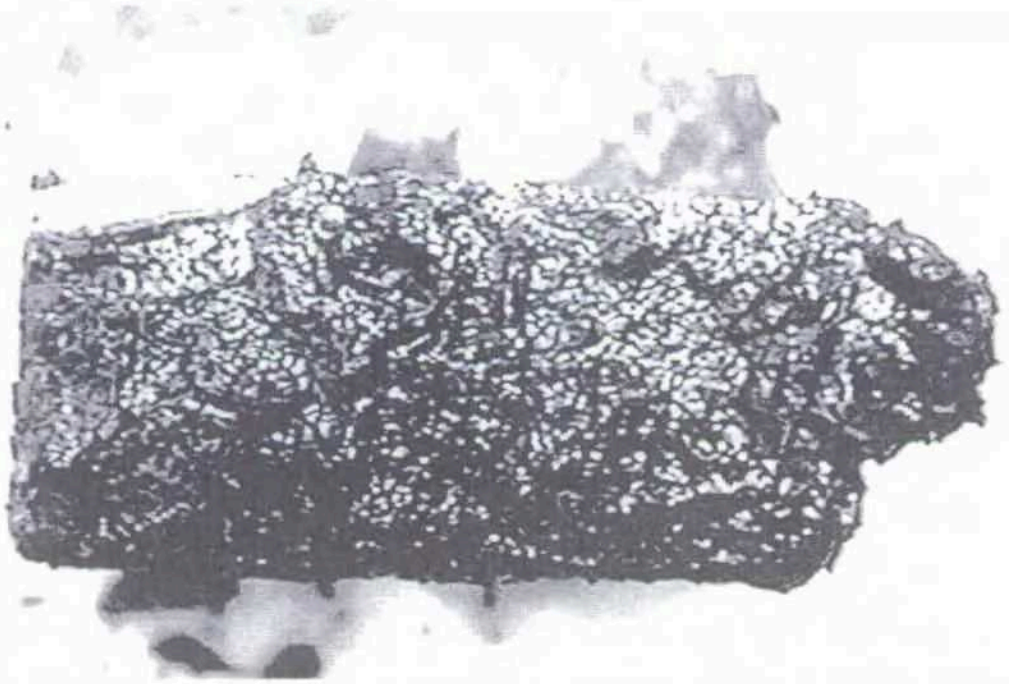

Figure 3-19. Photograph of test 3A uranium metal SNF sample after exposure to 2×10^{-4} M carbonate at a pH of 8 and 75°C showing increased roughness.

3.2.4.2 Galvanic Tests. Several experiments were planned to evaluate the potential for a mixed metal system, which could result in a galvanic condition and cause Stage 2 corrosion (see Section 3.2.1). First, an open circuit potential curve was generated for uranium metal, Type 304L stainless steel (the test cell material), and zircaloy-2 (N-reactor fuel cladding material) with respect to a calomel reference electrode. After 110 hours, the uranium had still not stabilized. A polarization resistance test with uranium in simulated J-13 well water was completed, resulting in a corrosion current density of 1×10^{-7} A/cm^2. Electrochemical tests were then performed with uranium coupled to 304L stainless steel and to Zircaloy-2. Both couples resulted in very similar current measurements, about 3×10^{-8} A/cm^2. The influence of the galvanic couple is very small compared to the uncoupled rate. In fact, 10^{-8} is near the measurement capability. Based on the electrochemical results, uranium coupled to zircaloy and stainless steel contributes a negligible amount to the dissolution rate.

In Section 3.2.4.1, flow through experiments with declad unirradiated uranium fuel were performed in electrically isolated vessels. Stage 2 corrosion was still indicated in at least the carbonate solution and simulated J-13 water. Coupled with the electrochemical results, it is clear that galvanic effects from a mixed metal system are not the cause of Stage 2 corrosion. Thus, the planned flow through tests to study galvanic couples were cancelled.

3.2.4.3 Anoxic Dissolution Tests. A second possible cause of Stage 2 corrosion is the oxygen content. Low available oxygen, creating anoxic conditions, has been reported as more aggressive to uranium metal than an oxic environment (see Reference 8). Oxic corrosion is believed to follow Equation (3-6) producing U(VI) as a dissolved ion. Anoxic corrosion, however, forms U(IV) as an oxide precipitate and hydrogen gas (Equation (3-7)). The oxidation of U(IV) in Equation (3-7) to U(VI) for dissolution is significantly influenced by the presence of oxygen in the water. Monitoring for hydrogen may provide a clue to the onset of anoxic reactions and, thus, was included in the experiments.

$$U + 3/2O_2 + H_2O \rightarrow UO_2^{+2} + 2OH^- \quad (3\text{-}6)$$

$$U + 2H_2O \rightarrow UO_2 + 2H_2 \quad (3\text{-}7)$$

Flow through tests with variable levels of oxygen were designed to compare oxic versus anoxic corrosion. A liquid/vapor separator was added to the exit stream immediately following the specimen cell (see Figure 2-1). The gas stream from the separator was fed into a gas chromatograph for hydrogen gas analysis. Unirradiated uranium metal was exposed to deionized water at 25°C with an air sparge in the feed solution. After 20 days, the feedwater sparge was changed to argon gas, removing the oxygen from the water. After about 20 more days, the sparge gas was returned to air. Uranium concentration in the exit solution and hydrogen was measured in the off-gas stream. Both measurements were used to calculate the dissolution rate. Equation (3-7) was used with the hydrogen measurements.

Results from the experiment are presented in Figure 3-20. The uranium dissolution rate in deionized water and oxic conditions is about 10 mg/m^2/d, similar to the unirradiated fuel tests with nitric acid and carbonate solution. No hydrogen was detected during this time. Once the argon sparge was initiated, the uranium-based dissolution rate began to drop and continued decreasing until the air sparge was reintroduced. However, after a short initiation period (4 days) and a large spike (to 1,600 mg/m^2/d), the hydrogen-based dissolution rate remained steady at about 300 mg/m^2/d. When the air sparge was again added to the feed, the hydrogen-based rate dropped back to zero. The uranium-based rate increased rapidly to about 100 mg/m^2/d and remained at that level until the test was terminated at 70 days. Sooty-like corrosion products were seen after the argon sparge period, but not after the air sparge sections.

These data do tend to support the theory of anoxic conditions resulting in increased uranium reaction rates. Regions where the feed solution was sparged with air produced a fairly stable concentration of uranium in solution with no hydrogen detected, comparing well with Equation (3-6). During the argon sparge period, hydrogen was produced but uranium in solution decreased to near zero, as predicted by Equation (3-7). Tests 3, 3A, and 3B had dissolution rates that dropped to zero, based on uranium concentration (see Figure 3-12). An anoxic condition similar to that seen during the argon purge may have existed with the low carbonate solution. Black, sooty-like corrosion products (U(IV) precipitate) and the detection of hydrogen agree with Equation (3-7). Several SNF and unirradiated fuel tests had visible corrosion products when the test was terminated (tests 3, 3A, 3B, 6, 9, and 10 with SNF and tests 1 and 9 with unirradiated fuel). However, only two other experiments were monitored for hydrogen in the off-gas, the carbonate test (Figure 3-16, test 1) and the second J-13 test (Figure 3-18, test 9) with unirradiated fuel. No hydrogen was detected at day 170 in Figure 3-16 although some corrosion products were seen at the end of the test on day 230. Note the dissolution rate based on uranium concentration was increasing. The simulated J-13 test with the higher flow rate shown in Figure 3-18 did

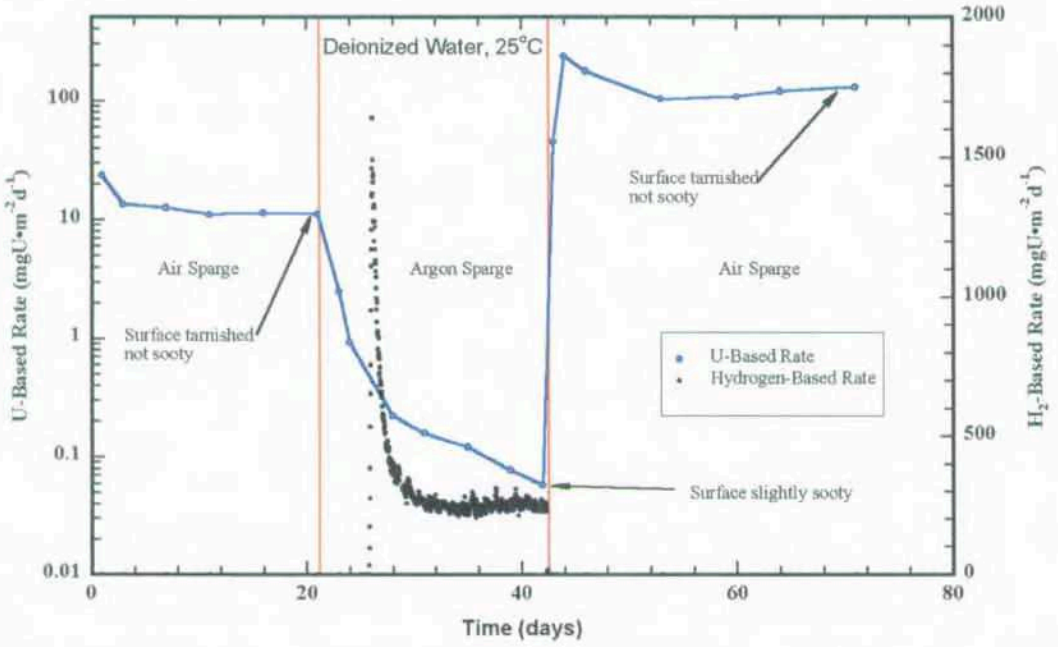

Figure 3-20. Unirradiated uranium metal dissolution test in deionized water at 25°C with air and argon gas sparge.

produce hydrogen and corrosion products were seen at the end of the test, suggesting anoxic corrosion (Equation (3-7)). However, uranium was detected in the solution. Figure 3-20 indicates that a completely oxygen free reaction would produce hydrogen, solid corrosion products, and no uranium in solution, whereas an oxygen-rich solution results in dissolved uranium oxide ion with no production of hydrogen. It appears that some oxygen was present, and both reactions are occurring simultaneously.

One additional flow through test was performed in an effort to define an oxygen limit for anoxic reactions. Unirradiated uranium metal was exposed to deionized water with an air sparge at 25°C. After 26 days, the sparge was changed to nitrogen with 2% oxygen. The results are presented in Figure 3-21. No hydrogen was detected at any time during the test, and very little change was seen in the uranium-based dissolution rate. Apparently very little oxygen is sufficient to keep the system in an oxic mode.

Anoxic corrosion may play a role in the initiation of Stage 2 corrosion with uranium metal. However, the data do not imply oxygen content is the complete explanation. It is doubtful that the experiments with SNF reached a completely oxygen free environment, and yet Stage 2 corrosion was apparent. This may be due to the complexity of oxygen affects on both the general corrosion rate and the dissolution of corrosion products. In addition, the definition of Stage 2 corrosion is rather ambiguous. It may be identified by uranium concentration dropping to zero, by sudden increases in the concentration of uranium or some other isotope (e.g., cesium), by the presence of hydrogen, or the appearance of black, sooty corrosion products. Surface area changes as the specimen degrades are another factor that affects corrosion. Dissolution rates are calculated based on an initial surface area and, thus, can appear artificially high if the surface area has increased significantly. This is particularly true if the metal is reacting incongruently, creating a rough surface. No consistency was seen between the onset of Stage 2 corrosion and controlled environmental factors such as pH, temperature, or chemistry.

The actual cause of increased degradation of uranium under some conditions is probably a combination of a number of factors. Equations (3-6) and (3-7) are competing with each other with varying

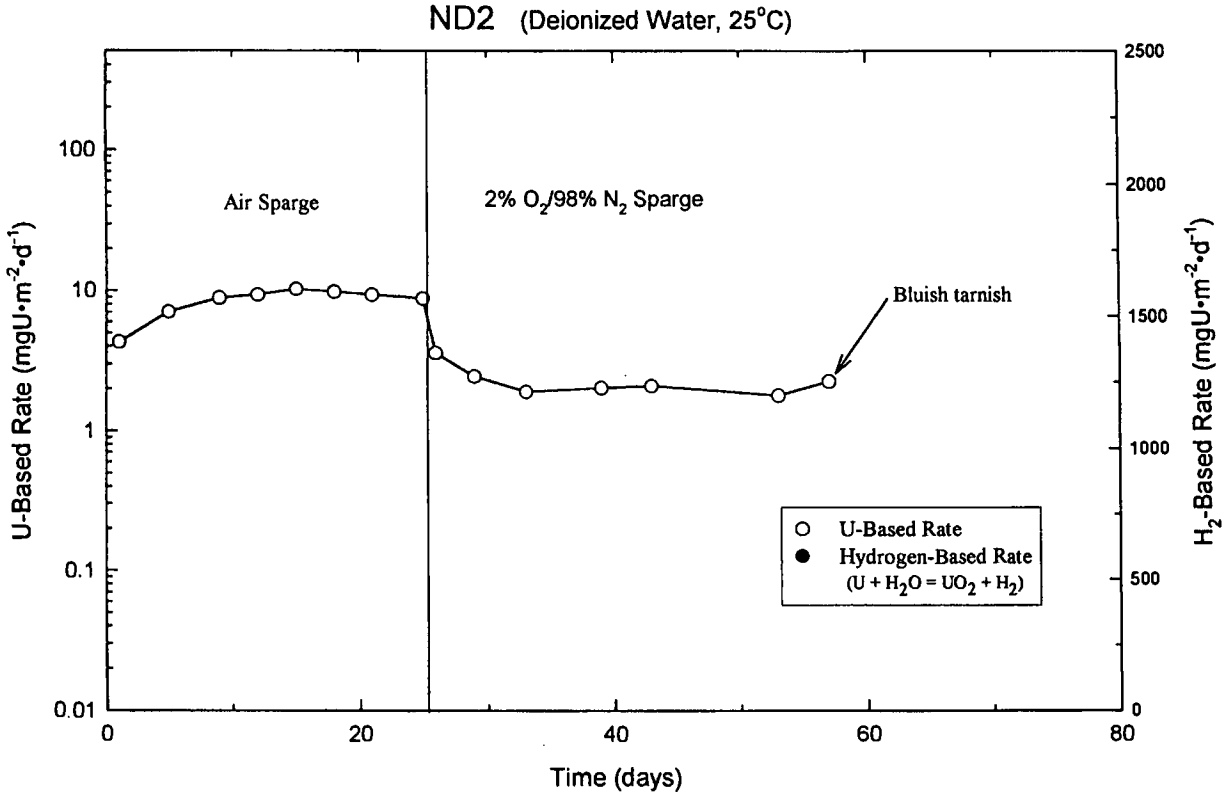

Figure 3-21. Unirradiated uranium metal dissolution test in deionized water at 25°C with air and nitrogen/2% oxygen sparge.

degrees of dominance. Initially, oxygen should readily react with the uranium surface, thus reaction 3-6 is dominant. As the sample begins to degrade, an oxide layer covers the surface and acts as a barrier to further oxidation. Eventually diffusion through the oxide layer becomes the limiting factor. It has been reported that the uranium oxide layer is a good ion and semiconductor with a structure that OH ions can readily move through but oxygen ions cannot.[10] Thus, the faster water reaction defined in Equation (3-7) becomes dominant after some indeterminate period of time.

3.2.5 Flow Through Test Conclusions

Flow through tests were performed with uranium metal SNF and unirradiated fuel in a variety of conditions. Dissolution rates with uranium metal fuel were higher than those found with commercial UO_2 fuel in every comparison. Simulated J-13 well water appears to be more aggressive than the nitric acid and most of the carbonate tests. Low carbonate concentration (0.01 M) tests at the higher temperature produced elevated dissolution rates (tests 3, 3A, and 3B).

Two stages of reaction were visible on graphs of dissolution rate versus time, Stage 1 and Stage 2 corrosion. Stage 1 was defined as relatively stable dissolution rates based on uranium concentration in the effluent, isotopic rates similar to uranium, and no visible corrosion products. In contrast, Stage 2 corrosion produced black, sooty corrosion products. Uranium concentration in the effluent dropped to zero whereas the cesium concentration began to increase rapidly. Galvanic interactions from the mixed metal system were ruled out as a possible cause of Stage 2 corrosion, because isolation did not prevent the Stage 2 corrosion indicators, and the electrochemical tests indicated very little influence when uranium was coupled with zircaloy or stainless steel. Anoxic conditions may have influenced the dissolution;

monitoring of hydrogen production lends support to this theory in some circumstances. Increasing the flow rate and decreasing the sample size reduced the effect of low oxygen. Sample preparation may also have contributed to the dissolution rate variations.

3.3 Unsaturated Drip Tests

Unsaturated drip tests are long-term experiments that simulate the expected repository environment. Small amounts of groundwater are dripped onto a fuel sample, which sits on a mesh that allows the solution to pass through. Thus, fuel is exposed to intermittent solution and moist air. Liquid and solids analyses provide data on release rates of selected radionuclides and their physical and chemical form, dissolution rates of the fuel matrix, paragenesis of alteration products, and the changing solution chemistry.[11] The experimental setup and method are described in Section 2.2.3. Initial tests with unirradiated uranium metal fuel resulted in solution backing up on the fuel holder (discussed in Section 3.3.2). Reacted material was generated and dispersed throughout the test cell so quickly that the mesh openings were plugged, allowing little solution to pass through. Thus, an improved design was developed which includes a three-stage fuel holder with successively smaller openings, as displayed in Figure 2-2. Subsequent tests verified this configuration prevents buildup of solution on the top stage, where the fuel sample sits.

3.3.1 Test Matrix and Sample Preparation

Unsaturated drip tests were completed with unirradiated uranium metal fuel and were initiated with irradiated SNF. Experiments with irradiated fuel were interrupted early (after about 1 year of exposure) due to the premature termination of the release rate project. All samples were exposed to EJ-13 (see Section 2.3 for composition) well water at 90°C. Two sets of experiments with the unirradiated fuel were performed at the high drip rate (injection of 0.75 mL solution every 3.5 days). Five experiments were planned with the SNF, two at the high drip rate, one at a low drip rate (0.075 mL injected every 3.5 days), one vapor test, and one control test. In the vapor test, water is added to the base of the test vessel but no injections of additional solution are made. Thus, the fuel is exposed to a water saturated air environment. Injections at the high drip rate are performed in the control test, but no fuel sample is added. Any solution contamination or vessel degradation products dissolving into solution will be identified in the control test. The test matrix is shown in Table 3-7 (see Reference 11).

Table 3-7. Test matrix for unsaturated drip tests with uranium metal fuel.

Test ID	Fuel Sample	Drip Rate	Solution	Temperature
UNNR1	Unirradiated	High	EJ-13	90°C
UNNR2	Unirradiated	High	EJ-13	90°C
UUT1	SNF	High	EJ-13	90°C
UUT2	SNF	High	EJ-13	90°C
—[a]	SNF	Low	EJ-13	90°C
—[a]	SNF	Vapor	EJ-13	90°C
Control	None	High	EJ-13	90°C

a. These tests have not been initiated.

Fuel samples were tested as a single monolith rather than the originally planned fragments because uranium reacts so quickly in water. Specimen preparation consisted of sectioning approximately1-gram samples with the cladding removed and polishing the exposed surfaces to a 600-grit finish. SNF samples were taken from element #4378 as discussed in Section 3.1. Efforts were made to select sections without significant cracking (see Reference 11).

Interim test analyses were performed on both the solution and the solids. Solution analyses included uranium and isotopic content, pH, ionic composition, and colloid determination. Solid corrosion products were analyzed using XRD, scanning electron microscopy (SEM), and TEM. Compositional changes in the test cell atmosphere were also monitored periodically (see Reference 11).

3.3.2 Unirradiated Fuel Tests

Experiments with unirradiated uranium metal fuel were performed prior to using SNF to evaluate the method and equipment applicability to this fuel type and to estimate test parameters. The first test was performed in the one stage test vessel described in Section 2.2.3. Initial injections of EJ-13 contacted the fuel and then rapidly drained through the 10-μm holes in the fuel holder mesh. However, excessive corrosion products plugged the holes causing the liquid to drain very slowly and accumulate in the holder, resulting in a pseudo-batch test. A subsequent test with unirradiated fuel was performed with a modified test assembly, which had three stages of different mesh size openings (see Section 2.2.3 and Figure 2-2). The fuel was placed on the top stage with the largest sized mesh. No fluid accumulated with this test configuration, and thus, it is being used in the irradiated fuel tests. Both experiments were performed at 90°C and included 0.75 mL injections of EJ-13 every 3.5 days (high drip rate).

3.3.2.1 Pseudo-Batch Test Results. Two monolithic specimens totaling about 1 gram were used in the initial unirradiated uranium fuel drip test. Corrosion was visible on the samples within 4 days, which included only one liquid injection. After 12 days of exposure, the reaction products had formed a sludge of sufficient volume to clog the 10-μm holes. Solution then accumulated on the sample holder resulting in a pseudo-batch condition rather than the desired unsaturated environment. The test was allowed to continue for 90 days, while periodically monitoring the sample weight, visual changes, solution pH, and composition of liquid and solids.

The tests were interrupted after 4, 12, 24, 33, 48, and 90 days and solid and liquid samples were removed for analysis. Oxidation of the fuel began immediately, as indicated by the visual appearance of degradation after only 4 days. Figure 3-22 shows the coupons at the end of the 90-day test. Weight changes (without cleaning) were recorded at three sample intervals. At 4 days, the coupons had a weight increase of 2%, but by day 48 they showed a loss of 21% and by 90 days they were at 55% of the original weight. Approximately half of the original samples had reacted and spalled off during this experiment.[12]

Corrosion products appeared primarily as a fine, black sludge (similar to what was seen in the flow through tests, Section 3.2). At day 24, XRD analyses indicated the sludge was primarily UO_2 with minor amounts of U_4O_9. By day 33, most of the material had oxidized to U_4O_9. Based on the diffracting units, the particle size is estimated as 10 to 20 nm. When the vessel was opened after 90 days, the finely divided black corrosion products were throughout the inside of the fuel sample holder, including the walls and the top. Figure 3-23 shows the holder and a portion of the accumulated corrosion products after the test was concluded (the gray and yellow mineral forms are evidence of the mixed uranium oxide phases produced). It appears the spalled corrosion products exhibit characteristics of hydrophobic films, moving with and aggregating at the leading edge of the solution.[13]

Solution samples were taken from the leachate collected in the bottom of the test vessel (Figure 2-2) and the liquid accumulated in the fuel holder cup. Table 3-8 shows the pH measurement of the samples. By the first sample at 4 days, the pH had begun to decrease in the leachate from the original

Figure 3-22. Unirradiated uranium metal fuel coupons after 90 days (UNNR1) in pseudo-batch test conditions.

Figure 3-23. Corrosion products from the pseudo-batch test with unirradiated uranium metal fuel after 90 days (UNNR1).

Table 3-8. Solution analyses from pseudo-batch tests with unirradiated uranium metal fuel (UNNR1).

Sample Day	pH in Leachate	pH in Cup
0	8.15	—
4	7.85	—
12	7.35	6.83
24	7.10	5.91
33	7.54	—
48	7.08	7.10
90	9.02	—

8.15. The pH remained down through the 48-day sample, but had increased to about 9 by the end of the test. The pH of the solution in the cup holder was generally less than what was found in the leachate, though it began to increase by day 48. A change in reaction mechanism may account for the abrupt increase in pH occurring somewhere between day 48 and 90 (see Reference 12).

Uranium content in the various samples was determined to find the distribution between phases. Release rates were then calculated based on the original geometric surface area of the coupons and the time of sampling. Table 3-9 shows the distribution between the different release paths. The dissolved fraction includes both solutes and any colloids present in the leachate samples. Test vessels were hot acid stripped at each sampling to remove any adsorbed material. Analysis of the resulting liquid includes solutes, colloids, and precipitates. Uranium in the solids was determined by weight changes of the coupon. As expected, most of the uranium is maintained in the solid corrosion products. However, a significant amount was adsorbed to the vessel walls and the amount appears to be increasing toward the end of the test. This phenomenon may be related to the increasing pH and the proposed change in reaction mechanism. It is possible much of the adsorbed material is colloid sized (the XRD indicated 10 to 20 nm particles in the corrosion products); this issue is addressed in Section 3.5.[14]

3.3.2.2 Unsaturated Test Results. A second drip test was initiated with unirradiated uranium metal fuel in a redesigned test vessel. The new fuel holder has three stages, each with successively smaller openings in the bottom to allow the liquid to drip through. One monolithic sample was placed on the top stage, which has 0.6-mm holes in the bottom gold mesh. The next stage has a gold mesh with 250-μm holes, and the bottom stage has a zircaloy-4 bottom with 10-μm laser-drilled holes. This arrangement ensures the sample is in the path of the injected water but not sitting in pooled liquid; hence the test conditions remain unsaturated. Analyses of the liquid and solids were similar to those in the pseudo-batch test, with the exception that sampling of the chamber vapors was included (see Reference 13).

Samples were removed from the test after 12, 28, 48, and 77 days. Reactions were again very quick, but no liquid pooled on the top stage. By day 77, the entire coupon had reacted. Weight changes were monitored and recorded as the fraction of weight loss. Figure 3-24 shows the fractional loss with respect to time for this test (UNNR2) compared to the loss in the pseudo-batch test (UNNR1). The loss per time increased at a relatively constant rate in test UNNR1; however, there was a marked jump between 50 and 80 days in test UNNR2. This could correspond to transition between reaction mechanisms, as proposed in the previous test based on pH and adsorbed uranium rates. Overall, unsaturated conditions caused the entire sample to react in less than 80 days, whereas the pseudo-batch tests resulted in about half of the sample reacting in 90 days. Based solely on these data, intermittent

Table 3-9. Uranium release rates from pseudo-batch tests with unirradiated uranium metal fuel (UNNR1).

Sample Day	Dissolved ($mg/m^2/d$)	Adsorbed ($mg/m^2/d$)	Solids ($mg/m^2/d$)
4	0.2	2.1	—
12	0.2	9.3	—
24	0.1	5.5	—
33	0.1	5.6	—
48	0.1	19.6	32,565
90	0.8	48.0	44,422

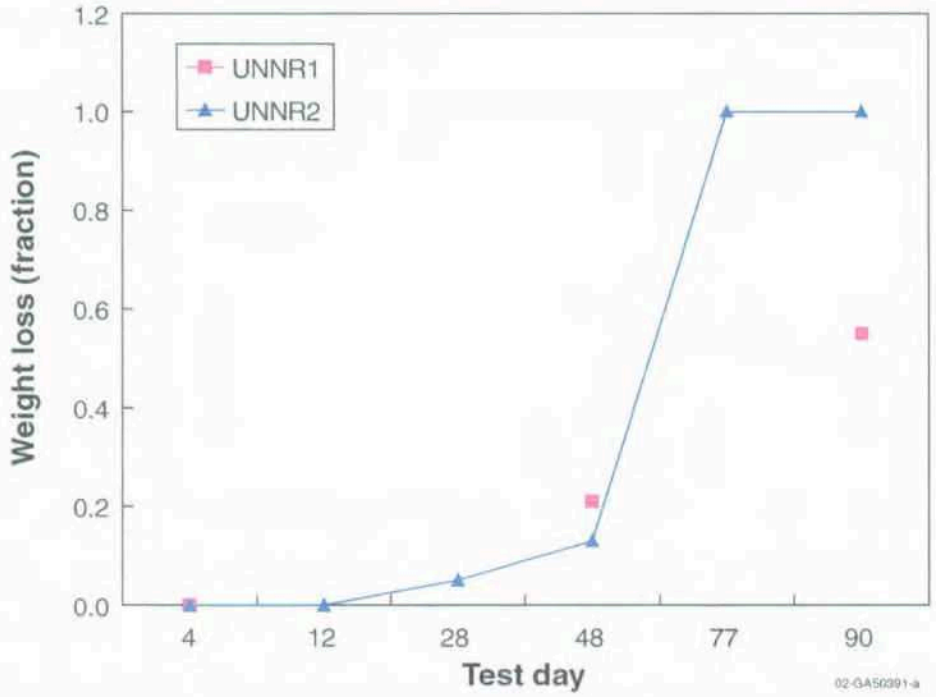

Figure 3-24. Fractional weight loss of unirradiated uranium metal fuel in pseudo-batch and unsaturated conditions (UNNR1 and UNNR2).

wetting and moist vapor conditions result in higher corrosion rates than immersing the sample in liquid (see References 12 and 14).

Samples of the corrosion products were removed and analyzed using XRD. Figure 3-25 shows the sample after 48 days of exposure. The black reaction products are uraninite (UO_2) and the yellow particles are schoepite ($UO_3 \bullet 2H_2O$) crystals. Further analysis of a crystal using SEM is shown in Figure 3-26, displaying the pseudo-hexagonal growth. After 77 days, the entire coupon had reacted to form a sludge composed of a combination of uranium oxides, oxyhydroxides, and possibly hydride, similar to the results seen in the pseudo-batch test (see Figure 3-27). However, uraninite was still the predominant species at the end of the test. Based on TEM analysis, the particle size is about 10 nm (see Reference 14).

Figure 3-25. Unirradiated uranium fuel sample after 48 days in unsaturated conditions showing uraninite and yellow schoepite crystals (UNNR2).

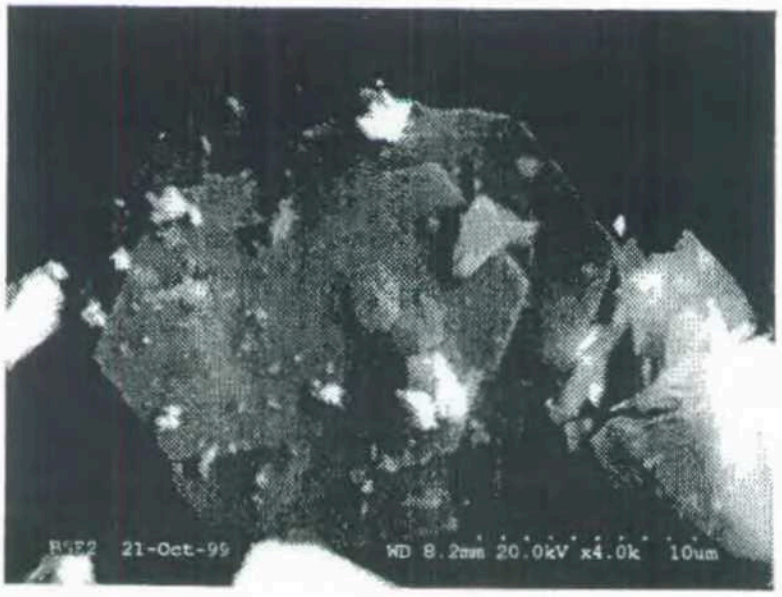

Figure 3-26. Scanning electron microscopy photomicrograph of schoepite crystal from Figure 3-25 displaying pseudo-hexagonal growth (UNNR2).

Figure 3-27. Sludge remaining after complete oxidation of an unirradiated uranium fuel sample after 77 days in unsaturated conditions.

Although solution did not accumulate in the top stage where the fuel sample was located, liquid did collect in the bottom stage (cup) with the 10-μm holes. As seen in the pseudo-batch test, corrosion products spalled from the coupon collected on this stage, plugging the holes, and thus the solution accumulated. Samples of the cup liquid as well as the leachate from the bottom of the test vessel were analyzed periodically during the experiment. Decreases in pH were seen in the cup and some of the leachate samples, but not as pronounced as in the earlier test. Final leachate pH was 9 in both experiments. Figure 3-28 shows a comparison of the pH evolution for both unirradiated fuel tests (see Reference 14).

Release rates of uranium were calculated for the dissolved, adsorbed, and solid fractions at four sample intervals. Most of the uranium was associated with solids, and the adsorbed fraction was greater than the amount dissolved. Any colloid sized particles would be included in the dissolved fraction. Larger values are seen in each fraction and at all time intervals than was seen in the pseudo-batch test results. In both tests, an increase in the adsorbed fraction was seen in the 48-day sample. As stated earlier, this may be an indication of a change in mechanism. A visual comparison of the distribution of release rates in dissolved, adsorbed, and solid fractions from the two tests is seen in Figure 3-29.[15]

Gas sampling capabilities were included for the upper chamber in the new drip test vessel design (see Figure 2-2). Samples were taken periodically and analyzed for hydrogen, nitrogen, oxygen, argon, and carbon dioxide. Figure 3-30 shows the results. Hydrogen increased during the first 12 days of the test indicating an emphasis on the anoxic reaction (Equation (3-7)) mechanism. However, the levels decreased in subsequent samples and were below detection limits at day 67 (when the sample had completely reacted). Oxygen increased at a fairly steady rate through day 48, but then also dropped to near zero on day 67. Nitrogen decreased slightly until the last sample; then it measured over 99% of the gas volume. Carbon dioxide concentration decreased at each sampling except one (43 days) and was below detection limits at test termination. Argon had a fairly stable concentration at about 0.9% until day 67, when it dropped to near zero. Gases were either generated or consumed during the active degradation of uranium metal. Sometime between the last two samples, 48 and 67 days, the coupon had completely reacted and the gas composition became almost entirely nitrogen (see Reference 14).

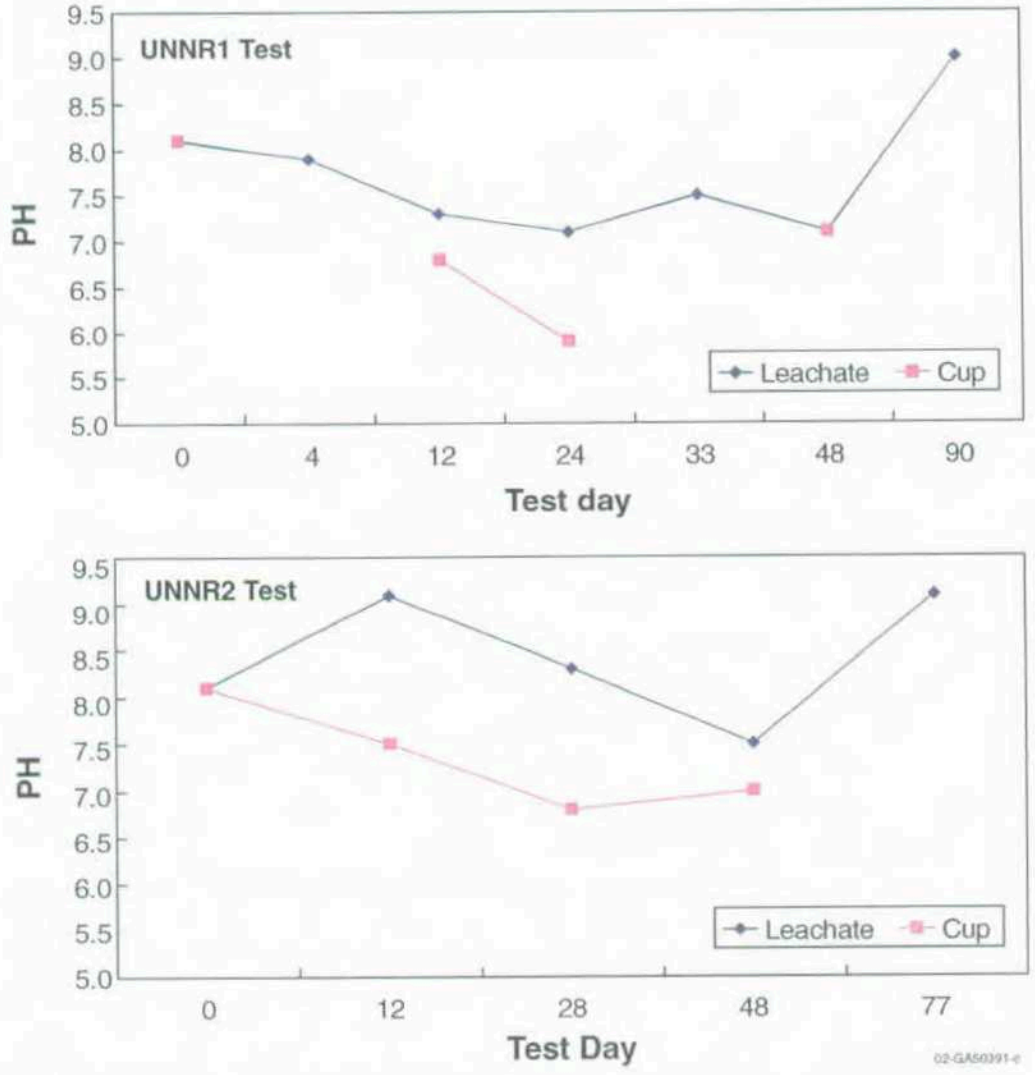

Figure 3-28. Leachate and collection cup solution pH in the unirradiated uranium metal fuel drip tests.

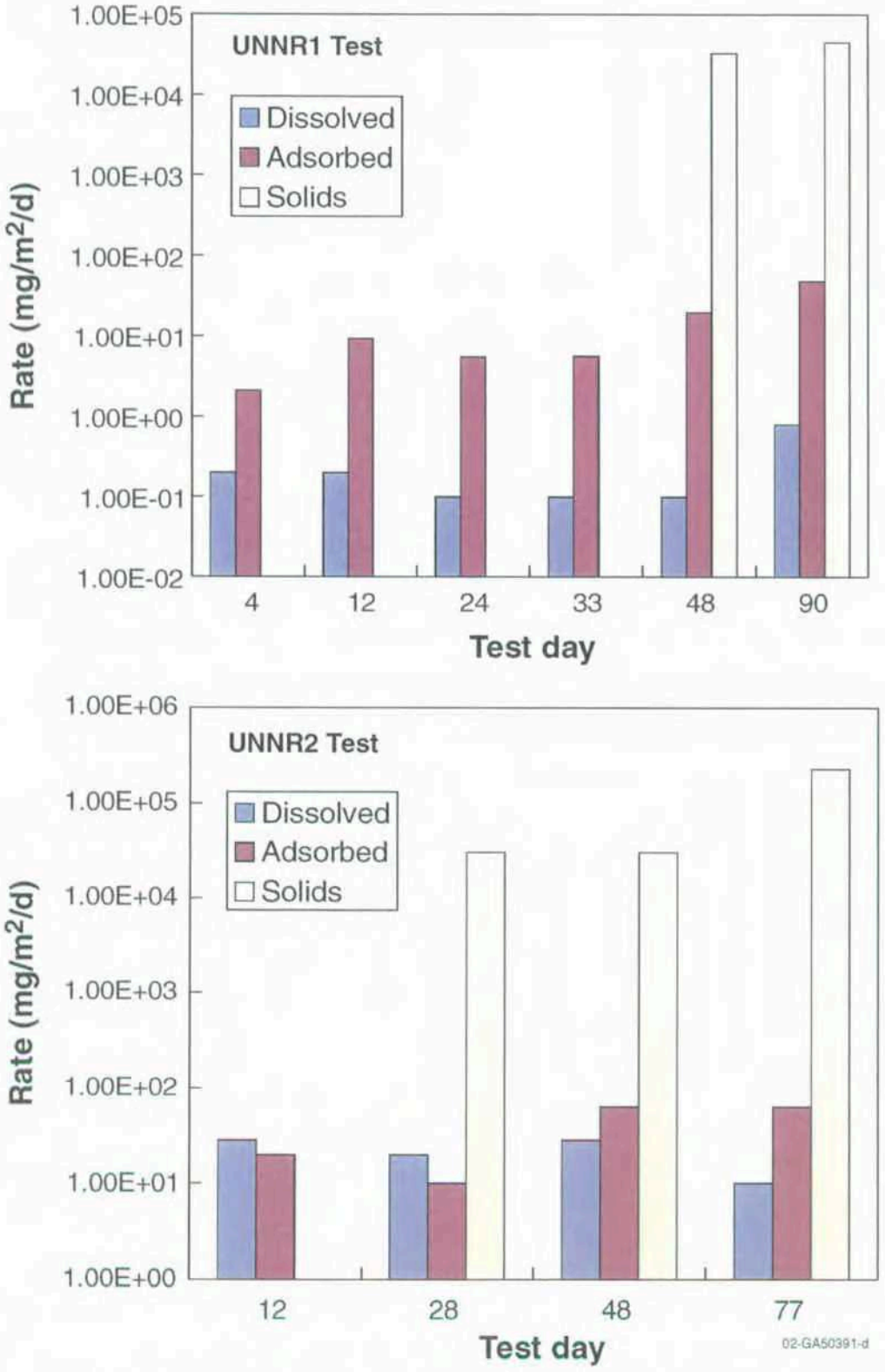

Figure 3-29. Uranium release rates from the unirradiated uranium metal fuel drip tests (UNNR1 and UNNR2).

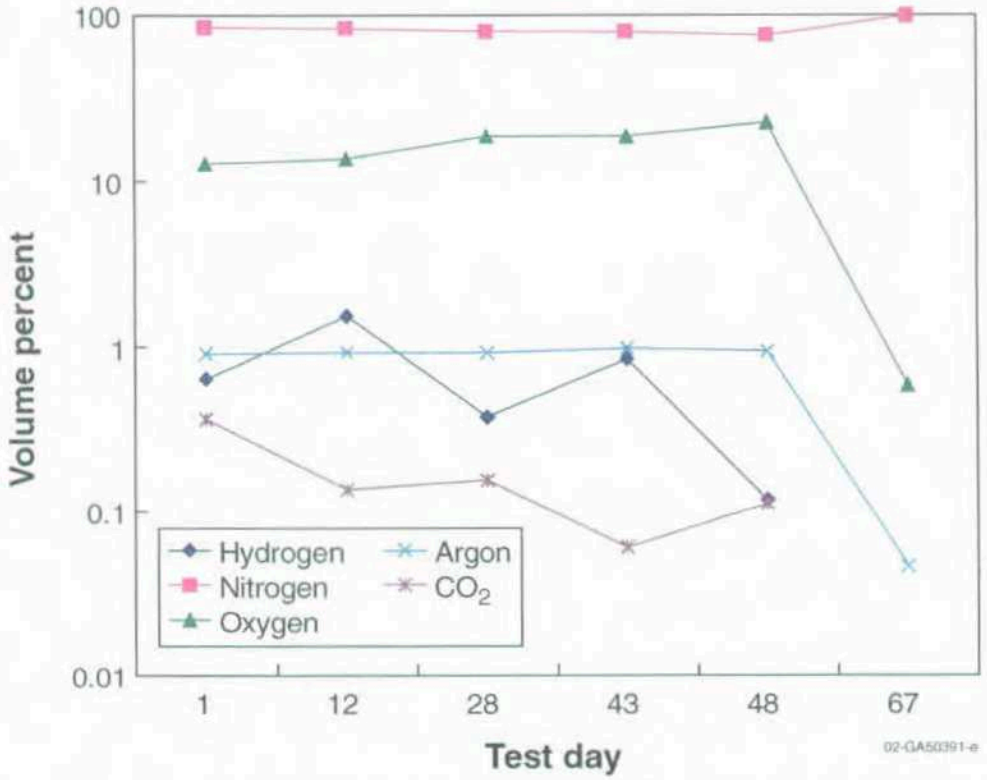

Figure 3-30. Gas analyses from the unirradiated uranium metal unsaturated drip test (UNNR2).

The second test with unirradiated uranium metal fuel with unsaturated drip conditions was a success. Solution did not accumulate where the sample was located, and thus, true unsaturated conditions were achieved. Confirmation of the rapid corrosion of uranium was seen, and a reasonable sampling schedule was defined for the irradiated fuel. Gas sampling was included in the new vessel design, and was shown to be effective. Therefore, the unsaturated drip tests with irradiated N-reactor fuel were initiated.

3.3.3 Irradiated SNF Test Results

Two tests with irradiated N-reactor fuel were evaluated in the high drip rate (0.75 mL/3.5 days) unsaturated tests. Sample selection and preparation are described in Section 3.3.1. Approximately one 0.5-g section of declad and polished SNF was placed in the top stage of each newly designed vessel. Pressure monitoring and head space gas sampling were available during the tests. As seen in previous experiments, the uranium reacted very quickly to form oxides. Uranium oxides have a larger specific volume than uranium (by a factor of two or more), and thus the alteration layer is highly strained and prone to mechanical spalling. Samples of these spalled corrosion products and the leachate were removed periodically for analysis to monitor the alteration of the fuel.[16]

Significant corrosion was visible on the fuel sample after only 7 days, and the material had completely reacted by 4 months. Figure 3-31 shows the early progression of the reacting surface. Corrosion products appeared primarily as a black sludge with some yellow particles. XRD analyses after about 1-month exposure revealed the sludge to be a very fine grained UO_2 with an estimated particle size of 10 nm. The yellow particles were metaschoepite. After about 4 months, the finely divided material began to agglomerate. Some of the reaction products were seen on the sides of the vessel by 7 months, though no flooding of the chamber was indicated. Additional XRD analyses after 8.5 months indicated the reaction products were a conglomeration of uranium oxyhydroxides, predominantly U_4O_9. The

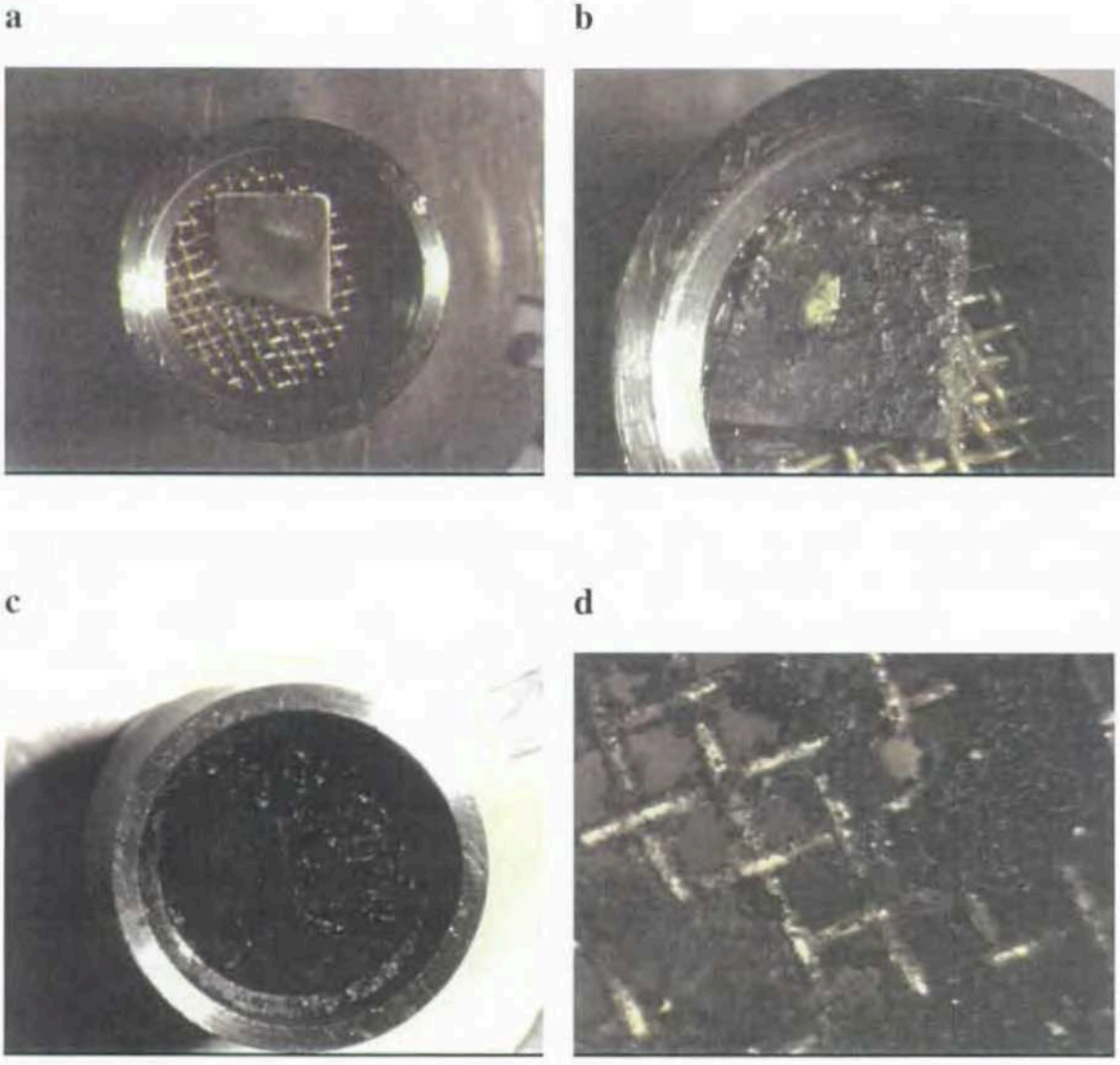

Figure 3-31. Progression of irradiated N-reactor fuel corrosion in an unsaturated drip test.

material is continuing to react to form higher oxides with additional exposure, similar to the behavior of oxide fuels, but with a larger effective surface area. Agglomeration of the finely divided material into larger particles, potentially becoming a solid mass, is also increasing over time.[17,18]

Uranium and plutonium distribution by size fraction in the leachate samples was measured using sequential filtration and ICP-MS. Filtration fractions included dissolved (<30 kD), <0.22 µm, and <0.45 µm. The particles identified in the <0.45 µm size fraction were considered colloidal. An analysis of the unfiltered solution was also performed for total release into solution. Samples were taken and analyzed after 7 days, 28 days, 8.5 months, and 11 months (see References 17 and 18).

Uranium was released in the leachate primarily as particulate material (>0.45 µm), initially at about 50% and increasing over time to 90% at 11 months. The dissolved fraction was fairly consistent in three of the four sample intervals, ranging from 10 to 15%. Only in the 1-month sample did the dissolved uranium concentration increase to about 35%. Initially, in the 7-day sample, 40% of the uranium was

associated with colloids. However, this value dropped to 10% after 1 month and then to zero in the 8.5 and 11-month samples. It does not appear that uranium colloids will be an issue under repository conditions. Table 3-10 shows the size distribution for each sampling interval. The increasing particulate fraction and decreasing colloidal portion may indicate agglomeration of smaller particles to form larger groupings (see References 17 and 18).

Similar trends were found in the plutonium distribution results. About 75% of the released plutonium after 7 days was associated with colloids. The amount dropped to 50% by 28 days and to 2% at the 8.5 and 11-month samplings. Plutonium dissolved in the leachate also decreased from 15%, to 5%, and finally to 2% in the 8.5 and 11-month samples. As reaction time continued, the particulate fraction above 0.45 μm increased from 10% at 7 days to 90% at 8.5 and 11 months. These data are presented in Table 3-11. As seen in the uranium analyses, smaller particles are decreasing in concentration and larger particles are increasing, suggesting agglomeration. In both cases the dissolved fraction is also decreasing to some degree, which may indicate attachment of plutonium and uranium ions to the particulate surface (see References 17 and 18).

Neptunium content was evaluated in the last two samples. At 8.5 months, 100% was dissolved in the leachate. However, at 11 months, only 70% was dissolved, and 30% was found in the particulate (>0.45 μm) fraction. Essentially no colloids of neptunium were present in either sample. Total release concentration decreased between the two samples from about 6 to 2 ppb. Neptunium may also be incorporated into the growing particulate mass or may be retained in the solid alteration products (see Reference 18).

Additional analyses were performed on the colloids found during the sequential filtration using SEM, TEM, and DLS. Two types of uranium-bearing colloids were identified. Small (~10 nm) spheres of uranium oxide particles were found after 1 month (see Figure 3-32), which were later incorporated in larger smectite clay colloids. Needle-like colloids of uranyl silicate were also identified. Both colloid types were seen in the unirradiated uranium metal fuel unsaturated drip tests as seen in Figure 3-33. DLS of samples from 7 days, 26 days, and 86 days revealed data supporting growth of small colloids. At 7 days, one peak was seen at about 200 nm. Only one peak was seen at 26 days also, though it was much broader (indicating a wider distribution) and centered at about 100 nm. However, by 86 days two peaks

Table 3-10. Uranium release by size from unsaturated drip tests with N-reactor SNF.

	Dissolved	Colloidal	Particulate (>0.45 μm)
7 Days	15%	40%	45%
28 Days	35%	10%	55%
8.5 Months	15%	0%	85%
11 Months	10%	0%	90%

Table 3-11. Plutonium release by size from unsaturated drip tests with N-reactor SNF.

	Dissolved	Colloidal	Particulate (>0.45 μm)
7 days	15%	75%	10%
28 days	5%	50%	45%
8.5 months	2%	8%	90%
11 months	2%	8%	90%

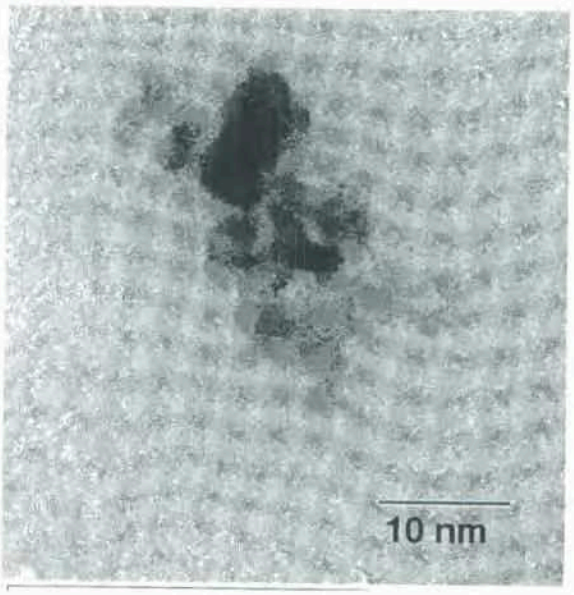

Figure 3-32. Uranium oxide spheres from N-reactor fuel after 1 month in an unsaturated drip test.

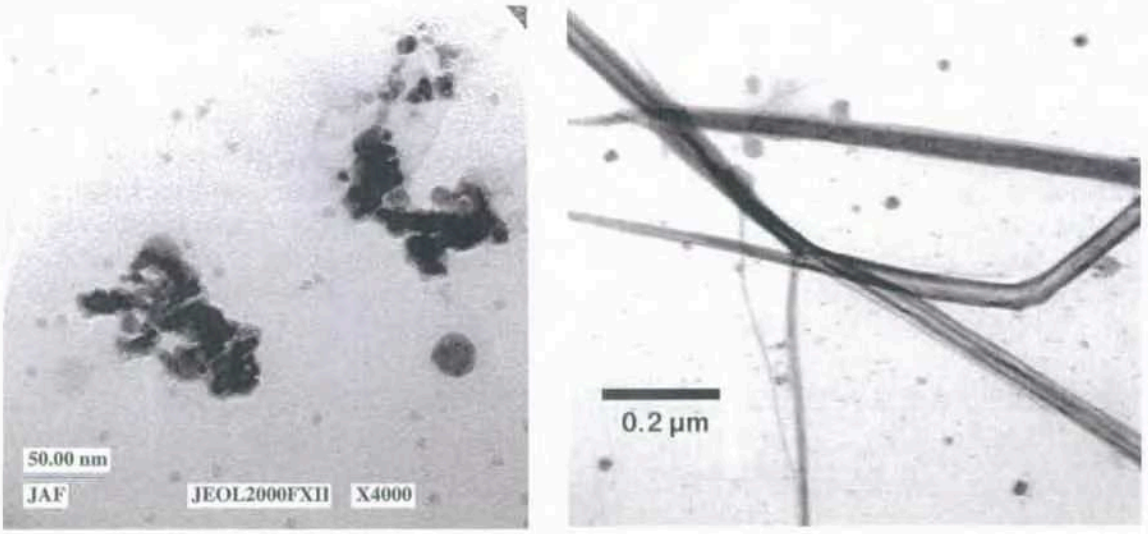

Uranium Oxide Uranium Silicate

Figure 3-33. Uranium oxide and uranium silicate colloids from unirradiated fuel tests in an unsaturated drip test.

were clearly seen, one broad peak at 5 nm and one sharper peak at 100 nm. These later results support the TEM data fairly well; small, spherical UO_2 colloids are incorporated into larger smectite clay colloids. The acicular uranyl silicate colloids are also found in the clay material. Samples from the unirradiated drip test that had been stored for about 1 year were evaluated again using DLS. The results were essentially the same, indicating that the colloids are stable under ambient conditions (see Figure 3-34) (see References 16 and 17).

3.3.4 Unsaturated Drip Test Conclusions

Unsaturated drip tests with unirradiated and irradiated N-reactor fuel showed uranium reacts very quickly in a water environment. Up to a gram of material can completely oxidize within a few months. Copious amounts of finely divided, black reaction products were produced, with occasional yellow particles. However, the corrosion products were not stable and continued to react to higher oxidation states. Initially, UO_2 was the predominant alteration phase, but after about 1 year, a collection of uranium oxyhydroxides had appeared with significant amounts of metaschoepite and U_4O_9. It is likely that over time the uranium will completely oxidize to UO_3, similar to the reaction sequence of commercial UO_2 fuels (although with a larger effective surface area) (see References 16 and 17).

Uranium is initially released into the leachate as nearly half colloids and half larger particles (>0.45 μm), with a small amount of dissolved material. By about 1 year, 90% of the uranium is larger particles with no colloids, but the dissolved fraction remains the same. Similar trends were found with the plutonium. Initially 75% was released as colloids and only 10% appeared as larger particles. After a year of exposure, the colloid fraction dropped to less than 10% and the particulate fraction increased to 90%. Unlike the uranium, the dissolved plutonium decreased to only 2% over the first year. Neptunium, however, was released almost entirely as dissolved material with about 30% in larger particles after 1 year and none associated with colloids. Although colloids may be an issue in the initial degradation stages, based on these tests, it should not pose a long-term concern (see References 17 and 18).

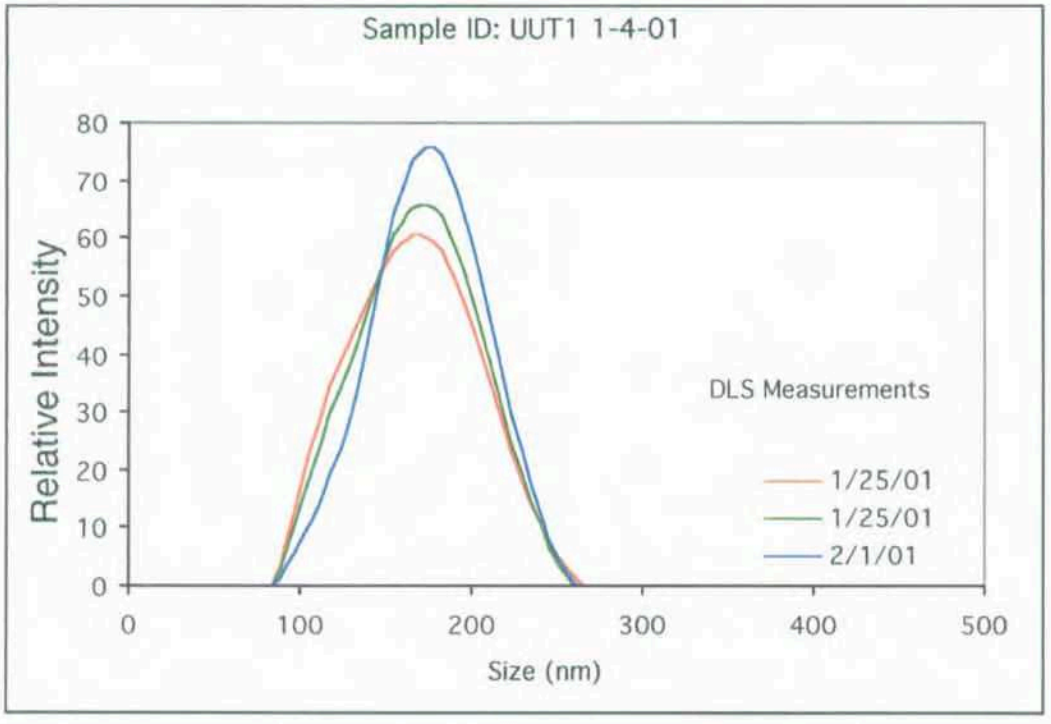

Figure 3-34. Dynamic light scattering results from an unirradiated uranium metal drip test before and after 1 year of storage.

TEM/SEM analyses of the colloids in the leachate formed during fuel degradation revealed two structures: small uranium oxide particles that were incorporated into a smectite clay colloid and acicular uranium silicate colloids. DLS analyses also revealed two size distributions, which may correspond to the UO_2 particles and the larger clay colloids. These results correlate well with the uranium and plutonium distribution results. Small particles of material, uranium oxide colloids, are released into the leachate during the fuel degradation process. Some uranium reacts with silicate in the EJ-13 water, forming the uranium silicate colloids. Clay colloids are present in the original well water prior to any chemical reactions, typical of groundwater. As the reactions continue and more material is released into the leachate, the small UO_2 and uranyl silicate colloids are entrained in the clay colloid matrix, forming larger colloids (see References 17 and 18).

One proposed mechanism for uranium degradation that describes the behavior seen in the N-reactor fuel tests is described in Langmuir by Danon et al. (see Reference 10). As uranium reacts with oxygen or water, a thin adherent UO_2 layer is formed on the surface. Figure 3-35 displays the surface layer concept. Either oxygen or hydroxide molecules must diffuse through this layer to the reaction surface where it can react with the uranium, resulting in a thicker outer layer of porous UO_{2+x}. The UO_2 crystal structure in the adherent layer is such that the OH^- ion diffuses more readily than the O^{-2} ion (see Figure 3-36). Thus, wet oxidation of uranium is a faster reaction than dry oxidation. Analysis of the corrosion products from the uranium metal fuel indicated UO_2 was generated initially, but over time higher oxides of uranium were formed. Because groundwater contains a variety of contaminants, compared to "pure" water used by Danon et al., other compounds such as silicates were also formed in the SNF tests. The porous UO_{2+x} layer has a larger specific volume than uranium metal, resulting in internal stresses that cause spalling of the alteration products. Uranium reacts so quickly with water that from a repository standpoint, the continuing reactions of the corrosion products will be as important as the fuel degradation (see References 17 and 18).

Irradiated uranium metal fuel was exposed to the unsaturated drip environment for approximately 19 months when the experiment was ended. However, due to the unexpected and complete termination of the test project, much of the later data are not available at the time of this document. Should additional information collected at a later date provide further insight into the degradation processes of uranium metal fuel, an addendum to this report will be prepared.

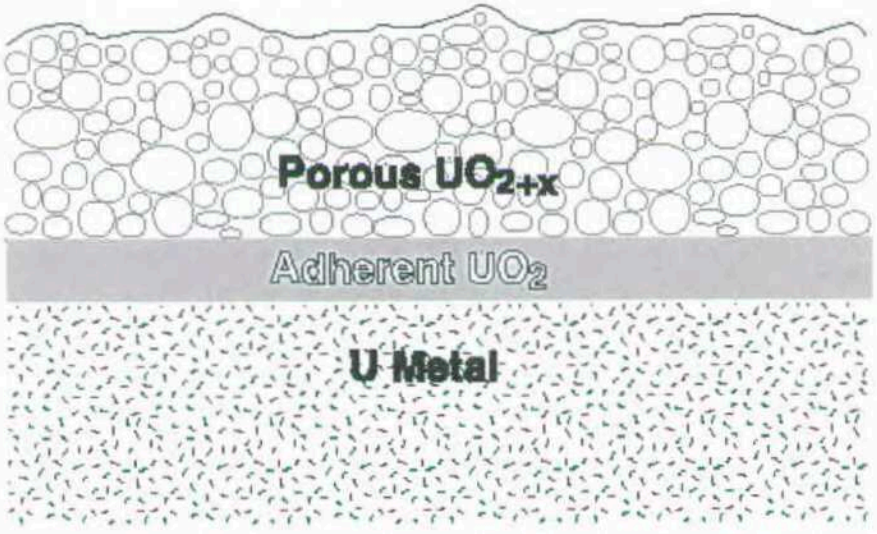

Figure 3-35. Uranium metal corroding surface diagram after Danon et al. (see Reference 10).

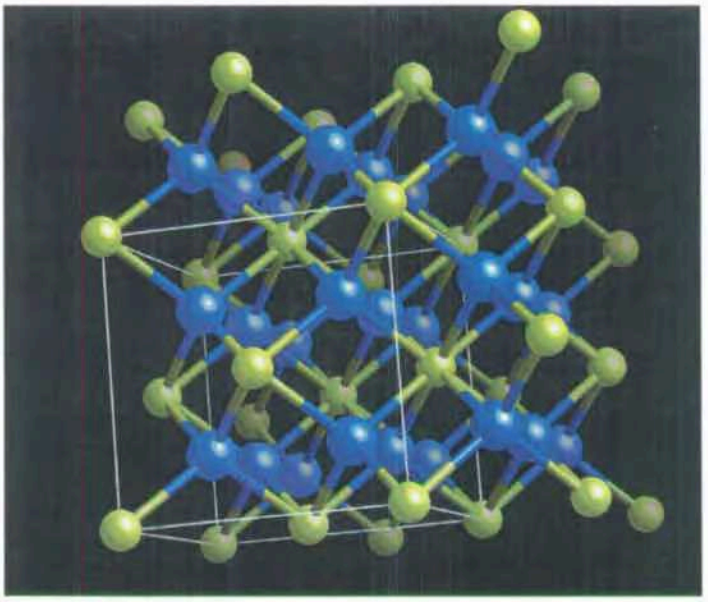

Figure 3-36. Uranium oxide crystal structure.

3.4 Static Batch Tests

Static batch tests were performed to evaluate the degradation of irradiated and unirradiated uranium metal fuel in oxygen-starved, water saturated conditions. Data from these tests will provide verification of the oxic/anoxic degradation mechanism as well as release rates for selected radionuclides, chemical and physical form of released radionuclides, changes in solution chemistry, and characterization of alteration products.[19] The test method and equipment are described in Section 2.2.4. A pressure gauge was added to the test vessel to monitor gas production. In order to ensure an anoxic atmosphere, a Plexiglass containment box was developed that sits inside a glovebox for double isolation. A nitrogen purge was used to maintain as low an oxygen content as possible. Monitoring of the atmosphere in the containment box indicated <50 ppm O_2 could be maintained during sampling and <10 ppm O_2 during undisturbed operation. Figure 3-37 is a photograph of the containment box. The storage box under the containment box is also sealed and is for sample vials prior to analysis.

3.4.1 Test Matrix and Sample Preparation

Batch tests were performed with unirradiated uranium metal samples and with sections from an irradiated N-reactor fuel element. Two tests with unirradiated fuel and one blank (with no fuel) were completed prior to the SNF experiments. The first unirradiated test was performed in a glovebox, but the atmospheric oxygen content was consistently about 2%. As seen with the flow through tests, this concentration is not sufficient to ensure anoxic conditions. Thus, the Plexiglass containment box shown in Figure 3-37 was designed and implemented with the second unirradiated fuel test. Oxygen content was then brought down to <10 ppm during the experiment. After a designated period of time, oxygen was allowed into the containment box and test vessel to convert the atmosphere to oxic conditions. Additional samples were taken to evaluate the effects of the changing environment. Irradiated SNF tests were performed in the same containment box while monitoring the off-gas and taking periodic samples of the liquid and the solids for analysis.

About 100-mg samples were sectioned from the unirradiated fuel element and the N-reactor SNF. All specimens had the cladding removed and the surfaces were polished with 600-grit SiC and then

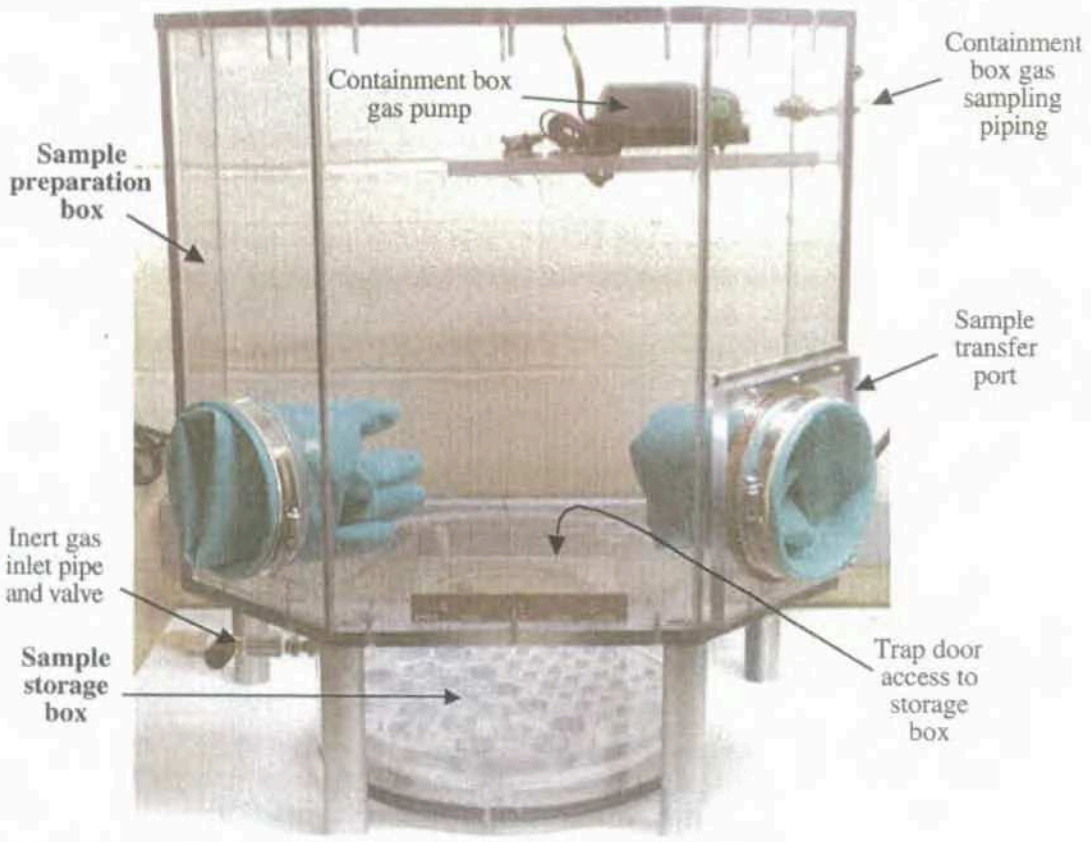

Figure 3-37. Containment box for atmosphere control of batch tests.

ultrasonically cleaned in deionized water for 2 to 3 minutes. The fuel was placed on the sample holder (see Figure 2-3) and inserted in the test vessel with about 15 mL of EJ-13 solution. Section 2.3 describes the preparation and expected composition of EJ-13. Analyses of the primary cations are shown in Table 3-12 compared to the nominal composition in Table 2-4. All experiments were performed at 90°C except during sampling. Liquid samples were periodically removed, cooled, and analyzed for pH, Eh, uranium concentration, dissolved oxygen, and colloid concentration. Samples from irradiated fuel tests were analyzed for the additional isotopes of plutonium and cesium. SEM with EDS capabilities and TEM analyses were also used to characterize any solid particles or colloids in the solution samples.

3.4.2 Unirradiated Fuel Test Results

Batch tests with unirradiated uranium metal fuel were conducted to evaluate the effects of an anoxic environment in a mockup test prior to using irradiated fuel. Test procedures and equipment can be optimized in a relatively nonhazardous configuration. The first unirradiated test was performed in a glovebox; however, the oxygen content was too high. A containment box was designed (see Figure 3-37), and the tests were repeated in a nearly oxygen-free test vessel. After a designated period of time, oxygen was introduced to the system to examine the immediate changes in solution chemistry and paragenesis. Once the test methods were well defined, experiments with SNF were initiated.

Table 3-12. Nominal and actual composition of EJ-13 solution used in batch tests with uranium metal fuel.

Element	Nominal (mg/L)	Actual (mg/L)
Al	600	500
B	200	80
Ca	9,100	8,400
K	NA	10,000
Mg	1,000	300
Na	50,000	46,000
Si	45,000	35,000

3.4.2.1 First Unirradiated Fuel Test (UUBT1). Liquid samples were taken from the first unirradiated fuel batch tests (test name UUBT1) on day 6, 17, 32, and 45. Visual inspection of the uranium specimen was also performed when the test vessel was opened. At 6 days, the fuel was intact and black, with a small volume of black UO_2 fines on the gold screen sample holder. After 17 days, the proportion of fines increased and consisted of a mixture of brown and black solids. The brown color of UO_2 is consistent with near stoichiometric UO_2, the presence of H_2, and reducing conditions. However, there was no appreciable gas detected at this time. The population of brown colored fines immediately surrounding the fuel had increased by day 32, and the fuel surface was brown with hints of black. Representative morphologies for uranium fines are shown in Figure 3-38. Exfoliated sheets of oxidized metal (<1 μm thick) and flaky agglomerations typically <30 μm in length are both represented in the figure. When the vessel was opened after 45 days, the fuel was about 80% to 90% disaggregated into brown fines.[20]

Hydrogen production is a characteristic of anoxic corrosion, as seen in Equation (3-6). No pressurization was detected during the first 30 days, then the levels increased to about 16 psig by day 60 and stabilized. Figure 3-39 shows the hydrogen pressure in the test vessel with respect to time (assuming hydrogen production is the only source of pressure increases). It is obvious that the uranium corrosion is described by at least two mechanisms. Initially the reaction produced no hydrogen describing one behavior. This was followed by a second mechanism that did create hydrogen. Gas production began before a sampling (when the oxygen levels in the vessel would be the least) and continued after the sampling, suggesting the onset of the second period is not dependent on the oxygen concentration. The altered fuel matrix on the specimen surface appears to be the controlling factor in defining the mechanism (see Reference 20).

Colloid analyses were performed on EJ-13 water and samples from day 6, 17, and 32. DLS intensities were not significant until the day 32 sample, when the results were about ten times the background (EJ-13) intensity. Stability was assessed by repeating the analysis on the day 32 sample after 9 months. Colloids were no longer detectable. It is not clear at this time what effect this will have on transport within a repository environment. Size distributions are not available because the polydispersity index was typically >0.5, higher than the 0.3 maximum needed for accurate size distribution data with DLS (see Reference 20).

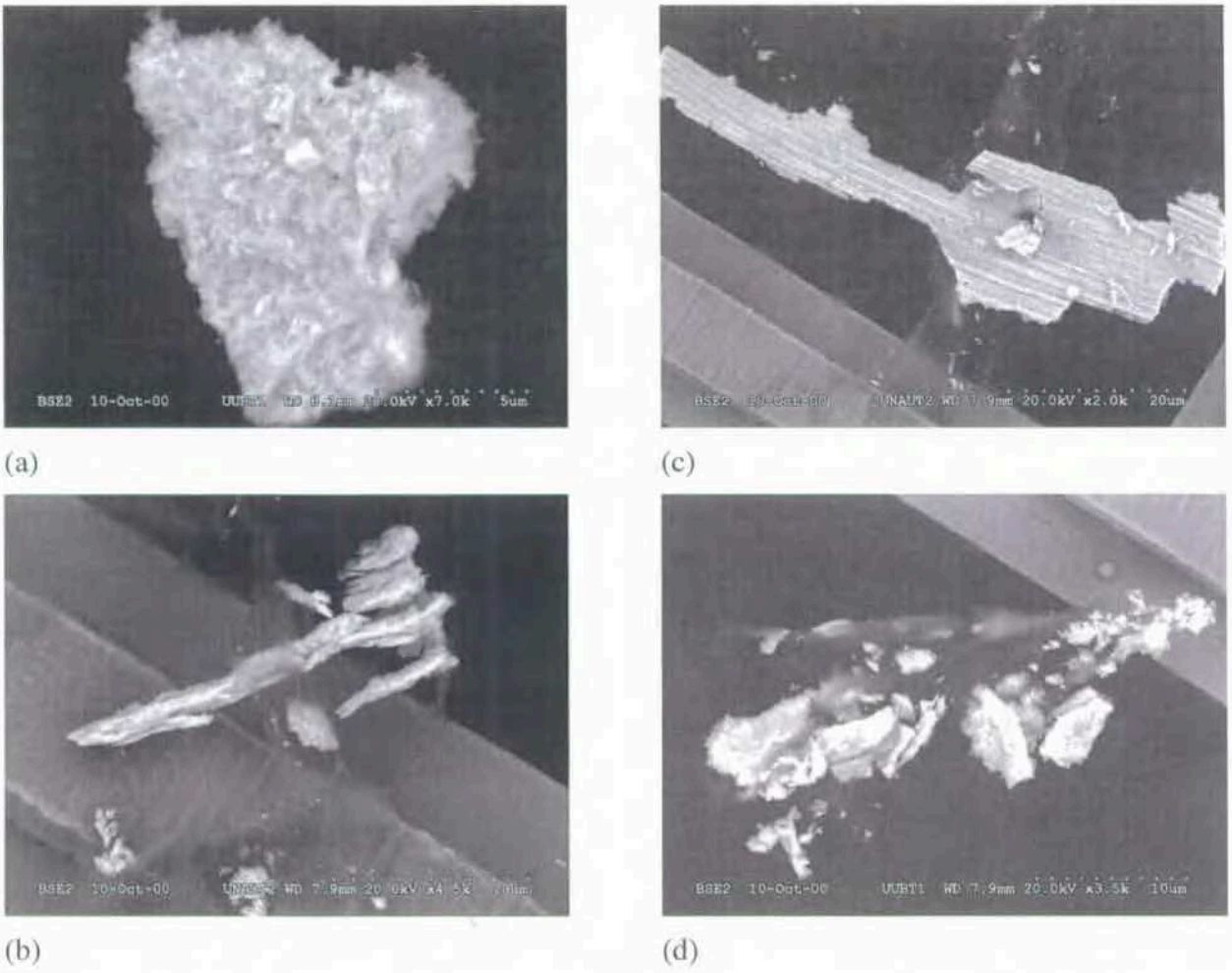

Figure 3-38. Examples of reaction products from the first unirradiated fuel batch tests after 45 days; a) expanded view, b and c) close-up view of exfoliated sheets, and d) flaky surface of fines.

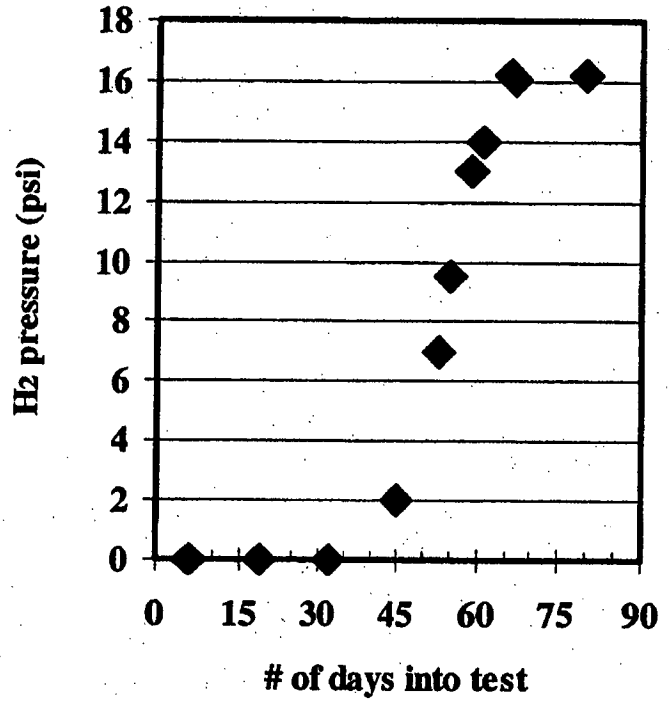

Figure 3-39. Inferred hydrogen gas produced during test UUBT1.

3.4.2.2 Second Unirradiated Fuel Test (UUBT2). Because the oxygen concentration maintained in the glovebox used for test UUBT1 was not sufficiently low (about 2 mol% oxygen), a second test, UUBT2, was run in a containment box with significantly lower oxygen (<50 ppm oxygen). As in UUBT1, the unirradiated fuel in UUBT2 produced spalled products but remained in good condition with sharp edges and corners after 6 days. Up to day 55, the original fuel piece was distinguishable but the vessel bottom was dominated by UO_2 fines. After 108 days, the fuel appeared to be completely converted to the UO_2 fines, which had a similar morphology as the UUBT1 products at test termination. Figure 3-40 is SEM images of uranium oxide particles after 55 days. The UO_2 spheres appear to form via cleavage along crystal domains 5–10 nm in size that are produced during oxidation of fuel. Thus, colloidal UO_2 is released directly during oxidation and is not limited to the kinetics of oxidation, dissolution, and precipitation of uranyl-type colloids (see Reference 20).

After 108 days of exposure, solid reaction products were collected and analyzed with XRD. Wide peaks were seen in the results making it difficult to resolve the exact phase. It is probably a higher oxidation uranyl oxyhydroxide such as schoepite, metaschoepite, or ianthinite. Quantitative evidence suggests U_4O_9 ($UO_{2.25}$) is a likely product form, which agrees with Haschke.[21] However, Baker[22] reported $UO_{2.06}$ as the dominant reaction product during anoxic conditions, but formed $UO_{2.2}$ when subsequently exposed to oxygen. It is possible the hyperstoichiometric UO_2 identified in this study underwent further oxidation during the analysis period. Mechanisms of uranium oxidation are discussed in more detail in Section 3.6. No uranium hydrides were detected (see Reference 20).

Hydrogen gas production was similar to that seen in test UUBT1. An initial period with little or no hydrogen detected was seen followed by an increase in pressure to about 15 psig. Figure 3-41 shows the hydrogen pressure (assuming H_2 is the only gas produced in the test vessel) with respect to the test duration. The induction period is shorter with the anoxic atmosphere from 35 days in test UUBT1 to about 10 days in tests UUBT2. The linear period between days 14 and 54 was used to estimate an oxidation rate of 0.94 mg/d, which corresponds to a loss of 39 mg of fuel over that time period. If this

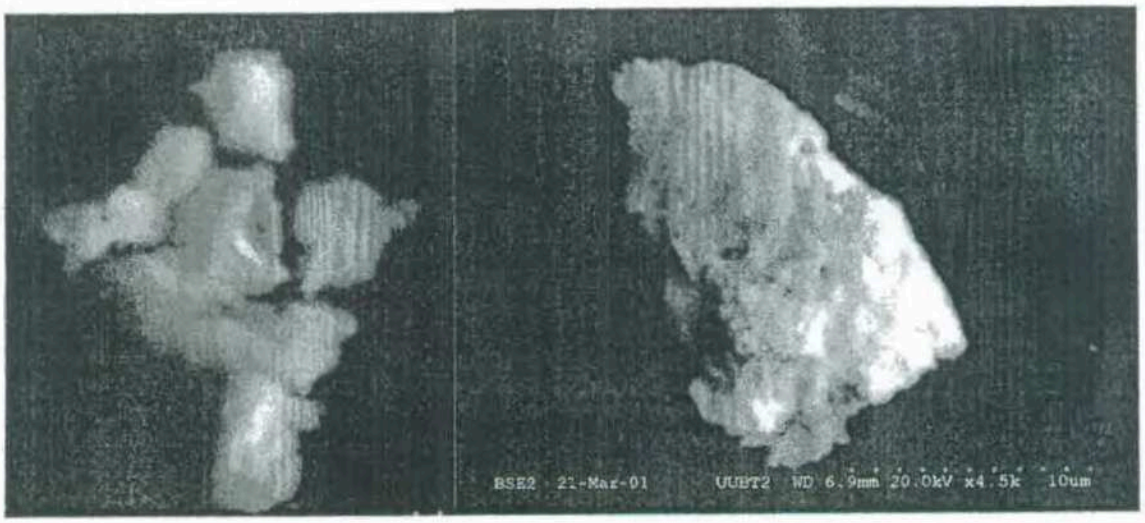

Figure 3-40. SEM images of suspended uranium oxide particles from test UUBT2 at 55 days.

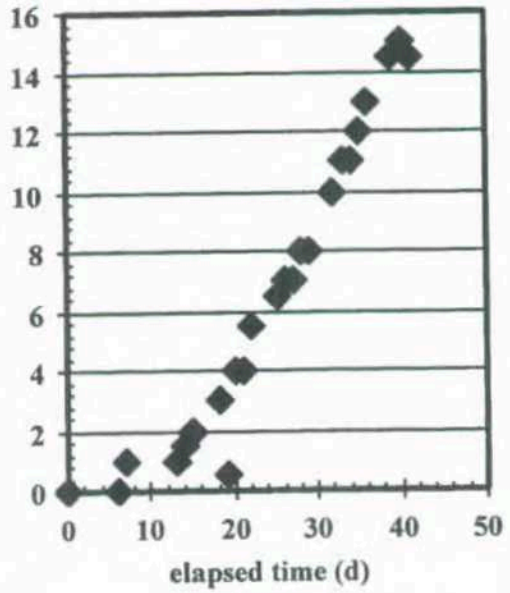

Figure 3-41. Inferred hydrogen gas produced during test UUBT2. The y axis indicates H_2 pressure, psi.

value is normalized to the original fuel geometric surface area (assumed the same as UUBT1, 23.2 mm^2), a highly conservative corrosion rate of 4×10^5 $mg/m^2/d$ is obtained. No hydrogen analyses were available after day 55, probably due to a gasket failure (see Reference 20).

Colloid analyses were performed on samples from day 28, 55, 108, and 115. An analysis of the blank sample was also done at day 116, resulting in a strong scattering intensity (170 kcps). Thus, colloids are either present in the groundwater or are produced in an anoxic environment. Table 3-13 shows the DLS data for the UUBT2 samples. Colloids were detected in every sample, although typically at the same intensity as the groundwater blank. The scattering intensity was very large in the samples from day 55 and 108 (1,100 kcps and 1,790 kcps, respectively). Stability was measured by repeating the analyses after a specific period of time. Day 28 sample dropped to about 5 kcps after 1 month, but returned to the original value after about 4 months. Both samples from day 55 and day 108 dropped in intensity over time. One sample was taken after the oxic stage of the test, at day 115. Colloids were also produced under these conditions. Some of the polydispersity indices shown in Table 3-13 were low enough to estimate a mean particle size. The sizes ranged from 190 (±170) to 310 (±260). Colloid particle concentrations were estimated by assuming the colloids scattering intensity were identical to either 100 or 300-nm-diameter latex spheres. Values were typically on the order of 10^{10} to 10^{12} particles per liter (see Reference 20).

Uranium concentration dissolved in solution and associated with the colloids was found for three samples. Solution that passed through a 30-kDa filter was considered dissolved. Solution that passed through a 0.45-μm filter but not a 30-kDa filter was assumed associated with colloids. As seen in Figure 3-42, colloidal uranium accounted for nearly all the detectable uranium at 55 days and approximately half the uranium in solution at day 108. No significant changes were apparent after the introduction of oxygen, shown after the vertical line (day 115). Additional analyses indicated nickel was in solution well in excess of its EJ-13 concentration and was partitioned to the colloidal range, suggesting that the stainless steel vessel may be contributing to the colloidal species. No other metals (e.g., silicon, calcium, iron, and aluminum) were found to be strongly partitioned to the colloidal phases (see Reference 20).

An aliquot of the sample from day 55 was wicked through a holey carbon grid and analyzed by TEM. Uranium appears either as agglomerations of tiny UO_2 spheres (<10 nm in diameter) or as UO_2 particles attached to silicate clay host materials. Figure 3-43 presents both colloid forms. View (a) shows the agglomeration of colloid-sized UO_2 spheres and an electron diffraction pattern of a similar structure. The uranium agglomerations vary in size from <50 μm to >200 μm. View (b) shows the morphology of the silicate phase, typical of layered smectite clays like those generated during waste glass corrosion.[23] Note the UO_2 spheres entrained in the clay (circled). Diversity in the UO_2 and smectite clay colloid-size distribution corroborates the DLS measurements where polydispersity was high (see Reference 20).

Other elements associated with the clay colloids in the TEM analyses include iron, nickel, and aluminum. Although the EJ-13 contains these elements, the concentration of nickel (and perhaps iron) in the colloids is too high for it to be the only source. Corrosion of the stainless steel vessel is the most likely cause of the increased nickel concentration. This differs slightly from the solution analyses, which only detected nickel in association with the colloid-size fraction (see Reference 20).

After the 108 days of anoxic conditions in the test environment, test UUBT2 was exposed to 12 hours of air and then resealed and returned to 90°C for continued reaction. A sample was withdrawn at day 115 (7 days in oxic conditions) and analyzed in the same manner as the anoxic samples. Very few changes occurred in this timeframe. Dissolved uranium concentration increased, as seen in Figure 3-42. The DLS signal intensity dropped from the 55 (1,100 kcps) and 108 (1,700 kcps) day samples to 552 kcps (shown in Table 3-13). Colloids identified with TEM were similar, UO_2 spheres and clays incorporating

Table 3-13. Measured light scattering data from the UUBT2 test samples.

Sample	Anoxic/ Oxic	Days in Storage	DLS Intensity @ 150 µm PMT (kcps)	DLS Intensity @ 500 µm PMT (kcps)	Poly-Dispersity Index	Mean Particle Size	Calculated Particle Conc.[a]	Colloidal U Conc. (ng/mL)	Dissolved U Conc. (ng/mL)
Day 28	Anoxic	6		160	0.32	310 ± 260	2×10^{11} (1×10^{10})		361
Day 28	Anoxic	26		4.5	>0.5	—[b]	8×10^{9} (3×10^{8})		
Day 28	Anoxic	124		160	0.36	—[b]	2×10^{11} (1×10^{10})		
Day 55	Anoxic	0	100	1,100	0.08	220 ± 220	2×10^{12} (7×10^{10})	3,822	8
Day 55	Anoxic	14	100		0.18	190 ± 170			
Day 55	Anoxic	15	100		0.16	212 ± 170			
Day 55	Anoxic	98		170	0.6	—[b]	2×10^{11} (1×10^{10})		
Day 108	Anoxic	5	90	1,790	0.4	—[b]	3×10^{12} (1×10^{11})	1,610	1,470
Day 108	Anoxic	33		253	0.5	—[b]	5×10^{11} (2×10^{10})		
Day 108	Anoxic	47		230	>0.6	—[b]	4×10^{11} (2×10^{10})		
Day 115	Oxic	0	50	552	>0.5	—[b]	1×10^{12} (4×10^{10})	1,680	2,250
Blank/ Day 116	Anoxic			160	>0.5	—[b]	2×10^{11} (1×10^{10})		

a. Particle concentration estimated assuming scattering intensity is identical to latex spheres of 100-nm diameter (300-nm diameter).

b. Could not resolve.

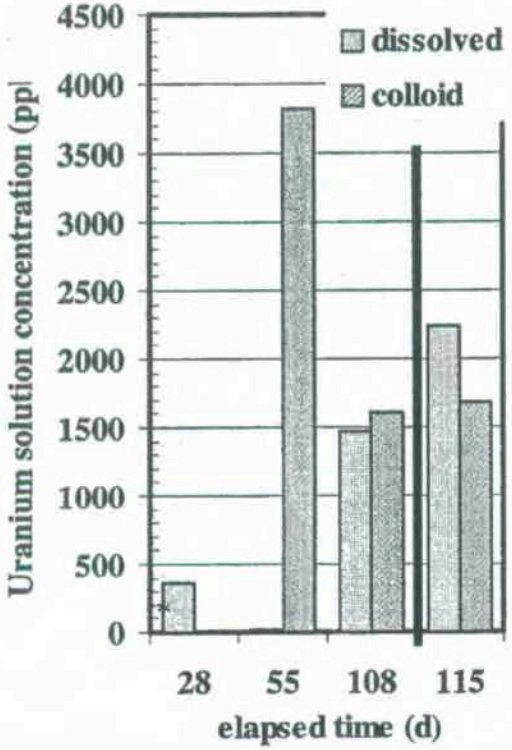

Figure 3-42. Dissolved and colloidal uranium concentrations in solutions from test UUBT2.

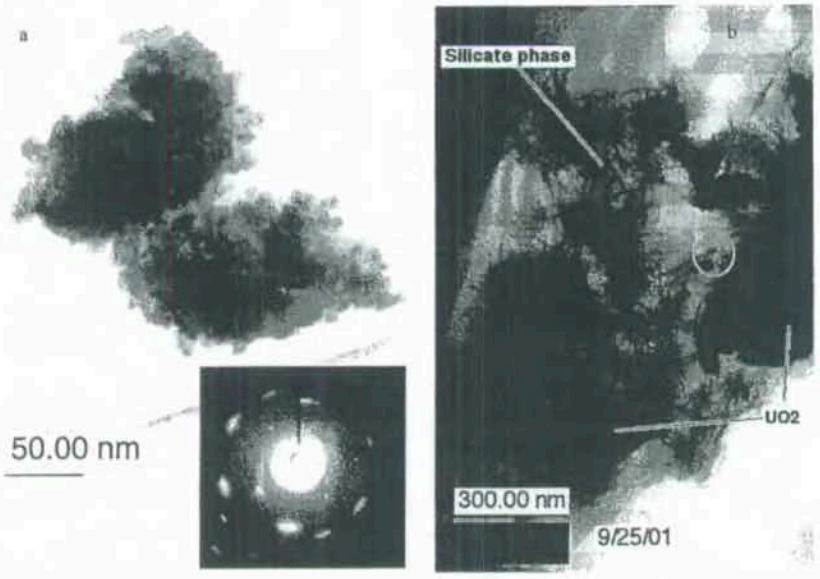

Figure 3-43. TEM images of two types of colloids found during test UUBT2, (a) UO_2 spheres and (b) silicate phase.

aluminum, nickel, iron, and magnesium. Calcium-rich colloids were also found and are shown in Figure 3-44. No changes were visible in the brown, reaction products (see Reference 20).

3.4.3 Irradiated SNF Test Results

Static batch experiments with irradiated uranium metal fuel were completed with a 100-day oxygen free environment followed by 65 days under oxic conditions. The same methodology and equipment that were used in the second unirradiated test were used in this experiment. A 100-mg sample of N-reactor SNF was placed with 15 mL of EJ-13 water in a sealed test vessel within the containment box for atmospheric control. Oxygen levels were maintained at less than 50 ppm during the initial 100 days through purging with argon. Results were similar to those found with the unirradiated fuel.[24,25]

After 28 days, significant degradation had occurred to the fuel resulting in brown alteration products, similar to what was found in UUBT1 and UUBT2. However, larger chunks of material were visible that were not seen in the earlier tests (Figure 3-45). The larger pieces continued to react until all the material appeared as fines. Brown, reaction products are indicative of stoichiometric UO_2, expected when atmospheric conditions are anoxic. Analysis of the reaction products was not available at the time of this writing, but it is expected a range of uranium oxyhydroxides will be seen that are typical of previous flow through and drip tests as well as the unirradiated batch tests (see References 24 and 25).

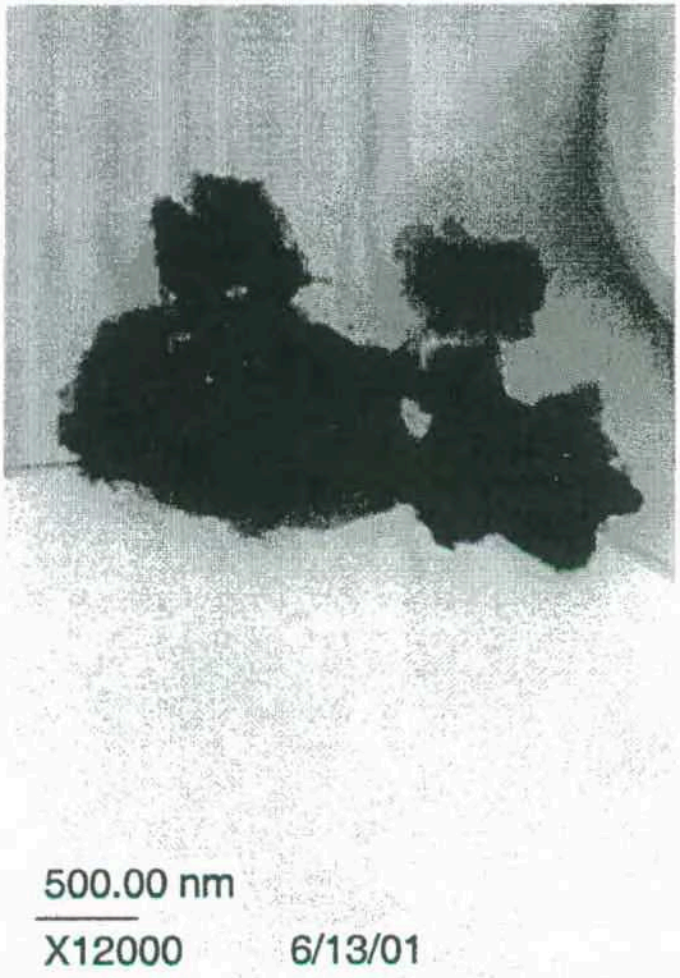

Figure 3-44. TEM micrograph of calcium-rich colloids from UUBT2 after oxic phase.

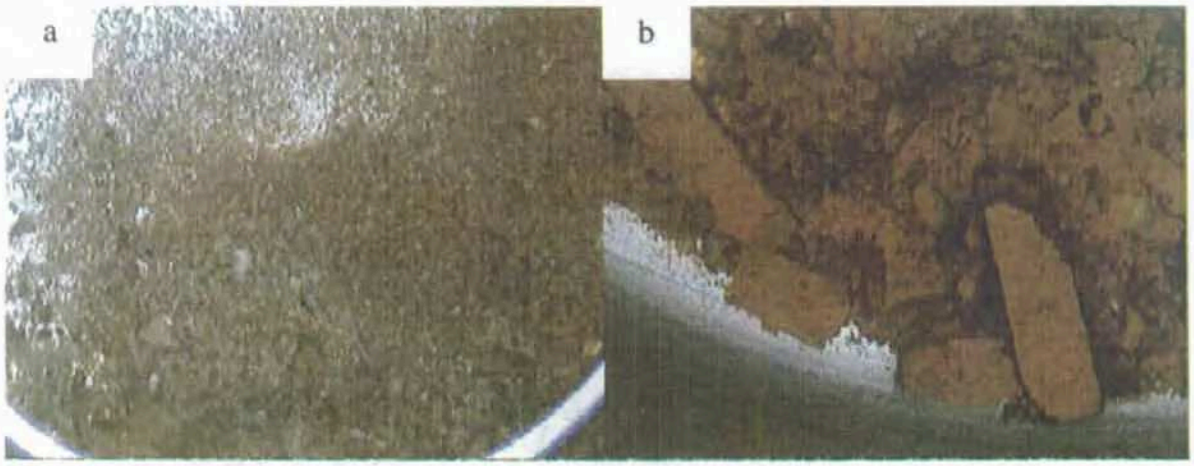

Figure 3-45. Irradiated N-reactor fuel after 28 days in anoxic static batch test conditions; field of view in a is ~15 mm and in b is ~5 mm.

Solution samples were taken after 2, 28, 41, 95, 130, and 165 days of exposure. Analyses indicate most of the uranium was released as U(IV) colloids during the anoxic stage but was oxidized to dissolved U(VI) in the oxic portion of the test. Figure 3-46 demonstrates the distribution between dissolved and colloid fractions in each sample. Note at 100 days the environment was changed from anoxic to oxic. After the introduction of oxygen, the dissolved uranium concentration increased, and the colloid fraction decreased. Somewhat similar behavior was seen in the unirradiated experiments, shown in Figure 3-42. Once oxygen was introduced into the system, the dissolved fraction increased. However, the colloid concentration was about the same as the sample just before the addition of oxygen. Figure 3-46 shows the colloids decreasing with time during the oxic phase of the test, and thus, the colloids from unirradiated fuel under oxic conditions may have decreased if the experiment had continued past 115 days (see References 24 and 25).

DLS analysis was performed to quantify colloid concentration and size. The results are presented in Table 3-14. Light scattering intensity was about 300 kcps for the first month then jumped to about 1,800 for the remainder of the anoxic portion of the test. The intensity dropped back down to about 300 once oxygen was added to the system. Using the groundwater concentration of colloids measured during the unirradiated test analyses (160 kcps), a significant amount of colloids were generated throughout the experiment. Storage time does not appear to have an impact on the results. Based on 100 nm and 300 nm polystyrene standards, the particle concentration was estimated to be between 10^{10} and 10^{12} particles per liter, similar to the results with the unirradiated fuel. Mean particle size was calculated between 170 to 250 nm, also very similar to what was found with the unirradiated samples (see Reference 25).

Additional characterization was performed on the colloids generated during the static batch tests. TEM results indicated two types of colloids. Spherical UO_2 colloids were identified, probably from spallation of the alteration layer. The spheres are approximately 100 nm in diameter and appear to be agglomerating. Clay colloids, rich in silicon, nickel, iron, and aluminum, were also found. Silicon and perhaps aluminum originated in the EJ-13 water. However, the nickel and iron are likely from degradation of the stainless steel test vessel. The UO_2 colloids were entrained in the spiked clay colloids, which were also agglomerating. Figure 3-47 shows a group of clay colloids collecting around an agglomeration of UO_2 colloids. Although this photograph is from the unirradiated fuel tests, the same phenomenon was found with the irradiated experiments (see References 24 and 25).

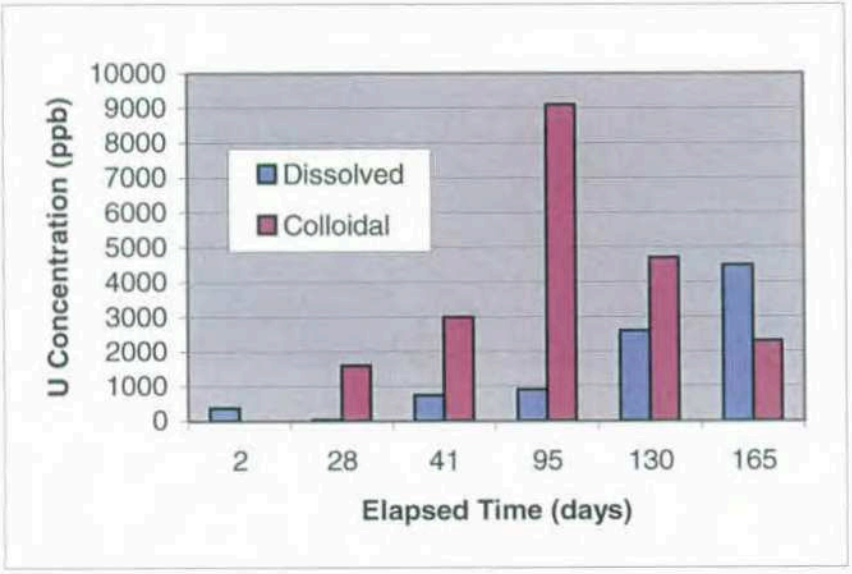

Figure 3-46. Colloid and dissolved uranium released into solution from irradiated uranium metal fuel during static batch tests.

Table 3-14. Dynamic light scattering (DLS) results from static batch tests with irradiated uranium metal fuel.

Sample	Anoxic/Oxic	Days in Storage	DLS Intensity (kcps)	Colloidal U Conc. (ng/mL)	Dissolved U Conc. (ng/mL)
Day 2	Anoxic	0	300	0	360
Day 28	Anoxic	0	260	1,600	38
Day 41	Anoxic	4	1,800	3,000	730
Day 95	Anoxic	32	1,700	9,100	900
Day 130	Oxic	122	280	4,700	2,600
Day 165	Oxic	80	320	2,300	4,500

Figure 3-47. UO_2 colloids attached to clay colloids from the static batch tests with unirradiated uranium fuel.

Plutonium and cesium released from the fuel into solution was also measured. Plutonium was released almost entirely as colloids before and after the addition of oxygen. All samples except one (about 0.5 ppb at 41 days) had a dissolved concentration of less than 0.2 ppb, whereas the colloid concentrations ranged from about 5 to 50 ppb. Disposition of the plutonium colloid, as a colloid or sorbed to a clay, could not be identified. Concentration of dissolved cesium ranged between about 120 and 370 ppb during the anoxic stage of the experiment. Cesium in solution dropped significantly to about 50 ppb once oxygen was added to the test vessel. The cesium may be sorbing onto the solid reaction products, but data are not available at this time to address the possibility. Figure 3-48 displays the change in cesium solution concentration over time.

Although the experimental portion of the unsaturated batch tests is finished, reporting of the results is not complete. Because of the premature termination of the release rate test project, some of the data from the irradiated batch tests have not been finalized. Thus, that information does not appear in this document. If any significant changes to the conclusions are evident from the finalized data package, a revision will be issued at that time.

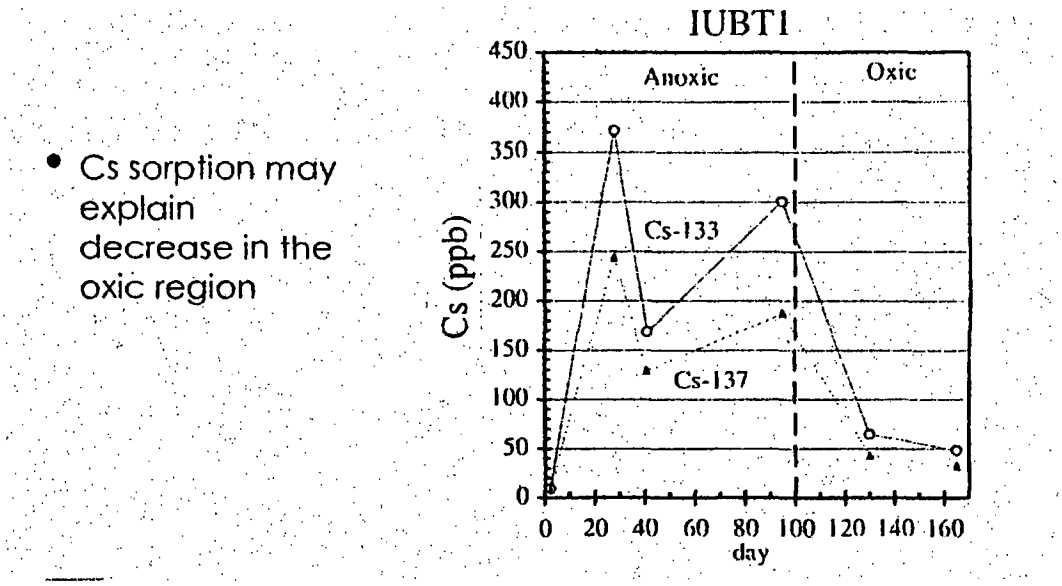

Figure 3-48. Cesium released into solution during static batch tests with irradiated uranium metal fuel.

3.4.4 Static Batch Test Conclusions

Three sets of static batch experiments were completed with uranium metal fuel to evaluate the degradation reactions under anoxic and oxic conditions. Two mockup tests were performed first with unirradiated fuel to ensure that the equipment and processes were adequate for determining the desired information. Initially, the oxygen levels were too high, at about 2%, to be considered an anoxic environment. A containment box was designed within the glovebox that held the test equipment and could be purged with an inert gas. Oxygen levels were then kept at less than 10 ppm. A final experiment with the modified equipment was then performed with irradiated N-reactor SNF.

Under anoxic conditions, the uranium fuel corroded to form nearly stochiometric UO_2, primarily as colloids. XRD diffracting domains show the particle size as less than 10 nm. No hydrides were detected. TEM analyses identified two types of colloids, spherical UO_2 and clays rich in silicon, nickel, iron, and aluminum. Both types were agglomerating, and the UO_2 colloids were entrained in the spiked clay colloids. DLS results estimate a mean particle size of 200 to 300 nm from both the irradiated and unirradiated experiments. Colloid concentrations are on the order of 10^{12} particles per liter. Plutonium was released almost entirely as colloidal, but the disposition could not be identified. It is likely that the clay colloids will adsorb other radionuclides, such as plutonium.

After a fixed time period, the atmosphere within the test vessel and the containment box was changed to air, thus allowing oxygen into the system and providing an oxic environment. The amount of uranium-bearing colloids decreased with the SNF, but did not change with the unirradiated fuel. It is possible the concentration would decrease if the unirradiated test had continued for a longer time. Uranium was released as U(IV) under anoxic conditions but was further oxidized to U(VI) when in an oxic atmosphere. Plutonium colloids, however, did not decrease after the addition of oxygen. Cesium concentration in solution decreased after the addition of oxygen, perhaps caused by sorption onto solids.

3.5 Colloid Tests

Results from other test methods indicate that colloids could play a significant role in radionuclide release predictions. Colloids are small particles that remain suspended in solution but are not considered dissolved, thus concentrations of specific elements can exceed the solubility limit. The presence of stable colloids (those that remain suspended in solution) in the repository groundwater that include radionuclides can potentially increase the predicted exposure at the site boundary. Understanding the characteristics of colloids is crucial to accurate modeling predictions of radionuclide releases. Therefore, a series of tests with uranium metal fuel was planned to define the amount and type of colloids produced during fuel degradation and their stability in a range of conditions. A general description of colloids is presented in Section 2.2.5.[26]

3.5.1 Test Matrix and Methodology

A range of temperatures, pH, ionic strength, and leachants were chosen for the static colloid test matrix. Test temperature planned for the first set of experiments was 30°C, for the second set it was 90°C, and finally 60°C, if necessary. Groundwater (EJ-13, see Section 2.3) from Yucca Mountain, deionized water (for a baseline), and three single component solutions (based on the expected reactivity with uranium) were selected for testing. The single component solutions include iron, silicon, and carbonate. Ionic strength was varied between 0.001, 0.01, 0.1 m. Adjustments were also planned to change the pH to 8, 5, and 11, depending on the initial pH. Only high purity, relatively inert chemicals were used to adjust the ionic strength and pH. Experiments with EJ-13 water were not adjusted for pH or ionic strength. One control test was also performed at each condition. It was assumed that some conditions would not need to be evaluated. For example, if the results at 30 and 90°C were equal, then the 60°C tests could be eliminated. Only a fraction of the experiments were completed prior to the premature termination of the release rate test project. Results are presented on the available data, but many gaps in the data are apparent. The complete planned test matrix (without the controls) is shown in Table 3-15 (see Reference 26).

Initial static experiments were performed with unirradiated uranium metal fuel, as in the unsaturated drip and static batch tests. Results were used to pare down the number of required tests using irradiated uranium metal SNF. A monolithic sample of approximately 200 mg was placed in the test vessel with about 10 mL of the selected leachant. The vessel was sealed and heated to the test temperature and allowed to react for a specified time (typically about 4 months). Aliquots of solution were removed periodically for interim test analyses. At test termination, solution and solids samples were removed, and the reaction vessel was acid stripped so any adsorbed material was included in the total release calculations (see Reference 26).

Table 3-15. Test matrix for uranium metal fuel colloid tests.

	pH	Ionic Strength (m)	Temperature (°C)	Replicates
EJ-13 Water	~8	~0.001	30, 90, 60	2
DI Water	4, 8, 11	0.001, 0.01, 0.1	30, 90, 60	1
Si Solution	4, 8, 11	0.001, 0.01, 0.1	30, 90, 60	2
Fe Solution	4, 8, 11	0.001, 0.01, 0.1	30, 90, 60	2
HCO_3/CO_3	4, 8, 11	0.001, 0.01, 0.1	30, 90, 60	2

Analysis of colloid particle size and distribution was done in situ using DLS. Sequential filtration and ICP-MS analysis of the filtrates provided information on elemental composition of each size fraction. XRD was used to identify the mineral species, and TEM was used to determine morphology, structure, and elemental composition. Solution chemistry changes were monitored using pH, ionic strength, and Eh measurements. Additional methods that were useful in determining colloid characteristics include size exclusion chromatography (for specific radionuclides at low concentration) and electrophoretic measurements (for surface charge). These techniques are discussed in Section 2.2.5 (see Reference 26).

In order to quantify the stability of the alteration phase layer on degrading fuel, a shear test was planned. The goal was to determine the hydrodynamic forces required to shear colloid-sized particles from the fuel surface. Only one test condition (temperature, pH, solution composition, ionic strength) was planned using this method, which was to be determined at the time of the experiment. This test was not completed due to the early termination of the project (see Reference 26).

3.5.2 Unirradiated Fuel Test Results

Unirradiated uranium metal fuel was used in the colloid tests prior to the SNF in order to establish the methodology and reduce the number of experiments required with irradiated fuel. Two sets of experiments were completed: all five solutions listed in Table 3-14 at 0.001-m ionic strength, 30°C, and pH of 8 and 4. Both sets were discontinued after about 4 months, with samplings at about 1-month intervals. Another set of experiments at 0.001-m ionic strength, pH of 8, and temperature of 60°C was initiated, but the experiments were interrupted too soon to produce any reportable data.

Visual examination of the coupons at test termination revealed that the most corrosion had occurred on the samples exposed to 1 mM silicate solution, regardless of pH. The EJ-13 and iron solutions also caused a large degree of alteration and deep pitting. Moderate degradation was seen on the material exposed to the carbonate solution and very minimal reaction had occurred in the deionized water. Figure 3-49 shows the fuel sample after 4 months of exposure to the five solutions at pH of 8 and 30°C.[27,28]

Samples of the alteration products from the experiments at pH of 8 were analyzed for composition. SEM analyses using EDS identified uranium and oxygen in every sample, including the lightly reacted deionized water test. Figure 3-50 shows an SEM micrograph of the products from the EJ-13 experiment. XRD was then used to identify the mineral species of the EJ-13, silicate, and carbonate solutions. Results were primarily a fine grained UO_2 (estimated 10 nm) product with varying amounts metaschoepite (1–5% for EJ-13, 25–50% for carbonate, and 5–10% for silicate solution). Na-boltwoodite was also identified in the EJ-13 sample. These data are similar to those found in the unsaturated drip and static batch tests. Initially, very fine UO_2 corrosion products are generated, but over time they begin to fuse together and higher oxidation phases are formed (Sections 3.3 and 3.4) (see References 27 and 28).

In situ DLS analyses of the solutions showed that the colloid concentration was not directly related to the amount of alteration on the fuel sample. Figure 3-51 shows the colloid concentration is based on 70 and 300 nm standards for each test solution at pH of 8. Carbonate solution generated by far the most colloids, even though only moderate corrosion was seen on the fuel sample. EJ-13 and the silicate solution produced a measurable amount of colloid-sized particles, but the iron solution had essentially none. Deionized water also produced no colloids, as expected. Size distribution using the DLS indicates a bimodal distribution (about 5 nm and 200 nm, shown in Figure 3-52) after exposure to EJ-13 water, similar to the unsaturated drip tests (Section 3.3). Silicate and carbonate solutions also resulted in a distribution of two peaks at about 5 nm and 200 nm (see References 27 and 28).

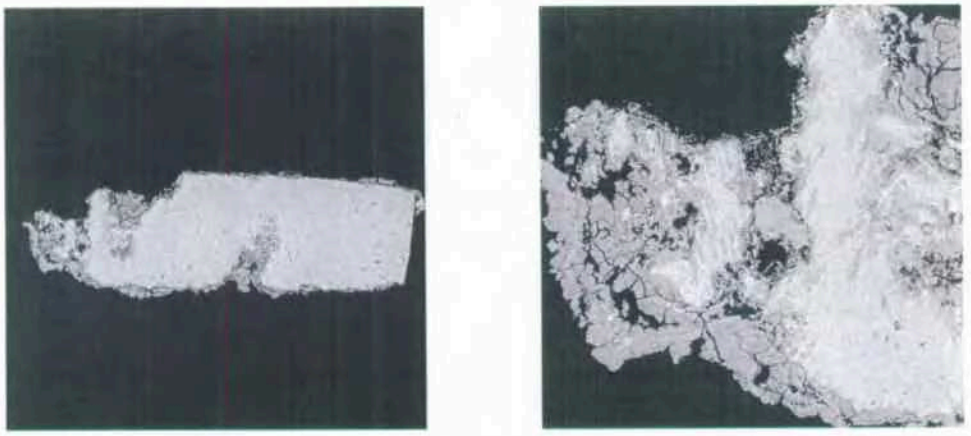

(a) Silicate solution

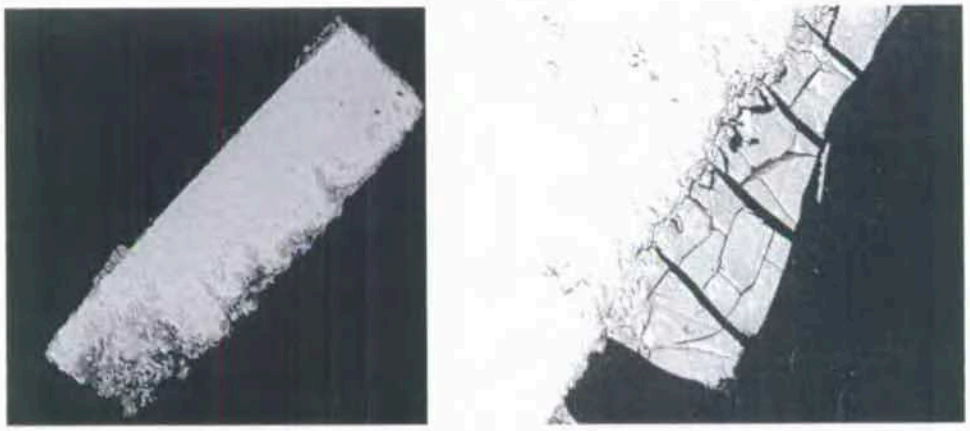

(b) EJ-13 water

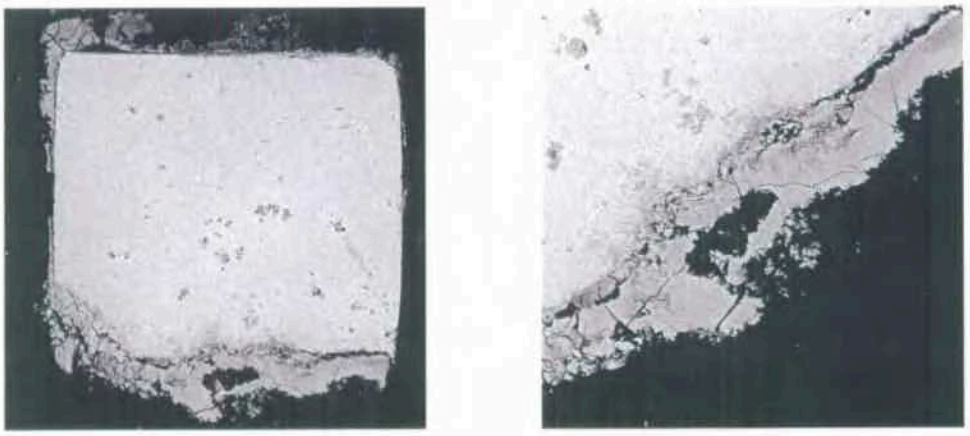

(c) Iron solution

Figure 3-49. Appearance of unirradiated uranium metal fuel after 4 months at 30°C and pH of 8 for (a) 1 mM silicate solution, (b) EJ-13 water, (c) 1 mM iron (III) solution, (d) 1 mM carbonate solution, and (e) deionized water.

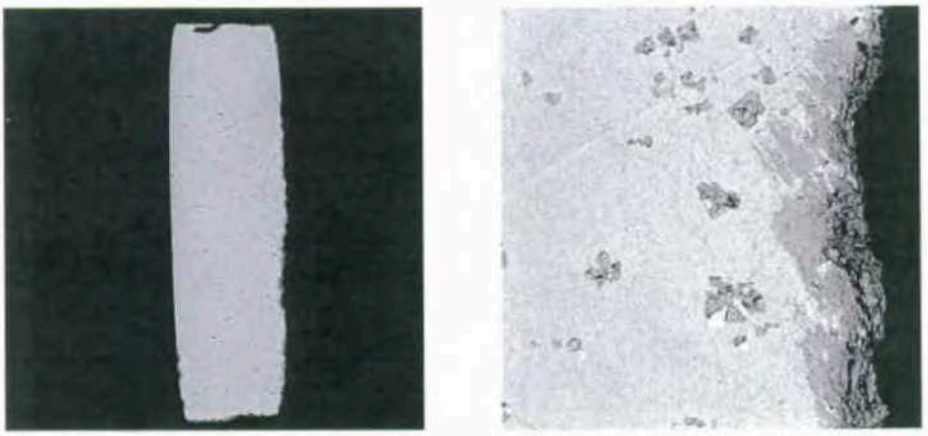

(d) Carbonate solution

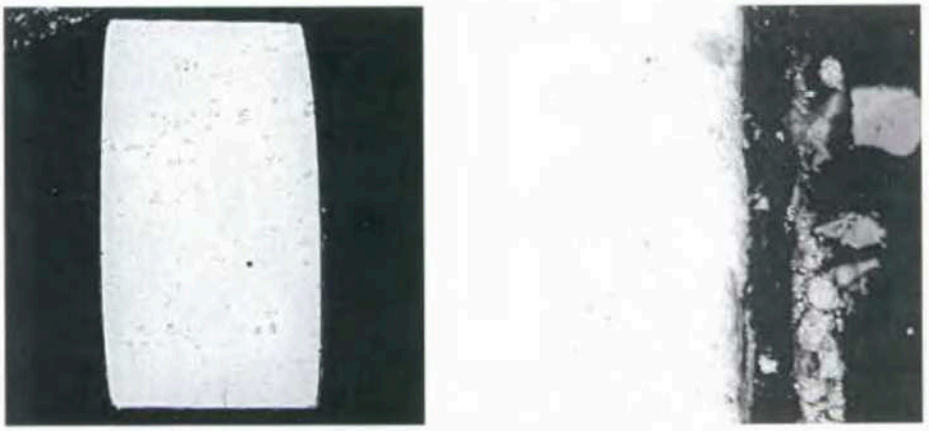

(e) Deinoized water

Figure 3-49. (continued).

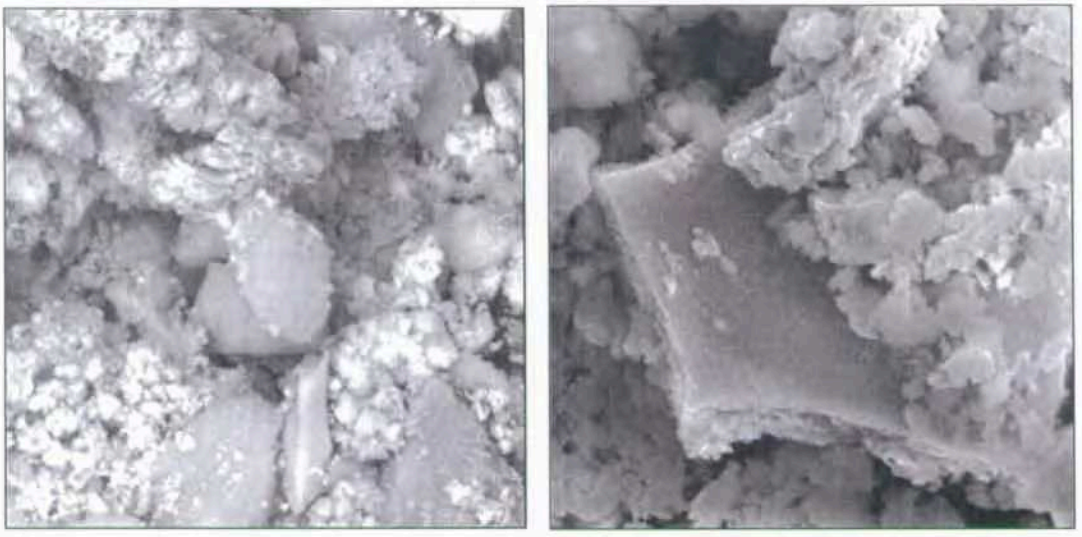

Figure 3-50. Scanning electron microscopy photo of alteration products from unirradiated uranium metal colloid test with EJ-13 water, pH of 8, and 30°C.

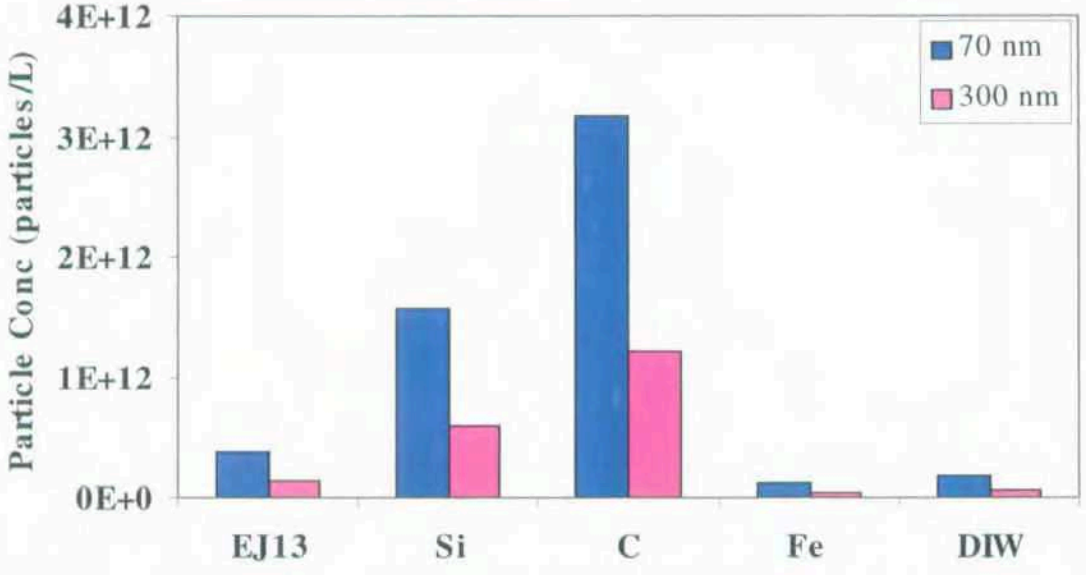

Figure 3-51. In situ dynamic light scattering colloid concentration from unirradiated uranium metal fuel colloid tests at a pH of 8 and temperature of 30°C using 70 and 300 nm standards.

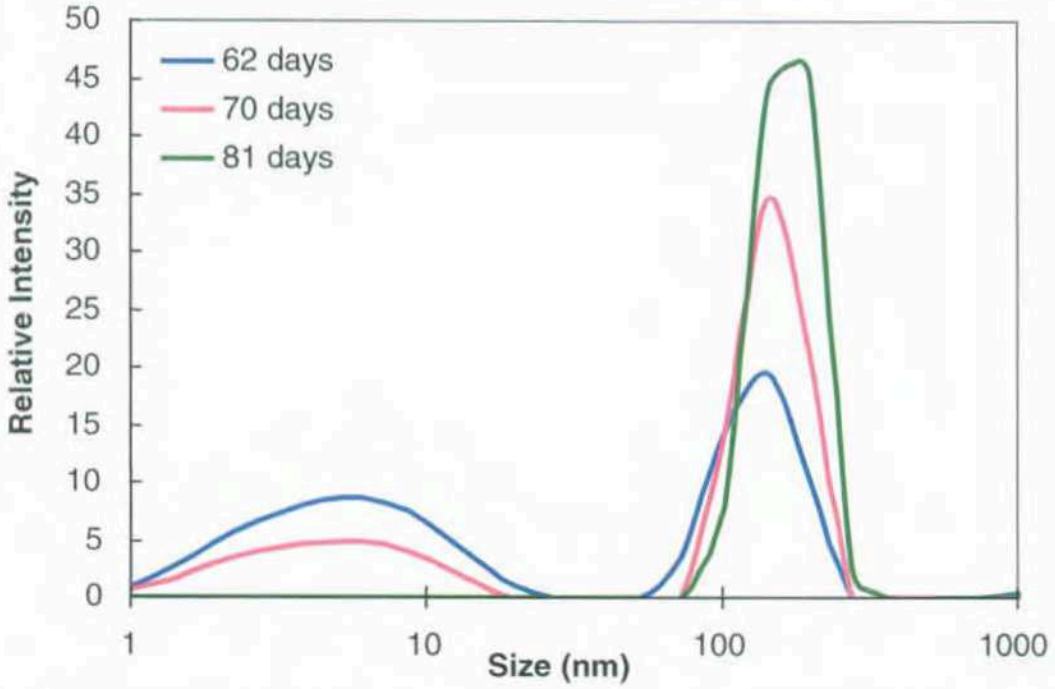

Figure 3-52. Uranium size distribution as a function of time from unirradiated uranium metal fuel colloid tests with EJ-13 at pH of 8 and 30°C.

Sequential filtration followed by ICP-MS analyses of uranium confirmed the DLS data. The size fractions evaluated were greater than 50 nm (large particles), less than 50 nm but greater than 5 nm (colloids), and less than 5 nm (dissolved). Colloid-sized particles comprise the highest percentage of uranium released in the 1 mM carbonate solution (pH of 8, 30°C). Most of the uranium was dissolved in the solutions from the silicate and EJ-13 tests. Few colloids were identified in the EJ-13, silicate, and iron solutions. The greatest total amount of uranium released was in the silicate solution. Figure 3-53 displays the uranium concentration distribution by solution chemistry for the pH of 8, 30°C tests (see References 27 and 28).

TEM analyses of recovered colloids from the silicate solution and the EJ-13 water were performed to evaluate the size distribution, morphology, and phase composition. Colloids from the silicate solution at pH of 8 and 30°C were measured as 100 to 1,000-nm particles. They had a morphology of spherical and plate-like aggregates and consisted of primarily silicon, calcium, magnesium, and uranium-rich phases (see Figure 3-54). Slightly different results were found with the colloids generated in EJ-13 water. The size distribution consisted of 100 to 200 nm aggregates of 5 to 10 nm spherical particles. Composition was dominated by uranium-rich phases, though some silicon-rich phases were also present. Additional TEM analyses were planned, however, results were not available when the release rate project was terminated and thus are not presented here (see References 27 and 28).

Measurements of Eh and pH during the test provide insight into the changing chemistry. Figure 3-55 shows the Eh for duplicate tests of each solution and a blank (no fuel added). Two test series are represented, an initial pH of 8 after 4 months and initial pH of 4 after 2 months. The largest change over time was seen in the carbonate and silicate solutions, dropping approximately as much as 50 mV over 4 months and in the pH 4 silicate solution dropping about 100 mV. Iron solution and EJ-13 showed a negligible change, smaller than was seen with the deionized water. One data point with EJ-13 and pH 4 showed a drop of about 40 mV (see References 27 and 28).

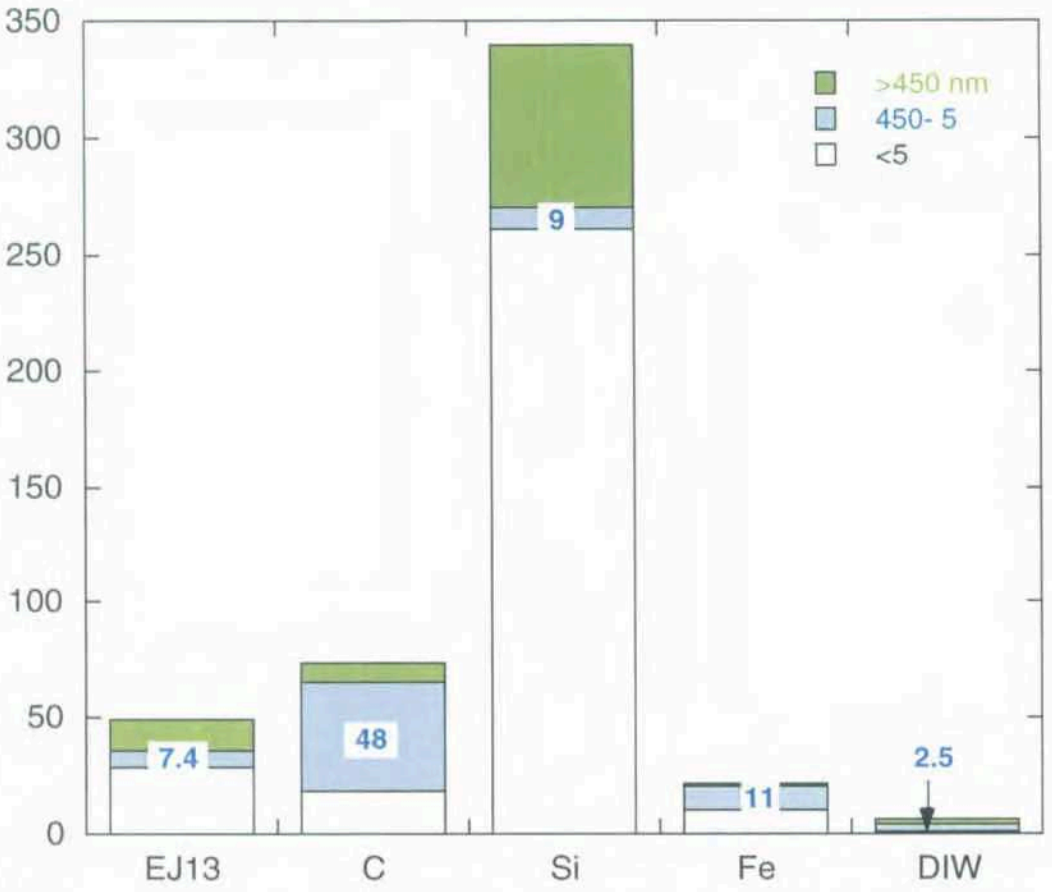

Figure 3-53. Uranium concentration by size fraction from unirradiated uranium metal colloid tests after 4 months (pH of 8, 30°C).

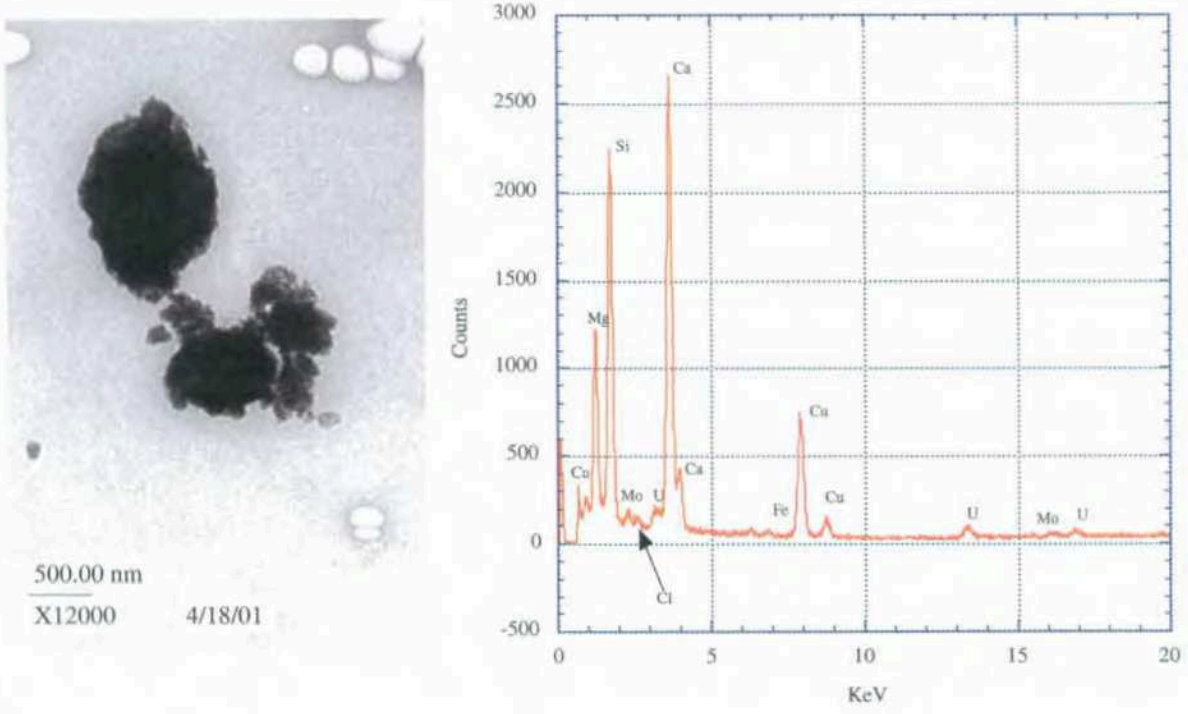

Figure 3-54. Example of silicon-rich colloid from an unirradiated uranium metal fuel experiment in 1 mM silicate solution at pH of 8 and 30°C.

Figure 3-55. Eh measurements from unirradiated uranium metal fuel colloid tests (0.001 ionic strength, 30°C, pH of 8 and 4).

A similar graph was prepared with the changes in pH values for each test sample, shown in Figure 3-56. The EJ-13 water and carbonate solution remained at a pH of about 8. However, pH in the silicate, iron, and deionized water samples all decreased, including the blanks. Iron and deionized water tests (including blanks) and the silicate blank sample dropped to a pH of about 7. However, the duplicate silicate test samples dropped to between 5 and 6. Results after 2 months of the experiments initially at a pH of 4 are also plotted on Figure 3-56. The largest change was in the iron tests, where the blank and both duplicate sample pH's increased to 7. Most of the samples from the EJ-13, carbonate, silicate, and deionized water had a final pH between 5 and 6. Apparently the solutions were not very stable at a pH of 4, hence, the upward shift in every case (including deionized water) (see References 27 and 28).

The first series of tests with irradiated uranium metal fuel was initiated. However, no data were available from the SNF tests when the release rate project was terminated. Thus, no discussion of colloids from irradiated N-reactor fuel is included.

3.5.3 Colloid Test Conclusions

The proposed colloid experiments with uranium metal fuel were not completed, and many gaps in the data are apparent. However, several conclusions can be drawn from what is available. Visible degradation of the fuel sample is not necessarily an indication of the amount of colloids generated. Uranium metal in the presence of silicate solution was visibly the most corroded and released the most uranium, but the carbonate solution produced the greatest concentration of colloid-sized particles. Both the DLS and the ICP-MS (on sequentially filtrated samples) gave these results. Reaction products were primarily fine grained UO_2 with varying amounts of metaschoepite. Na-boltwoodite was also identified in

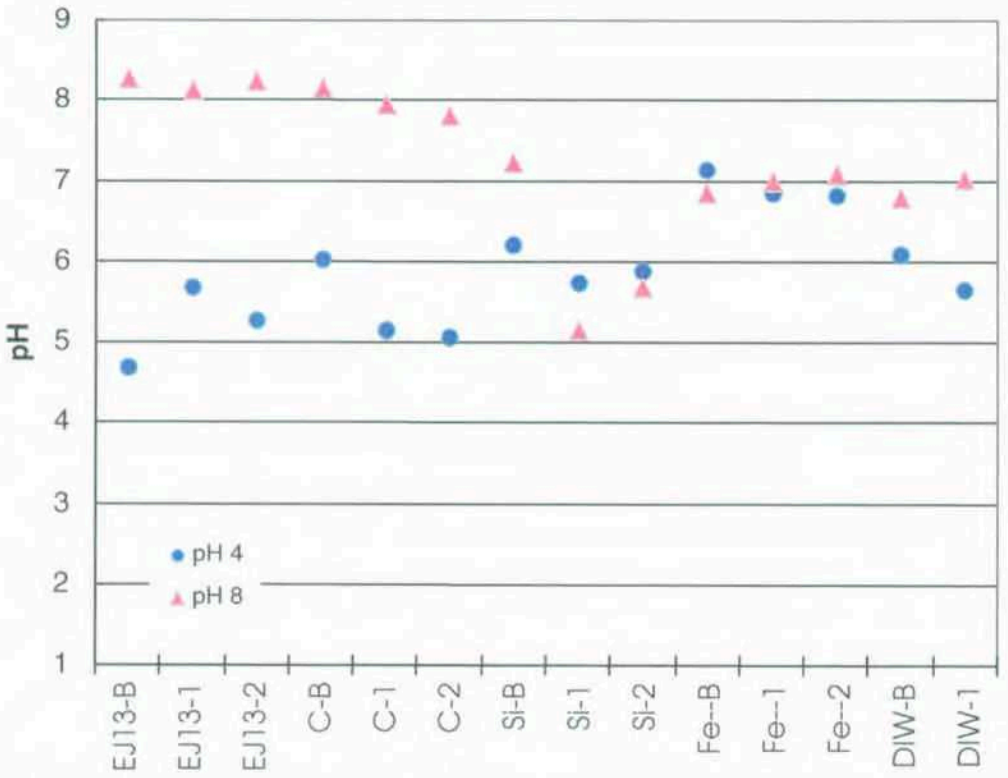

Figure 3-56. pH measurements from unirradiated uranium metal fuel colloid tests (0.001 ionic strength, 30°C, pH of 8 and 4).

the EJ-13 water test. More complex mineral species are expected with the EJ-13 water because it contains a variety of components in solution. Based on these results, the amount of colloids released will be primarily dependent on the carbonate concentration in the water.

Higher pH resulted in larger particle count rates in nearly every solution. Iron and deionized water had very low particulate concentrations regardless of the pH. Size distribution for EJ-13 colloids was bimodal with similar diameters in both pHs. At a pH of 4, the only other size estimate made was for colloids from the silicate test. Although the dimension was similar in the neutral and acidic silicate solutions, a second large size (>1,000 nm) was also seen at a pH of 8. This is likely from agglomeration of the smaller particles, as seen in Figure 3-54. Agglomeration of colloids was seen in the unsaturated drip and static batch tests. Based on the data collected from the release rate experiments with uranium metal fuel, generation of a large number of colloids (at least 10^{12} particles per liter) can be expected. However, they quickly begin to agglomerate into a smaller number of large particles. At some point they may become large enough to settle out of solution, but the data are not sufficient to make that determination at this time.

Table 3-16 summarizes the colloid experimental results using unirradiated uranium metal fuel. Most the solution pHs tend to move to a more neutral point, with the exception of silicate solution originally at a pH of 8. Changes in temperature, ionic strength, and the effects of irradiation were not evaluated due to the premature termination of the release rate test project. Any additional data that change the conclusions set forth in this document will be addressed in a revision at a later date.[29]

Table 3-16. Summary of unirradiated uranium metal colloid test results.

Solution	Initial pH	Final pH	Corrosion	U Released (ppm)	U Colloids (ppm)	Average Size (nm)	Counts (kcps)
EJ-13	8	8.2	Severe	50	7.4	5.8 137	130
C	8	7.9	Moderate	75	48	69	770
Si	8	5.4	Severe	345	9	86 >1,000	110
Fe	8	7.1	Severe	25	11	—	3
DIW	8	7.0	Minor	5	2.5	—	2
EJ-13	4	5.5				4.4 104	30
C	4	5.1				—	3
Si	4	5.8				74	7
Fe	4	6.8				—	7
DIW	4	5.6				—	6

3.6 Comparison with Literature

Many experimenters have studied degradation of uranium in various environments over the last 50 years. For the purposes of release rate, only the oxidation of uranium in water environments will be considered. A comprehensive survey of the available literature on uranium metal oxidation was reported by Hilton.[30] Mechanisms and kinetics referenced in this review will be discussed, followed by a comparison to the experimental results found with the flow through, batch, and drip test methods. Examination of the effects of oxygen on the corrosion rate will be included. A similar literature review

was completed on the generation and stability of colloids.[31] Results from the uranium fuel experiments will be compared to the literature data. Finally, conclusions based on the available information for the expected behavior of uranium metal in the proposed repository will be presented.

3.6.1 Uranium Oxidation Review

Many researchers have extensively studied oxidation of uranium metal in water systems. Hilton summarized the different experiments and attempted to draw a comprehensive description of the reactions (see Reference 30). Uranium corrosion in oxygenated water was found to be the same as uranium in saturated water vapor. Of primary concern are the roles of oxygen and water in the chemical reaction. Anoxic and oxic reactions have been assumed to occur independently in some reports; however, McGillivray et al., proposed they are simultaneous. Uranium oxides are formed according to the following combined equation (*a* and *b* are the fraction of contributions from water and oxygen, respectively).[32]

$$U + a(2 + x)H_2O + b(2+x)/2\ O_2 \rightarrow UO_{2+x} + a(2+x)H_2 \qquad (3\text{-}8)$$

The reaction product UO_{2+x} is nearly stoichiometric, with x less that 0.1. Hydrogen generation, however, is less than expected, ranging between 70 and 95%. It has been proposed that uranium hydride formation may account for the discrepancy in the reaction (see Reference 30). As the contribution from oxygen disappears, *b* equals zero, and *a* equals one, reducing Equation (3-8) to Equation (3-7) for anoxic behavior (assuming stoichiometry) presented in Section 3.2.4.

The mechanism for uranium metal oxidation is not fully understood, but several aspects have been generally accepted as accurate. Initially, an adherent oxide layer forms on the surface of the uranium metal. Then a second layer of adsorbed ions, O^{-2} or OH^-, forms on the oxide layer. Oxygen and hydroxide molecules must diffuse through the oxide layer in order to react with the uranium as electrons diffuse out to the bulk solution (see References 10 and 30). Thickening of the oxide layer will continue until internal stresses from the increased volume cause cracking and spalling of the corrosion products. Competition between the oxic and anoxic reactions is described in a variety of ways. Hilton discussed preferential adsorption of oxide molecules on the oxide layer that prevents hydroxyl ions from diffusing to the uranium metal surface, inhibiting the anoxic reaction. Only when the oxygen content in solution is reduced does anoxic corrosion begin to dominate. Transition from oxic to anoxic dominance is related to temperature and time. Below 70°C, oxygen strongly inhibits the reaction of uranium with water during the initial 1,200 to 1,800 hours. At lower temperatures, the time required to transition from oxic to anoxic is longer. It appears that as oxygen is being consumed by the reaction with uranium, a minimum level of dissolved oxygen necessary for oxic corrosion is reached. Figure 3-57 depicts the range of temperature and dissolved oxygen levels necessary for oxic and anoxic reactions of uranium in water (see References 30).

Reaction kinetics for uranium in oxygenated and anoxic water are linear. As stated earlier, the rate and mechanism of uranium oxidation in water is considered the same as saturated water vapor. In addition, the rate in oxygenated water over long periods of time becomes the same rate as in anoxic water. Thus, only the anoxic water/uranium oxidation kinetics was considered. Hilton collected data reported by Burkart,[33] Troutner,[34] and Trimble[35] and derived a single Arrhenius expression that described all the data. Because each of the earlier documents included some of the same data from the literature, the four equations are nearly identical. Equation (3-9) is the expression derived by Hilton and is valid between temperatures 20 and 300°C (see References 30).

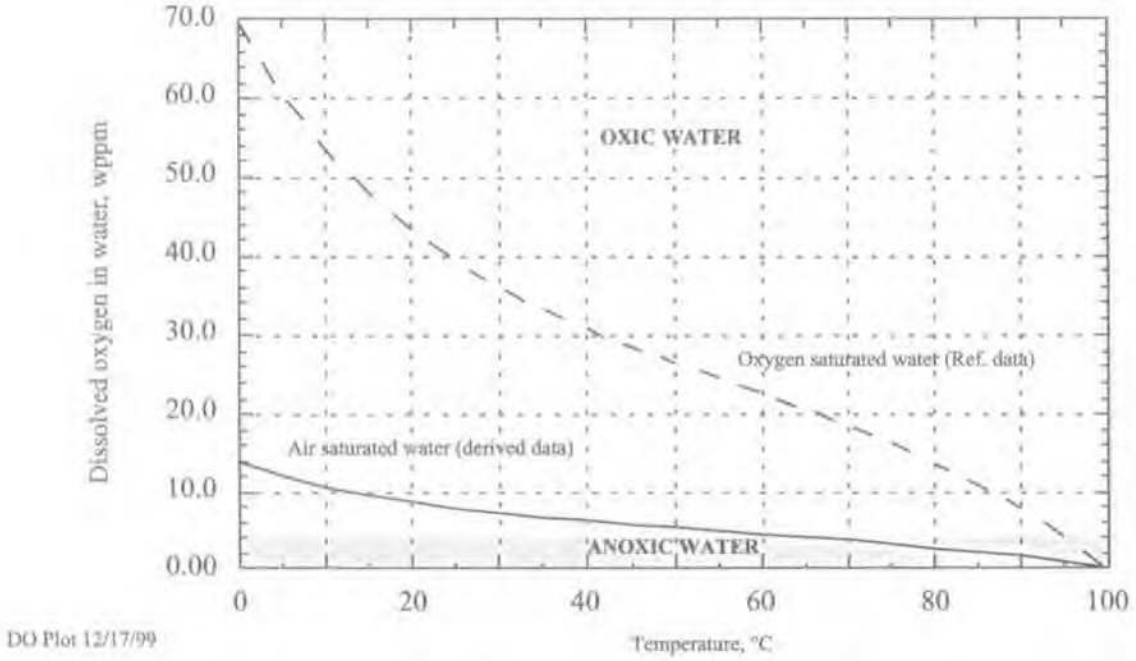

Figure 3-57. Temperature and dissolved oxygen in water necessary for oxic and anoxic corrosion of uranium metal.

$$k_1 = 5.03 \times 10^9 \exp[(-66.4 \pm 2.0 \text{ kJ/mol})/RT] \quad (3\text{-}9)$$

where

k_1 = linear reaction rate in mg U/cm^2/h

R = gas constant equal to 8.314 J/mol/L

T = absolute temperature in K

Hilton also evaluated the reported effects of irradiation on the oxidation of uranium metal. Typically, the metal swelled during the irradiation process, increasing the open porosity. The kinetics of oxidation did not change, however. Irradiation caused swelling resulting in an increase in surface area, and thus the apparent reaction rate (based on surface area) correspondingly increases. For low burnup fuels, little difference is seen between the unirradiated fuel and SNF (see Reference 30).

3.6.2 Experimental Data Comparison

Little information on the physical characteristics of the oxide corrosion products was presented in the Hilton report. The evaluation was focused on reaction kinetics rather than reaction products and water impurities were not considered. However, similar results are seen between the different test methods used in the release rate project. Uranium is oxidized first to UO_2, either as a solid or dissolved in solution. The reaction is fairly rapid, and achieving true dissolution conditions in the flow through tests proved quite challenging. Corrosion products were small particles that dispersed easily, demonstrated by the coating of the unirradiated drip test sample holder. Further oxidation of UO_2 was seen in each test and is assumed to continue until all the material is UO_3. Most of the alteration products were black, but some brown UO_2 (characteristic of stoichiometric composition) was seen in the batch tests. XRD analyses of the products

from all test methods typically produced schoepite and uraninite with minor quantities of other minerals formed with the solution components (such as uranyl silicate in the colloid experiments). Because of the large volume of small particles, a study of colloid generation and stability was included in the work and is discussed in Section 3.6.3 (see References 7, 13, and 25).

Uranium distribution was evaluated in the drip tests indicating about half of the uranium released initially was colloid size, but this value approached zero after eleven months. The colloidal particles appeared to be agglomerating, and by 1 year 90% of the released uranium was larger particles with 10% dissolved (see References 16, 17, and 18). Static batch tests with uranium metal fuel were run for 95 days under anoxic conditions, resulting in 90% of the released material as colloidal and 10% dissolved. Once oxygen was introduced into the system, the colloid fraction decreased, and the dissolved fraction increased (to 35% and 65%, respectively, after an additional 70 days). Agglomeration of the colloids, as seen in the drip tests as well as the increased oxygen supply, may have contributed to the change in distribution (see References 20, 24, and 25).

Other isotopes found in the sludge (corrosion products) from the flow through tests include americium, plutonium, cesium, technetium, and strontium. Table 3-4 lists the percent retention of each isotope assuming a uniform degradation rate and based on the original composition listed in Table 3-3 (see Section 3.2.3). On an average, 100% of the americium and plutonium, about 50% of the technetium, 33% of the strontium, and 10–15% of the cesium remained in the sludge product. (Only the experiments using simulated J-13 well water are presented here. Other solutions had slightly different distributions.) Plutonium release rates, calculated from solution analyses, were generally equal to or less than the uranium values. Low rates are expected because nearly 100% was found in the solids material. Cesium, however, was nearly always much higher, and technetium was at or above uranium rates. In some cases, it appears that cesium release rates increased as Stage 2 corrosion dominated the reaction. The solution analyses agree with the sludge results; very little of the cesium and about half the technetium was found in the solids (see Reference 7).

Some isotopic data were collected from the static batch tests. Plutonium was essentially all colloidal regardless of the amount of oxygen available. Colloid analyses were not performed on flow through samples, but the tests revealed little to no plutonium dissolved in solution. It is possible that the colloidal plutonium seen in the short batch tests agglomerates and precipitates over time and eventually becomes part of the reaction products as seen in the flow through tests. However, the conditions of the two test methods are very different, and the results should not necessarily be the same. Cesium was released at fairly high levels during the anoxic portion of the batch tests, but dropped significantly (from as high as 370 ppb to 50 ppb) when oxygen was supplied to the atmosphere. It appears that the increase in cesium concentrations during Stage 2 corrosion may be attributed to the change from an oxygenated system to an anoxic environment. No estimates of isotopic distribution were predicted in the literature review because the data were collected on uranium metal and not on spent fuel.

Some information was available in the literature regarding the effects of irradiation on uranium metal oxidation. Swelling and subsequent increased porosity were correlated to generate an enhancement factor for irradiation (Equation (3-10)). It was hypothesized that the swelling caused the oxide alteration layer to crack, providing additional pathways to the surface for further oxidation. It was also reported that at low burnup rates, as in the N-reactor fuel, the enhancement factor is negligible (see Reference 30). This does not agree with the results found in the flow through tests. As shown in Table 3-6, the reaction rates with SNF were approximately ten times what was seen with unirradiated fuel. Surface finish may have played a role in the difference, but no data are available to predict the extent of the contribution (see Reference 7). The data from the drip and batch tests are not consistent or complete enough to perform a comparison between the irradiated and unirradiated rates.

$$EF = 0.444 \exp[7.86 \times 10^{-2} S] \quad (3\text{-}10)$$

where

EF = enhancement factor

S = per cent swelling

Data from the flow through tests resulted in an average reaction rate for a specific set of conditions. Drip and batch tests are designed more for the characterization of reaction products and distribution of the isotopes of interest. However, one estimate of the reaction rate from the unirradiated drip test and one from the anoxic stage of the unirradiated batch test was calculated. A summary of the rates with the corresponding test conditions is shown in Table 3-17. The regression equation proposed by Hilton is based on an anoxic environment, and thus should be the upper bound for all the experiments performed (see Reference 30). It is shown as the line on Figure 3-58. Data points from Table 3-17 are also plotted on the graph, and they do indeed fall at or below the line. The three data points that are on the regression line include two flow though test results reported as Stage 2 corrosion and one from the anoxic batch test.

Table 3-17. Summary of uranium metal reaction rates from flow through, drip, and batch tests.

Test Method/Number	Temperature (°C)	pH	Solution	Reaction Rate ($mg/m^2/d$)
Flow—1—SNF	25	8	0.02 M CO_3	155
Flow—2—SNF	75	10	0.02 M CO_3	2,030
Flow—3—SNF	75	8	0.0002 M CO_3	150
Flow—4—SNF	25	10	0.0002 M CO_3	50
Flow—5—SNF	25	5	0.02 M CO_3	63
Flow—6—SNF	75	5	0.0002 M CO_3	199
Flow—7—SNF	25	5	1×10^{-5} M HNO_3	38
Flow—8—SNF	25	3	1×10^{-3} M HNO_3	127
Flow—9—SNF	25	8.5	J-13	3,000
Flow—10—SNF	75	8.5	J-13	—
Flow—1—U	25	8	0.02 M CO_3	10
Flow—8—U	25	3	1×10^{-3} M HNO_3	7
Flow—9—U	25	8.5	J-13	2,300
Flow—9[a]—U	25	8.5	J-13	4
Drip—UNNR1	90	8.5	EJ-13	44,422
Batch—UUBT1	90	8.5	EJ-13	40,000

a. Higher flow rate and smaller surface area.

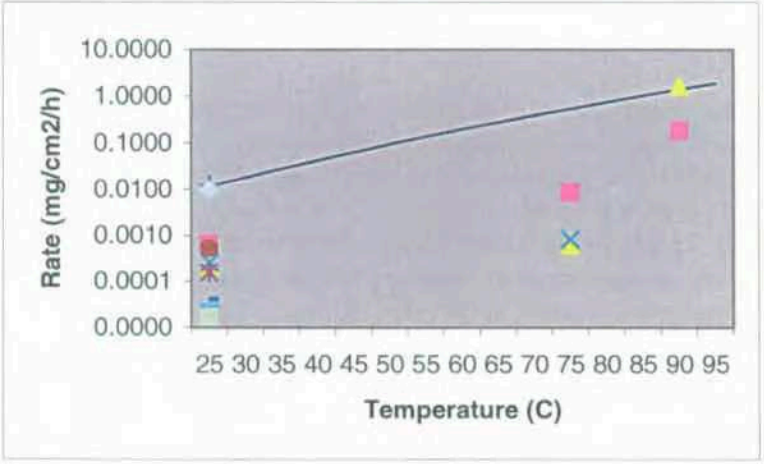

Figure 3-58. Uranium metal oxidation rate from literature compared to experimental data.

Flow through test results with N-reactor SNF indicated two stages of corrosion: one initial, relatively stable reaction followed by a rapid, unpredictable rate. One proposed cause of the apparently different regimes is the amount of oxygen available for reaction. When sufficient oxygen is present, uranium reacts and is dissolved into solution. If the system becomes anoxic, then uranium forms solid reaction products, and hydrogen is produced. An experiment demonstrating the oxic and anoxic effects on uranium degradation using the flow through test method was discussed in Section 3.2.4.3. The results presented in Figure 3-20 showed distinct differences in the two regions and supported the theory of anoxic conditions causing Stage 2 corrosion (a drop in uranium liquid sample concentration, production of hydrogen, generation of reaction solids). A second oxic/anoxic test was performed with the batch test configuration. Hydrogen was produced during the anoxic stage, and dissolved uranium increased during the oxic portion, similar to the flow through results. An induction period prior to detection of hydrogen, even in strongly anoxic environments, may be due to the formation of transient hydrides. Increases in cesium release (discussed earlier) during the anoxic portion of the test may correlate with a similar trend in flow through tests during Stage 2 corrosion (see References 7 and 20).

3.6.3 Uranium Colloid Review

An extensive literature review of the colloid issues that have relevance to a geological repository was completed for the NSNFP. Radionuclide-associated colloids generated in the SNF degradation process could increase the release values of specific sparingly soluble isotopes. Recent field investigations have found that radionuclides associated with colloids have been transported significantly farther than anticipated by the current mathematical models.[36,37,38] Colloids generally are classified as aquatic (groundwater), real, or pseudocolloids. Real colloids and pseudocolloids were introduced in Section 2.2.5. Groundwater colloids are naturally occurring particles of either inorganic or organic material. Natural abundance can range between 10^8 to 10^{17} particles/L. Stability of colloids, defined as remaining suspended in solution, is dependent on ionic strength, temperature, Eh, and pH. Colloid size can also be a factor for transport concerns because the particle typically must pass through the soil porosity. Redox potential controls the speciation and solubility of radionuclides, which affects their ability of form real colloids as well as pseudocolloids. Surface charge defines the attraction of the colloid to a solid surface (such as soil), which can remove a colloid from the bulk solution (from charge attraction) or enhance the colloid transport (through charge repelling). The point of zero charge is the unique pH where each mineral surface has a charge of zero. Above the point of zero charge, the surface charge is positive; and below the point of zero charge, the surface charge is negative. The closer the pH is to the point of zero

charge for the particular mineral, the more stable the colloid. Thus, changing the pH can result in alterations in the colloid stability, transport, and adsorption characteristics (see Reference 31).

Of particular importance to disposal of DOE fuels is the potential for specific radionuclides to be released as colloids in solution concentrations above the solubility limit. Protactinium, thorium, uranium, plutonium, radium, neptunium, technetium, and iodine releases have been in question due to either an expected high potential for release or the uniqueness to DOE fuels. Traexler reviewed the speciation, sorption, laboratory test results, and field data for each element in question. As expected, a large amount of information is available on uranium, and nothing could be found concerning protactinium; at least some information was presented on each of the other elements. Traexler also reviewed colloid studies from natural analogs and high-level waste glasses (see Reference 31).

Uranium will be present in one of two valences, U(IV) or U(VI). U(V) exists but is not applicable to repository conditions. The uranyl ion, UO_2^{2+}, dominates in oxidizing environments like that found in the proposed repository at YMP and is soluble in the parts per million range. U(IV) is far less soluble (parts per billion) and dominates in a reducing environment. Uranium also complexes readily with many elements including carbonate, silicate, potassium, and calcium (readily available in groundwater) forming various compounds depending on pH and redox potential. Sorption studies have been performed with iron oxides, silica, kaolinites, and phosphates at various ionic strengths and pH. Reasonable models were developed with empirical parameters, but additional work is required before an effective theoretical model can be proposed. Most of the uranium laboratory experiments were performed with high-level waste glass and commercial spent fuel (primarily UO_2). Although colloid releases were initially high, they soon began to decrease due to agglomeration. As the solid surface area to solution volume ratio increased, the time for the colloid concentration to drop decreased. Degradation of the waste form glass also causes an increase in solution ionic strength (primarily from the silica) that decreases the stability of colloids and may cause the decrease in concentration. Sources of the colloids included spalling of waste form reaction products, real colloids of radionuclides, and pseudocolloids. The minerals identified from the glass experiments were uranium silicate, weeksite, schoepite, and soddyite. SNF tests produced these as well as more complex forms with cesium, barium, molybdenum, iron oxides, and phosphates. Lower burnup fuel released ten times as many actinides as the higher burnup fuel. Cesium was released into solution 100 times faster than uranium, plutonium was 0.1 times less, and neptunium was 0.001 times less. Generally, unirradiated UO_2 provided a reasonable surrogate for SNF and showed a paragenetic sequence similar to natural uraninite deposits (see Reference 31).

Plutonium chemistry is much more complex than uranium as it exists in five oxidation states and forms cationic, anionic, and neutral species. Solubility is low in all reported environments but the ability to form colloids varies considerably (ranges from 0% to 100%) based on temperature and pH. Laboratory tests with high-level waste indicated plutonium was leached faster under oxic conditions than anoxic due to the change in valence. As much as 99% was released as colloids. Plutonium was found to adsorb onto smectites and manganese oxides but not to iron minerals and was effectively retarded by bentonite. Field tests at the Nevada Test Site found plutonium had traveled over 1.3 km in 30 years via adsorption to natural colloids, though the true concentration at the site is questionable. Plutonium and americium were detected in two cases at Los Alamos National Laboratory farther than would be expected by transport models that do not consider colloid-assisted mobility. Other analyses at the Savannah River Site indicated about 50% of the plutonium in a secondary cooling system pond appeared to be associated with colloids (see Reference 31).

Neptunium has five valence states and forms a number of hydroxy-carbonate compounds, reflecting the complexity of its chemistry. A number of sorption experiments have been performed by several researchers using silica, iron minerals, alumina, volcanic tuff, bentonite, and montmorillonite. Resulting adsorption coefficients differed by orders of magnitude, and some neptunium species did not

sorb to the materials evaluated. A strong dependence on pH and redox conditions was also indicated. Some evidence of enhanced neptunium transport due to bentonite colloids was presented, but montmorillonite proved to be effective in retarding transport. Neptunium-associated colloids have been identified in laboratory column tests and appeared to be maximized at low concentrations and near standard redox potentials (see Reference 31).

Technetium typically forms TcO_4^-, the pertechnate anion, under oxidizing conditions. The negative charge on the ion results in behavior different than the positive charge found on most metals groups. Pertechnate is highly soluble and not easily sorbed, nor is it expected to be incorporated into the SNF alteration phases due to the negative charge. Tc(IV) may also be present in small amounts but is more prevalent in reducing environments. It is less soluble and readily sorbs to minerals and clays, so it is more likely to form colloids. Iodine will also be present as a negative ion, I^-. Although sorption to mineral surfaces is not likely due to the charge, organic material may have an influence. In addition, mineral colloids with neutral points of zero charge could be altered to a positive surface charge by changes in the solution pH. Although some field data presented in the literature claimed iodine associated colloids were responsible for observed transport behavior, wind usually accounts for most of the movement (see Reference 31).

Thorium has a stable isotope in the plus four state that is often used as a proxy for uranium, plutonium, and neptunium IV, which are not very stable. Some data are available on sorption to silica, alumina, titanium oxide, and natural systems but little information is specific to colloids. As much as 50% of the thorium found in a uranium ore deposit was associated with colloids, and in one case 78% was colloidal in Gulf of Mexico samples. In most cases, it was concluded that thorium does not readily desorb (see Reference 31).

Very little data are available on radium. Radium readily sorbs to bentonite and smectite and is generally retained by clays and soils. No information was found on radium-associated colloids (see Reference 31).

Predictive models have been formulated for the transport of certain radioisotopes based on reversible and irreversible sorption coefficients and assumed environmental conditions. Sensitivity studies are then performed to define the susceptibility of the system to specific parameters. Unfortunately, the available input data are very small compared to the complexity of the system. Each possible mineral phase has different sorption characteristics at different pH, Eh, temperature, and ionic strengths. In addition, there are hundreds of potential minerals. It is clear that the model will necessarily have to incorporate certain assumptions on behavior, followed by parameter variations to estimate sensitivities (see Reference 31).

3.6.4 Colloid Data Comparison

Colloid generation and characterization data are available from the uranium metal colloid experiments described in Section 3.5 and the unsaturated drip and static batch tests (Sections 3.3 and 3.4, respectively). Although a number of uranium oxyhydroxides were produced, the most common were uraninite, schoepite, and metaschoepite, regardless of test method. Colloids of clay minerals, particularly smectite and uranyl silicates, were also identified. It was proposed that most of the colloids were either waste form particles spalled from the corroding fuel or pseudocolloids from minerals present in the groundwater. Reports in the literature generally make the same observations (see References 14, 16, 17, 20, 27, 28, and 31).

In all test methods, the colloids appear in two size ranges, about 5–10 nm and 100–300 nm. Further analyses indicate that small colloidal particles of uranium oxide agglomerate and attach to clay

colloids that are also agglomerating. Eventually the uranium colloid concentration drops, probably due to particles destabilizing as they grow too large to remain suspended. Traexler reported that colloids probably did not play a major role in transport of uranium or other radionuclides in natural systems. Although they were identified in some cases, it appears the capacity for transport was low. This observation may be related to the agglomeration phenomenon seen in the laboratory tests, or the colloids could be strongly sorbed to the soil surface (see References 14, 16, 17, 20, 27, 28, and 31).

Drip test results indicated uranium colloids were initially high (about 40% of the released uranium) but had dropped to essentially none after about 1 year. Uranium colloids from the batch tests were significant, as much as 90%. However, the tests were designed to compare oxic and anoxic conditions for a short duration. Colloid concentrations dropped when oxygen was introduced to the test. Time of exposure may have played a role in the decrease due to agglomeration and may have occurred eventually without the addition of oxygen. The colloid tests were run for 4 months in different solution chemistries with varying results. In silicate solution, only about 3% of the uranium released were colloidal, increasing to about 15% in EJ-13 and to 50% or more in the iron, carbonate, and deionized water. Laboratory test results in the literature report the same phenomenon, initially a large release of uranium colloids that decreases over time. Agglomeration of the particles has been seen by TEM analysis, which could account for the decrease in colloid concentration. Increases in pH in the colloid tests indicated larger sized particles; data on the amount generated were not available at the time this document was printed due to early termination of the project. The effects of ionic strength and temperature were also not completed due to project termination (see References 14, 16, 17, 20, 27, 28, and 31).

Plutonium colloid concentrations in the drip tests also started out high, at 75%, and ended at about 8% after 11 months. In the batch tests, plutonium was essentially all colloidal during the entire experiment (oxygen content had no effect). Literature data indicate that plutonium-associated colloid concentrations range from near zero to 100% depending on environmental conditions, but appear to be at the higher range most often. Neptunium (evaluated in the drip tests) and cesium (from the batch tests) did not appear as colloid-sized particles during the experiments. Literature data on neptunium indicated low solubility and a low propensity for colloid formation. No other isotopes were evaluated in the release rate tests due to low concentrations. Only unirradiated fuel was examined in the colloid tests because the project was cancelled prior to initiation of the irradiated fuel experiments (see References 14, 16, 17, 20, 27, 28, and 31).

3.6.5 Conclusions

Four different experimental methods have been used to increase our understanding of the degradation processes of uranium metal fuel. The results were compared with two literature reviews to evaluate for consistency. Several conclusions, which are outlined below, can be made about the expected uranium metal SNF degradation in a repository.

Hilton's review of the published data on oxidation of uranium metal indicated that eventually the corrosion became dominated by the anoxic reaction, regardless of the available oxygen in the bulk environment. A regression of the anoxic data resulted in an expression that should be a reasonable upper bound for modeling uranium metal fuel degradation (Equation (3-9)). Figure 3-58 displays the expression with the data generated by the release rate experiments. Based on these tests, Equation (3-9) is indeed an upper limit for modeling purposes.

Alteration products from uranium metal consist of initially fine grained UO_2 that are followed by a variety of uranium oxyhydroxides as oxidation continues. Eventually the products would be entirely UO_3 as U(IV) is oxidized to U(VI) if no other elements were present during the reactions. However, contaminants in the water also combine with the uranium to form potentially hundreds of different

mineral compounds. The most common form was uraninite, schoepite, and metaschopite. Uranium reacts very quickly in water, as shown in the kinetics expression above. At some point in the reaction sequence, the reaction appears to accelerate. The actual cause of increased degradation of uranium under some conditions is probably a combination of a number of factors. Equations (3-6) (oxic) and (3-7) (anoxic) are competing with each other with varying degrees of dominance. Initially, oxygen should readily react with the uranium surface; thus reaction 3.6 is dominant. As the sample begins to degrade, an oxide layer covers the surface and acts as a barrier to further oxidation. Eventually diffusion through the oxide layer becomes the limiting factor. The uranium oxide layer is a good ion and semiconductor with a structure that OH ions can readily move through but O_2 ions cannot. Thus, the faster water reaction defined in Equation (3-7) becomes dominant after some indeterminate period of time. An intermediate hydride may also form and then subsequently react further to release hydrogen at a later time. This would account for the apparent induction period seen during the anoxic region of the flow through test displayed in Figure 3-20 and identified in the anoxic batch test shown in Figures 3-39 and 3-41.

Significant changes to the sample surface occur during the dissolution process. Increases in the roughness result in larger surface areas, which cause dissolution rate calculations to appear artificially high (see Equation (3-1)). Uranium metal SNF specimens were sectioned with either a slow-speed wafering saw or a milling machine; thus the original surface was relatively smooth. Figure 3-19 is a photograph of an SNF specimen after exposure to test 3A showing obvious surface roughness. Increases in the surface area likely played a role in the calculated increases in dissolution rates.

A large percentage of the uranium released early in the degradation process appears as colloid-sized particles. They were present as spherical UO_2 and entrained in clay colloids. Size distributions of about 10 nm and 200 nm represent the two types of colloids. Over time, the particles agglomerated, and the percent of uranium released as colloids dropped to nearly zero. Literature documents report a similar phenomenon. The amount of plutonium released as colloids varied in the literature, but was often high. Results from the release rate tests indicated plutonium colloids were near 90%. No other isotope evaluated in the experiments showed a tendency toward colloid formation.

Data on isotopic distribution were collected during the experiments, and some general observations were made. The plutonium was incorporated into the reaction products rather than released into solution. However, what was released was nearly all colloids. About half of the technetium was found in the alteration products and half in the solution; no analysis for technetium colloids was performed. Only a small amount of the cesium was entrained in the reaction products, and none appeared as colloidal. Most of it was dissolved in solution.

3.7 References

1. B. J. Makenas, "Activity Plan for Release Rate Testing of Uranium Metal Spent Nuclear Fuel," DOE/NSNF/PP-012, Revision 0, June 1998.

2. M. M. Goldberg, "Test Plan for Reactions Between Irradiated Uranium Metal Fuel and J-13 Well Water Under Unsaturated Conditions," SNF-3A-052, Revision 0, December 18, 1998.

3. S. C. Marschman, T. D. Pyecha, and J. Abrefah, "Metallographic Examination of Damaged N Reactor Spent Nuclear Fuel Element SFEC5,4378," PNNL-11438, UC-602, August 1997.

4. T. S. Bray, "Test Plan for the Characterization of Metallic Uranium Fuel," SNF-3A-078, Revision 0, May 17, 1999.

5. T. S. Bray and R. V. Strain, "Characterization of N-Reactor Fuel Samples," Argonne National Laboratory Intra-Laboratory Memo, October 4, 2000.

6. W. J. Gray and R. E. Einziger, *Initial Results from Dissolution Rate Testing of N-Reactor Spent Fuel Over a Range of Potential Geologic Repository Aqueous Conditions*, DOE/SNF/REP-022, PNNL-11894, UC-802, Revised April 1998.

7. W. J. Gray, "Test Plan for Dissolution Rate Testing of Hanford N-Reactor Spent Nuclear Fuel," April 1998.

8. W. D. Wilkinson, *Uranium Metallurgy, Volume II: Uranium Corrosion and Alloys*, New York: Interscience Publishers, 1962.

9. W. J. Gray, "Addendum 1 to Test Plan for Dissolution Rate Testing of Hanford N-Reactor Spent Nuclear Fuel," February 1999.

10. Danon, J. E. Koresh, M. H. Mintz, "Temperature Programmed Desorption Characterization of Oxidized Uranium Surfaces: Relation to Some Gas-Uranium Reactions," *Langmuir*, Vol. 15, No.18, 1999, pp. 5913–5920.

11. M. M. Goldberg, "Test Plan for Reactions Between Irradiated Uranium Metal Fuel and J-13 Well Water Under Unsaturated Conditions," SND-3A-052, Revision 0, December 18, 1998.

12. C. V. Shelton-Davis, INEEL, to W. L. Hurt INEEL,"ANL-E Release Rate Test Program Review Trip Report," M. M. Goldberg and D. L. Bowers Presentation, June 22, 1999.

13. M. M. Goldberg, D. L. Bowers, J. A. Fortner, "Corrosion of Unirradiated N-Reactor Fuel in Unsaturated Test Conditions," Draft.

14. C. V. Shelton-Davis, INEEL, to Distribution, "Release Rate Test Team Meeting Minutes from November 4, 1999," M. M. Goldberg and D. L. Bowers Presentation, November 16, 1999.

15. C. V. Shelton-Davis, INEEL, to Distribution, "May 11, 2000, Release Rate Test Review Meeting Minutes," M. M. Goldberg Presentation, August 10, 2000.

16. J. A. Fortner, C. J. Mertz, M. M. Goldberg, C. V. Shelton-Davis, "Corrosive Alteration of N-Reactor Fuel Exposed to Simulated Groundwater," 9th International High-Level Radioactive Waste Management Conference, May 2001.

17. C. V. Shelton-Davis, INEEL, to Distribution, "Meeting Minutes from NSNFP Release Rate Test Program Held on May 3, 2001," J. A. Fortner Presentation, June 7, 2001.

18. C. V. Shelton-Davis, INEEL, to Distribution, "NSNFP Release Rate Test Meeting Minutes from November 14, 2001," J. A. Fortner Presentation, December 19, 2001.

19. M. D. Kaminski, "Test Plan for Reactions Between Irradiated Metallic Uranium Fuel and J-13 Well Water Under Saturated Conditions," SNF-3A-209, Revision 0, January 26, 2001.

20. M. D. Kaminiski, "Batch Tests with Unirradiated Uranium Metal Fuel Program Report," ANL-01/33, December 2001.

21. J. M. Haschke, "Corrosion of Uranium in Air and Water Vapor: Consequences of Environmental Dispersal," *Journal of Alloys and Compounds*, Vol. 278, August 21, 1998, pp. 149–160.

22. M. M. Baker, L. N. Less and S. Orman, "Uranium + Water Reaction Part 1. Kinetics, Products, and Mechanism," *Transactions of the Faraday Society*, Vol. 108, No. 62, 1966, pp. 2513–2524.

23. C. A. Mertz, "Colloid-Associated Radionuclide Concentration Limits," Office of Civilian Radioactive Waste Management Analysis Model Report, ANL-EBS-MD-000020, Revision 00, ICN 01, June 20, 1999.

24. C. V. Shelton-Davis, INEEL, to Distribution, "Meeting Minutes from NSNFP Release Rate Test Program Held on May 3, 2001," M. D. Kaminski Presentation, June 7, 2001.

25. C. V. Shelton-Davis, INEEL, to Distribution, "NSNFP Release Rate Test Meeting Minutes from November 14, 2001," M. D. Kaminski Presentation, December 19, 2001.

26. Argonne National Laboratory, "Test Plan for the Characterization of Spent Nuclear Fuel Colloids," SNF-3A-121, Revision 0, March 6, 2000.

27. C. V. Shelton-Davis, INEEL, to Distribution, "Meeting Minutes from NSNFP Release Rate Test Program Held on May 3, 2001," C. J. Mertz Presentation, June 7, 2001.

28. C. V. Shelton-Davis, INEEL, to Distribution, "NSNFP Release Rate Test Meeting Minutes from November 14, 2001," C. J. Mertz Presentation, December 19, 2001.

29. M. M. Goldberg, ANL, to C. V. Shelton-Davis, INEEL, "Monthly Report for February 2001," July 30, 2001.

30. B. A. Hilton, *Review of Oxidation Rates of DOE Spent Nuclear Fuel, Part 1: Metallic Fuel*, DOE/SNF/REP-054, Revision 0, September 2000.

31. K. A. Traexler and R. C. Ewing, *Colloid Formation and the Potential Effects on Radionuclide Transport in a Geologic Repository for Spent Nuclear Fuel*, DOE/SNF/REP-070, January 2002.

32. G. W. McGillivray, D. A. Geeson, and R. C. Greenwood, "Studies of the Kinetics and Mechanism of the Oxidation of Uranium by Dry and Moist Air—a Model for Determining the Oxidation Rate Over a Wide Range of Temperatures and Water Vapour Pressures," *Journal of Nuclear Materials*, Vol. 208, 1994, pp. 81–97.

33. M. W. Burkart and ed. "Development and Properties of Uranium-Base Alloys Corrosion Resistant in High-Temperature Water, Part III. Corrosion Mechanism of Uranium Base Alloys in High Temperature Water," WAPD-127-Part III, Westinghouse Electric Corporation, Pittsburgh, PA, 1957.

34. V. H. Troutner, "Mechanisms and Kinetics of Uranium Corrosion and Uranium Core Fuel Element Ruptures in Water and Steam, HW-67370, Hanford Atomic Products Operation, 1960.

35. D. J. Trimble, "Reaction Rate Constant for Uranium in Water and Water Vapor," HNF-2853, Duke Engineering & Services Hanford, 1998.

36. A. B. Kersting, D. W. Efurd, D. L. Finnigan, D. J. Rokop, D. K. Smith, and J. L. Thompson, "Migration of Plutonium in Ground Water at the Nevada Test Site," *Nature (London)*, Vol. 396, No. 6714, 1999, pp. 56–59.

37. J. F. McCarthy and J. M. Zachara, "Subsurface Transport of Contaminants," *Environmental Science and Technology*, Vol. 23, 1989, pp. 496-502.

38. J. L. Means, D. A. Crerar, and J. O. Duguid, "Migration of Radioactive-Wastes-Radionuclide Mobilization by Complexing Agents," *Science*, Vol. 200, No. 4349, pp. 1477–1481.

4. ALUMINUM-BASED FUEL

Aluminum-based fuel group has a fairly high fissile content and is third highest in the amount of technetium and neptunium available for release (see Table 4-1). Samples are also readily available, and early modeling evaluations indicated a potential for a significant impact on the performance assessment. Thus, samples from this group were chosen for experimental studies. An activity plan was prepared outlining the recommended test methods: fuel characterization, flow through tests, unsaturated drip tests, static batch tests, and electrochemical tests.[1] Most of the testing done to date was performed according to the test protocols outlined in ASTM C 1431-99.[2] Colloid tests were added to the planned test matrix after the activity plan was issued because early results indicated aluminum colloids were produced during dissolution and they could pose a negative effect on the performance assessment. Quality assurance requirements were also defined in the activity plan. Test method details are discussed in Section 2. The flow through, electrochemical, characterization, unsaturated drip tests (with unirradiated fuel), and some colloid analyses were completed prior to project shutdown.

Four plate fuel types from the aluminum-based fuel group were selected for release rate tests including uranium aluminum alloy (UAl), uranium aluminide (UAl_x), uranium silicide (U_3Si_2), and uranium oxide (U_3O_8). All the aluminum-based fuels addressed in this study consist of particles (either UAl alloy, UAl_x, U_3Si_2, or U_3O_8) dispersed in a continuous aluminum phase. Only the UAl fuel had a small amount of uranium (<1%) dissolved into the aluminum matrix. In addition, a melt-dilute process was planned with highly enriched aluminum fuels to reduce their criticality risk. These materials are expected to be metallurgically very similar to the UAl_x material. Samples from each of the four fuels were used in the flow through test matrix. Unirradiated surrogates of a wide variety of compositions were used in the electrochemical experiments and comparative flow through tests. Below is list of the specific fuel samples selected for testing.[3] The irradiated aluminide fuel sample shown below (or melt-dilute samples, if available) was selected for the unsaturated drip, static batch, and colloid tests because it can also simulate the melt-dilute waste form. However, none of these experiments will be performed because the release rate project ended prior to test initiation.

4.1 Characterization

Four coupons of each SNF selected in Table 4-1 were sectioned, and the aluminum cladding was removed from one side to expose the actual fuel material. One coupon from each group was used for characterization and metallography. Photomicrographs of the metallographic samples were made for subsequent image analysis. Measurements of 5 to 12 different areas of each photomicrograph provided the percentage of the surface area that consisted of fuel particles. Total geometric areas were then measured so the fuel particle area and aluminum matrix areas could be calculated. Figure 4-1 shows the microstructure of the four fuel types that are included in this test matrix (see References 3 and 4).

Table 4-1. Aluminum-based spent nuclear fuel release rate test samples.

Fuel Type	Plate Number	Enrichment (%^{235}U)	Burnup (%)
UAl	Mk-22, 46-30	80	40
UAl_x	NLE 451	45	73
U_3O_8	T292X	45	72
U_3Si_2	A-90	20	93

Figure 4-1. Photomicrograph of uranium aluminum alloy spent nuclear fuel, plate number Mk-22, 46-30.

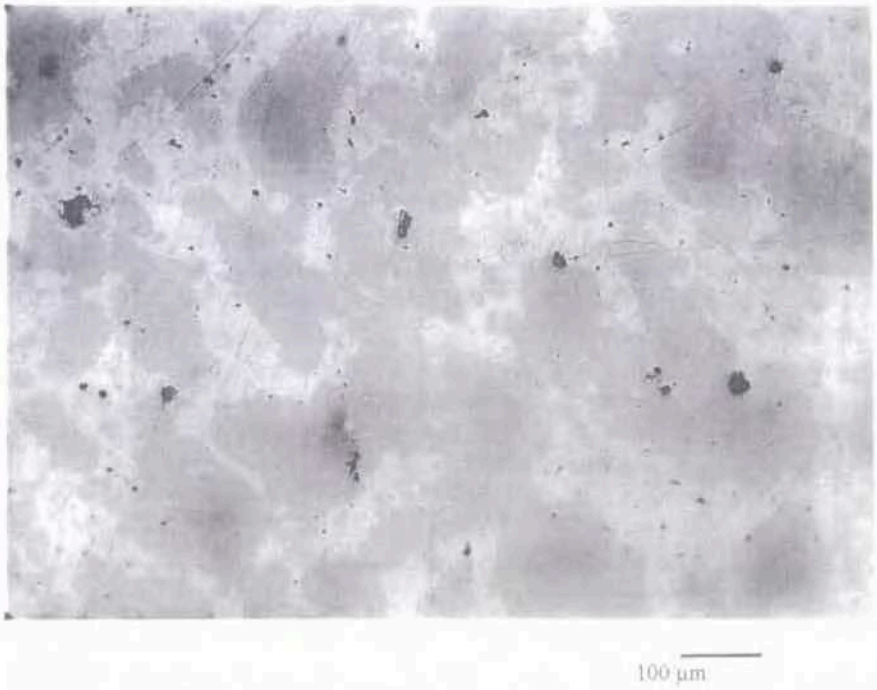

Figure 4-2. Photomicrograph of uranium aluminide spent nuclear fuel, plate number NLE 451.

Figure 4-3. Photomicrograph of U_3O_8 spent nuclear fuel, plate number T292X.

Figure 4-4. Photomicrograph of U_3Si_2 spent nuclear fuel, plate number A-90.

Three more sections (about 1 gram samples) from each fuel characterization coupon were dissolved and analyzed in triplicate. Dissolution consisted of an initial immersion in hydrochloric acid (HCl) followed by an addition of nitric acid (HNO_3). The U_3Si_2 fuel did not completely dissolve. Thus the remaining material was fused with potassium hydroxide (KOH) and then dissolved in the HCl/HNO_3 mixture. All solutions were analyzed for aluminum, uranium, $^{239/240}Pu$, ^{238}Pu, ^{137}Cs, ^{99}Tc, and ^{90}Sr. The U_3Si_2 residue was predominantly silicon with a negligible amount of other elements or radionuclides. Table 4-2 lists the results from the image analysis and inventory analyses (see References 3 and 4).

4.2 Dissolution Tests

Flow through dissolution experiments with aluminum-based fuel were performed at two test facilities, PNNL and the Savannah River Site. Some tests were performed with irradiated spent fuel (conducted at PNNL), and some were done with unirradiated surrogates (at both facilities). Additional static and electrochemical experiments with unirradiated samples were conducted at the Savannah River Site. A matrix of solution, temperature, and material composition was designed to provide information on a variety of environmental conditions and disposal configurations. Specific conditions are discussed below for each test method.

4.2.1 Unirradiated Sample and Solution Preparation

Unirradiated uranium aluminum alloy fuel surrogates were used to simulate aluminum-based spent fuel. Four alloy compositions were prepared: 10%, 13.2% (eutectic), 19%, and 25% uranium in aluminum. The 19-UAl composition is comparable to the irradiated UAl fuels evaluated by this experimental project. Other alloy compositions were chosen to simulate possible melt-dilute products. (Some of the high activity aluminum-based spent fuels will be melted and diluted with low activity aluminum fuels to reduce criticality risks after disposal.) Bulk aluminum (1,100 Al) ingots were melted with depleted uranium in an induction furnace and then cast into molds and air cooled. Metallographic analyses indicated a fairly uniform composition across the surface of the alloy samples. A portion of the 13.2-UAl and 25-UAl and all of the 19-UAl alloys were subsequently extruded and rolled to produce a wrought structure. Coupons were then cut from the cast or wrought material and polished with 1-μm diamond paste. PNNL evaluated only the 19-UAl alloy, but the Savannah River Site tested all four compositions (see References 3 and 4).

Table 4-2. Average composition of triplicate aluminum-based SNF test samples.

Fuel Type	UAl	UAl_x	U_3O_8	U_3Si_2
Fuel particle area (%)	31	67	51	66
Al (g/g)	0.763	0.796	0.763	0.387
U (g/g)	0.144	0.122	0.134	0.449
Initial U (g/g)	0.212	0.182	0.198	0.550
$^{239/240}Pu$ (mCi/gU)	0.61	1.74	1.69	1.26
^{238}Pu (mCi/gU)	28.8	21.3	16.5	15.5
^{137}Cs (mCi/gU)	1,210	1,230	1,140	500
^{99}Tc (mCi/gU)	0.108	0.113	0.106	0.040
^{90}Sr (mCi/gU)	1,050	1,020	960	410

SEM examinations were made of the surfaces prior to any testing. Photomicrographs of selected samples are shown in Figure 4-5. View (a) shows the 10-UAl cast material; the dark areas are the primary aluminum phase, and the light skeletal areas are the eutectic phase. As expected, the 13.2-UAl had the greatest fraction of the eutectic phase and appears as lamellae of aluminum and the UAl_4 phase in View (b). Some UAl_3 phase is also present as the light blocky structures. View (c) is the 25 UAl cast material, showing more of the UAl_3 phase and small amounts of the UAl_4 phase (seen as diamond shapes with a dark, aluminum center). The last view demonstrates the crushing and alignment of 13.2 UAl material after rolling to create a wrought structure. Additional SEM analyses were performed after exposure to the test environment to evaluate possible degradation processes (see Reference 4).

At PNNL, three solutions were evaluated with unirradiated fuel samples at ambient temperature (~25°C): 2×10^{-2} M carbonate solution (pH = 8), 10^{-3} M HNO_3 solution (pH = 3), and simulated J-13 well water (pH ~8) (see Reference 3). The simulated J-13 well water was prepared as described in Section 2.3. Flow through tests at the Savannah River Site evaluated variations of simulated J-13 well water including low pH (modified with nitric acid to a pH of about 3), high pH (modified with sodium hydroxide to a pH of about 11), and high chloride content (modified with sodium chloride to about 60 ppm Cl^-). Some experiments were at 25°C, and others were at 90°C (see Reference 4).

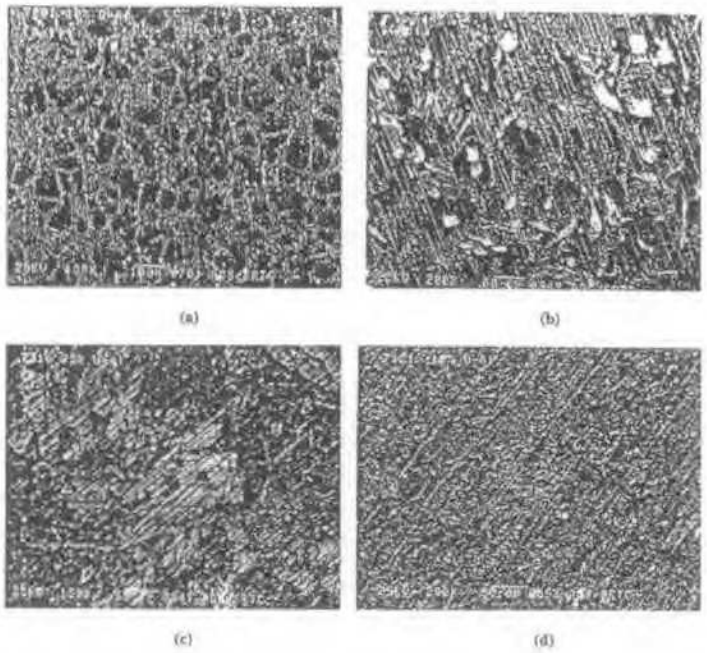

Figure 4-5. Microstructures of (a) 10-UAl cast material, (b) 13.2-UAl cast material, (c) 25-UAl cast material, and (d) 13.2-UAl wrought material.

4.2.2 Irradiated Flow Through Tests

Flow through tests with irradiated spent fuel were conducted at PNNL with the test equipment described in Section 2.2.2. Four aluminum-based fuel types were tested, as identified in Table 4-1. The aluminum cladding was removed from one side by polishing with 1 µm diamond paste, exposing fuel meat on five of the six surfaces. Three solution chemistries were evaluated with each of the four SNF materials:

- Bicarbonate, 2×10^{-2} M $NaHCO_3$, pH = 8

- Nitric Acid, 10^{-3} M HNO_3, pH = 3
- J-13, simulated groundwater from J-13 well near the YMP site (Section 2.3).

All twelve tests (four materials using three solutions each) were conducted at ambient temperature, about 25°C. Solution flowed upward through the specimen cells at a rate of approximately 0.2 mL/min. A quartz liner was added to the test vessel to prevent galvanic interaction. Samples were initially taken twice per week, but were reduced to once per week or less after the system was stabilized. Blanks were used during sampling to determine the potential for contamination in the sampling process. A problem was found early in the tests with J-13. The source was identified and eliminated, but some of the J-13 test data (prior to day 50) were not used in the final analysis (see Reference 3).

Dissolution rates were calculated from the concentration of uranium, aluminum, or other isotopes measured in the samples taken from the effluent. Data were normalized to the effective surface area based on the geometric area and on the fuel particle area for the component of interest (U, Al, Pu, Cs, Tc, or Sr). The following formulas were used to calculate the rates.

$$R_g = (C_i F)/(A_1) \quad (4\text{-}1)$$

$$R_f = (C_i F)/(A_2 f_i) \quad (4\text{-}2)$$

$$R_a = (C_a F)/(A_3) \quad (4\text{-}3)$$

where

R_g = component i dissolution rate based on fuel meat surface area ($mg/m^2/d$)

C_i = concentration of component i in effluent (mg/mL)

F = flow rate of test solution (mL/d)

A1 = geometric surface area of fuel meat, five of the six surfaces (m^2)

Rf = component i dissolution rate based on the particle surface area ($mg/m^2/d$)

A2 = surface area of fuel particles (m^2)

fi = initial inventory concentration of component i relative to uranium (mg/mg)

Ra = aluminum dissolution rate based on the geometric surface area ($mg/m^2/d$)

Ca = concentration of aluminum in effluent (mg/mL)

A3 = geometric surface area of coupon, six surfaces, less particle surface area (m^2)

Equation (4-1) gives the dissolution rate of a component (uranium, plutonium, cesium, technetium, or strontium) based on the exposed fuel meat surface area (one side of the coupon is unexposed due to the aluminum cladding layer). Although most of the isotopes will be released only from the fuel particles within the aluminum matrix, that information may not be readily known about each fuel element. These data provide a general estimate of overall dissolution that can be applied to bulk quantities of fuel. Thus, rates based on the exposed fuel meat may be readily applicable to release rate models used in the performance assessment (see Reference 3).

Dissolution rates of selected components based on the fuel particle surface area are calculated using Equation (4-2). These data may be useful for fuel elements that have fuel particle loadings significantly different than the majority of the inventory. In addition, isotopic rates derived from this equation have been normalized to the original uranium concentration. Thus, all isotopes will have the same rates if they dissolve congruently. Any incongruency will be readily visible on a graph of all the selected isotopes (uranium, plutonium, cesium, technetium, or strontium) showing dissolution rates versus time. Information on isotopic dissolution may be useful in the detailed system models, which are rolled up into performance assessment summary models (see Reference 3).

The dissolution of aluminum from aluminum-based fuel is more complex than the other elements. Aluminum released from the matrix and the cladding will likely be similar and are represented by Equation (4-3). However, aluminum can also dissolve from the UAl and UAL_x fuel particles and any aluminum that may have reacted into the U_3O_8 and U_3Si_2 particles. It is not possible to distinguish the fraction of aluminum released from the fuel particles using this test method. Thus, aluminum dissolution rates were based on the total geometric area (fuel meat plus cladding) less the fuel particle area, recognizing that it includes an inherent error. The uncertainty can be reduced by comparing the results with other experiments performed with unirradiated uranium-aluminum material, as discussed in Section 4.2.3 (see Reference 3).

4.2.2.1 Test Results. Dissolution rates for uranium and other isotopes were plotted on a graph with respect to time. An average rate was calculated over a period of time where the data seem to be relatively consistent. Because this is somewhat ambiguous, general criteria for acceptance into the average rate calculation were formulated. The initial transient period was not included, usually a few days but could be as long as a few weeks. Data that fall within +/-30% over a few weeks with little or no trends either higher or lower are included in the average calculation. Rates that begin to change after a long period of time are excluded regardless of whether an obvious change in conditions has occurred. Average dissolution rates are reported in Table 4-3 (see Reference 3).

Uranium dissolution rates were calculated based on the fuel particle and the fuel meat surface areas (Table 4-3). It is clear from the particle surface area results that UAl is more vulnerable to degradation than the other three fuel compositions. Rates in simulated J-13 well water were significantly less than the bicarbonate or nitric acid for all four materials. Little difference is seen between the two surface area bases, except with UAl fuel. This is due to the fraction of the material that consists of fuel particles. UAl alloy fuel has only 31% fuel particles, whereas the other three fuels are between 50 and 70% (see References 3 and 4).

Only one experimental condition can be used for a comparison between aluminum-based fuel and commercial LWR (UO_2) fuel. LWR spent fuel dissolution tests in 2×10^{-2} molar bicarbonate solution ranged between 1.5 and 4.1 $mg/m^2/d$.[5,6] Aluminum fuels were much more reactive, with dissolution rates a

Table 4-3. Average uranium dissolution rates ($mg/m^2/d$) based on fuel particle and fuel meat surface areas.

	Bicarbonate		Nitric Acid		J-13 Well Water	
	Particle	Meat	Particle	Meat	Particle	Meat
UAl	107	33	320	99	0.55	0.17
UAl_x	33	22	42	28	0.28	0.19
U_3O_8	65	33	61	31	0.28	0.14
U_3Si_2	56	36	54	36	0.34	0.22

factor of ten or more faster (ranging between 33 and 107). There are some significant differences between UO_2 fuels and the aluminum-based fuels, besides the obvious presence of aluminum. LWR has a much lower burnup, about 3%, compared to the 40 to 93% seen with the selected aluminum fuel samples. Enrichment is also high in the aluminum fuel, up to 80%. Other metallic fuels have also been found to react faster than oxide fuels, as seen in Section 3. In previous LWR tests, preoxidized UO_2 was found to be more reactive then unconditioned fuel (similar to the U_3O_8).[7] These data indicate that a single package has a greater impact in the repository than a package of commercial fuel. However, the total number of commercial fuel packages is far greater than all DOE-owned fuel packages (see Reference 3).

Only a few samples near the beginning and at the end of each test were analyzed for aluminum concentration. In bicarbonate solutions, the aluminum initially dissolves at a higher rate than uranium, but equilibrates to about the same rate by the end of the tests (~230 days). Aluminum dissolution was clearly faster that uranium in the nitric acid experiments, as demonstrated in Figure 4-6 for UAl_x fuel. No comparison can be made in simulated J-13 well water because the aluminum concentrations were near or below the detection limit of 60 µg/L. The dissolution rate associated with the detection limit of aluminum concentration would be about 100 times the uranium dissolution rate. Aluminum may have dissolved faster than uranium, but it cannot be verified with these restrictions on analysis (see Reference 3).

Tables 4-4 through 4-6 list the average dissolution rates of uranium, plutonium, cesium, technetium, and strontium for the twelve experiments based on Equation 4-2. Under certain conditions the standard deviations are fairly high, particularly in the J-13 water and in some of the nitric acid solution tests. However, several trends comparing the radionuclide dissolution rates to uranium dissolution are discernible. These are demonstrated more clearly in Tables 4-7 through 4-10. A ratio of one indicates uniform dissolution, less than one indicates the radionuclide is dissolving slower, and greater than one indicates the radionuclide is released at a faster rate than uranium (see References 3 and 4).

The plutonium to uranium ratio (Table 4-7) is less than one under every condition, though in a few cases it was close to one (UAl alloy in J-13 water, UAl alloy in nitric acid, and U_3O_8 in nitric acid). Plutonium may be present in the fuel as a separate phase, may have deposited on the specimen cell wall, or may be in a form undetectable by the analytical method employed with test samples. Cesium and strontium (Table 4-8 and 4-10) dissolved at a rate close to uranium in most cases. UAl in simulated J-13 well water is the most notable exception, with ratios of 9.1 and 7.6, respectively. Ratios of cesium and strontium from U_3Si_2 in all three solutions were also significantly higher than one, possibly indicating preferential leaching of cesium and strontium or a separate phase in the fuel. A low ratio was seen in one case, U_3O_8 in simulated J-13 well water. It is not clear why this ratio differs significantly. Technetium-to-uranium dissolution ratios (Table 4-9) were high for all fuel types in the bicarbonate solution and for the UAl alloy in the nitric acid solution and low for U_3O_8 in the nitric acid. No data were available for the simulated J-13 well water, because the concentrations were too near the detection limit of technetium. Preferential leaching of technetium with respect to uranium appears to have occurred in most cases. Mechanistic experiments, such as the unsaturated drip tests, could provide more information on the potential causes for these incongruent dissolution rates if they were performed (see References 3 and 4).

4.2.3 Unirradiated Flow Through Tests

Flow through experiments with unirradiated aluminum material were performed at both PNNL and the Savannah River Site. The test equipment at PNNL was identical to that used with other fuel types and with the irradiated fuel samples, and is described in Section 2.2.2. The Savannah River Site used two systems that were both similar to the PNNL design. One system used gravity feed rather than a pump, although the pump provided a more consistent flow rate. Four coupons, in contrast to one at PNNL, were suspended in each test cell, and no filters were used.

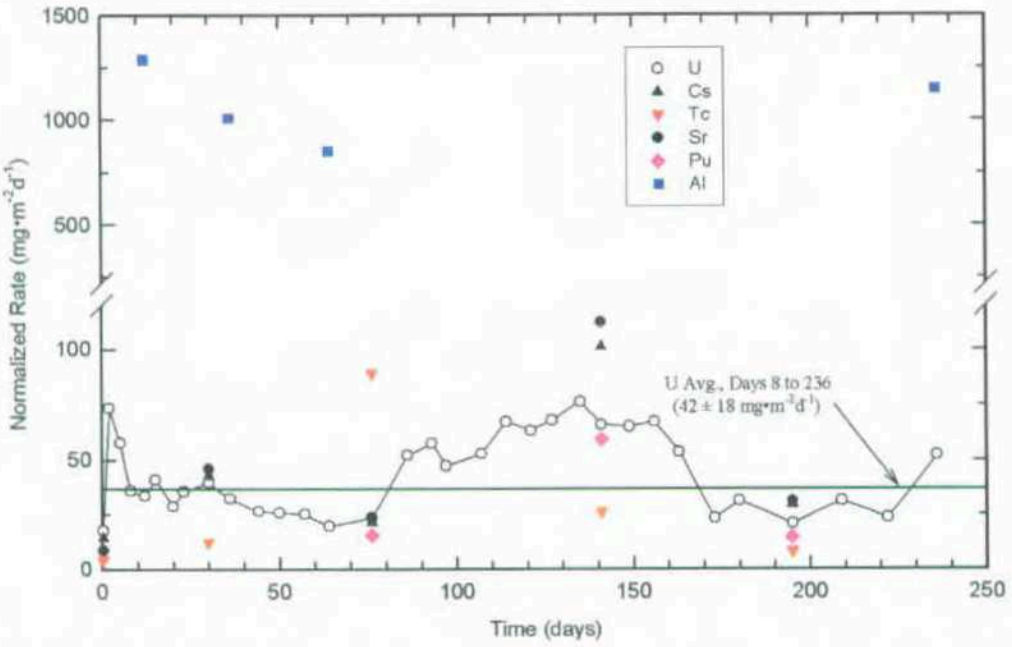

Figure 4-6. Dissolution rates of uranium aluminide spent fuel in 10^{-3} M nitric acid, pH ~3, at 25°C.

Table 4-4. Average dissolution rates ($mg/m^2/d$) based on fuel particle surface area in 2×10^{-2} M sodium bicarbonate solution.

	Uranium		Plutonium		Cesium		Technetium		Strontium	
	Avg	σ	Avg	σ	Avg	σ	Avg	σ	Avg	σ
UAl	107	7	65	15	120	16	200	41	96	30
UAl_x	33	5	13	0.3	43	10	61	16	45	1
U_3O_8	65	19	21	2	75	11	120	22	68	1
U_3Si_2	56	16	20	9	150	63	230	85	160	53

Table 4-5. Average dissolution rates ($mg/m^2/d$) based on fuel particle surface area in 10^{-3} M nitric acid solution.

	Uranium		Plutonium		Cesium		Technetium		Strontium	
	Avg	σ	Avg	σ	Avg	σ	Avg	σ	Avg	σ
UAl	320	104	280	90	300	60	590	490	320	60
UAl_x	42	18	30	26	49	36	34	38	53	41
U_3O_8	61	19	56	7	84	14	21	7	86	16
U_3Si_2	54	16	39	8	140	21	48	14	150	33

Table 4-6. Average dissolution rates ($mg/m^2/d$) based on fuel particle surface area in simulated J-13 well water.

	Uranium		Plutonium		Cesium		Technetium		Strontium	
	Avg	σ	Avg	σ	Avg	σ	Avg	σ	Avg	σ
UAl	0.55	0.24	0.50	0.22	5.0	4.7	NA	NA	4.2	0.7
UAl_x	0.28	0.11	0.11	0.07	0.31	0.21	NA	NA	0.33	0.18
U_3O_8	0.28	0.11	0.06	0.04	0.06	0.02	NA	NA	0.08	0.03
U_3Si_2	0.34	0.11	0.10	0.06	0.64	0.58	NA	NA	1.6	1.0

Table 4-7. Ratio of plutonium dissolution rates to uranium dissolution rates (Pu/U).

	Bicarbonate	Nitric Acid	J-13 Well Water
UAl	0.61	0.91	0.88
UAl_x	0.39	0.39	0.71
U_3O_8	0.32	0.21	0.92
U_3Si_2	0.36	0.29	0.72

Table 4-8. Ratio of cesium dissolution rates to uranium dissolution rates (Cs/U).

	Bicarbonate	Nitric Acid	J-13 Well Water
UAl	1.12	0.94	9.1
UAl_x	1.30	1.17	1.11
U_3O_8	1.15	1.38	0.21
U_3Si_2	2.68	2.59	1.88

Table 4-9. Ratio of technetium dissolution rates to uranium dissolution rates (Tc/U).

	Bicarbonate	Nitric Acid	J-13 Well Water
UAl	1.87	1.84	NA
UAl_x	1.85	0.81	NA
U_3O_8	1.85	0.34	NA
U_3Si_2	4.11	0.89	NA

Table 4-10. Ratio of strontium dissolution rates to uranium dissolution rates (Sr/U).

	Bicarbonate	Nitric Acid	J-13 Well Water
UAl	0.90	1.00	7.6
UAl_x	1.36	1.26	1.18
U_3O_8	1.05	1.41	0.29
U_3Si_2	2.86	2.78	4.7

4.2.3.1 PNNL Flow Through Test Results. PNNL performed flow through tests with unirradiated 19-UAl coupons in carbonate, nitric acid, and simulated J-13 well water. The uranium data were normalized to the surface area of the fuel particles (discussed in Section 4.1.2) and the fuel meat, whereas the aluminum data were normalized to the area of the matrix (total geometric area less the fuel particle surface area). Aluminum appeared to dissolve faster than uranium in nitric acid and in simulated J-13 well water (although aluminum concentrations for the latter test were near the detection limit) but at the same rate in the bicarbonate solution. The rates for both elements were significantly higher in nitric acid than either of the other two solutions and were the slowest with the simulated J-13 well water. Most of the rates with the unirradiated fuel were similar to those seen with the irradiated UAl SNF reported in Section 4.2.2.1. Figure 4-7 shows the dissolution rate of unirradiated 19-UAl in the nitric acid solution over time. This is the only test that indicated a significant (greater than a factor of 2) difference between irradiated and unirradiated fuel. Average dissolution rates for aluminum and uranium for each solution are shown in Table 4-11 (see Reference 3).

SEM photomicrographs of the coupon surface before and after exposure to each of the three solutions are shown in Figures 4-8 through 4-11. (Dark areas are the aluminum matrix and the light areas are the fuel particles.) Prior to any testing, the microstructure clearly shows the UAl particles dispersed in an aluminum matrix, (Figure 4-8). After 113 days of exposure to the carbonate solution (Figure 4-9), the surface had a mud-cracked appearance typical of aluminum hydroxide (although no compositional analysis was performed). Aluminum probably reacted with the carbonate preventing the formation of the protective aluminum hydroxide film. Exposure to nitric acid (Figure 4-10) caused excessive corrosion of both the aluminum and uranium. Aluminum reacted at a faster rate, and thus UAl particles are seen to protrude from the surface. Simulated J-13 well water had a negligible effect on either the aluminum matrix or the fuel particles (Figure 4-11) (see Reference 3).

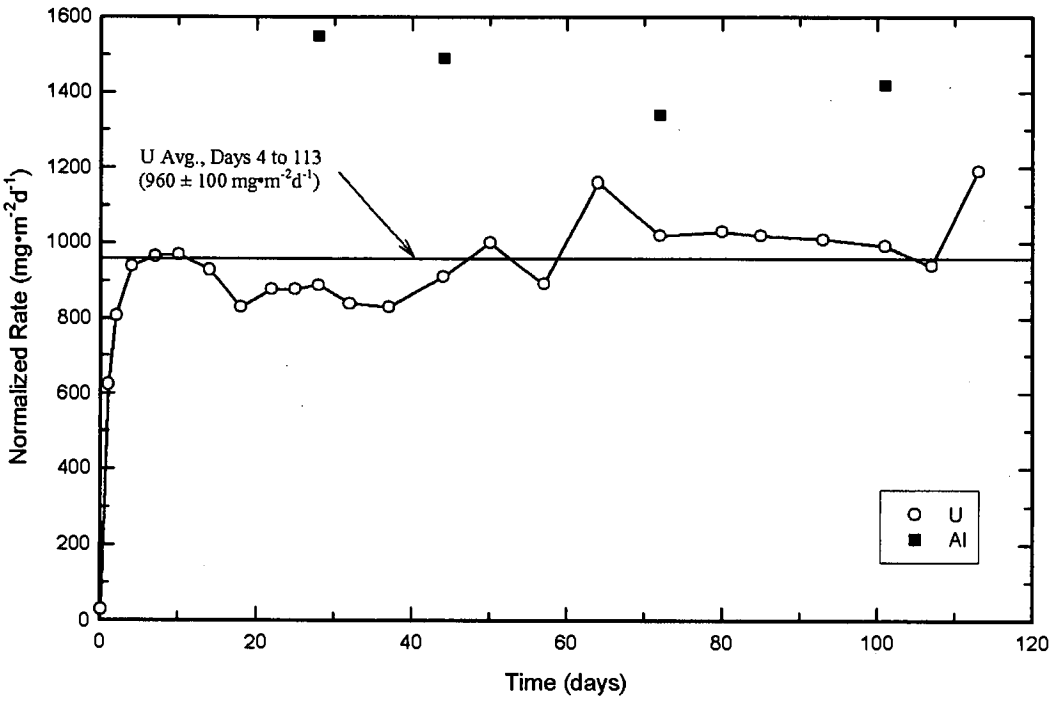

Figure 4-7. Dissolution rates of unirradiated 19-UAl in 10^{-3} M nitric acid (pH = 3, temperature = 25°C).

Table 4-11. Flow through dissolution rates of unirradiated 19-UAl and UAl SNF in three solutions at 25°C (mg/m^2/d) based on aluminum and uranium concentrations.

	Bicarbonate		Nitric Acid		J-13	
	Particle	Meat	Particle	Meat	Particle	Meat
PNNL—Uranium	103	25	960	230	0.84	0.20
SNF—Uranium	107	33	320	99	0.55	0.17
PNNL—Aluminum	~100	—	~1,450	—	—[a]	—
SNF—Aluminum	~100	—	~1,500	—	—[a]	—
SRS—Uranium	—	—	—	—	—	1.8

a. Below detection limits.

PNNL = Pacific Northwest National laboratory
SNF = spent nuclear fuel
SRS = Savannah Rive Site

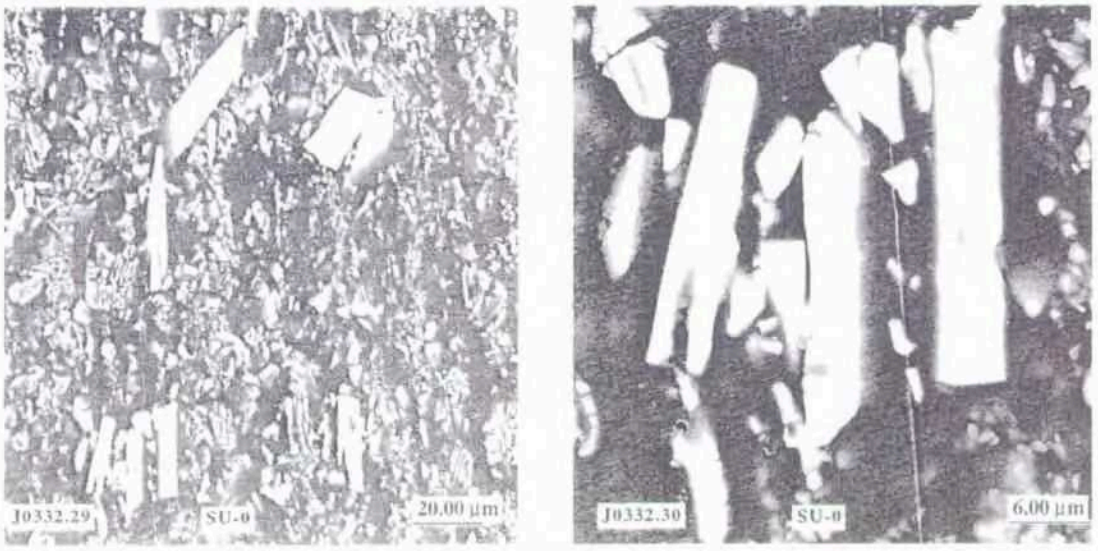

Figure 4-8. Unirradiated 19-UAl microstructure before testing.

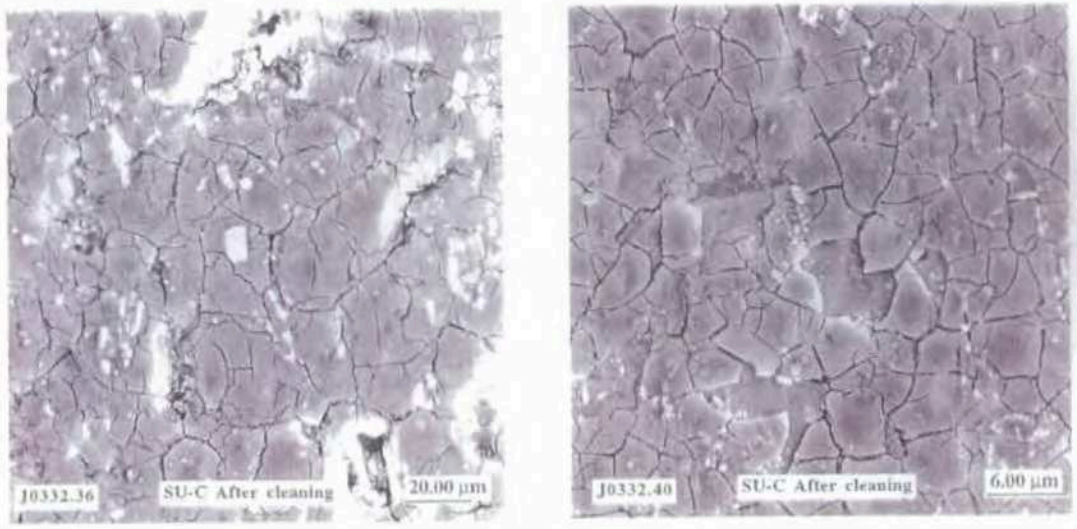

Figure 4-9. Unirradiated 19-UAl microstructure after exposure to carbonate solution.

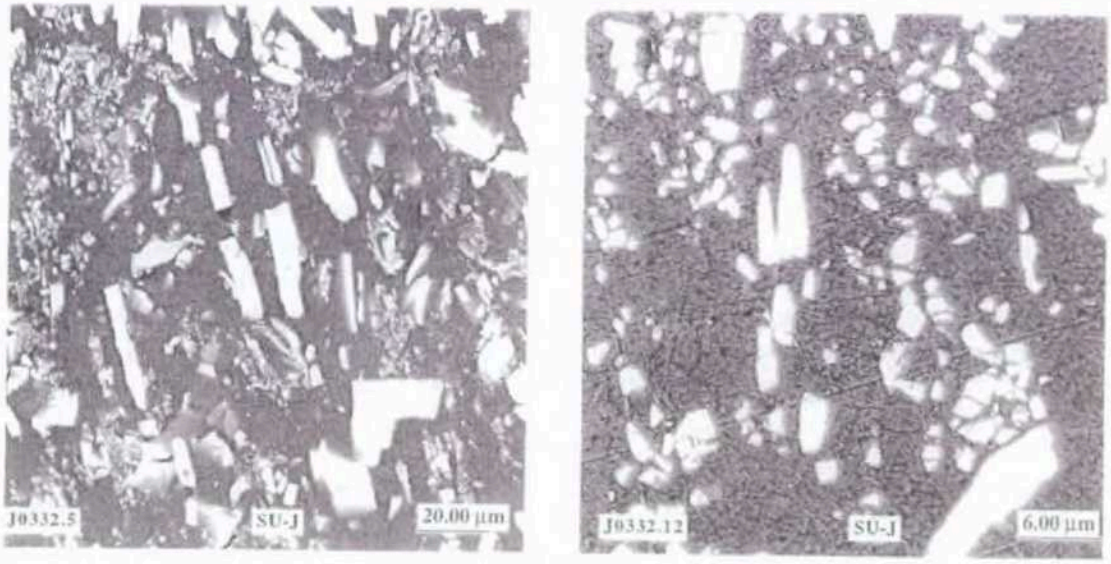

Figure 4-10. Unirradiated 19-UAl microstructure after exposure to nitric acid.

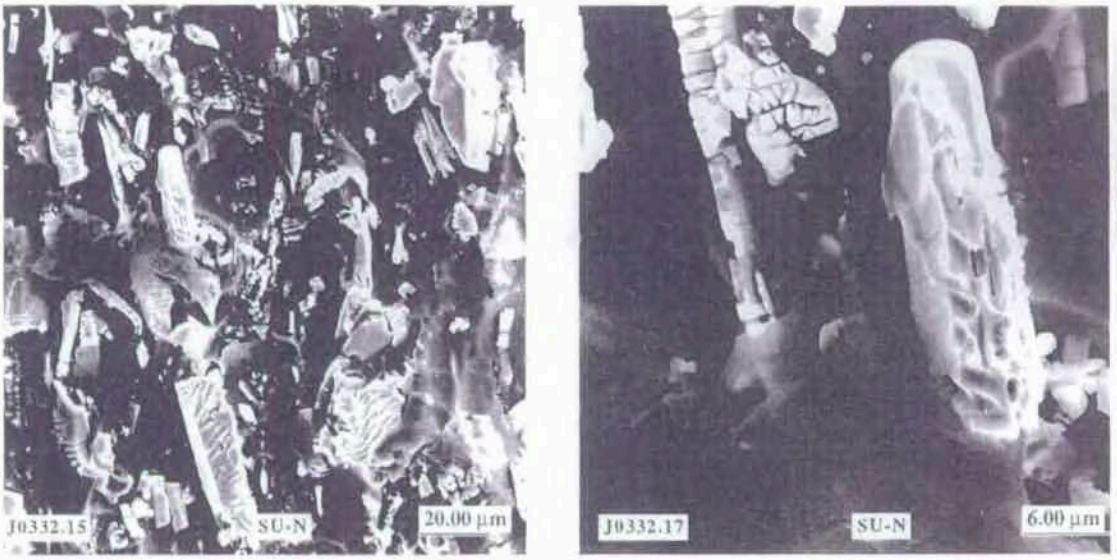

Figure 4-11. Unirradiated 19-UAl microstructure after exposure to simulated J-13 water.

4.2.3.2 SRS Flow Through Test Results. Flow through tests with different material compositions, temperatures, and solution chemistries were performed to evaluate mechanisms with respect to microstructure and environmental conditions. Four solutions were evaluated (nominal simulated J-13 well water, low pH J-13 water, high pH J-13 water, and high chloride J-13 water) with four uranium-aluminum alloy compositions. Temperature and material fabrication (cast or wrought) were also varied with these tests (see Reference 4).

Table 4-12 summarizes the results for each condition tested. Not all conditions were evaluated, thus blank cells appear in the table where no data are available. All rates were calculated based on the geometric surface area of the coupon. Variation in the data is represented by σ, which is significant in a number of cases. However, some conclusions can be made based on trends that are consistent regardless of other parameters. For example, aluminum reacts preferentially to uranium in simulated J-13 well water, regardless of the solution or material modifications. This result was also seen in the flow through tests at PNNL. It is also clear that increasing the temperature and either raising or lowering the pH causes a higher dissolution rate for both uranium and aluminum. Tables 4-13 and 4-14 show these comparisons more clearly. Chloride content does not appear to have a significant effect on the rate (see References 4 and 8).

A comparison of dissolution rates at 90°C for cast versus wrought fabrication and eutectic (13.2-UAl) versus 25-UAl composition can be made from Tables 4-12 through 4-14. No significant variances are seen based on the aluminum rates. However, uranium concentration did change based on fabrication. The 13.2-UAl cast material had higher rates than the 13.2-UAl wrought coupons in nominal J-13, low pH, and high chloride solutions. In the high pH solution, the wrought material resulted in a higher rate. Uranium content in the alloy (13.2 versus 25) did not have an effect on the dissolution rate except in the low pH solution (see References 4 and 8).

Table 4-12. Uranium and aluminum dissolution rates (mg/m^2/d) from the Savannah River Site flow through tests.

		25°C				90°C			
		Uranium		Aluminum		Uranium		Aluminum	
Alloy/fab	Solution	Mean	σ	Mean	σ	Mean	σ	Mean	σ
13.2/cast	J-13	1.7	0.9	—[a]	—	24.2	53.8	225	228
13.2/wrt		—	—	—	—	8.2	5.6	102	120
25/cast		—	—	—	—	26.9	27.7	120	121
19/wrt		1.8	0.8	—[a]	—	—	—	—	—
13.2/cast	Low pH	139	78	1,110	544	215	120	1,350	699
13.2/wrt		—	—	—	—	188	15	1,110	501
25/cast		227	111	973	544	420	444	1,333	712
13.2/cast	High pH	—	—	—	—	86	57	5,250	3,045
13.2/wrt		—	—	—	—	248	210	5,440	2,731
25/cast		—	—	—	—	96	1.5	4,710	2,034
13.2/cast	High Cl	1.4	0.6	—[a]	—	18	9	198	143
13.2/wrt		—	—	—	—	8.4	3.9	157	163
25/cast		2.6	3.0	—[a]	—	14	7.0	134	97

a. Below detection limit.

Table 4-13. Dissolution rates (mg/m^2/d) at different temperatures.

Test Conditions	25°C	90°C
Uranium (13.2, cast, J-13)	1.7	24.2
Uranium (13.2 cast, low pH)	138	215
Uranium (25 cast, low pH)	227	420
Uranium (13.2 cast, high Cl)	1.4	18
Uranium (25 cast, high Cl)	2.6	14
Aluminum (13.2 cast, J-13)	—[a]	225
Aluminum (13.2 cast, low pH)	1,110	1,350
Aluminum (25 cast, low pH)	973	1,333
Aluminum (13.2 cast, high Cl)	—[a]	198
Aluminum (25 cast, high Cl)	—[a]	134

a. Below detection limit.

Table 4-14. Dissolution rates (mg/m^2/d) at high and low pH and high chloride.

Test Conditions	Nominal	Low pH	High pH	High Cl^-
Uranium (13.2, cast, 25°C)	1.7	139	—	1.4
Uranium (13.2 cast, 90°C)	24	215	86	18
Uranium (25 cast, 90°C)	27	420	96	14
Uranium (13.2 wrought, 90°C)	8.2	188	248	8.4
Aluminum (13.2 cast, 25°C)	—[a]	1,110	—	—[a]
Aluminum (13.2 cast, 90°C)	225	1,350	5,250	198
Aluminum (25 cast, 90°C)	120	1,333	4,710	134
Aluminum (13.2 wrought, 90°C)	102	1,110	5,440	157

a. Below detection limit.

The test with 19-UAl was performed for a comparison with the work conducted at PNNL (see Table 4-11). Uranium dissolution rate was approximately ten times greater in the Savannah River Site tests than in the PNNL experiments. Investigations into possible variations in surface preparation and analytical techniques have been initiated to explain the inconsistency between the two laboratories (see References 4 and 8).

Microstructural changes following exposure to the selected solutions were observed. At 90°C, the materials exposed to nominal J-13 well water (13.2-UAl cast, 13.2-UAl wrought, and 25-UAl cast) were generally darker with spotty regions of shiny metal. The shiny areas were regions not covered by corrosion products but where aluminum was attacked preferentially to the UAl phase; see Figure 4-12. Various amounts of white corrosion products and roughening were also seen. Sulfur, uranium, silicon, and calcium compounds were found in the reaction products. In low pH solutions, the surfaces were smooth with a brown/white oxide layer. High pH solutions caused heavy layers of corrosion products. Generally, the reaction products on the surface trapped the uranium-aluminum particles if the layer was thick enough. Localized corrosion (pitting) with the typical white corrosion products was seen in materials exposed to the high chloride solution. At the lower temperature of 25°C, similar results were found but were less extensive (see References 4 and 8).

Aluminum reaction products are typically referred to as aluminum oxide (see References 3, 4, and 12). However, recent research indicates they are actually aluminum tri-hydroxides, and the true aluminum oxide is only formed at high temperatures (~360°C) or very long time periods. White corrosion products may be gibbsite, hydrargillite, or bayerite. Aluminum hydroxide forms poly nuclear rings that deprotonate to form hydroxide gels, which were found in these experiments.

4.2.4 Unirradiated Static Tests

Static tests were performed with unirradiated aluminum-based fuel at the Savannah River Site to evaluate variations in temperature, material, fabrication, and solution chemistry (similar to the flow through tests performed at the Savannah River Site). Three of the unirradiated sample compositions described in Section 4.2.1 were used for these tests: 10 UAl cast, 13.2 UAl cast and wrought, and 25 UAl cast and wrought. Simulated J-13 well water and modifications for high pH, low pH, and high chloride as described in Section 4.2.1 were used with each material. The experiments were run at 25°C and 90°C for

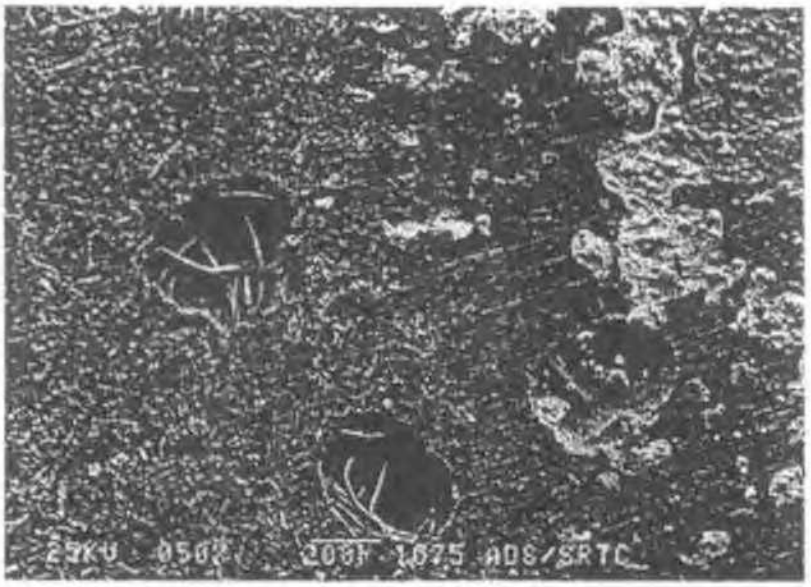

Figure 4-12. Surface of 25-UAl cast material after exposure to nominal J-13 well water.

1 month with samplings at 7, 14, and 28 days. Possible effects of galvanic interaction were also evaluated in the static tests by coupling the samples to either aluminum or stainless steel. Degradation was evaluated using weight changes, solution chemistry, visual examination, and SEM microstructural analysis (see References 4 and 8).

4.2.4.1 Weight Change Measurements. Weight measurements of the coupons were made before and after exposure to the test environment. An increase in weight would indicate oxidation of the aluminum resulting in a hydroxide layer on the surface. Decreases in the weight occur when the alloy material is dissolved into solution or aluminum compounds have spalled off the surface. Table 4-15 lists the change in weight at the end of the tests for coupons coupled to aluminum and to stainless steel (negative numbers indicate a weight loss, positive numbers a weight gain). Galvanic interaction with stainless steel increased the amount of attack under nearly every condition. The wrought material and 25-UAl cast in J-13 pose an interesting exception. Data with 13.2-UAl wrought are close enough to be considered equivalent, indicating no galvanic effect, and the 25-UAl cast in nominal J-13 is so low it could be an anomaly. Generally, the wrought material was more resistant to attack than either of the cast materials, which is similar to the flow through test results. In particular, the cast materials were attacked (either a loss or a gain) more severely by the low and high pH solutions. Composition did not have a strong effect on the dissolution in any solution. Table 4-16 compares the weight changes of 13.2-UAl cast material at 25°C and 90°C. There is some indication that increased temperature increases the degradation of the simulated fuel, but not in every case (similar to the variations in solution chemistry and material fabrication) (see References 4 and 8).

4.2.4.2 Solution Chemistry Analysis. Solution samples were removed for analysis of uranium and aluminum concentration from the static tests at 7, 14, and 28 days. Weight loss measurements provided an indication of the total amount of material that had reacted, whereas the solution chemistry analyses provided more precise data on the amount of a specific element that had reacted. Tables 4-17 and 4-18 present the range of uranium and aluminum results for each test. Not all conditions and analyses were performed with every material, and thus some spaces appear in the tables. Results are similar to those found in the weight loss measurements. Galvanic coupling to stainless steel increased the reaction

Table 4-15. Weight changes ($\mu g/dm^2$) of UAl alloys in static tests coupled to stainless steel and aluminum at 90°C.

Solution	13.2-UAl Cast	13.2-UAl Wrought	25-UAl Cast
Stainless Steel Couple			
J-13	-1,000 to –6,000	-2,500 to 3,500	-100 to -50
Low pH	-10,000 to 43,000	-15,000 to -3,500	-2,000 to -43,000
High pH	-25,000 to -36,000	-1,000 to -4,000	500 to 30,000
High Cl^-	2,000 to 5,000	1,500 to 6,000	5,000 to 20,000
Aluminum Couple			
J-13	200 to 900	1,200 to 4,000	1,500 to 3,000
Low pH	0 to 13,000	500 to 4,000	-1,000 to -9,000
High pH	-4,000 to -2,500	NR	-2,000 to 10,000
High Cl^-	0 to 2,200	NR	1,000 to 4,000

NR = no results

Table 4-16. Weight changes ($\mu g/dm^2$) of 13.2-UAl cast material in static tests coupled to stainless steel.

Solution	25°C	90°C
J-13	500 to -5,500	-1,000 to -6,000
Low pH	-5,000 to -30,000	-10,000 to 43,000
High pH	-100 to 2,000	-25,000 to -36,000
High Cl^-	-100 to -22,000	2,000 to 5,000

Table 4-17. Uranium concentrations (ppm) in static test solution samples at 90°C coupled to stainless steel and aluminum.

	10-UAl cast	13.2-UAl Cast	13.2-UAl Wrought	25-UAl Cast	25-UAl Wrought
Stainless Steel Couple					
J-13	0.2–0.8	0.6–0.7	0.5–0.6	0.5–0.6	0.6–0.7
Low pH	0.5–0.6	2.5	2.0–2.5	1.0–2.0	2.5–3.0
High pH	1.0–4.0	3.5–4.5	1.0–1.2	3.0–4.0	15–20
High Cl^-	0.2	0.25–0.3	0.2–0.25	0.25–0.4	0.3
Aluminum Couple					
J-13	NR	0.05	0.05	0.1	0.05–0.2
Low pH	NR	1.0–1.5	0.5–0.8	0.25–0.75	0.9–1.0
High pH	NR	0.1		2.0	1.2–1.4
High Cl^-	NR	0.05		0.08–0.1	0.1

NR = no results

Table 4-18. Aluminum concentrations (ppm) in static test solution samples at 90°C couple to stainless steel and aluminum.

	10-UAl Cast	13.2-UAl Cast	13.2-UAl Wrought	25-UAl Cast	25-UAl Wrought
Stainless Steel Couple					
J-13	2.0–2.5	2.0–3.0	1.5–2.0	2.5–4.0	2.8–3.0
Low pH	1.0–5.0	4.0–9.0	5.5–11.8	1.0–3.0	3.2–12.5
High pH	91–114	36–40	1.0–8.0	11–15	50–63
High Cl^-	2.1–4.4	3.5–6.2	1.0–4.0	2.2–9.6	2.8–4.5
Aluminum Couple					
J-13	NR	5.0–6.5	5.0–5.5	2.5–4.0	3.1–3.7
Low pH	NR	3.5–6.0	2.0–4.5	0.5–4.0	3.0–7.8
High pH	NR	63–80		12–13	113–138
High Cl^-	NR	8–15		2.5–4.2	2.1–3.5

NR = no results

rate; therefore, the uranium concentration was higher than with samples coupled to aluminum (no galvanic interaction). Aluminum did not show the same trend in all cases; in fact with some test conditions the aluminum couple resulted in higher solution concentrations of aluminum. This is likely from the couple material (aluminum) also corroding into the test solution (see References 4 and 8).

Increasing the pH had the most pronounced effect on both the uranium and aluminum concentration in the test samples, resulting in significant increases over the nominal J-13 results. Low pH also increased the concentration of both elements in most cases. Uranium concentrations were equal or lower for all alloys in the high chloride solution compared to the nominal J-13 chemistry, but most of the aluminum results were higher. This reflects the known aggressiveness of chloride and caustic solutions with aluminum that may not be duplicated with uranium.

Material composition and fabrication had a minimal effect on the uranium or aluminum concentrations in the static test solution samples. High pH solutions show some variation between cast and wrought, but not consistently. The 25-UAl wrought material reacted more than the 25-UAl cast when coupled to stainless steel, but less when coupled to aluminum. The 13.2-UAl cast resulted in higher uranium concentrations than the 13.2-UAl wrought. No predictable trends can be drawn from these data.

Table 4-19 shows the uranium and aluminum concentrations of samples from the 13.2-UAl static tests coupled to stainless steel at 25°C and 90°C. Increasing the temperature produced an increase in both uranium and aluminum concentration in all the solutions. Temperature, galvanic coupling, and solution composition significantly affect the dissolution of aluminum-based fuel, but alloy composition and fabrication trends are less certain. Increased chloride concentrations preferentially attack the aluminum, but do not increase the overall corrosion rates (see References 4 and 8).

4.2.4.3 Visual and Microstructural Analysis. Coupons were examined both visually and with a SEM after exposure to the test conditions and compared to the structure prior to testing. Nominal J-13 solution caused very little damage to any of the materials, only a few white corrosion products typical of aluminum pitting, and original grinding marks were still visible. However, preferential attack of the aluminum matrix was indicated by the slightly protruding uranium-aluminum particles. Evidence of

Table 4-19. Uranium and aluminum concentration (ppm) in static test solution samples of 13.2-UAl cast material coupled to stainless steel.

	Uranium		Aluminum	
Solution	25°C	90°C	25°C	90°C
J-13	0.05–0.09	0.6–0.7	0.25	2.0–3.0
Low pH	0.5–0.7	2.5	4.0–7.4	4.0–9.0
High pH	0.03	3.5–4.5	0.25	36–40
High Cl^-	0.08–0.13	0.25–0.3	0.25	3.5–6.2

preferential corrosion of the aluminum was seen in all four solutions, regardless of alloy material. This was most apparent in the high pH solution and is seen in Figure 4-13 (13.2-UAl cast material at 90°C). Corrosion, essentially from reaction of the aluminum around the fuel particles, forms a positive surface charge that prevents diffusion of Al^{+3} ions. The UAl_x particles disrupt the film and aluminum will react under the particle, eventually dislodging it. Both UAl_3 and UAl_4 particles were found on the filtrate from solution samples of the 25-UAl wrought test in high pH J-13 at 90°C (see References 4 and 8).

In low pH solutions, a whitish film was observed on the coupon surface but no white corrosion products. A black film with no white products was seen on the material that was exposed to high pH solutions. The microstructure of 13.2-UAl cast material, which is exposed to high pH simulated J-13 well water at 90°C, is shown in Figure 4-13. A black film was also seen on coupons tested in the high chloride solution, but numerous white corrosion products were also visible. Increasing the temperature and coupling with stainless steel resulted in the same results only more pronounced; the amount of attack was increased, but the mechanism did not change (see References 4 and 8).

In summary, the visual and SEM analysis indicated that both increasing the temperature and creating a galvanic condition increased the amount of corrosion. Preferential attack of the aluminum compared to the uranium-aluminum particles was apparent for all conditions. White corrosion products typical of aluminum pitting were visible on the nominal J-13 and the high chloride solutions, but the high pH solution caused the most severe general attack. Alloy composition and fabrication appeared to have a negligible effect on the degree of degradation or the mechanism.

4.2.5 Unirradiated Electrochemical Tests

Coupons for the electrochemical tests were taken from the 10-UAl, 13.2-UAl, and 25-UAl cast materials. Effects of temperature, composition, and solution chemistry were evaluated from the corrosion potential, linear polarization resistance (R_P), and the polarization scan characteristics. A corrosion rate was calculated from the R_P based on density and equivalent weight of aluminum. Table 4-20 lists the calculated corrosion rates for the three alloys in each of the four solutions at 25°C and 90°C. Variations in alloy composition appeared to have a negligible effect on the corrosion rate. Increasing the temperature increased the rate in nominal J-13 solution, but had little effect in the other solutions. Corrosion rates were fairly equal at 90°C regardless of solution chemistry with the exception of the high pH solution. Increasing the pH increased the corrosion rate by a factor of about 10. At 25°C, the low pH solution had a small effect (increased the rate by less than 10), but the high pH solution increased corrosion by a factor of over 100 (see References 4 and 8).

Similar results are seen in a comparison of the corrosion potentials (Table 4-21). The only parameter that appears to affect the corrosion potential is the high pH solution, which resulted in a significant increase. Neither temperature nor material composition had a readily apparent effect on the potential (see References 4 and 8).

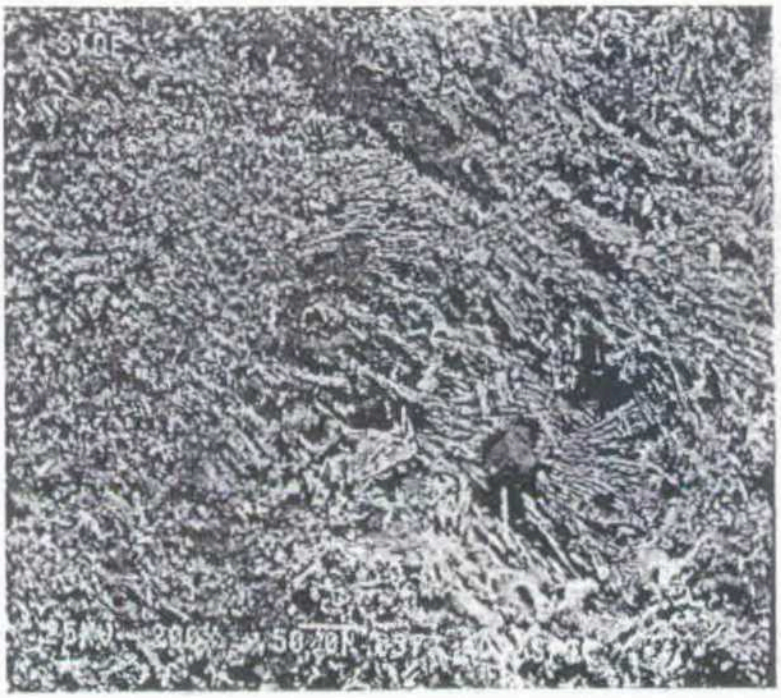

Figure 4-13. SEM photomicrograph of 13.2-UAl cast material in high pH J-13 solution at 90°C.

Table 4-20. Aluminum alloy corrosion rates (mpy) from linear polarization resistance tests.

	25°C		90°C		
Solution	13.2-UAl	25-UAl	10-UAl	13.2-UAl	25-UAl
J-13	0.6	0.5	5.9	3.4	6.0
Low pH	2.1	3.6	2.2	3.8	3.5
High pH	73.0	58.0	49.8	58.8	49.4
High Cl^-	0.8	1.3	2.4	1.0	4.9

Table 4-21. Aluminum alloy corrosion potentials (V) from electrochemical tests.

	25°C		90°C		
Solution	13.2-UAl	25-UAl	10-UAl	13.2-UAl	25-UAl
J-13	-0.27	-0.45	-0.45	-0.31	-0.48
Low pH	-0.26	-0.40	-0.26	-0.33	-0.35
High pH	-1.47	-1.51	-1.22	-1.19	-1.23
High Cl^-	-0.46	-0.48	-0.53	-0.86	-0.56

The primary degradation mechanism indicated by the polarization curves is low general corrosion with some pitting. Specific pitting and repassivation potentials were generally not seen, probably because the pitting potential was near the corrosion potential (see References 4 and 8).

4.2.6 Dissolution Test Conclusions

Four sets of experiments have been described in this section: (1) flow through tests with irradiated fuel, (2) flow through tests with unirradiated fuel, (3) static tests with unirradiated fuel, and (4) electrochemical tests with unirradiated fuel. Although some variations in the results were found, some conclusions on behavior were consistent throughout all or most of the test methods. Aluminum reacts faster than uranium (or the uranium-aluminum particles) with nearly every condition and test method. All of the static tests with unirradiated alloys indicated aluminum dissolution rates higher than uranium, and the visual and SEM examinations confirmed preferential degradation of the aluminum matrix. Similar results were seen with the unirradiated flow through tests at the Savannah River Site; aluminum rates were higher than uranium regardless of material composition, solution chemistry, or temperature. Flow tests at PNNL with both irradiated and unirradiated fuel indicated higher aluminum rates in the nitric acid solution and possibly in simulated J-13 well water (aluminum concentration in the samples was near the detection limits making conclusions difficult). However, in pure bicarbonate solution, aluminum and uranium had similar dissolution rates for both unirradiated and irradiated fuels. Under repository conditions, the aluminum matrix will react faster than the uranium-aluminum fuel particles. The particles may be released from the fuel until a fairly thick hydroxide layer is created on the surface, then the particles will remain trapped in the layer. This redistribution of fuel may be a concern from a criticality standpoint. As such, research has been initiated investigating the addition of neutron absorbers into the melt-dilute waste form.

Environmental characteristics generally had a significant effect on the dissolution results. Increasing the temperature clearly increased the reaction rate of uranium in the unirradiated flow through tests and in the solution analyses from the static tests. The coupon weight changes from the static tests and the electrochemical tests were less certain; in some cases the rates decreased with increasing temperature, but in some cases it did not. However, it is likely that the reaction rates will increase at elevated temperatures.

Solution chemistry was varied in the flow through, static, and electrochemical experiments. Only the flow through tests at PNNL examined pure bicarbonate and nitric acid solutions; the Savannah River Site modified simulated J-13 well water for high and low pH and high chloride solutions. High and low pH levels would be expected to increase the corrosion rate of aluminum based on the Pourbaix diagram (Figure 4-14).[9] All four irradiated fuel types and the unirradiated aluminum alloy fuel had dissolution rates significantly lower in the simulated J-13 well water than in either nitric acid or bicarbonate. Rates in nitric acid were much higher than bicarbonate for the UAl alloy fuel. Although nitric acid was not used in the static, electrochemical, or flow through tests at the Savannah River Site, low pH (~3) solutions were evaluated. The flow through test results were similar to those found at PNNL; low pH solutions caused an increase in the dissolution rate. Increasing the pH also increased the dissolution rate in the Savannah River Site flow through tests. Changing the pH in the static tests increased the overall corrosion rate (based on weight changes) compared to the nominal J-13 solution in most cases, but not all. Based on the uranium concentration in solution, modifications to the pH increased the corrosion rate regardless of material configuration and temperature. Aluminum concentrations were not consistently higher in the altered J-13 solution, possibly indicating different corrosion products with different exposure conditions. Increasing the pH had the most pronounced effect in the static tests and the electrochemical experiments.

Increasing the chloride content had very little effect on uranium concentration with any of the experimental methods. Aluminum concentrations did not change in the flow through tests but some increase was found in the static tests. Visual examination indicated that the chloride caused pitting of the

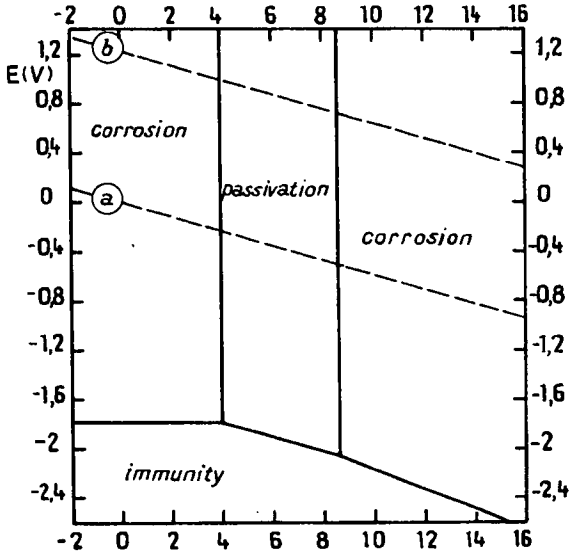

Figure 4-14A

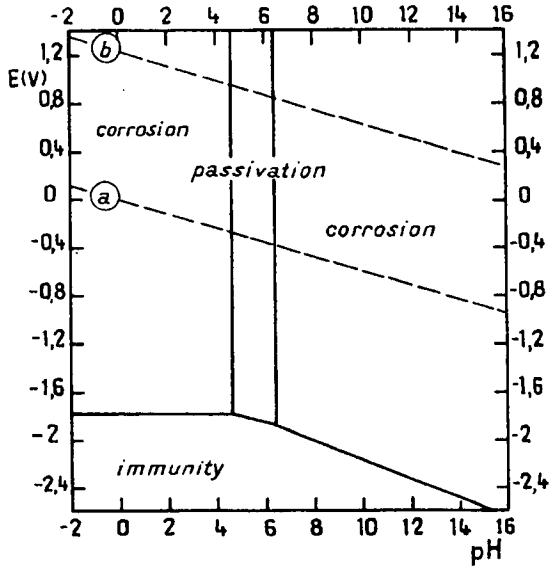

Figure 4-14B

Figure 4-14. Pourbaix diagram of (A) hydrargillite Al_2O_3 and of (B) böhmite Al_2O_3 $3H_2O$.

aluminum, forming adherent corrosion products that may not be detected by changes in solution chemistry. Higher chloride concentrations do not appear to have a detrimental effect on uranium corrosion, but does cause localized attack in the form of pitting to the aluminum. This is a well-documented consequence of chloride in contact with aluminum.[10]

An evaluation of galvanic effects was included in the static tests. Unirradiated UAl fuel coupled to stainless steel had higher corrosion rates than those coupled to aluminum based on weight loss, uranium solution chemistry, and visual examination. Thus, stainless steel in contact with the fuel will increase the reaction rates.

Four uranium-aluminum alloy compositions, some cast and some wrought material, were used in the static, flow through, and electrochemical tests at the Savannah River Site. Composition had a negligible effect on degradation rates regardless of test method or solution chemistry. Fabrication did show some variations, however. The cast material had higher dissolution rates than the wrought alloy for three out of four solutions in the flow through tests. The fourth solution produced the opposite effect. In the static tests, weight changes indicated the cast material was more susceptible to attack, but visible examination and liquid sample analyses indicated no significant variations. Fabrication effects were not examined in the electrochemical tests. Based on these variable results, no conclusive trends can be made; but wrought material may provide more resistance to degradation than cast alloys.

Selected radionuclides were examined in the SNF flow through tests at PNNL. Plutonium, cesium, technetium, and strontium dissolution rates were compared to uranium rates for the four fuel types. Rates were typically higher for the UAl fuel than the UAl_x, U_3O_8, and U_3Si_2 fuels for uranium as well as plutonium, cesium, technetium, and strontium. Under most conditions, the plutonium rates were less than uranium, the cesium and strontium were similar to uranium, and the technetium was greater. Notable exceptions are with cesium and strontium in the UAl alloy fuel and cesium, strontium, and technetium in the U_3Si_2 fuel (discussed in Section 4.2.2.1).

A summary of the conclusions derived from the dissolution tests discussed in this section is listed below.

1. Aluminum in the matrix was dissolved preferentially to the aluminum-uranium fuel particles.

2. Increasing the temperature resulted in increases in the dissolution rate.

3. Low pH (including nitric acid) and particularly high pH solutions increased the dissolution rate of UAl alloy fuels.

4. Higher chloride concentrations caused localized corrosion in the form of pitting to the aluminum matrix.

5. Galvanic coupling to stainless steel increased the corrosion rate of UAl alloy fuels.

6. Material composition had a negligible effect on the degradation of UAl alloy fuels in all solutions tested.

7. Wrought material may provide more resistance to attack than cast alloys, but the results are not conclusive.

8. Dissolution rates were higher with the UAl alloy fuel than the UAl_x, U_3O_8, and U_3Si_2 fuels.

9. Plutonium dissolution rates were typically lower than uranium; technetium rates were higher; and cesium and strontium were about the same.

4.3 Unsaturated Drip Tests

Unsaturated drip tests with aluminum-based fuel were planned to evaluate radionuclide release rates and alteration product characteristics under repository relevant conditions. The methodology is similar to that used in the uranium metal drip tests (Section 3.3) and is described in Section 2.2.3. Experimental objectives stated in the test plan include dissolution rates, release rates of fission products and radionuclides, chemical and physical form of released elements, chemistry of solutions in contact with the fuel, and type and sequence of alteration products.[11] Initial tests with unirradiated aluminum-based metal fuel were completed. However, the program was terminated before any tests with irradiated SNF could be performed. Results of the initial tests are presented below.

As discussed in the flow through Section 4.2, several types of aluminum-based fuel are available, and four representatives were evaluated in the flow through tests. Included were UAl alloy, UAl_x, U_3Si_2, and U_3O_8. The Savannah River Site also examined different ratios of uranium to aluminum in the UAl_x as part of the melt and dilute program. However, only one material was chosen for the unsaturated drip tests, UAl_x. The primary reason for choosing this material was that it simulated the melt and dilute product, which was the expected disposal form for most aluminum fuels. (The melt and dilute process was subsequently eliminated as a possible disposal form of aluminum-based fuel.)[12]

Some initial characterization of the selected samples was performed for a baseline to compare with post test analyses. The sample had an enrichment of 19.75% ^{235}U, with 70.2 wt% uranium in the fuel meat (balance is aluminum). Aluminum fuel is fabricated by sandwiching the UAl_x dispersed in a continuous aluminum matrix between AG3NE alloy cladding (see Figure 4-15). Samples were cut from the center of the plate, and the cladding was removed from one face by polishing. Drip tests with unirradiated fuel were performed with EJ-13 well water at the high drip rate, 0.75 mL/3.5 days, at 90°C.

Two experiments with duplicate samples under identical conditions and a blank (no fuel) were completed. Specimen 1 was sampled after 33, 67, 118, and 183 days, and Specimen 2 was sampled after 16 and 55 days. Test results are discussed below (see References 12 and 13).

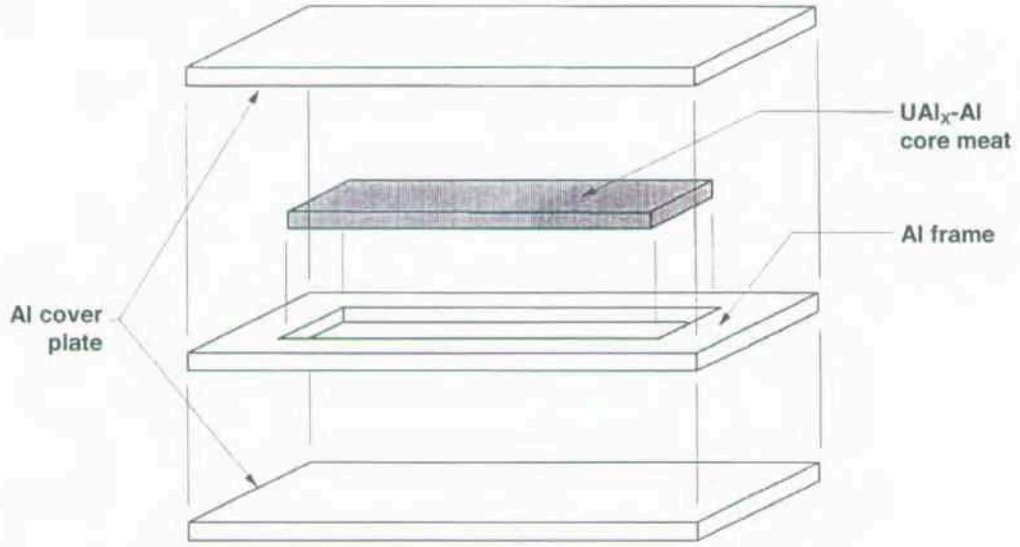

Figure 4-15. Fabrication diagram of UAl_x aluminum-based fuel.

4.3.1 Unirradiated Fuel Test Results

Aluminum-based fuel reacted to dripping EJ-13 well water very differently than the uranium metal fuel. The samples remained intact throughout the experiments, and no spallation of the material was seen. Uranium was released into solution at a cumulative rate between 0.2 and 2.9 $mg/m^2/d$ from both tests. Results from the experiments are shown in Figure 4-16. Included is uranium sorbed to the vessel walls and sample holder, which accounts for 41 to 91% of the released uranium. Between 62 and 98% of the aluminum was also sorbed on the vessel. In addition, silicon was found adsorbed but to a lesser degree, from 4 to 68%. Flow through tests with UAl_x at 90°C in simulated J-13 well water had release rates of 8.2 (13.2% uranium wrought material), 24.2 (13.2% cast material), and 26.9 (25% uranium cast material) $U/m^2/d$ (see Section 4.2). These rates are about an order of magnitude higher than what was seen in the drip tests. However, the rates should be higher in flow through tests because they were designed to generate a forward reaction rate, the maximum release of uranium (see References 12 and 14).

DLS and TEM analyses were performed on liquid samples to evaluate the presence of colloids. A widely dispersed bimodal distribution was identified, with particles at about 10 and 300 nm, similar to what was seen in the uranium metal tests. After 8 months of storage, the colloids were still stable in solution. Composition was found to be silicates and aluminum silicates, but no uranium was detected (see References 12 and 14). The colloids may provide sites for transport of fission products, but tests with irradiated aluminum-based fuel were not performed and are no longer scheduled.

Alteration products were closely monitored using SEM analysis. Figure 4-17 shows a microscopic view of the fuel meat and its composition (UAl_3) prior to test initiation. A thin gel layer of aluminum hydroxide was found across the sample surface after only 16 days, and remained throughout the experiment. Composition of the gel was identified as boehmite ($Al_2O_3 \cdot H_2O$), which agrees with results from Savannah River Site experiments. Silicon and calcium were also found within the hydrogel layer.

Figure 4-18 is a closer view of the hydrated aluminum hydroxide (block-like crystals). The smaller spherical particles are uranium compounds (see References 12, 13, and 14).

Spherical uranium-rich patches embedded throughout the gel layer, shown in Figure 4-19, were identified as uranyl oxyhydroxides with aluminum, silicon, and calcium present. The spheres

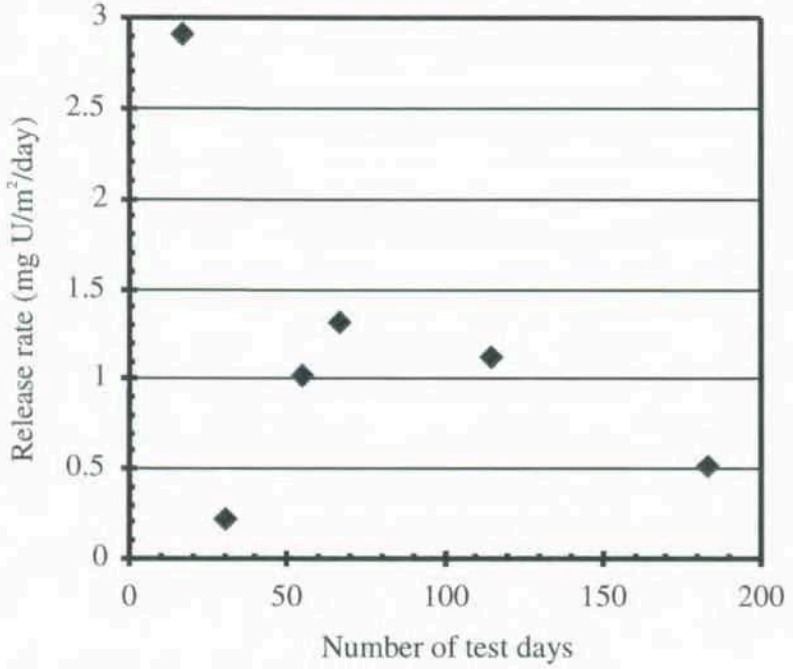

Figure 4-16. Uranium released into solution during drip tests.

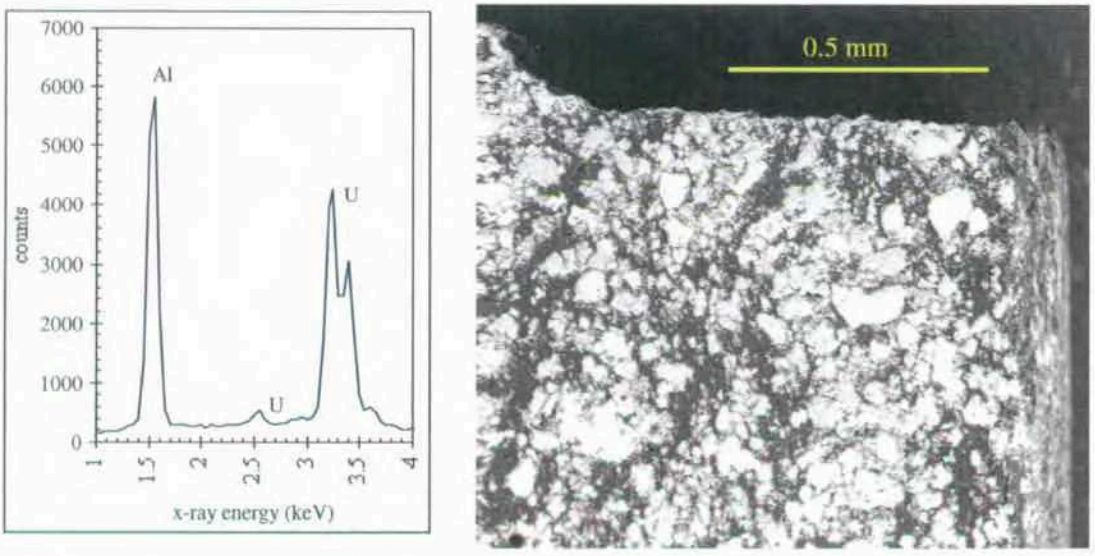

Figure 4-17. Initial surface and composition of unirradiated UAl_x fuel.

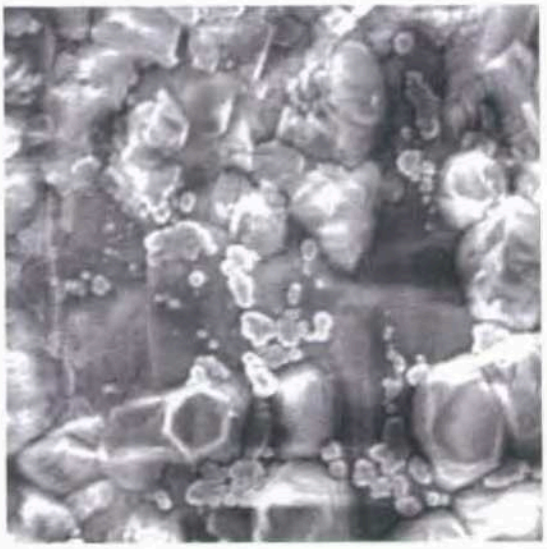

Figure 4-18. Hydrated aluminum oxide crystals in hydrogel.

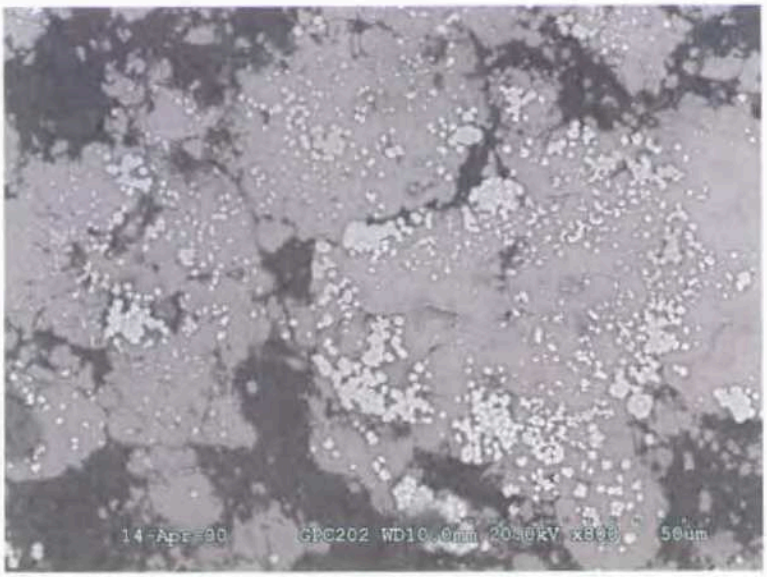

Figure 4-19. Uranium-rich spheres embedded in an aluminum oxide gel layer.

agglomerated and then began to break apart as seen in Figure 4-20. Eventually, after drying, the patches crystallized to form small platelets as shown in Figure 4-21. Analyses identified the platelets as schoepite and becquerelite measuring 1 to 5 μm on a side. A needle-like structure was also visible in the SEM analyses, but the composition could not be discerned. Savannah River Site personnel have also seen this structure and were not able to identify the composition, shown in Figure 4-22. Figure 4-23 is a closeup of the elongated structure showing triple-terminating crystals. It appears that the uranium was preferentially dissolved from the UAl_x particles and then precipitated within the aluminum hydroxide gel layer (see References 12, 13, and 14).

4.3.2 Unsaturated Drip Test Conclusions

The aluminum matrix within the UAl_x fuel reacts first with EJ-13 well water to form a thin gel layer of boehmite. UAl_x grains disassociate prior to leaving the layer, thus uranium releases are controlled by this hydrogel. Uranium leached from the fuel initially appears as spherical uranyl oxyhydroxide patches that quickly begin to agglomerate. When dried, these patches become platelets of schoepite and becquerelite containing calcium, silicon, and aluminum. Another uranium phase was found later in the experiments, appearing as elongated crystals, but the specific composition could not be discerned.

Significant amounts of uranium and aluminum were sorbed to the vessel walls; as much as 91 and 98% respectively. Colloids were identified as a bimodal distribution, consisting of silicates and alumino-silicates. No uranium was associated with the colloids. The release rate of uranium into solution (including the sorbed fraction) ranged between 0.2 and 2.9 $mg/m^2/d$. Previous flow through tests at 90°C with unirradiated fuel reported release rates between 8 and 27 $mg/m^2/d$. Higher rates are expected because flow through tests are designed to generate the forward reaction rate.

Figure 4-20. Uranium-rich aggregates breaking apart.

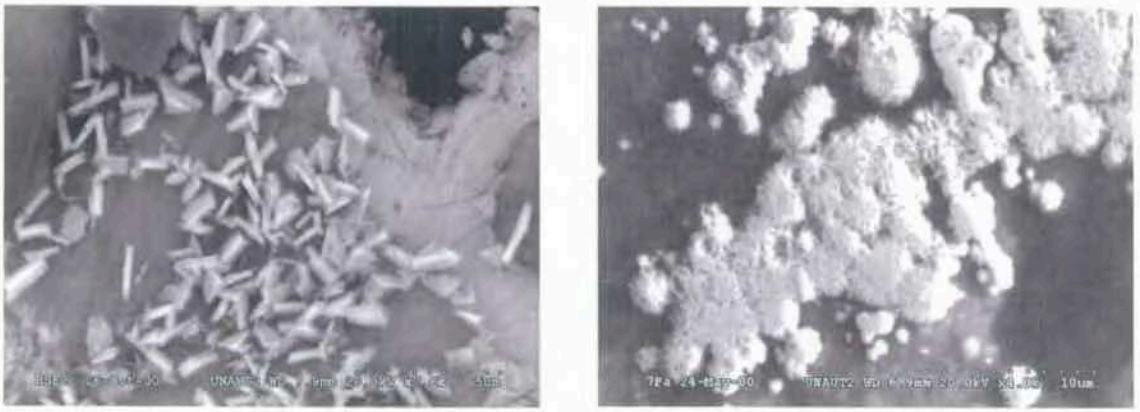

(a) (b)

Figure 4-21. Platelets crystallized from the uranyl oxyhydroxide patches.

Figure 4-22. Needle-like structure with an unknown composition.

Figure 4-23. Triple-terminating crystals of unknown composition.

4.4 Comparison with Literature

Aluminum corrosion in most waters occurs by localized attack, typically pitting. Thus, general corrosion rates can be very misleading and often confusing due to the high variability in values. Similar results have been seen with the aluminum-based fuels. Pitting of the aluminum matrix was identified in the flow through and static tests. Aluminum corroded preferentially to the uranium-aluminum particles, possibly indicating a galvanic effect. In the drip tests, an aluminum hydroxide (as boehmite) gel formed on the surface that controlled the release of uranium. Various environmental conditions (temperature, solution chemistry, etc.) altered the dissolution rate from that found with simulated J-13 well water. Some variations in degradation were found with different fuel types (UAl alloy fuels were the most reactive), and incongruent dissolution was seen with plutonium and technetium.

An extensive review of publications regarding aluminum alloy oxidation in air and water systems was documented in Reference 15. A regression analysis of all available data resulted in the rate expressions shown in Table 4-22. Note these are Arrhenius expressions that do not consider any environmental conditions except temperature.

Most of the data generated in the dissolution tests were for UAl alloy fuels and in the drip tests were for the UAl_x fuel. Figure 4-24 shows the dissolution rates from flow through tests presented in Section 4.2.2 (UAl alloy fuel only), drip tests discussed in Section 4.3.2, and the regression expression for those two fuel types from Table 4-22. Only one equation is used to represent water and saturated water vapor conditions because the literature shows little difference in the reactions (see Reference 15). Dissolution test results using simulated J-13 fall near or below the UAl alloy line, indicating the expression is a fairly good representation of the expected repository reactions. As expected, changing the water chemistry (high pH, low pH, carbonate, and nitric solutions) increased the reaction rate, and the regression was no longer applicable. The high chloride solutions resulted in release rates near those found with J-13 water.

Drip tests, however, with EJ-13 water were significantly lower than predicted from the literature data. Release of uranium in these tests was controlled by the gel layer, which was not described in the dissolution tests. This could be a transitional phase that releases larger amounts of uranium after an initial

Table 4-22. Reaction rate expressions from regression of literature data for aluminum-based fuels.

Fuel Type/Environment	Rate Expression (mg/cm^2/hr)	Temperature Range
UAl Alloy/water	$k = 4.29\exp[-32.8\pm1.8/RT]$	25–360°C
UAl_x/water	$k = 5.20\exp[-34.9\pm2.3/RT]$	178–350°C
U_3Si/oxygen	$k = 1.65 \times 10^7\exp[-70.5\pm17.9/RT]$	350–550°C
U_3Si_2/oxygen	$k = 8.19 \times 10^1\exp[-22.6\pm2.7/RT]$	300–400°C
$U_3Si(\delta)$/water	$k = 6.38 \times 10^4\exp[-56.1\pm6.1/RT]$	100–343°C
U_3Si(cast)/water	$k = 4.37 \times 10^7\exp[-62.7\pm33.7/RT]$	100–125°C

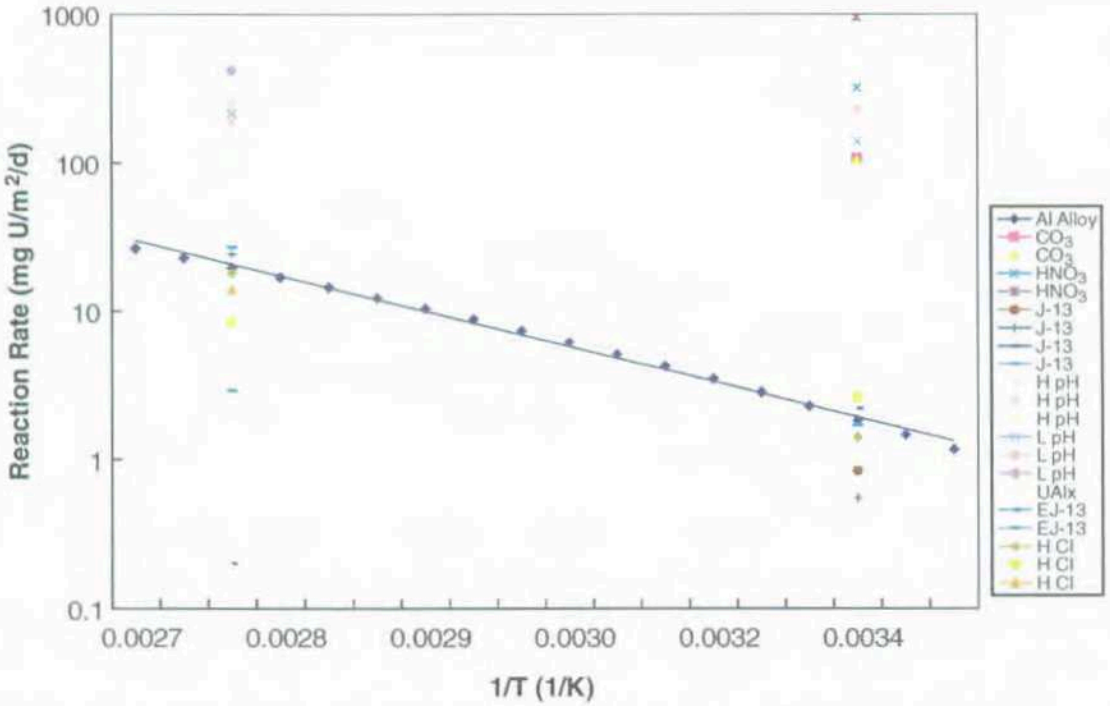

Figure 4-24. Regression analysis from literature and experimental data of UAl alloy and UAl_x fuel tests.

time period. Or it may be a phenomenon associated with the test methodology that was not identified in the flow through or the static tests (flow through tests are designed to produce a maximum release rate, and static tests provide a continuous supply of reactant). No further investigations are currently planned to study aluminum-based fuel in a drip test, and thus the cause of the lower release rates will remain a question.

Only a few experimental data points from the flow through tests are available for each of the other three fuel types and all are at 25°C. (These data are not shown in Figure 4-24.) The UAl_x fuel group includes U_3O_8 resulting in six values (three solution chemistries for each fuel). Using the equation for UAl_x in Table 4-22 at 25°C, the dissolution rate would be 0.95 mg/m^2/d. This value bounds the rates of UAl_x (0.19 mg/m^2/d) and U_3O_8 (0.14 mg/m^2/d) in simulated J-13 water. However, the rates in bicarbonate solution (22 mg/m^2/d for UAl_x and 33 mg/m^2/d for U_3O_8) and nitric acid (82 mg/m^2/d for UAl_x and 31 mg/m^2/d for U_3O_8) were above the literature regression, as was true for the UAl alloy fuel. Several models for silicide fuels were derived from the literature, but none for U_3Si_2 in water, which is the only

laboratory data generated. It is expected the same trend would be found with this fuel group; the regression describes the reaction in J-13 water fairly well but underestimates the rates in other solution chemistries.

Predictive models to be used in the license application for DOE owned SNF in the proposed repository at YMP are presented in an analysis/model report.[16] For simplicity, all aluminum fuels are assumed to follow the same degradation mechanism. The estimates for the aluminum-based fuel release/degradation model were extracted from the Analysis/Model Report and are shown below. No dependence on temperature is presented, although absolute values are given at two temperatures. The best estimate model is based on the uranium dissolution rate from flow through tests with irradiated U_3Si_2 SNF in simulated J-13 well water at 25°C. A factor of ten is applied to estimate the higher temperature value. A similar method was applied to the conservative model, using the flow through dissolution rate of U_3Si_2 SNF in bicarbonate solution at 25°C. The upper limit assumes all radionuclides within a waste package are available for transport at the moment the canister is breached.

Upper limit model:	full release over Total System Performance Assessment time (same for all fuels)
Conservative model:	36 mgU/m^2/d @ 25°C 360 mgU/m^2/d @ 90°C
Best-estimate model:	0.22 mgU/m^2/d @ 25°C 2.20 mgU/m^2/d @ 90°C

Table 4-23 presents all the experimental data collected during the release rate test project using aluminum-based fuel as well as the Analysis/Model Report estimates and the UAl alloy regression predictions in bold. Most of the tests were performed with unirradiated UAl alloy fuels. However, the best estimate and conservative model values in the Analysis/Model Report were based on irradiated U_3Si_2 fuel. At 25°C, the best estimate model predicts the four irradiated fuel tests in nominal J-13 water fairly well, but not under any other conditions, including the unirradiated tests in nominal J-13. As mentioned earlier, the same test at two different facilities resulted in dissolution rates that differed by about a factor of 10 (19-UAl wrought material in nominal J-13 water at 25°C, rates of 0.26 and 2.2 mgU/m^2/d). All values shown in Table 4-23 that are below 1.0 mgU/m^2/d are from tests performed at PNNL. It may be that a discrepancy between the test methods is causing significant differences in the test results. If so, using one of the data points from one of the laboratories may not be the best estimate of what will actually occur in a repository. For groundwater conditions at ambient temperatures, the literature regression is probably the best model, or a single value of about 2.0 mgU/m^2/d. A value that encompasses all the data produced with the various test methodologies would be the optimum conservative model, at least 300 mgU/m^2/d for 25°C.

A similar condition exists at the elevated temperature of 90°C. The best estimate value is less than all the results except the drip tests with unirradiated UAl_x fuel. Release rates from the drip tests were reported as a range between 0.2 and 2.9 mg U/m^2/d, but only the two end points are shown. Regression of the literature data resulted in about 20 mgU/m^2/d at 90°C, which is a better approximation of the available data. A conservative estimate of at least 450 mgU/m^2/d would encompass the experimental results generated by this project.

Table 4-23. Model predictions and experimental data of aluminum-based fuel dissolution rates in $mgU/m^2/d$.

Data Source	25°C	Data Source	90°C
U_3O_8 SNF, nominal J-13	0.14	*UAlx, drip test, EJ-13*	0.2
UAl SNF, nominal J-13	0.17	***Best estimate model***	***2.20***
UAl_x SNF, nominal J-13	0.19	UAlx, drip test, EJ-13	2.9
U_3Si_2 SNF, nominal J-13	0.22	13.2-UAl, wrought, nominal J-13	8.2
Best estimate model	***0.22***	13.2-UAl, wrought, high chloride	8.4
19-UAl, wrought, nominal J-13	0.26	25-UAl, cast, high chloride	14.0
13.2-UAl, cast, high chloride	1.4	13.2-UAl, cast, high chloride	18.0
13.2-UAl, cast, nominal J-13	1.7	***Regression from literature***	***19.6***
Regression from literature	***1.8***	13.2-UAl, cast, nominal J-13	24.2
19-UAl, wrought, nominal J-13	2.2	25-UAl, cast, nominal J-13	26.9
25-UAl, cast, high chloride	2.6	13.2-UAl, cast, high J-13	86
UAl_x SNF, bicarbonate	22	25-UAl, cast, high J-13	96
UAl_x SNF, nitric acid	28	13.2-UAl, wrought, low J-13	188
U_3O_8 SNF, nitric acid	31	13.2-UAl, cast, low J-13	215
19-UAl, bicarbonate	32	13.2-UAl, wrought, high J-13	248
U_3O_8 SNF, bicarbonate	33	***Conservative model***	***360***
UAl SNF, bicarbonate	33	25-UAl, cast, low J-13	420
U_3Si_2 SNF, bicarbonate	36		
U_3Si_2 SNF, nitric acid	36		
Conservative model	***36***		
UAl SNF, nitric acid	99		
13.2-UAl, cast, low J-13	139		
25-UAl, cast, low J-13	227		
19-UAl, nitric acid	298		

4.5 References

1. N. Iyer, "Activity Plan for Release Rate Testing of Aluminum Based Spent Nuclear Fuel," SRT-MTS-98-2021, Revision 0, April 1998.

2. ASTM C1431-99, "Standard Guide for Corrosion Testing of Aluminum-Based Spent Nuclear Fuel in Support of Repository Disposal," 1999.

3. W. J. Gray, "Dissolution Rates of Aluminum-Based Spent Fuels Relevant to Geologic Disposal," PNNL-11979, WSRC-TR-2000-00042, February 2000.

4. B. J. Wiersma and J. I. Mickalonis, "Preliminary Report on the Dissolution Rate and Degradation of Aluminum Spent Nuclear Fuels in Repository Environments (U)," WSRC-TR-98-0290 (U), August 1998.

5. W. J. Gray and C. N. Wilson, "Spent Fuel Dissolution Studies: FY 1991 to 1994," PNL-10540, 1995.

6. W. J. Gray, "Spent Fuel Dissolution Rates as a Function of Burnup and Water Chemistry," PNNL-11895, Pacific Northwest National Laboratory, 1998.

7. W. J. Gray and L. E. Thomas, "Initial Results from Dissolution Testing of Various Air-Oxidized Spent Fuels," Scientific Basis for Nuclear Waste Management XVIII, Vol. 333, Ed. A. Barkatt and R. A. Van Konynenburg, Materials Research Society, 1994.

8. B. J. Wiersma, J. I. Mickalonis, M. R. Louthan, Jr., "Evaluation of Test Methodologies for Dissolution and Corrosion of Al-SNF," ANS 3rd DOE Spent Nuclear Fuel and Fissile Material Management Topical Meeting, 1998.

9 M. Pourbaix, *Atlas of Electrochemical Equilibria in Aqueous Solutions*, London, Pergamon Press, 1966.

10. "Corrosion of Aluminum and Aluminum Alloys," Metals Handbook, Ninth Edition, *Corrosion*, Volume 13, 1987.

11. M. D. Kaminski, "Test Plan for Reactions Between Irradiated Uranium-Aluminum Fuel and J-13 Well Water under Unsaturated Conditions," SNF-3A-087, Revision 0, November 29, 1999.

12. M D. Kaminski and M. M. Goldberg, "Corrosion of Breached Aluminide Fuel under Potential Repository Conditions," 2001 International High Level Radioactive Waste Management Conference, 2001.

13. C. V. Shelton-Davis, INEEL, to Distribution, "May 11, 2000, Release Rate Test Review Meeting Minutes," CCN 00-012071, M. D. Kaminski Presentation, August 10, 2000.

14. C. V. Shelton-Davis, INEEL, to Distribution, "Meeting Minutes from NSNFP Release Rate Test Program Held on May 3, 2001," M. D. Kaminski Presentation, June 7, 2001.

15. B. A. Hilton, *Review of Oxidation Rates of DOE Spent Nuclear Fuel, Part 1: Metallic Fuel*, DOE/SNF/REP-054, Revision 0, September 2000.

16. T. A. Thornton, "DSNF and Other Waste Form Degradation Abstraction," ANL-WIS-MD-000004, Rev. 00, February 2000.

5. MIXED OXIDE FUEL

MOX fuel was chosen for experimental testing based primarily on the high fissile content of the inventory (1,329,113 curies, third largest group per Table 2-2.) and a plutonium content significantly higher than other oxide fuels. An activity plan was prepared describing the purpose of testing MOX fuel and the tasks planned for this particular fuel type, including sample selection.[1] Four tasks, or test methods, were discussed in the MOX activity plan: (1) fuel characterization, (2) unsaturated drip tests, (3) static batch tests, and (4) flow through dissolution tests. Colloid studies were added to the program at a later date as it became apparent that they could have an effect on the performance assessment. Each of these is described in Section 2. Quality assurance requirements were also defined in the activity plan. Characterization and some flow through tests were completed; static batch, unsaturated drip, and colloid tests were in progress at the termination of the project.

Two MOX fuel pins irradiated in the Experimental Breeder Reactor-II as part of a US/Japan cooperative program were chosen as representative material for the release rate test program. Selection was based on the relatively high plutonium content (~25 wt%) and high burnup. The fuel was fabricated at Los Alamos National Laboratory to specifications for the driver fuel for the Fast Flux Test Facility and the Japanese MONJU reactor. They were both irradiated under steady state conditions for a total of 833 effective full power days to provide benchmarks for sibling pins that were subsequently subjected to transient overpower tests. Outside diameter of the stainless steel cladding was originally 7.50 mm and 0.404 mm thick. Fuel pin UW02010 was enriched to 67% ^{235}U and had a peak burnup of 13.9 at.% (atomic percent of heavy metal atoms). Initially, the pin contained annular fuel pellets with an outside diameter of 6.538 mm and a 2.16-mm-diameter center hole. Pin UW08036 contained solid fuel pellets with the same diameter. Enrichment of this fuel was 54% ^{235}U and the peak burnup was 12.7 at.% (see References 1 and 2).

5.1 Characterization

5.1.1 Nondestructive Analysis

Characterization of the fuel included nondestructive techniques (dimensioning, gamma scan) and destructive analysis (ceramography, microprobe, and dissolution) as described in the test plan. ANL-E performed an axial gamma scan to provide a distribution of selected radionuclides for the full length of the pins. The ^{137}Cs profile gives a good indication of the movement of volatile fission products, and most have migrated to the ends of the fuel. The $^{95}Nb/^{95}Zr$ profile is a reasonable representation of the axial burnup as if forms a stable solid solution in the fuel and does not migrate. The distribution indicates a maximum in the center of pin with a minimum at the top. Little change in dimensions were found, only a small increase in diameter located where the cesium peaks were seen. Formation of lower density compounds from reactions between the cesium and fuel may have caused this phenomenon (see Reference 2).

5.1.2 Ceramography

Irradiation at Experimental Breeder Reactor-II resulted in a high centerline temperature (~2,100°C) and a steep temperature gradient (from 2,100 to 600°C over 3 mm). Cross sections were taken at three locations from UW02010 (1, 5.1, and 10.6 inches above the bottom) and one location from UW08036 (10.4 inches above the bottom) for metallographic examination at ANL-E. Massive grain restructuring and central voids were found as seen in Figures 5-1 and 5-2. Porosity was greatest in pin UW02010 at the 5.1-inch position, where highest power and fuel temperatures were seen. A gap region filled with a ceramic-like material was seen between the cladding and fuel meat. Three zones within the

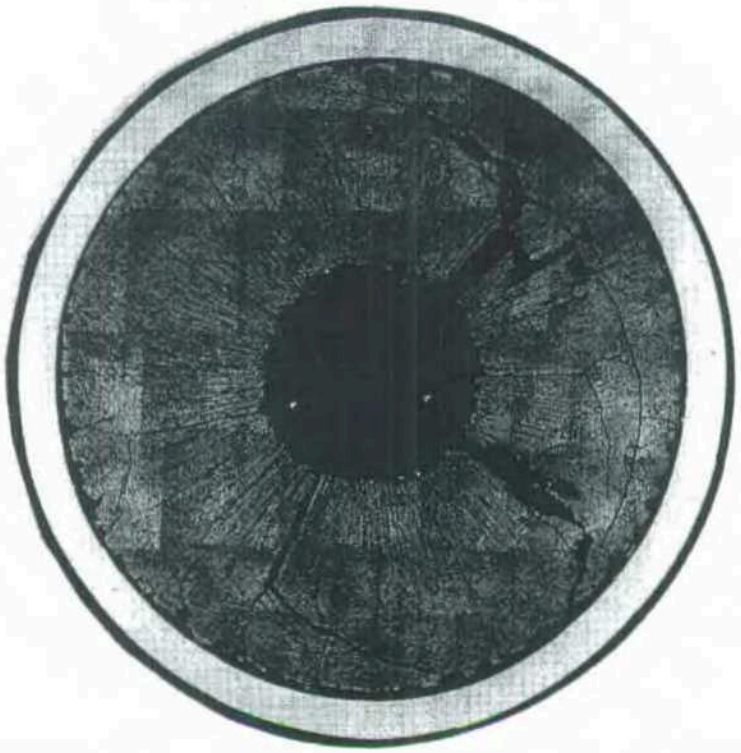

Figure 5-1. Cross section of pin UW02010 about 5.1 in. above the bottom of the fuel column.

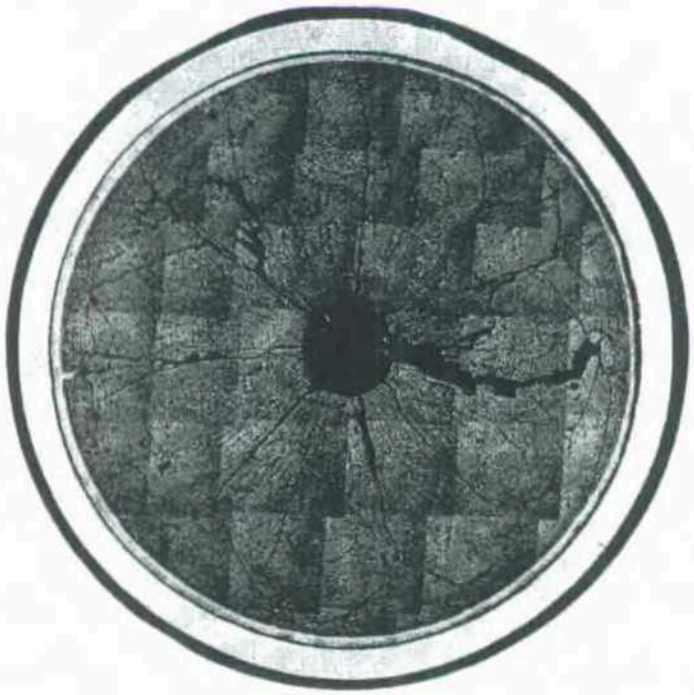

Figure 5-2. Cross section of pin UW08036 about 10.4 in. from bottom of the fuel column.

fuel were clearly visible, an inner zone of columnar grains, a central region of equiaxed grains, and an outer region with unrestructured grains (see Figure 5-3). Some indication of the operating temperature can be inferred from the size of the columnar equiaxed grains. For example, the larger zones exhibited by pin UW02010 indicate it operated at a higher temperature than pin UW08036. Cracking in the samples occurred during the rapid cooling once the reactor was shut down (see Reference 2).

5.1.3 Electron Microprobe Examination

Microprobe analysis was performed at ANL-E on a cross section from 10.6 inches above the bottom of pin UW02010 to determine the distribution of various radionuclides. Peak heights were measured for nine fission products at four locations, (1) the outer unrestructured area, (2) the equiaxed grain zone, (3) the columnar zone, and (4) the edge of the columnar zone near the void. As shown in Table 5-1, the results are quite variable. However, the fission products were generally at higher concentrations near the outer edge where no restructuring had taken place. Further analyses found that the more noble fission products (ruthenium, rhodium, technetium, molybdenum, etc.) were concentrated in metallic inclusions dispersed throughout the fuel. Plutonium concentration was fairly evenly distributed, with a maximum near the void and a minimum where the equiaxed and columnar grains meet. Uranium had an opposite distribution, the highest concentration at the equiaxed-columnar interface and the lowest near the void, but is even more uniform than the plutonium. Cesium, tellurium, and molybdenum appear to have migrated to the gap region between the fuel meat and the cladding. Iron, nickel, and chromium were also found in the gap material, and the cladding inner surface was irregular, indicating some fission product attack of the cladding, though to a small extent (see Reference 2).

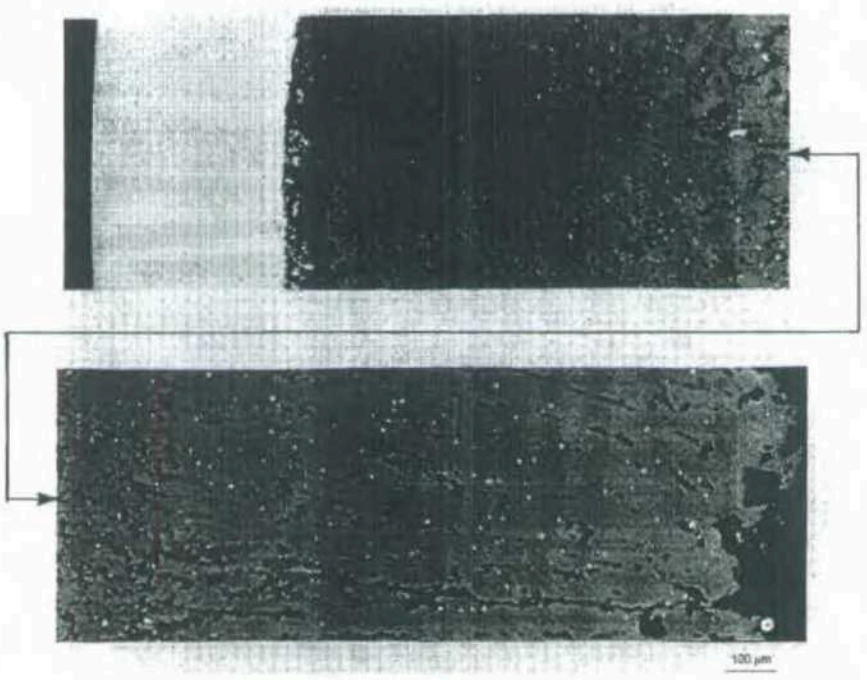

Figure 5-3. Radial micrograph of pin UW02010 about 10.6 in. from bottom of the fuel column.

Table 5-1. Microprobe x-ray peak heights from four locations of mixed oxide pin UW02010.

Element	Outer Edge (Counts)	Equiaxed Zone (Counts)	Columnar Zone Near Void (Counts)	Columnar Zone Mid-region Counts
Cs	12	9	ND	12
Zr	49	23	32	27
Mo	30	25	11	13
Ru	51	16	25	25
Rh	21	7	13	16
Pd	10	9	38	18
La	28	11	5	40
Pr	72	52	44	81
Nd	42	42	ND	23

ND = Not detected.

5.1.4 Dissolution Analysis

Isotopic composition of the MOX spent fuel was calculated using the computer code ORIGEN.[3] The composition was also checked by total dissolution of duplicate samples of the fuel at PNNL followed by analysis of the resulting solutions for uranium and certain radionuclides. The dissolution procedure consisted of heating the spent fuel in 8 M HNO_3 in a distillation apparatus designed to trap the iodine. The small amount of undissolved residue remaining in the vessel was fused using Na_2O_2 and, subsequently, dissolved with 6 M HCl. Analyses of the two solutions provided a measure of the inventories of selected isotopes in the fuel.[4,5]

Table 5-2 shows the average concentrations of uranium and selected radionuclides in the duplicate samples of dissolved MOX spent fuel. The measured fuel inventories are in reasonable agreement with the calculated inventories with the exceptions of ^{238}Pu, ^{129}I, and ^{99}Tc. For ^{238}Pu, the actual inventory is quite small, and the calculated value is based, in part, on the amount of ^{238}Pu that was assumed to be present in the fuel before irradiation. Because the starting value for ^{238}Pu was not well known, it was assumed, for computational purposes, to be the same as in certain elements of uranium metal fuel from Hanford's N-Reactor. Based on the measured value for the spent MOX fuel, it seems likely that the starting ^{238}Pu concentration that was assumed for the calculation was too low (see Reference 5).

Table 5-2. Inventories of uranium and certain radionuclides in mixed oxide fuel.

	U (μg/g)	^{129}I (μg/g)	$^{239/240}Pu$ (μCi/g)	^{238}Pu (μCi/g)	^{137}Cs (μCi/g)	^{99}Tc (μCi/g)	^{90}Sr (μCi/g)
Measured	5.58×10^5	376	1.70×10^4	3.93×10^3	2.59×10^5	16.4	1.57×10^5
Calculated	5.97×10^5	587	1.57×10^4	1.21×10^3	2.56×10^5	38.7	1.70×10^5

In the case of ^{129}I, there are at least two possible reasons why the measured value could be low. First, some of the ^{129}I could have migrated to the cooler plenums at the ends of the fuel rod under the influence of temperature gradients during reactor operation. Second, some of the ^{129}I could have escaped as a vapor from the fuel rod after it was cut open and before sampling took place at PNNL. The measured value for ^{99}Tc could be low because some of the technetium is present in the form of ε-phase metallic particles that do not readily dissolve. Despite the fact that a Na_2O_2 fusion procedure was used during dissolution with the objective of getting the technetium into solution, it is possible that less than 100% of the ε-phase technetium actually dissolved (see Reference 5).

5.1.5 Grain Boundary and Gap Analysis

As demonstrated by the microprobe examination in Section 5.1.3, mobile radionuclides migrate under the influence of temperature gradients during reactor operation into the grain boundaries and the gap region between the fuel and the cladding. In the gap regions, these soluble elements are available for immediate contact by any water that might penetrate the waste container and fuel cladding. Soluble elements that are concentrated within the grain boundaries are not as accessible to water as they are in the gaps, but they can still be preferentially leached from the fuel over a period of months to a few years.[6] Knowledge of the amount of these elements (primarily ^{129}I and ^{137}Cs) located in the gaps and grain boundaries allows assessment of the potential for their release into the biosphere (see Reference 5).

PNNL performed a two-step process to measure the ^{129}I and ^{137}Cs inventories in the gap and the grain boundaries of the MOX spent fuel. Cladding was removed from a 12-mm long fuel segment, and both portions were leached with KI. The solution was analyzed for ^{129}I using ICP-MS, uranium using a Scintrex UA-3 analyzer, and ^{137}Cs using gamma-energy spectroscopy. Uranium measurements were used to estimate the amount of iodine and cesium released from the fuel matrix. It was assumed that the cesium and iodine dissolved congruently with the UO_2/PuO_2 matrix. Based on inventory measurements described in Section 5.1.4, 59 to 92% of the total ^{129}I inventory and about 81% of the total ^{137}Cs inventory had migrated to the gap regions of the fuel. The lower value listed for ^{129}I was based on the calculated total inventory listed in Table 5-2, and the higher value was based on the measured total inventory. These high percentages (compared with values of <1% to about 20% found in LWR spent fuels)[7] undoubtedly occurred because of the high temperatures during reactor operation, which caused the volatile elements to migrate to cooler regions of the fuel (see References 4 and 5).

Following the gap inventory measurements, the cladding was discarded and the fuel was ground to grain and subgrain-sized particles, exposing the grain boundary surfaces. The powdered fuel was then leached with KI, and the solution was analyzed for uranium, iodine, and cesium concentrations as before. Grain boundary measurements of ^{129}I and ^{137}Cs were less than 1% of their total inventories. Thus, while these volatile elements must migrate along grain boundaries to the cooler regions of the fuel, it is clear that little or none of the iodine and cesium remained within the grain boundaries. As noted above, most of these elements were deposited in the gap regions of the fuel (see Reference 5).

5.2 Flow Through Dissolution Tests

Flow through dissolution tests with MOX fuel were performed at PNNL to define the forward reaction rate and to evaluate the effects of varying the temperature, pH, carbonate level, and oxygen content (see Reference 4). Samples from element UW08036, described in Section 5.1, were used in the experiments. Similar tests have also been conducted with LWR spent fuel, thereby allowing direct comparisons (see Reference 5).

Approximately 100 to 200 mg of grain-size MOX fuel was placed in the specimen cell with a flow rate of 12 mL/hr (see Section 5.2.2 on sample preparation). This combination of test specimen size

and water flow rate leads to concentrations of uranium and other sparingly soluble elements, such as plutonium, that are below solubility limits but are high enough to be readily measurable.[8] Periodically (one to three times per week initially but later reduced to once per week), the outlet solution was collected over a period of about an hour. To ensure the dissolved elements remained in solution, a small amount of nitric acid was placed in the collection vials prior to sampling.[9] The samples were analyzed for concentrations of uranium and selected radionuclides (see Reference 5).

5.2.1 Test Matrix

Twelve experiments were planned with the MOX spent fuel grain particles to evaluate varying conditions and for comparison with LWR fuel test results. Two concentrations of carbonate/bicarbonate, two temperatures, two pH values, and two oxygen levels were planned as well as variations to the J-13 water chemistry, as shown in Table 5-3. Tests M1 through M8, which was conducted with pure carbonate/bicarbonate solutions, represents half of a full factorial matrix of four variables with two levels of each variable (see Reference 4). It also includes four of the tests used in earlier testing of LWR spent fuel (see Reference 8), which allows for direct comparisons under those conditions.

Oxygen concentration was included as a test variable, even though the proposed Yucca Mountain repository is expected to be generally in equilibrium with the atmosphere, because localized oxygen concentrations could be reduced by reactions with waste package components such as iron. Oxygen pressures greater than atmospheric were not considered credible, so the variation was only downward. Temperatures of 25 and 75°C are expected to allow the dependence of the dissolution rate on temperature to be determined without approaching the boiling point where experimental difficulties might be encountered. Differences spanning two orders of magnitude were chosen for each of the other variables. Total carbonate/bicarbonate concentrations ranged from 10-fold higher to 10-fold lower than in J-13 well water. (The nominal carbonate content of J-13 well water is 2×10^{-3} molar.) Carbonate and oxygen concentrations and pH will be maintained by sparging with an appropriate gas. In addition, tests M11 and M12 were added because it is possible for small amounts of nitric acid to be generated via radiolysis of the moist air environment in a repository. Adjustments to the pH of J-13 well water will be made with HNO_3 (for pH of 4) and NaOH (pH of 10) (see Reference 4).

Two additional tests were planned with MOX fragments using the conditions shown in Table 5-3 test numbers M3 and M9. Fragment sizes were about 0.1 to 5 mm. Results from the fragment tests are used to determine the extent of water penetration into the grain boundaries and aid in extrapolation of the grain tests to repository conditions (see Reference 4).

5.2.2 Test Specimen Preparation

Special preparation of the test specimens was required to achieve the optimum size distribution of particles. First, the fuel was discharged from a 12-mm-long section of cladding and crushed until most of it passed through a screen with 25-μm openings. The MOX fuel grains ranged from a low of ~10 μm up to a few 10s of μm in size as a result of columnar grain growth toward the central regions of the fuel pellets (see discussion in Section 5.1). Screening eliminated most of the particles larger than a single 20-μm grain. Next, the fine subgrain particles produced by the crushing were removed from the screened fuel by washing, first with 2×10^{-4} M Na_2CO_3 solution (pH ~10) and then with deionized water to remove the Na_2CO_3. This process may also remove any restructured "rim" material from the test sample. Figure 5-4 shows the screened and washed powder consisting predominantly of single grains or grain fragments (see Reference 9) with few small subgrains remaining. The surface area of this powder was measured using the BET method[10] to be 0.22 m^2/g (see Reference 5).

Table 5-3. Test matrix planned for mixed oxide spent fuel flow through grain tests.

Test Number	Oxygen (% of atm)	Temperature (°C)	$[CO_3^{-2}]+[HCO_3^-]$ (molar)	pH
M1	0.2	25	2×10^{-4}	8
M2	20	75	2×10^{-4}	8
M3	20	25	2×10^{-2}	8
M4	0.2	75	2×10^{-2}	8
M5	20	25	2×10^{-4}	10
M6	0.2	75	2×10^{-4}	10
M7	0.2	25	2×10^{-2}	10
M8	20	75	2×10^{-2}	10
M9	20	25	Simulated J-13	~8
M10	20	75	Simulated J-13	~8
M11	20	25	Simulated J-13	4
M12	20	25	Simulated J-13	10

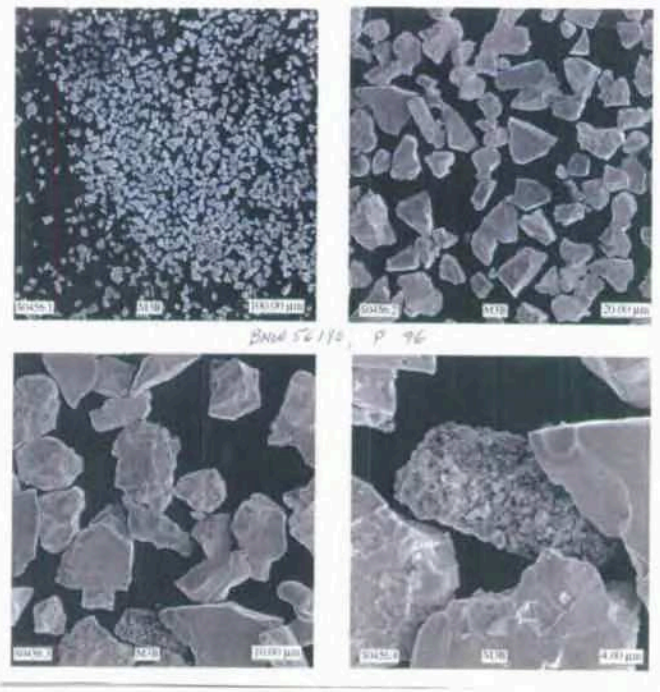

Figure 5-4. Screened and washed particles of mixed oxide spent fuel.

The fuel specimen prepared by this method exhibits two important characteristics relative to measurement of the UO_2/PuO_2 matrix dissolution. First, the surface area measured by the BET method is thought to be a good representation of the surface that is contacted by water during the dissolution measurements. A good surface area measurement is required if flow through test results from different fuel specimens are to be compared. In the absence of crushing the fuel down to grain size powder, water can partially penetrate into the grain boundaries, and this portion of the water-contacted surface area cannot be adequately measured (see Reference 8). Second, elevated concentrations of elements, such as cesium, along grain boundaries are removed by the washing of the screened powder. Subsequent flow through tests then provide information on the behavior of the UO_2/PuO_2 matrix without interference by preferential dissolution of cesium from the grain boundaries (see Reference 5).

Fragments of MOX fuel were also tested for comparison with the grain size specimens. A similar method was used to collect particles measuring about 0.1 to 5 mm on any one side. The surface areas for the fragments were determined assuming they all had cube geometrical shapes according to the following equation. A roughness factor of 3 was subsequently applied to the calculated surface area (see Reference 5).

$$A = 6.0\left(\frac{M}{\rho}\right)^{2/3} cm^2 \qquad (5\text{-}1)$$

where

A = surface area (cm^2)

M = weight (g)

ρ = density of spent fuel (assumed to be 10.08 g/cm^3).

5.2.3 Solution Preparation

Two types of solution were used in the MOX flow through tests, pure carbonate/bicarbonate solutions and simulated J-13 well water. Bicarbonate/carbonate solutions were prepared ten times more concentrated (2×10^{-2} molar) and ten times less concentrated (2×10^{-4}) than the nominal J-13 well water (2×10^{-3} molar). Simulated J-13 was prepared according to Section 2.3 and two tests were performed with modified J-13 well water. One was prepared at a pH of 4 using HNO_3 to simulate possible nitric acid from radiolysis of the moist air environment in a repository. The other solution had a pH of 10, using additions of NaOH, to simulate the presence of other degradation products. Below are analytical results from three samples of simulated J-13 well water compared to the nominal composition (Table 5-4) (see References 4 and 5).

5.2.4 Flow Through Test Results

Nine of the fourteen planned experiments (twelve with grain particles and two with fragments) were completed. Table 5-5 shows the conditions for the tests that have been completed and identifies the test number for coordination with Table 5-3. All of the tests to date were exposed to atmospheric oxygen, ~20%. Reduced oxygen tests were planned for the future, but will not be performed due to the abrupt termination of the project. The specimen used in test M3 was also used in test M8, and specimen M5 was used in test M2. Temperature was not measured in the test vessel, so the average hot cell or oven set temperature is reported in Table 5-5. Flow rates and pH shown are the average values for the entire test period. Anticipated values for pH are in parentheses. Tests with fragments are identified with an F as part of the test number (see Reference 5).

Table 5-4. Composition of simulated J-13 well water for MOX flow through tests.

Ions	Nominal Concentration (mg/liter)	ICP Analytical Concentrations (mg/liter)		
		F28-J13	F29-J13	F30-J13
Ca	13.2	10.3	11.2	11.0
K	5.3	5.8	4.9	5.4
Mg	1.9	1.9	1.9	2.0
Na	44.4	45.0	46	50
Si	33.2	33.3	35	34
Cl	7.1	6.7	NM	NM
F	2.3	2.2	NM	NM
NO_3	8.1	11.1	NM	NM
SO_4	18.1	15.8	NM	NM
HCO_3	124	NM	NM	NM

Table 5-5. Conditions of completed flow through tests with mixed oxide spent fuel.

Test No.	Surface Area (cm^2/g)	Sample Weight (g)	Temp. (°C)	Flow Rate (mL/min)	Chemistry $[CO_3^{-2}]+[HCO_3^-]$ (molar)	pH	CO_2 Sparge (ppm)
M3	2,210	0.1719	25	0.217	2×10^{-2}	8.33 (8)	11,000
M5	2,210	0.1860	25	0.251	2×10^{-4}	8.52 (10)	0.9
M9/ M10	2,210	0.1717	25	0.238	J-13	8.04 (8)	None
M11	2,210	0.1740	25	0.234	J-13	3.50 (4)	None
M12	2,210	0.1705	25	0.235	J-13	9.45 (10)	None
M2	2,210	0.1719	75	0.222	2×10^{-4}	7.05 (8)	125
M8	2,210	0.1860	75	0.240	2×10^{-2}	9.92 (10)	55
M3F	12.1	2.5088	25	0.214	2×10^{-2}	8.13 (8)	11,000
M9F	12.1	2.0017	25	0.208	J-13	8.13 (8)	None

Throughout the course of testing, samples were collected from the flow through tests one to three times per week initially and once per week later on. Each of these samples was analyzed for uranium content and some were analyzed for other isotopes. Dissolution rates were normalized from uranium analyses according to the following equation (see Reference 5).

$$R = \frac{C_i F}{M A f_i} \tag{5-2}$$

where

R = dissolution rate based on component i ($mg/m^2/d$)

C_i = concentration of component i in effluent (mg/mL or Bq/mL)

F = flow rate (mL/d)

M = mass of test specimen (mg)

A = surface area of test specimen (m^2/mg)

f_i = concentration of component i in test specimen (mg/mg or Bq/mg).

A graphical representation of dissolution rates calculated using Equation (5-2) versus time was prepared for each test completed. Once steady state is visually apparent on the graph, an average dissolution rate is calculated. By normalizing the data prior to plotting, the points at a given time for all isotopes should fall on top of one another if the fuel dissolved congruently. By averaging the data over time, comparisons between MOX and commercial LWR (UO_2) fuel and the effects of variations in environmental conditions can also be evaluated.

5.2.4.1 Comparison of Isotopic Dissolution Rates. Grain size MOX fuel particles (discussed in Section 5.2.2) were tested in the flow through apparatus with varying environmental conditions. Specific conditions by test number are shown in Table 5-3. Figure 5-5 below is a graph of test M3 (first section) and M8 (second section). A solution of 2×10^{-2} M Na_2CO_3 was used in both tests, but the temperature (from 25 to 75°C) and pH (from 8 to 10) were modified at about 157 days. Figure 5-6 shows tests M5 (first section) and M2 (second section) at a lower carbonate concentration of 2×10^{-4} M Na_2CO_3 with an increase in temperature (from 25°C to 75°C) and a decrease in pH (from 10 to 8) at about 157 days. A third graph, Figure 5-7, presents the results from test M9 and M10 in simulated J-13 well water with a change in temperature from 25 to 75°C at 100 days (see Reference 5).

Perhaps the most notable feature in the three graphs is the large difference between the results for $^{239/240}Pu$ and ^{238}Pu. Separation of plutonium isotopes could only occur if the different isotopes dissolved predominantly from different phases at different rates. Fabrication of this MOX fuel type was from sintering a mixture of UO_2 and PuO_2 powders resulting in islands of PuO_2 particles in a UO_2 matrix rather than atomic-scale mixtures of the UO_2 and PuO_2. The original PuO_2 consisted mostly of ^{239}Pu and very little ^{238}Pu. During irradiation, ^{238}Pu builds into the UO_2 phase, which was enriched to 54% ^{235}U. In this way, the spent MOX fuel consists of a UO_2 phase that contains much of the ^{238}Pu and a separate PuO_2 phase that contains most of the $^{239/240}Pu$. Data in the figures clearly show that the PuO_2 phase, where most of the $^{239/240}Pu$ resides, dissolved much more slowly than the UO_2 phase, where much of the ^{238}Pu is found (see Reference 5).

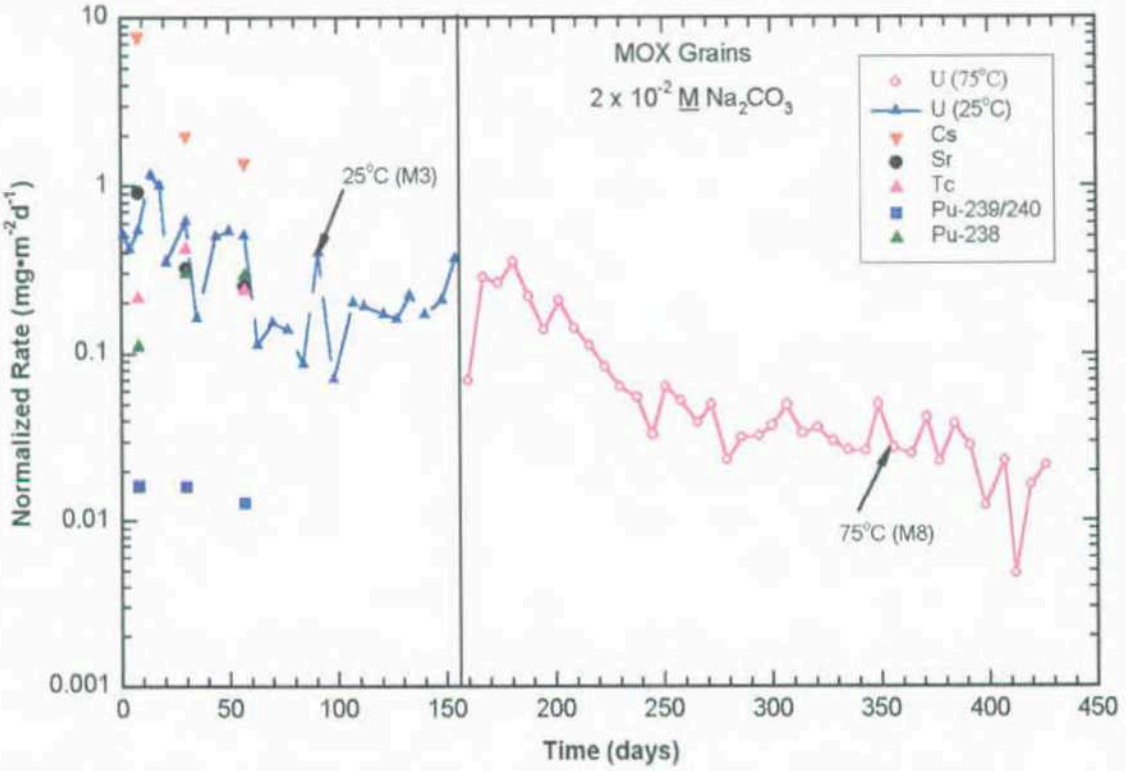

Figure 5-5. Dissolution rate of mixed oxide fuel in 2×10^{-2} M carbonate, tests M3 (pH = 8, temperature = 25°C) and M8 (pH = 10, temperature = 75°C).

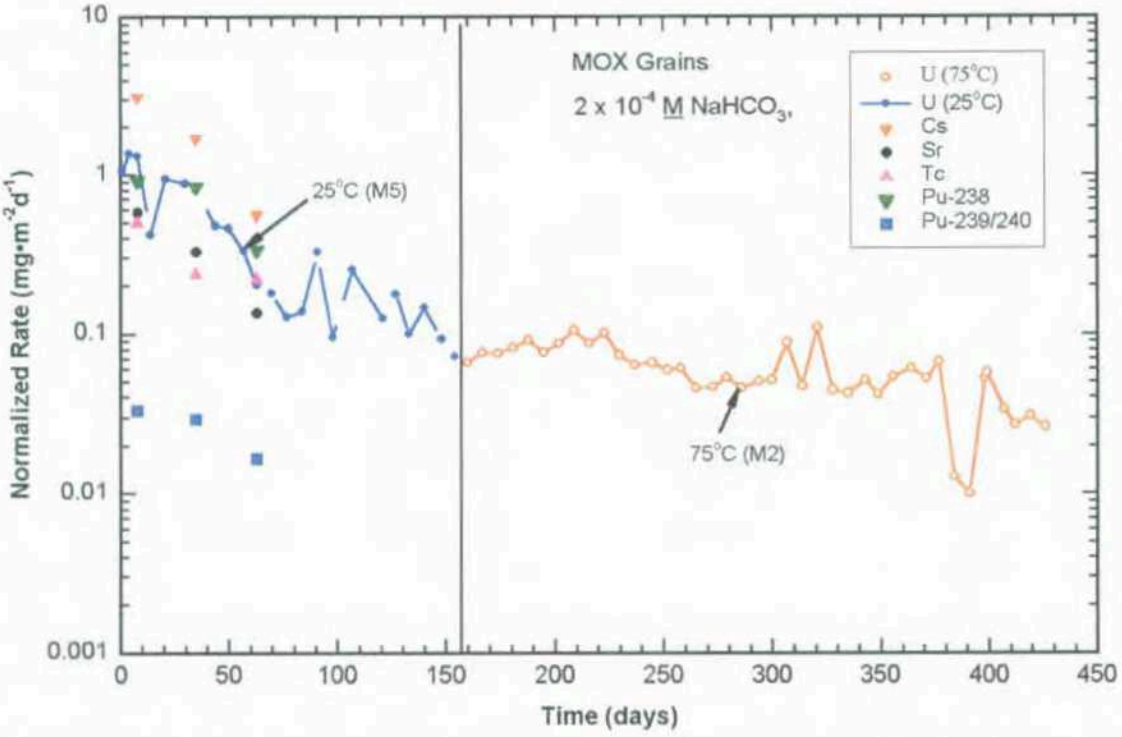

Figure 5-6. Dissolution rate of mixed oxide fuel in 2×10^{-4} M carbonate, tests M5 (pH = 10, temperature = 25°C) and M2 (pH = 8, temperature = 75°C).

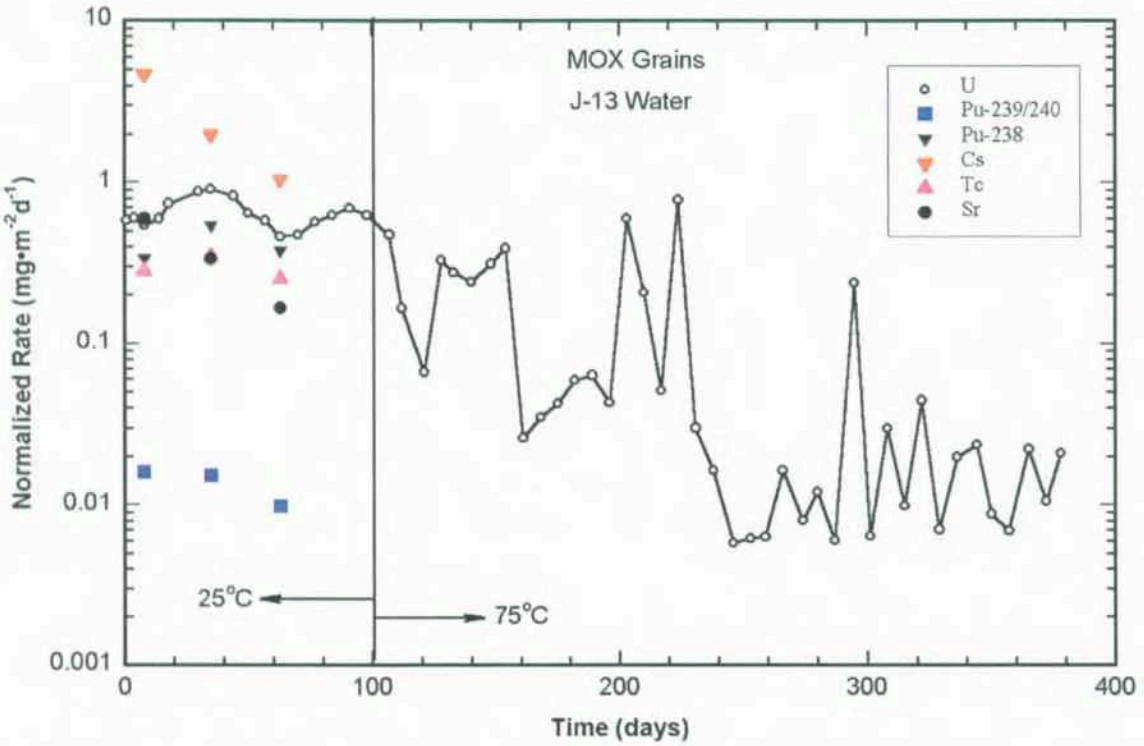

Figure 5-7. Dissolution rate of mixed oxide fuel in simulated J-13 well water, tests M9 (temperature = 25°C) and M10 (temperature = 75°C), both at pH ~8.

Another potential reason for the slower dissolution rate of PuO_2 is related to the reaction process. Dissolution of UO_2 is preceded by the oxidation of uranium to the +6 valence state (see Reference 6), which is easily accomplished in oxygenated systems, and then readily dissolved. On the other hand, PuO_2 is fairly stable and quite insoluble; therefore, it will dissolve more slowly than UO_2. Unlike uranium, small amounts of PuO_2 probably dissolve as a Pu^{+4} species, which are then oxidized in solution to the +5 or +6 valence state.[11] The results of MOX spent fuel dissolution tests with reduced concentrations of dissolved oxygen may have shed some light on this question, but they are not currently planned.

Support for the argument that the PuO_2 phase dissolves slower than the UO_2 phase can also be found in the strontium data. In LWR (UO_2) spent fuels, strontium typically dissolved congruently with the uranium (see Reference 8). However, Figures 5-6 (low carbonate solution) and 5-7 (simulated J-13 well water) show that the strontium dissolved slower than uranium from the MOX spent fuel. This is to be expected if the PuO_2 phase dissolves much slower than the UO_2 phase, because about 20% of the strontium is located in the slowly dissolving PuO_2 phase. This is a consequence of about twice as many fissions occurring in the UO_2 phase as in the PuO_2 phase plus the ^{90}Sr has a 2.7-fold higher fission yield from ^{235}U than ^{239}Pu (see Reference 5).

An argument like that for strontium could also be made for technetium. However, the technetium data are subject to greater uncertainty simply because the concentrations in the samples are near detection limits. Also, a portion of the technetium is found in ε-phase metallic particles that do not dissolve readily, so it does not always dissolve congruently with the UO_2 (see Reference 5).

Cesium results are high compared to the uranium data in all three cases. The rates shown are normalized to the amount of ^{137}Cs expected in the UO_2 and PuO_2 matrixes after accounting for the amount migrated to the gap region. Cesium in the gap region should have been eliminated during preparation of

the fuel specimen. The fact that the normalized ^{137}Cs rates are higher than uranium probably means that either an incorrect cesium inventory in the UO_2 and PuO_2 matrixes was assumed or cesium is preferentially leached out of the matrix (see Reference 5).

5.2.4.2 Comparison with Commercial LWR (UO_2) Dissolution Rates. Most of the dissolution test results are variable over time, and thus, reported average rates are approximate numbers. Single values are useful for comparison purposes, but ranges and error bands need to be considered when long-term degradation rates are being calculated. The initial data for MOX dissolution in a high carbonate solution, Figure 5-5 test M3, show the average uranium dissolution rate of about 0.2 $mg/m^2/d$ after an initial transient period. Faster dissolution rates, with a reported average of 4 $mg/m^2/d$, have been observed for LWR (UO_2) spent fuels under these same conditions.[12,13] Test M8 (also in Figure 5-5) resulted in a rate of 0.02 $mg/m^2/d$ with the MOX fuel compared to 14 $mg/m^2/d$ reported for LWR fuel at the same conditions. In the low carbonate solution (Figure 5-6), test M5 conditions produced the same average dissolution rate as with the LWR fuel, 0.5 $mg/m^2/d$. Test M2 conditions, also shown in Figure 5-6, resulted in a dissolution rate of about 10 $mg/m^2/d$ with LWR fuel and about 0.1 $mg/m^2/d$ with MOX fuel. Table 5-6 presents a comparison between the two fuel types with the respective test conditions (see Reference 5).

It appears the uranium dissolution rate of MOX fuel is less than what was found with LWR (UO_2) fuel, and a statistical comparison confirmed the theory. Possible reasons for slower dissolution of the UO_2 phase in MOX spent fuel relative to LWR spent fuel are highly speculative. The only known differences, besides the presence of a PuO_2 phase in the MOX fuel, are the higher burnup of the MOX fuel and associated higher concentrations of fission products. It is tempting to suppose that the higher fission product concentrations may somehow stabilize the UO_2 phase, perhaps making it harder to oxidize uranium to the +6 valence state and thereby making it dissolve slower. However, the fission product concentrations in the UO_2 phase of MOX fuel are only slightly higher than in moderately high burnup (50 MWd/kg) LWR fuel. The total fission product concentration in MOX fuel is about 2.2 times greater than in the LWR fuel, but about half of that is in the PuO_2 phase (see Reference 5).

Another difference between MOX and LWR spent fuels is the high temperatures encountered during reactor operation. This may have caused diffusion of plutonium into the UO_2 phase from the PuO_2 phase of the MOX fuel, resulting in more atomically dispersed plutonium in the UO_2 phase. As discussed in Section 5.1.1, the centerline temperatures were sufficiently high to cause melting, resulting in a central void and columnar grain growth adjacent to the central void. It is possible some atomic-scale mixing of the two phases also occurred. If the UO_2 phase of the MOX spent fuel contains a large amount of plutonium relative to LWR spent fuel, the plutonium (which is more difficult to oxidize than the uranium) might stabilize the U(IV) valence state. Such stabilization of valence states in solid solutions with fixed-valence cations has been reported.[14,15] If the U(IV) valence state is stabilized, then the rate of dissolution would be reduced because of the need to oxidize uranium to the +6 state prior to dissolution (see Reference 5).

Table 5-6. Comparison of mixed oxide and light water reactor flow through dissolution rate tests.

	Test M3	Test M8	Test M5	Test M2
Temperature (°C)	25	75	25	75
pH	8	10	10	8
CO_3 (M)	2×10^{-2}	2×10^{-2}	2×10^{-4}	2×10^{-4}
LWR rate (mg $U/m^2/d$)	4	14	0.5	10
MOX rate (mg $U/m^2/d$)	0.2	0.02	0.5	0.1

5.2.4.3 Effects of Environmental Conditions. Tests varying temperature, pH, and carbonate concentration were completed, but the oxygen dependency tests have not been done. Data from the LWR experiments resulted in the following expression to describe the rate dependence on temperature, pH, carbonate, and oxygen pressure (see Reference 8).

$$\log(R) = 9.310 + 0.142\log[CO_3] - 16.7\log(P_{O2}) + 0.140\log[H] - 2{,}130/T + 6.81\log(T)\log(P_{O2}) \quad (5\text{-}3)$$

where

R = reaction rate in $mg/m^2/d$

CO_3 = carbonate concentration in moles/L

P_{O2} = O_2 pressure in atm

$\log[H]$ = pH

T = temperature in kelvin

Oxygen pressure was significant to the dissolution rate of LWR fuel and may play an important role with MOX fuel. However, a similar relationship cannot be derived for MOX fuel at this time because the experiments with various oxygen pressures are not complete. Based on the four data points available, no terms (pH, temperature, or carbonate concentration) made a statistically significant impact on the dissolution rate. For example, the rates at 75°C were lower than the rates found at 25°C, but the variation is within the error expected with the small database.

A further study of the effects of varying temperature and pH was performed with simulated J-13 well water. Figure 5-7 displays the change in temperature at a constant composition, and Figure 5-8

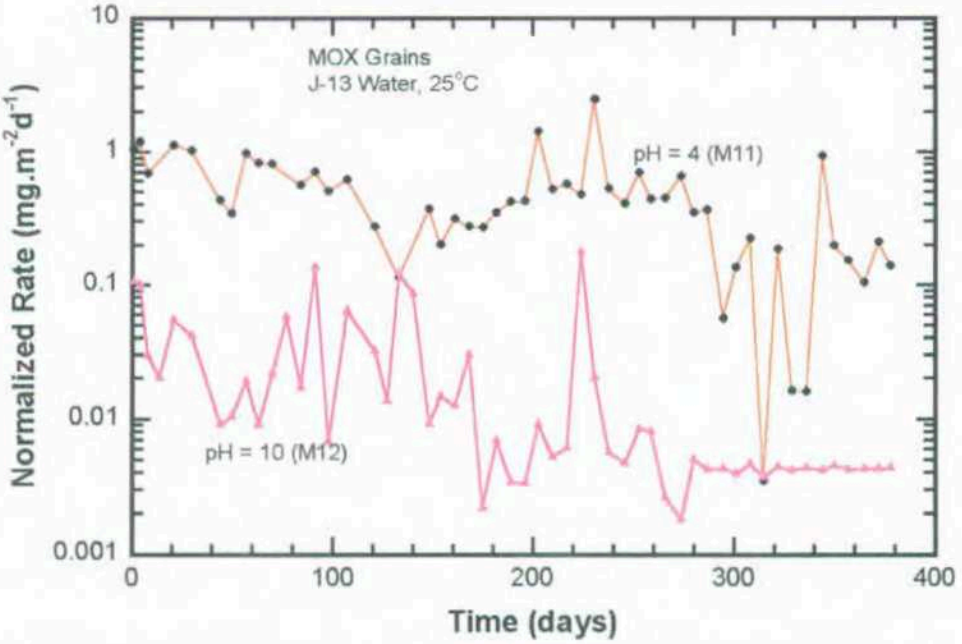

Figure 5-8. Dissolution rate of mixed oxide fuel in simulated J-13 well water, tests M11 (pH = 4) and M12 (pH = 10), both at 25°C.

shows the effects of varying pH from ~8 to 4 and to 10 at a constant temperature. Data for all four conditions with simulated J-13 well water are shown on Figures 5-7 and 5-8. Decreasing the pH clearly increases the dissolution rate; however, most of the data are erratic. One possible reason for the variability is the formation of secondary phases during the testing. A buildup of secondary phases on the particulate surfaces followed by spallation could be causing the up and down behavior observed. Similar behavior was seen with the carbonate solutions (Figures 5-5 and 5-6), but less pronounced (see Reference 5).

Another observation that may support the secondary phase formation for MOX in the J-13 water is plate out of the uranium in the sample cell and the outlet stainless steel tubes. In addition, no sample was left at termination in the sample cells with high and low pH (tests M11 and M12). The time of complete dissolution is unknown and the cumulative uranium dissolution measurements did not account for the initial mass (only 4.2% uranium from M11 and 0.2% uranium from M12 was recovered). Because the mass balance is so poor, these data cannot be used in any predictive fashion, and thus, no analyses have been performed. The cause of this apparent increased dissolution rate has not been resolved, but the presence of colloids may have played a role (see Reference 5).

5.2.4.4 Effects of Particle Size. Figure 5-9 shows the dissolution kinetics of MOX fragments (see Section 5.2.2) in two water chemistries. The dissolution rate of fragments in the carbonate/bicarbonate solution was higher than in simulated J-13 well water. However, dissolution of MOX grains in carbonate/bicarbonate solution and simulated J-13 well water were essentially equal (Figure 5-10). The erratic data for the MOX dissolution rates in simulated J-13 well water for both grain and fragment sizes complicate the comparison (see Reference 5).

The comparison for the MOX grains and fragment dissolution kinetics is shown in Figure 5-11 for a carbonate/bicarbonate solution. Similar to the data for LWR spent fuel, the MOX fragments appear to have a higher dissolution rate than the MOX grains. This may be partially due to the difficulty in making accurate assessments of the actual surface area of the samples used. The grain surface area is measured by the BET technique, and the fragment surface area is determined by the mass density method (Section 2.3.1). Discontinuous dissolution may also play a significant role. Accelerated attack of the grain boundaries, available in the fragments but not in the grains, has been postulated in the literature.

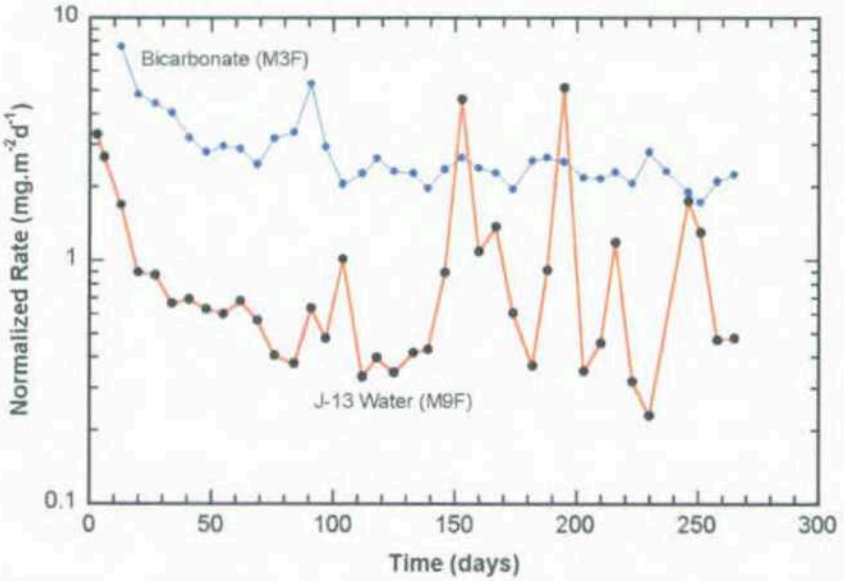

Figure 5-9. Dissolution rate of mixed oxide fuel fragments in carbonate/bicarbonate solution (test M3F) and simulated J-13 well water (test M9F) at 25°C.

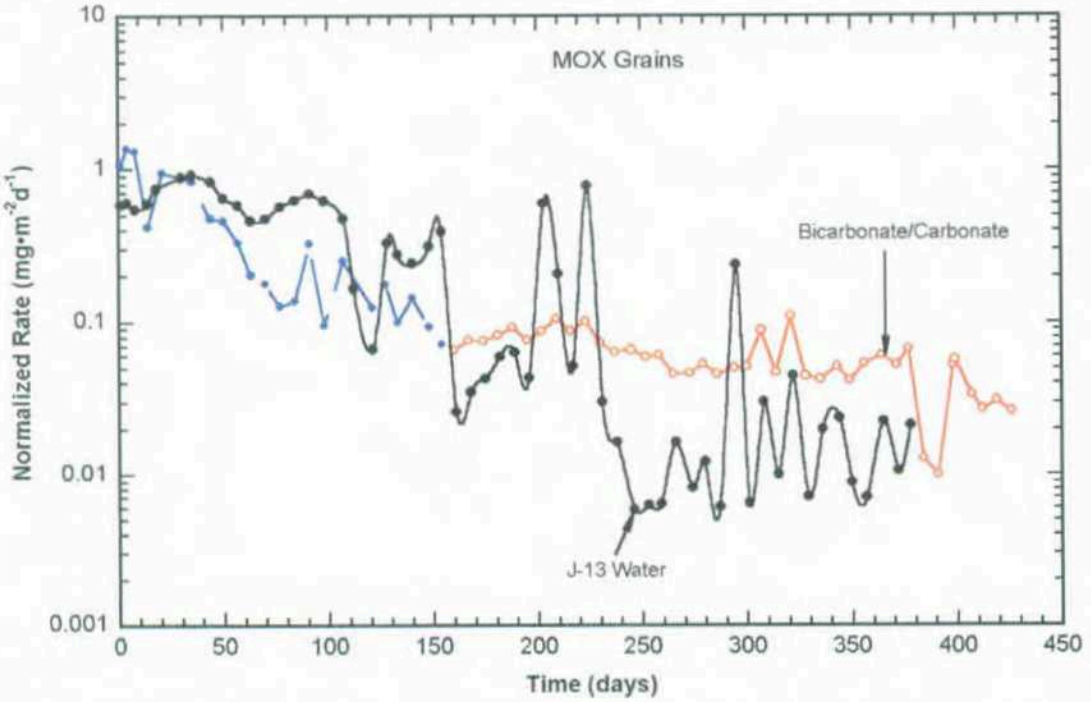

Figure 5-10. Dissolution rate of mixed oxide fuel grains in bicarbonate/carbonate solution (tests M2 and M5) and simulated J-13 well water (tests M9 and M10) at 25°C.

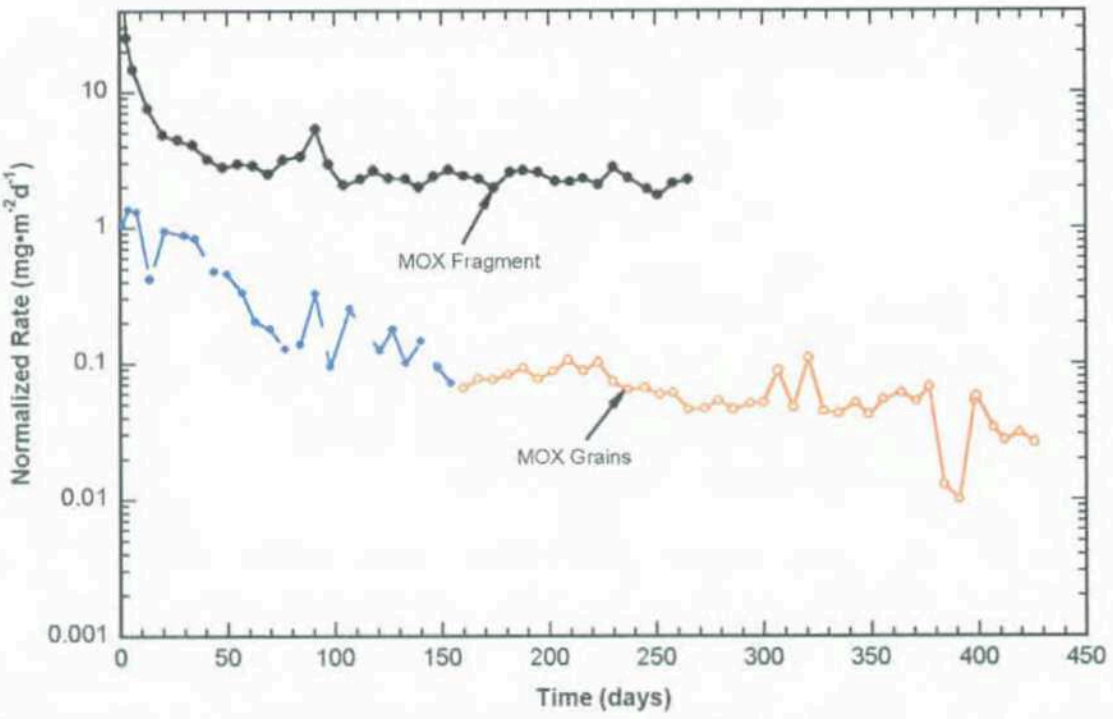

Figure 5-11. Dissolution rate of mixed oxide fuel grains (tests M2 and M5) and fragments (test M3F) in bicarbonate/carbonate solution at 25°C.

Comparison of the dissolution rates of fragments and grains in simulated J-13 well water is more difficult to analyze due to the large variability in the data. But the dissolution rate appears to be higher with the fragments than the grains (similar to the results in carbonate/bicarbonate solution) (see Reference 5).

5.2.5 Flow Through Test Conclusions

Although four of the planned flow through experiments with MOX fuel have not been completed and some of the data are questionable (particularly the simulated J-13 tests at high and low pH), several conclusions can be made from the test results. Below is a summary of these conclusions (see Reference 5).

1. The pellet/cladding gap contains most of the semivolatile fission products, I-129 (59–92%) and Cs-137 (~81%). Total inventory of these isotopes at the grain boundaries was less than 1%, suggesting fast diffusion along the grain boundaries.

2. Average dissolution rates for the UO_2 phase in MOX fuel are slower than LWR UO_2 spent fuel.

3. The PuO_2 phase had a slower dissolution rate than the UO_2 phase in the MOX fuel matrix.

4. ^{238}Pu formed in the UO_2 phase by neutron capture in ^{235}U showed congruent dissolution kinetics with the uranium matrix.

5. Dissolution rates for the MOX fragments are greater than for grain-sized particles for both simulated J-13 well water and carbonate/bicarbonate solution. This observation is similar to the behavior of LWR spent fuel dissolution in the two water chemistries.

6. The dissolution rate did not show a significant change when the temperature was increased from the ambient condition (i.e., 25°C) to about 75°C.

5.3 Unsaturated Drip Tests

Unsaturated drip tests with MOX fuel were performed to evaluate the release of radionuclides in a repository relevant environment. Test apparatus similar to that used in the commercial LWR fuels was used, with a one-stage holder (see Section 2.2.3) that had 20-μm diameter holes in the base. Reactions with MOX fuel are significantly slower that uranium metal fuel, and thus the three-stage holder designed to prevent plugging of the mesh from alteration products was not needed. Objectives of this test method include chemistry changes of the exposure solution over time, dissolution rate of the fuel matrix, rate and form of released radionuclides, and the composition of alteration products.[16] These tests were initiated in 1998. Thus about 3.5 years worth of exposure were completed prior to the project termination.

5.3.1 Test Matrix and Sample Preparation

Samples from each of the two fuel elements, UW02010 and UW08036, characterized in Section 5.2, were used in the drip tests. No unirradiated tests were performed. Experiments included a high drip rate (0.75 mL/3.5 days), a low drip rate (0.075 mL/3.5 days), and vapor test. A vapor atmosphere was created by placing 10 mL of solution in the base of the test apparatus. Element UW02010 segments were exposed to all three conditions, but element UW08036 was only exposed in the vapor test. All tests were performed at 90°C, and EJ-13 well water was used as the exposure solution (see Section 2.3 for description and composition). Because of the relatively slow reaction rates (compared to uranium metal fuel), liquid and alteration product samples were taken approximately every 6 months. Visual, microscopic, SEM/EDS, XRD, and TEM examinations were planned for the solid samples and

pH, ICP-MS, and sequential filtration/DLS (for colloid identification) were used with the liquid samples. Because of the high radiation field associated with the solid samples, changes in analytical staff, and the early termination of the release rate project, no information on the alteration products was produced (see Reference 16).

Sections of the two MOX fuel elements were removed and washed with alcohol to remove any fines. Figure 5-12 shows the burnup profile of the two fuels and the location where the test samples were sectioned. Cladding was removed from the samples by an extraction method. The fuel meat was then crushed, and the fragments were placed in the test apparatus. Surface area was estimated based on geometric calculations as about 1 to 2×10^{-3} m^2/g (see References 16, 17, and 18).

ORIGEN code calculations were used to predict the composition distribution of the fuel elements based on their irradiation history. However, it does not model the diffusion of nuclides due to a heat gradient. Because this gradient was so steep across the 3-mm MOX fuel radius (from 2,100°C at centerline to 600°C at the surface), extensive movement of volatile radionuclides was expected. Section 5.1 discusses the measurements made on the fuel samples, which were then compared to the ORIGEN calculated values. Ratios of measured to calculated values of uranium, plutonium, and neptunium were between 0.85 and 1.0, indicating the model is a reasonable representation. However, technetium, molybdenum, cesium, and iodine ratios were less than 0.4. Cesium and iodine are volatile elements known to accumulate in the gap region, where measurements were not made. These variations were taken into account when the release fractions were calculated for test samples.[19]

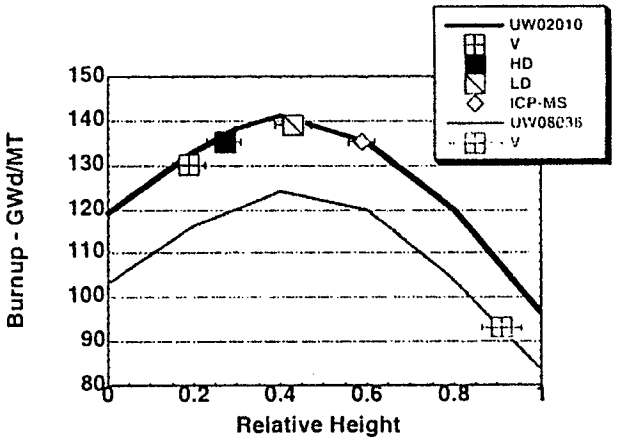

Figure 5-12. Mixed oxide fuel element burnup profile and test sample location.

5.3.2 Irradiated Test Results

Experimental results are available through the 2.5-year sampling. The test project was terminated prior to the removal of the 3.5-year sampling, and analysis of the 3-year samples was not complete. Visual inspection of the fuel fragments after 30 months did not show significant alteration, although radionuclides were being released into solution at small concentrations. In contrast, obvious reaction products were visible on commercial fuel after that length of time. One distinct crystal was seen after 1.5 years, but identification was not completed prior to the project termination (Figure 5-13). A variety of radionuclides could be traced during the analyses due to the high enrichment and large burnup of the original fuel element. Release fractions were defined as the mass of a specific radionuclide divided by the original nuclide mass in the sample (based on measured or ORIGEN calculated values). The release rate was then found by dividing the release fraction by the number of exposure days. Graphical representations of release rates with respect to test time show changes in release characteristics and allow

Figure 5-13. Alteration phase from mixed oxide vapor test after 1.5 years of exposure.

for comparisons with commercial fuel. Both fuel types are uranium oxide, though the MOX also contains a significant amount of plutonium oxide (~25%). Thus, rates were expected to be similar for most radionuclides (see References 18 and 20).

By examining cumulative releases of a number of radionuclides in the high drip rate tests, it is clear that reactions are not congruent. Larger fractions (at about 0.5) of ^{129}I, ^{137}Cs, and ^{97}Mo were released and smaller fractions (about 10^{-5}) of ^{239}Pu and ^{237}Np were seen. Other nuclides (^{99}Tc, ^{90}Sr, and ^{238}U) evaluated were released at fractions of about 10^{-3}. Figure 5-14 displays the cumulative fractional releases through 2.5 years of exposure. Note for nearly every isotope (all but ^{237}Np), initial releases at the 0.3-year sampling were low, but have remained stable since the 0.6-year sampling. Neptunium has been stable since about 1.5 years of testing. Table 5-7 converts the fractional releases to percent and lists the cumulative amount of each isotope released after 2.5 years (see Reference 18).

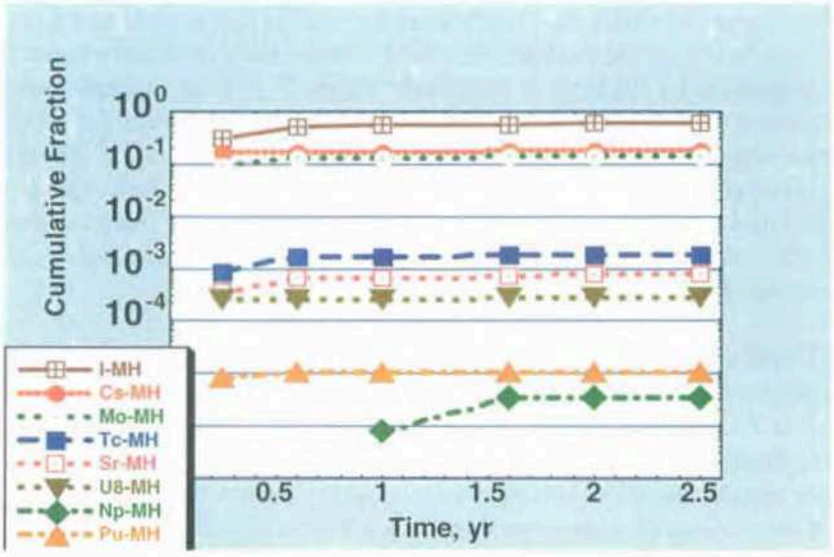

Figure 5-14. Cumulative fractional releases of selected radionuclides from the high drip rate tests with mixed oxide fuel.

Table 5-7. Percent of selected radionuclides released in high drip rate mixed oxide tests.

Radionuclide	Percent Released after 2.5 Years
^{129}I	>60%
^{137}Cs	17%
^{97}Mo	14%
^{99}Tc	0.2%
^{90}Sr	0.08%
^{238}U	0.03%
^{239}Pu	0.001%
^{237}Np	0.0003%

5.3.2.1 Comparison with Commercial LWR (UO_2) Fuel. A comparison of fractional release rates of each radionuclide discussed above from MOX and LWR commercial fuel high drip tests was graphed over time. Figures 5-15 to 5-18 show the comparison of selected radionuclides (^{238}U, ^{137}Cs, ^{129}I, and ^{99}Tc). In every case there was an initial higher rate of fractional release, which typically leveled out after about 1.5 years. Generally, the trends between MOX and LWR fuel were similar for each isotope but the difference in actual values varied by radionuclide. After 2.5 years of testing, release rates of ^{137}Cs, ^{97}Mo, ^{238}U, ^{239}Pu, and ^{237}Np from MOX and LWR experiments were within an order of magnitude with each other (Figure 5-15 is an example). At that point in time, all but ^{237}Np values were higher from the MOX tests, though ^{238}U and ^{239}Pu rates had fluctuated back and forth over the course of the experiment (Figure 5-16). Neptunium rates were the same for both fuel types at nearly every sample time. Although the trends for ^{129}I and ^{99}Tc were similar to other nuclides, the final spread between MOX and LWR fuel was about twice, or two orders of magnitude. MOX rates were consistently higher for iodine (Figure 5-17), but LWR fuel rates with technetium were larger throughout the test (Figure 5-18) (see Reference 18).

5.3.2.2 Effects of Water Volume. Comparisons were also made between the high drip, low drip, and vapor tests after 2 years of exposure. Trends were not readily discernable and a great deal of variation was visible in the data. In the 2-year samples, fractional release rates of most radionuclides were within about an order of magnitude for the three test methods. Figure 5-19 is an example showing similar trends and values of ^{129}I release rates regardless of the test conditions throughout the experiment. Exceptions include ^{137}Cs (with a variation of nearly four orders of magnitude), ^{239}Pu, and ^{237}Np. However, for some nuclides, samples taken at earlier times had very different results. For example, results of ^{90}Sr at 2 years were similar for the three test conditions, but varied nearly three orders of magnitude at 1.5 years (Figure 5-20). Based on these data, it is not clear that the solution drip rate or only vapor makes any difference on the resulting release of radionuclides (see Reference 19).

Average release rates were calculated through 2.5 years of testing for two radionuclides, ^{129}I and ^{97}Mo. Based on a geometric surface area of 2×10^{-3} m^2/g, the release rate of ^{129}I was 43 $mg/m^2/d$ and for ^{97}Mo was 14 $mg/m^2/d$. Cumulative releases of uranium were about two orders of magnitude less (Figure 5-14). Flow through tests (Section 5.2) reported release rates of uranium that were also about two orders of magnitude smaller. Results from the two test methods (flow through and unsaturated drip) would be similar if the volume of water exposure did not have a significant effect on the degradation rate (see Reference 18).

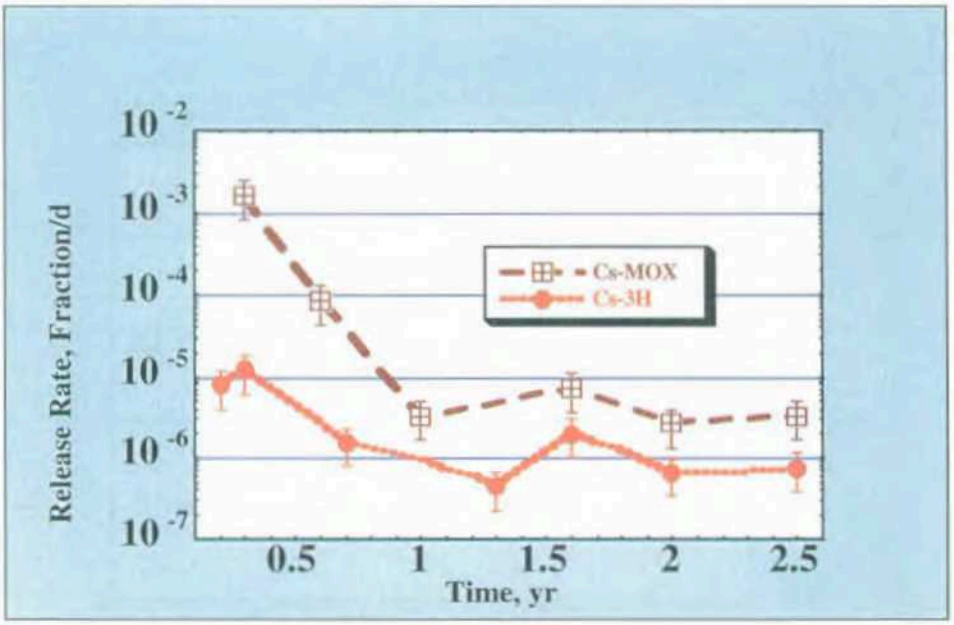

Figure 5-15. Fractional release rate with time of ^{137}Cs in mixed oxide and light water reactor fuels.

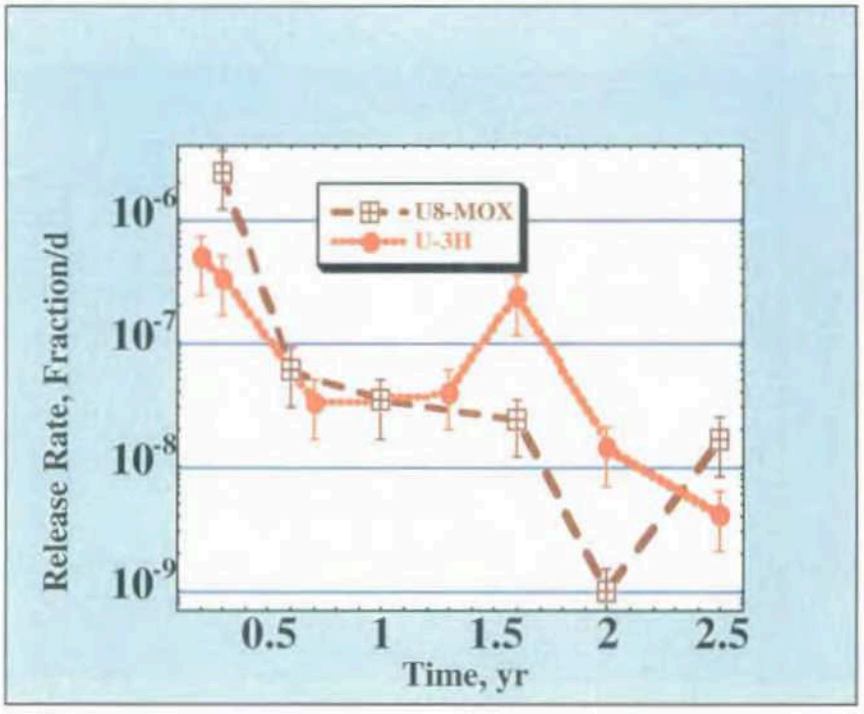

Figure 5-16. Fractional release rate with time of ^{238}U in mixed oxide and light water reactor fuels.

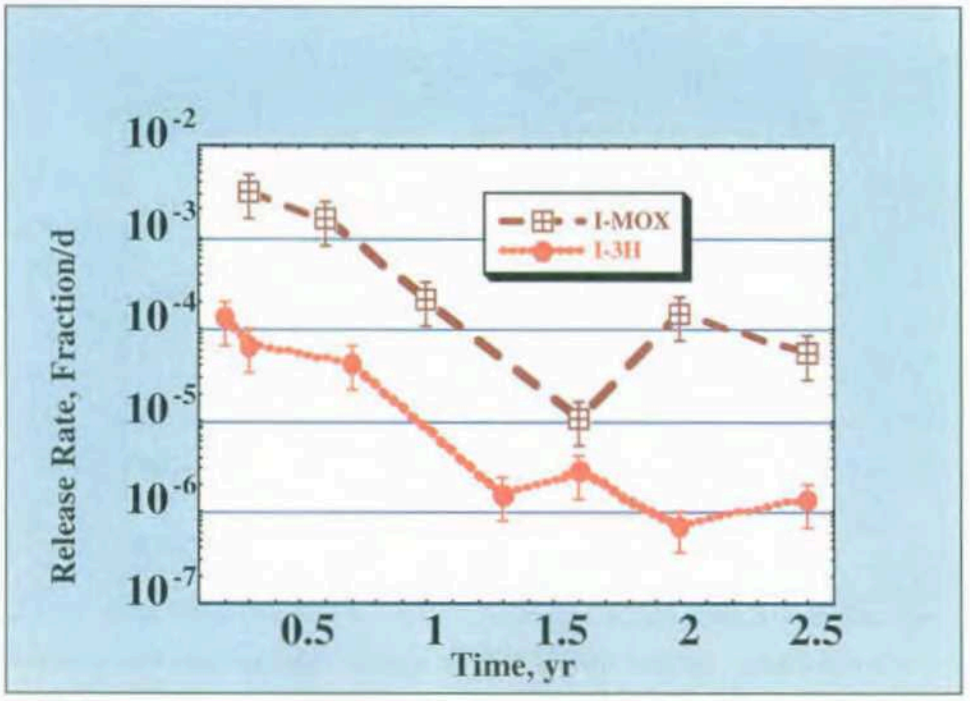

Figure 5-17. Fractional release rate with time of ^{129}I in mixed oxide and light water reactor fuels.

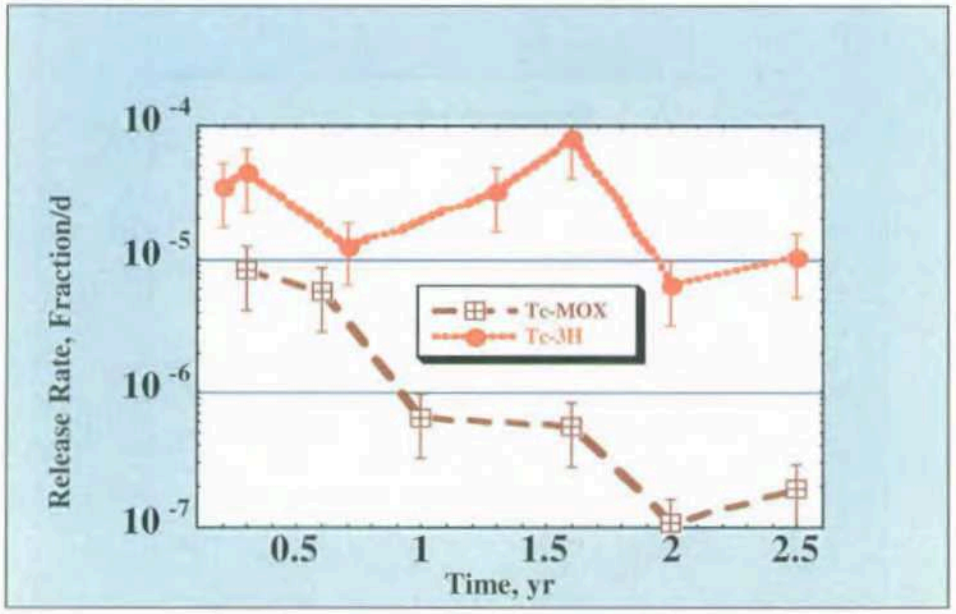

Figure 5-18. Fractional release rate with time of ^{99}Tc in mixed oxide and light water reactor fuels.

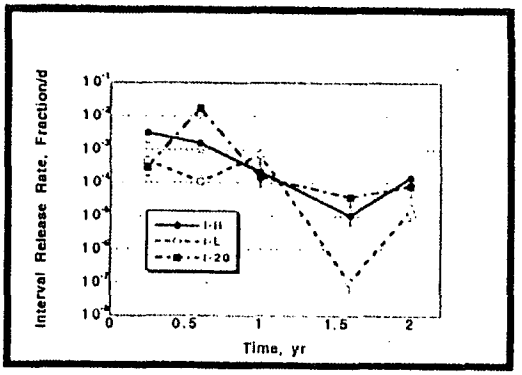

At 2 yr, the three ^{129}I release rates were within an order of magnitude.

H = High-drip
L = Low-drip
20=Vapor

Figure 5-19. Fractional release rate of ^{129}I from mixed oxide fuel in a high drip, low drip, and vapor drip test.

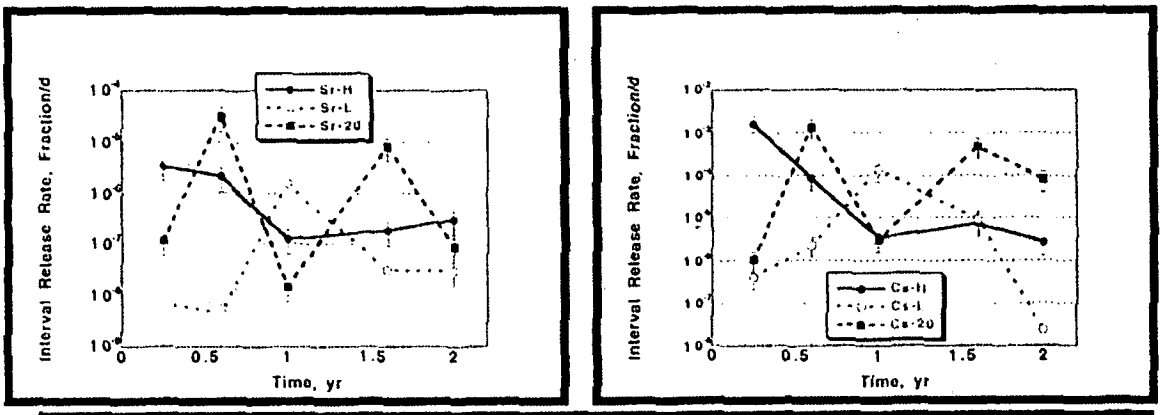

At 2 yr, the three ^{90}Sr release rates were within an order of magnitude of each other. However, the three ^{137}Cs release rates varied widely from each other.

Argonne National Laboratory
Chemical Technology Division

H = High-drip
L = Low-drip
20=Vapor

Figure 5-20. Fractional release rate of ^{90}Sr from mixed oxide fuel in a high drip, low drip, and vapor drip test.

Changes in pH of the EJ-13 well water collected in the base of the test vessel for each test condition was also recorded. Initial values were about 8.5, but they quickly dropped in all three tests. After 0.6 years, a minimum pH of about 5 was reached in the high drip tests, and then the level increased to about 9 by the 2-year sample. Results from the low drip test are similar but delayed slightly. A minimum pH of about 5.5 was reached after 1 year, and then it began to increase (no value was reported for two years). The vapor test also indicated a minimum pH at 6, but not until 1.5 years. This solution had increased to 8 by the 2-year sample. It appears the same phenomenon is occurring in all three tests, though fastest in the high drip experiment and slowest in the vapor test. Figure 5-21 displays the changes in pH for each test (see Reference 19).

5.3.3 Colloid Analyses

Portions of the liquid samples extracted from the unsaturated drip tests were analyzed for the presence of colloid-sized particles. Radionuclide associated colloids could potentially increase the concentration of a specific species above the solubility limit and ultimately release radionuclides at rates higher than anticipated. Of primary concern with the MOX fuels is the distribution of plutonium due to its high content in the fuel.

Liquid samples from the high drip rate test were first filtered into specific size fractions to differentiate between colloids and larger particles. Sorbed material was included from acid washing the test vessel. Plutonium content from each size fraction was then determined, and a bar graph was prepared with the plutonium distribution, shown in Figure 5-22 after 2.5 years. Plutonium in the sorbed state dominates in all but the first sampling at 0.6 years. In fact, at 1 year and 2.5 years essentially all of the plutonium was sorbed to vessel walls (see Reference 18).

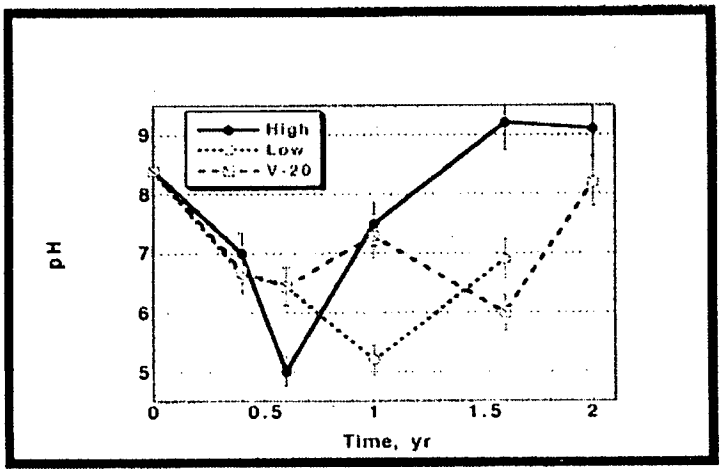

Figure 5-21. Changes in EJ-13 well water pH after exposure to mixed oxide fuel in the high, low, and vapor drip tests.

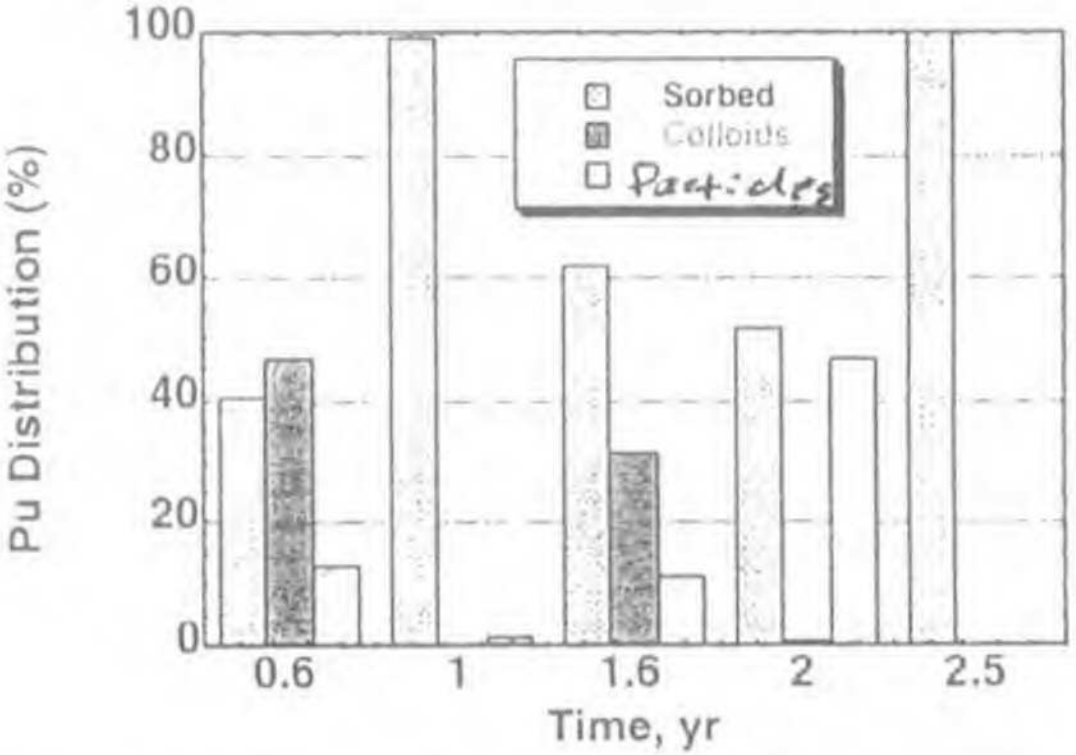

Figure 5-22. Plutonium distribution from sequential filtration of mixed oxide high drip rate tests.

DLS analysis was performed to define the size distribution of the plutonium colloids from the drip tests. However, the colloid concentration was too low for the technique to resolve dimensions. Plutonium concentration in the colloidal and dissolved fractions from the sequential filtration was analyzed using ICP-MS. Again, the concentrations were below the limit for resolution (<0.01 ppb) (see Reference 18).

5.3.4 Unsaturated Drip Test Conclusions

Data are available from 2.5 years of unsaturated drip tests with MOX fuel under three test conditions (high drip, low drip, and vapor). Liquid and solid samples were removed at about every 6 months for analysis. Solution analyses included the concentration of specific radionuclides, pH, and colloids. No alteration was visible on the fuel fragments and solids characterization is not available. Iodine had the largest cumulative fraction released (>60% after 2.5 years) and neptunium had the smallest (0.0003%). Table 5-7 lists the nuclides analyzed in order of fractional releases. The wide range of values indicates radionuclides are not released congruently.

Release rates in fraction per day of specific radionuclides were compared to commercial fuel (UO_2) test results. Generally, the MOX rates were higher than UO_2 fuel for all nuclides except ^{99}Tc. In addition, after 2.5 years the release rates of all radionuclides except ^{129}I and ^{99}Tc were within an order of magnitude for the two fuel types. Iodine and technetium were about two orders of magnitude apart. The trend over time was also similar for MOX and UO_2 fuels, initially high and then decreasing to a fairly stable value after 1.5 to 2.0 years.

Variations in water exposure did not result in any consistent behavior between radionuclides. Comparisons were made of fractional release rates over time for the high drip rate, low drip rate, and

vapor tests. After 2.5 years, ^{99}Tc, ^{97}Mo, ^{90}Sr, ^{129}I, and ^{238}U were fairly close in fractional release rates (about one order of magnitude variation or less), but ^{137}Cs, ^{239}Pu and ^{237}Np were not (greater than one order of magnitude variation). However, the comparison results were different at each sample time. Average release rates were calculated for ^{97}Mo and ^{129}I, resulting in values about two orders of magnitude higher than what was found for uranium in the flow through tests. Iodine and molybdenum fractional releases were also about two orders of magnitude larger than uranium in the drip tests. This may provide a weak argument that volume of water has no effect on the release characteristics.

Plutonium was released from MOX fuel as finely divided particles that readily sorb to metals. Most of the radionuclide released was sorbed to the vessel, but colloids were also detected. However, the concentrations are so low that it is doubtful MOX fuel will make a significant contribution to plutonium releases in the repository.

Based on the results from 2.5 years of unsaturated drip tests with MOX fuel, the following results can be summarized:

- Radionuclides are released from the MOX fuel incongruently.
- The largest radionuclide releases were of ^{129}I, ^{137}Cs and ^{97}Mo, whereas the smallest was of ^{239}Pu and ^{237}Np.
- Initial release rates are elevated but reach steady state within a year for most radionuclides.
- Release rates from MOX fuel were faster than the rates from commercial for all radionuclides examined except ^{99}Tc.
- The amount of water used to expose the material samples probably did not make a contribution to the rate of release.
- Plutonium releases are very small, but what is released is primarily sorbed onto the vessel walls.

5.4 Static Batch Tests

Static batch tests were performed with MOX fuel as a slightly accelerated test to evaluate the reactions in a thin film of water adjacent to the fuel. Results of these tests will provide data on the changes to the reacting solution and alteration phases and provide input into the mechanism of the MOX corrosion process. Details of the test method are found in Section 2.2.4. Briefly, samples of the crushed fuel are exposed to a small amount of EJ-13 well water over different timeframes to examine the progression of the reactions.[21]

A 1-inch section of a MOX fuel pin from Experimental Breeder Reactor-II (Section 5.0) was crushed and sieved to a uniform size fraction between 75 and 45 μm. About 0.2 g of the particles were used for each test vessel with 0.5 g of EJ-13 well water (Section 2.3) to create a solid surface area to liquid volume ratio of at least 3,000 to 5,000 m^{-1}. Actual surface areas were found using the BET analysis method. All tests were performed at 90°C. Initially, four tests and one blank (no fuel samples added) were planned for various exposure times. Planned exposure times were 1 week, 1 month, 2 months, and 4 months of exposure. The blank would be removed after 4 months. Additional test sets were assumed possible based on the interim results (see Reference 21).

Samples of the liquid in contact with the fuel, as well as selected solids, were removed when each test was terminated. Liquid analyses provided data on the changes in pH and the concentration of various radionuclides released into solution. Video microscopy was available in the hot cell to visually monitor

alterations in the appearance of the fuel fragments. A small portion of the solids was removed to identify alteration products and examine potential entrainment of radionuclides (see Reference 21).

5.4.1 Batch Test Results

MOX static batch tests were first started in FY-99. However, when the first sampling was attempted, difficulties with the method became obvious. The weight decrease was significant enough to indicate a faulty seal resulting in unacceptable losses of water. All tests were stopped, and a new vessel sealing method was developed. Experiments were restarted after the sealing procedure was perfected. In addition, the solid particles selected for sampling had a radiation field too high to remove from the hot cell. Based on ORIGEN calculations, it was assumed the cesium and iodine were causing the high readings. A process to wash and filter the sample and then select the smaller particles was developed. This proved to be an effective method for sampling the solids.[22]

By the end of the second set of experiments, very little alteration was visible on the fragment surfaces and XRD analysis of solid samples indicated any released particles were fuel not reaction products. The static batch test did not accelerate the corrosion of MOX fuel as was seen with other materials (commercial fuel and high level waste glass). Apparently, longer exposure times were necessary to evaluate the chemistry changes of the water in contact with the fuel. The experiments were restarted several times, eventually using longer sampling intervals. Data from 650 days of exposure were reported in November 2001. Although some discoloration and occasional gray material were seen, no significant visible corrosion was identified on the fuel. A sample of suspended particles was collected for TEM analysis. Results indicated clay colloids (probably from the groundwater) and fuel particles, but no alteration products, were released (see References 22 and 23).

Concentrations of selected radionuclides were analyzed in the liquid samples from different tests. Interim results from the experimental sets showed little consistency in releases. Figures 5-23 to 5-26 display ^{239}Pu and ^{235}U concentration in the contact solution at each sample interval for two consecutive sets. (Series R was completed prior to Series B initiation.) Although it appears from Series R that a maximum for plutonium and uranium is reached at 66 days, Series B does not follow the same trend (see Reference 22).

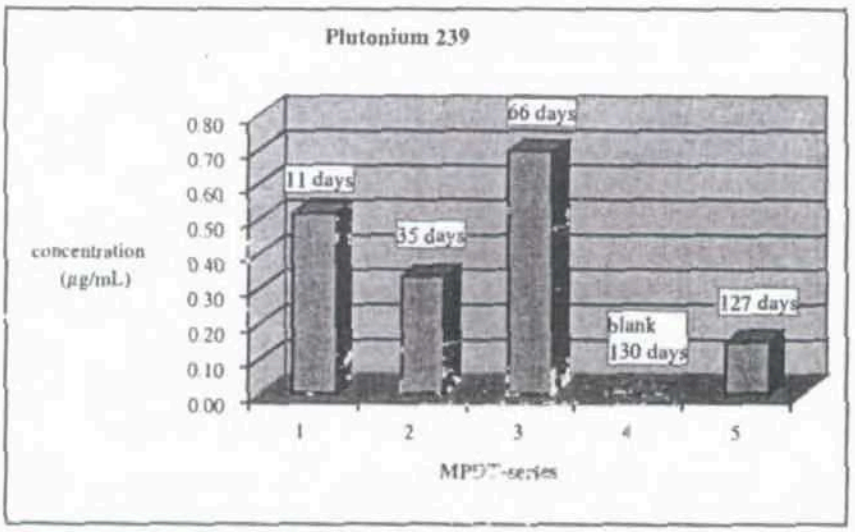

Figure 5-23. Plutonium releases from Series R mixed oxide batch tests.

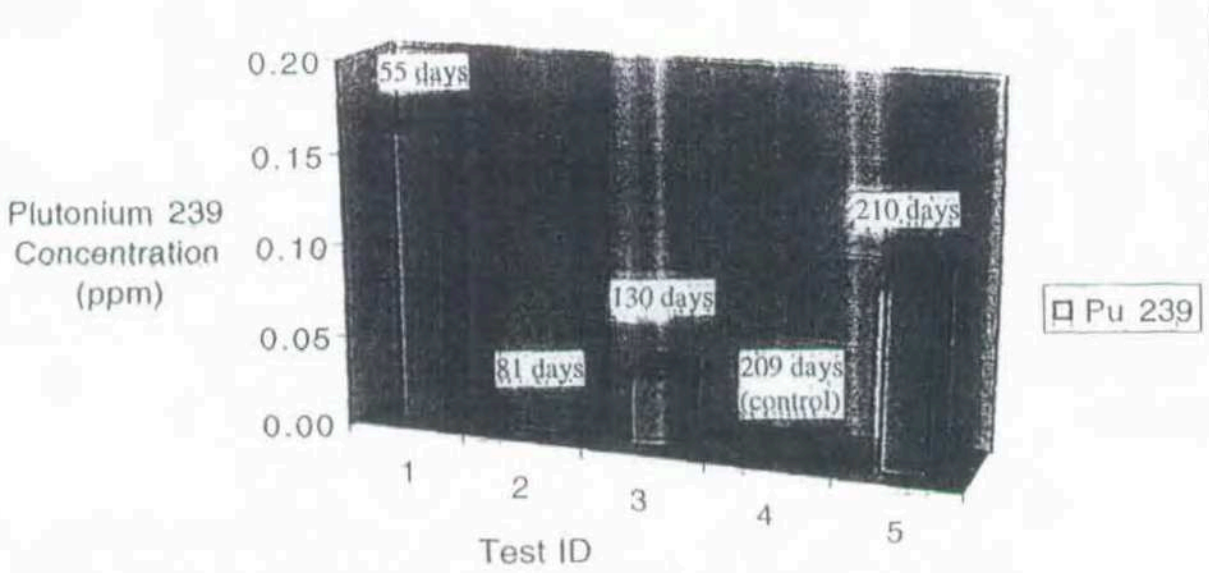

Figure 5-24. Plutonium releases from Series B mixed oxide batch tests.

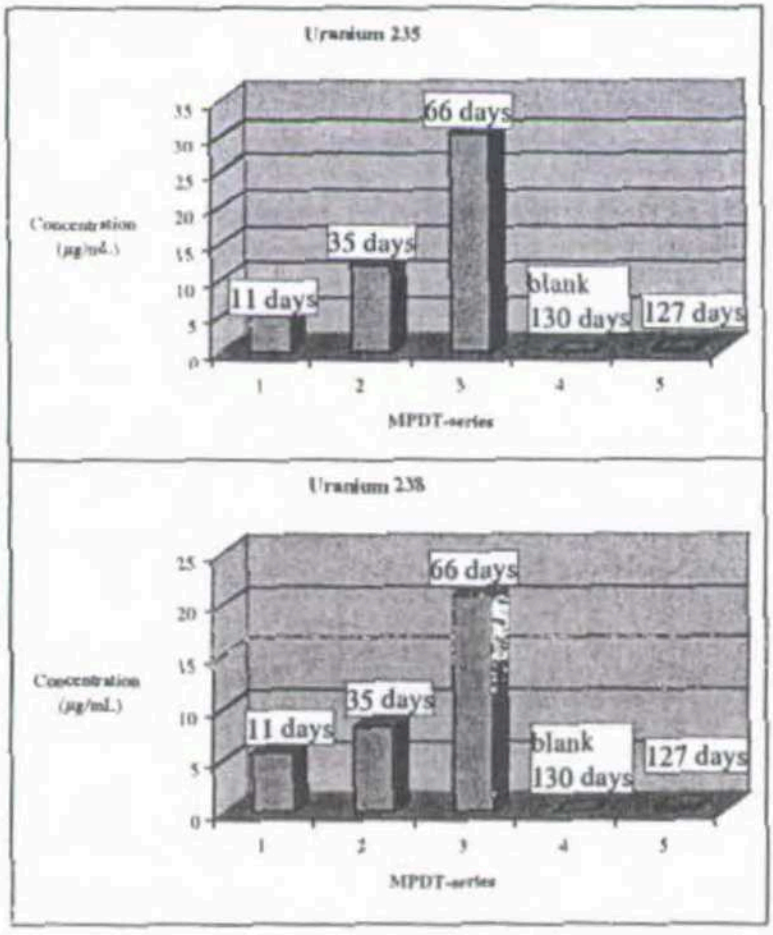

Figure 5-25. Uranium releases from Series R mixed oxide batch tests.

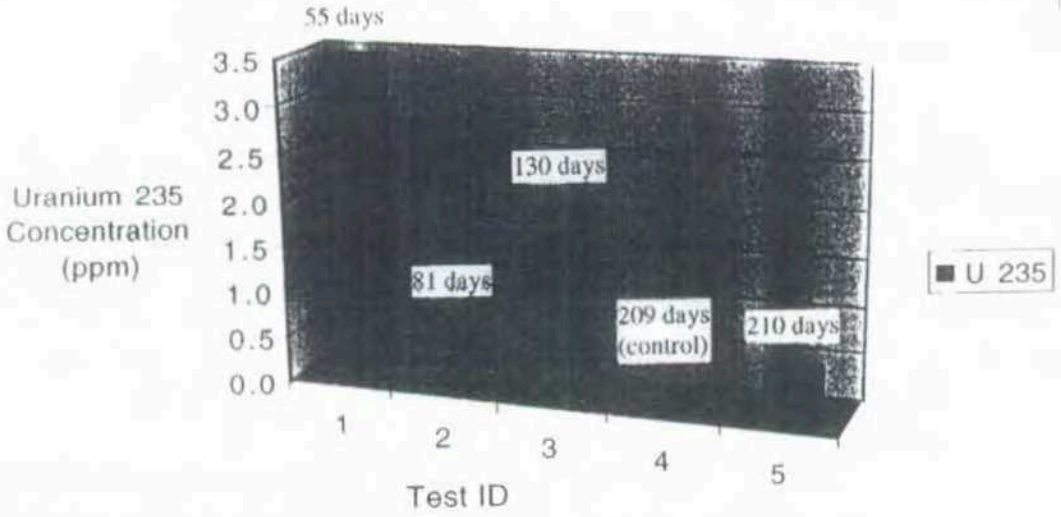

Figure 5-26. Uranium releases from Series B mixed oxide batch tests.

Longer test intervals were selected after Series B in an effort to reach an equilibrium reaction. However, releases still varied considerably between samples with no discernable trends. Figure 5-27 displays the results for plutonium through 650 days of exposure. (Uranium results were similar, but all values were larger than the plutonium.) The values include dissolved and colloidal nuclides, but do not include the material acid stripped from the test vessel. Because different sample intervals were used during the experiment, another graph was prepared to ensure there was no dependency on the interval time. Again, no trends were identified (Figure 5-28) (see Figure 23).

Additional radionuclides were evaluated in the Series R tests. Figures 5-29 to 5-31 show the concentration in the contact water of neptunium (Figure 5-29), cesium (Figure 5-30), molybdenum and technetium (Figure 5-31). Figures 5-23 and 5-25 show the concentration values from Series R for ^{235}U and ^{239}Pu, respectively, for comparison. Note the blank (or control) had a value of zero in every case, which it should if there is no external contamination in the test method. Cesium was released in the largest amounts with neptunium released in the least amount. Initial concentrations were high for cesium, technetium, and molybdenum. This could be attributed to the removal of fines or leaching of those nuclides concentrated in grain boundaries from restructuring during fuel irradiation. However, an increase was also seen with the same nuclides in the 127-day sample. Neptunium and uranium increased in concentration through the first three samples, then decreased in the 127-day sample. Alteration phase composition and subsequent retention or release of nuclides or preferential leaching of the fuel matrix are possible causes of the variability between releases of radionuclides. Solids analysis was not completed prior to the project termination, so investigation into its contribution is not possible (see References 22 and 24).

Release rates of selected radionuclides normalized to the original surface area were calculated. Approximate rates of the four samples taken from Series R are shown in Table 5-9, assuming a surface area of 2.75 m^2/g. Both the unsaturated drip and flow through tests had uranium releases typically on the order of 10^{-1} $mg/m^2/d$, much faster than what was seen in the batch tests. It may be that compositional changes in the continuous thin layer of solution on the fuel fragments from reaction products affect the reaction. Further investigation into this potential variation in reaction mechanism was not performed prior to the project termination.

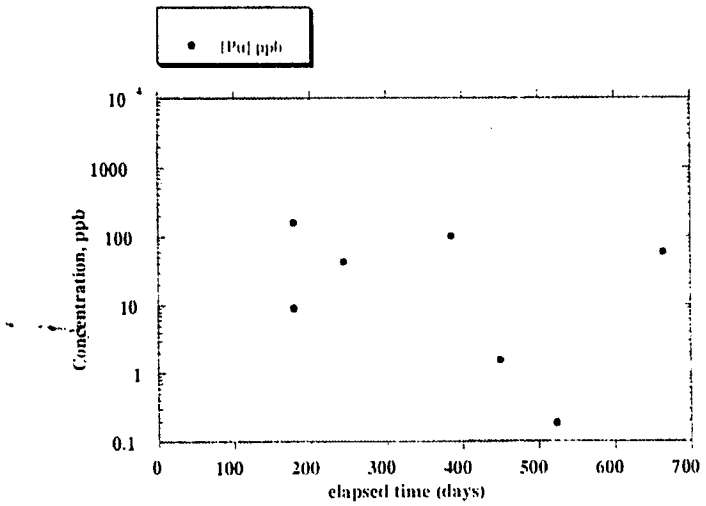

Note very high Pu release in leachate. Includes dissolved and colloidal Pu < 0.45 μm.

Does not include "acid-strip" quantity.

(100 ppb = 4 x 10^{-7}M)

pH range = 5-8.

No significant trends observed with time.

Figure 5-27. Plutonium released over time from the mixed oxide batch tests.

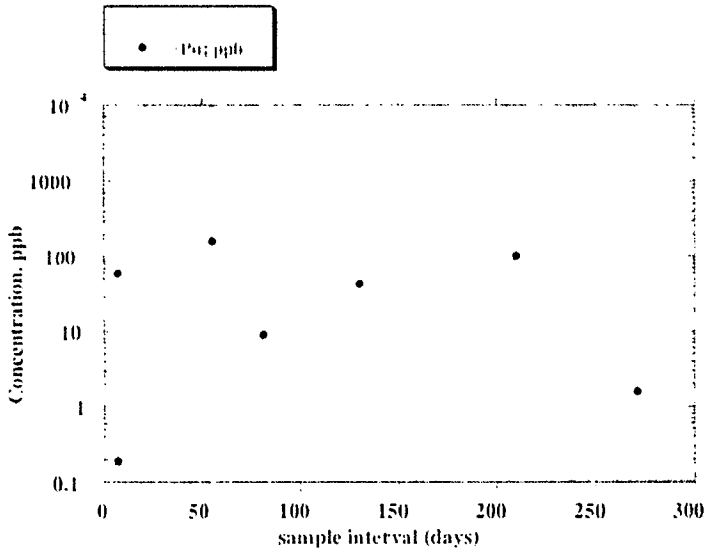

No trend in release vs. sample interval after 50 days.

Figure 5-28. Plutonium released based on sample interval from mixed oxide batch tests.

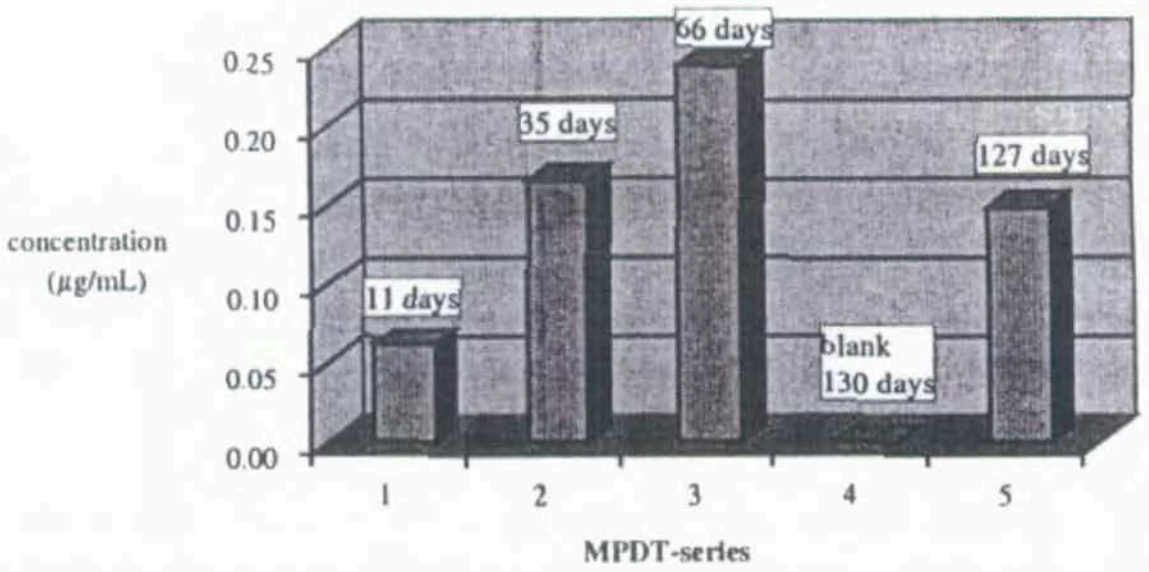

Figure 5-29. Solution concentration of ^{237}Np after exposure to Series R mixed oxide static batch tests.

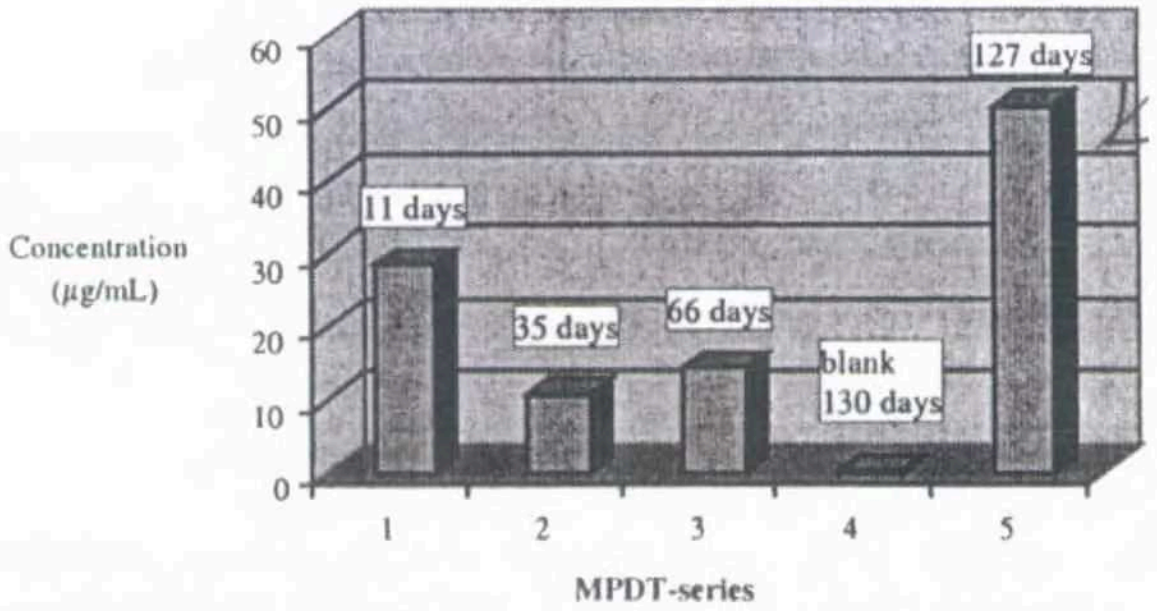

Figure 5-30. Solution concentration of ^{137}Cs after exposure to Series R mixed oxide static batch tests.

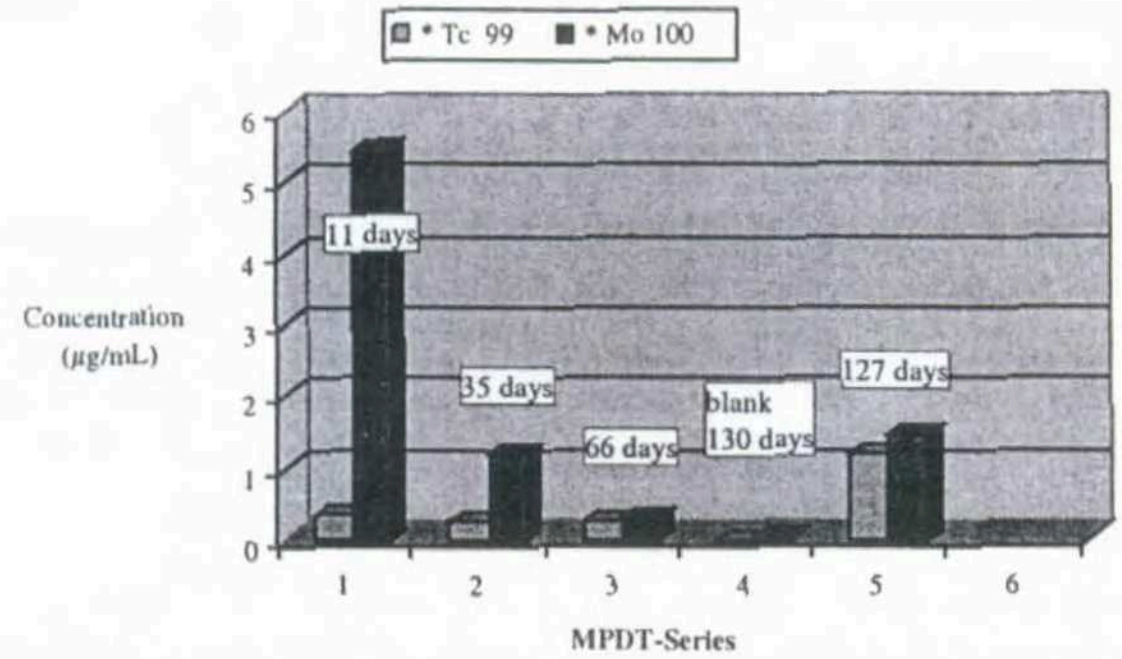

Figure 5-31. Solution concentration of ^{100}Mo and ^{99}Tc after exposure to Series R mixed oxide static batch tests.

Table 5-9. Radionuclide release rates from mixed oxide batch test.

Radionuclide	Release Rate
Plutonium	$< 4 \times 10^{-6}$ mg/m^2/d
Uranium	$< 2 \times 10^{-5}$ mg/m^2/d
Technetium	$< 2 \times 10^{-2}$ mg/m^2/d
Neptunium	$< 2 \times 10^{-2}$ mg/m^2/d
Cesium	$< 5 \times 10^{-2}$ mg/m^2/d

The pH was monitored during the experiments and ranged between about 5 and 8 from the original EJ-13, which had a pH of 8.4. No major excursions were seen and this range is similar to what was seen in other test methods.

5.4.2 Batch Test Conclusions

Static batch tests with crushed MOX fuel consisted of a small volume of EJ-13 well water covering the fragments to make a thin film. The surface area to volume ratio was designed to be at least 3,000 to 5,000 m^{-1}. Uranium and plutonium releases into solution were recorded for 650 days of exposure. A wide variability with no discernable trends was found for both nuclides.

Very little alteration was visible on the surface of the fuel fragments and characterization of released particles indicated fuel material, not alteration products. Approximate release rates were several orders of magnitude less than what was found in either the flow through or the unsaturated drip tests. In spite of the wide variability in the reaction rates, it is clear that the static batch test method decreased the reaction rate with MOX fuel, rather than accelerated the reaction as planned.

5.5 Comparison with Literature

There has been very little published research on the degradation of mixed uranium and plutonium oxides. However, a significant amount of work has been performed with uranium oxide and some with plutonium oxide individually. Commercial fuel falls into the UO_2 category, though commercial fuel is typically intact whereas many DOE-owned fuels have been damaged or are unclad (over 81 MTHM). A report is in progress summarizing research conducted on metal oxide degradation as it applies to DOE-owned SNF. In the "Waste Form Characteristics Report," a distillation of the experimental data on UO_2 degradation is presented in support of modeling commercial fuel behavior in a repository.[25] YMP has also prepared an Analysis/Model Report with a reaction model that will be used for predicting commercial fuel degradation. Finally, the total system performance assessment-license application document for predicted DOE-owned SNF behavior at YMP is being prepared. Results from these evaluations are discussed below with a comparison to the data obtained during the release rate testing project.

5.5.1 Uranium/Plutonium Oxide Degradation Review

Oxidation of uranium oxide in a water environment is a complicated process involving intermediate reactions as the U(IV) in UO_2 is oxidized to U(VI) in UO_3, as discussed in the section on uranium oxidation. Dissolved oxygen diffuses into the fuel through the grain boundaries where it reacts first. The reaction products cause stresses in the fuel matrix resulting in cracking, which exposes more surface available for reaction. Oxygen subsequently diffuses into the UO_2 matrix as an interstitial forming the hypostochiometric UO_{2+x}. Further oxidation forms U_3O_7, then UO_2^{2+}, and eventually UO_3. Oxidation rates were found to be dependent on temperature, but degree of dependence varied significantly with reported activation energies ranging from 18 to 64 kJ/mole. The variation was attributed to solution parameters such as composition, pH, and complexing agents. Because the activation energy has such a strong dependence on environmental conditions other than temperature, a general kinetic expression based on literature data was not derived for this system. Variations in pH had little effect over small ranges (5 to 10); however, larger pH ranges can effect the solubility resulting in changes in the dissolution rate. Carbonate does not have a direct effect of dissolution but acts as a strong complexing agent for UO_2^{2+}, decreasing the corrosion product layer thickness and decreasing the diffusion path for matrix dissolution. Other elements in solution have a strong effect on the SNF dissolution rate.[26]

Degradation of commercial UO_2 fuels was studied extensively by the YMP. Most of the test methods used were similar to those employed by the NSNFP release rate project, including flow through, unsaturated drip, and static batch tests. Semi-static tests were also included in the commercial fuel test matrix, where solutions were replaced after sampling. Turkey Point Reactor and H. B. Robinson Reactor pressurized water reactor spent fuels were evaluated in the semistatic tests with undamaged fuel samples, sealed sections with laser-drilled holes, sealed sections with a machined slit, and fuel particles with the cladding removed but included in the sample. Deionized water and J-13 well water were compared, and temperature was varied from 25 to 85°C. The bare fuel experiment indicated the largest releases. Typically, increased temperature reduced the measured releases, perhaps due to the formation of secondary phases. Radionuclides ^{137}Cs, ^{90}Sr, ^{99}Tc, ^{129}I, and ^{14}C were released at rates significant enough to approach the limit of 10^{-5} fraction of inventory per year. Plutonium, americium, and curium filtration data indicate they were present as colloids (see Reference 25).

Flow through experiments were performed to examine the effects of temperature and important water chemistry variables. Parameters evaluated in the test matrix included temperature (25 to 75°C), dissolved oxygen (0.002 to 0.2 atm overpressure), pH (8 to 10), and carbonate concentrations (0.2 to 20 mmol/L). Carbonate is expected to be the most aggressive component of J-13 groundwater, and thus, it was included in the study. Unirradiated samples and SNF with peak burnups ranging between 30 and 50 MWd/kgM) were used in the experiments. Uranium dissolution rates from SNF varied widely

depending on the conditions, which ranged from 0.5 to 14 mg/m^2/d, but 80% of the values are less than or equal to 5 mg/m^2/d. Unirradiated UO_2 had higher rates than SNF for most conditions, ranging from 0.1 to 77 mg/m^2/d with 86% below 13 mg/m^2/d. One particularly high value for each sample type (14 mg/m^2/d for SNF and 77 mg/m^2/d for UO_2) was exposed to the most aggressive conditions (75°C, 20 mmol/L carbonate, 20% oxygen, and pH of 10). However, the trends were basically the same for both materials. Oxygen content had the most significant effect, followed by temperature and carbonate to a smaller degree. Changes in pH had little effect on the dissolution rates (see Reference 25).

Unsaturated drip tests were also performed with unirradiated UO_2 and SNF to evaluate long-term behavior in a simulated repository environment. After 8 years of exposure, the UO_2 results indicated reacted uranium was primarily entrained in the alteration phases (94%) rather than released into solution. SNF exposure, of 3.7 years found similar results, 74% in the alteration phases. Congruent release with ^{238}U was not seen for most radionuclides, though ^{239}Pu, ^{237}Np, and ^{241}Am did have comparable rates. Nuclides ^{99}Tc, ^{129}I, ^{90}Sr, and ^{137}Cs were released at much higher rates than ^{238}U. A number of uranyl oxyhydroxides were identified in the alteration products, including sodium, potassium, calcium, silicon, and magnesium (see Reference 25).

Distillation of the data was input into Butler-Volmer equation resulting in a twelve-term model for release rate based on carbonate concentration, oxygen partial pressure, pH, temperature, burnup, and a series of interacting components. This provided the best fit to the data collected from the tests described above. However, some of terms (particularly the interaction terms) were found to not be statistically significant. A simpler version was recommended for the total system performance assessment-site recommendation that provided an acceptable fit to the behavior (±1.5 orders of magnitude) (see Reference 27):

For pH > 7:

$$\text{Log}_{10}\, DR = a_o + a_1 * IT + a_2 * PCO_3 + a_3 * PO_2 + a_4 * pH \qquad (5\text{-}4)$$

where

DR = dissolution rate in mg/m^2/d

IT = inverse temperature in K

PCO_3 = [-Log_{10}] carbonate concentration in mol/L

PO_2 = [-Log_{10}] oxygen partial pressure in atm

pH = [-Log_{10}] hydrogen ion concentration in mol/L

For basic conditions (pH > 7):

a_o, a_1, a_2, a_3, a_4 = 4.69, -1,085, -0.12, -0.32, 0.0

For acidic conditions (pH ≤ 7):

a_o, a_1, a_2, a_3, a_4 = 7.13, -1,085, 0.0, -0.32, -0.41

This expression can be written in the form of an Arrhenius equation as follows:

For basic conditions (pH > 7):

$$K = 4.9 \times 10^4 [CO_3]^{0.12} [O_2]^{0.32} \exp[-20.8 \text{ kJ/mol/RT}] \text{ mg } UO_2/m^2/d \quad (5\text{-}5)$$

For acidic conditions (pH ≤ 7):

$$K = 1.35 \times 10^7 [H^+]^{0.41} [O_2]^{0.32} \exp[-20.8 \text{ kJ/mol/RT}] \text{ mg } UO_2/m^2/d \quad (5\text{-}6)$$

where

K = reaction rate

CO_3 = carbonate concentration in mol/L

O_2 = oxygen partial pressure in atm

H^+ = hydrogen ion concentration in mol/L

R = ideal gas constant in

T = temperature in K.

DOE-owned uranium oxide fuels are very similar to the commercial fuel except that a significant portion is damaged. The current model assumes the rate would be the same but with a much higher surface area. Therefore, a factor of 10 is added to Equation (5-4) to compensate for the disrupted fuel.[28]

A minimal amount of information has been published on oxidation of plutonium oxides in water. However, plutonium degradation processes are not as complex as uranium because it primarily forms Pu(IV) with a small amount of Pu(VI). It has been shown that the reaction product PuO_{2+x} has a maximum x value of 0.27 between the temperatures of 25 and 350°C. Based on this value, the oxidation reaction is described by Equation (5-7). The resulting kinetics expression is shown in Equation (5-8), which indicates the rate is significantly slower than the dissolution rate for UO_2 [Equations (5-5) and (5-6)] (see Reference 26).

$$PuO_2 + 0.27H_2O \rightarrow PuO_{2.27} + 0.27H_2 \quad (5\text{-}7)$$

$$K = 4.46 \times 10^4 \exp[-39 \pm 3 \text{ kJ/mol/RT}] \text{ mg } PuO_2/m^2/d \quad (5\text{-}8)$$

5.5.2 Experimental MOX Degradation Comparisons

MOX fuel degradation is significantly slower than either the uranium metal or the aluminum-based fuels. Little reaction was seen on the fuel samples from flow through, batch or unsaturated drip tests. Characterization of the reaction products that were formed was limited because the activity was high enough to cause problems with handling in standard analytical equipment. Based on morphology, color, and other experiments, it was assumed that most of the products were a uranyl silicate, schoepite, or other uranyl-oxyhydroxide form.

Release of radionuclides was not congruent in any of the test methods. Cesium was released much faster than uranium in all cases. Iodine was released significantly faster than any other nuclide in

the drip tests, but was not analyzed in the other test methods. This is likely due to the migration of these nuclides to the grain boundaries during irradiation and the subsequent increased availability for release after crushing. Plutonium releases were similar to or less than uranium. Flow through test results found that ^{238}Pu was released at the same rate but $^{239/240}Pu$ was slower than uranium. The two isotopes are found in different forms; the $^{239/240}Pu$ appears as oxide particles in the initial fuel matrix whereas the ^{238}Pu is a product of irradiation located within the UO_2 particles. Technetium releases were less than uranium in the batch tests, more than uranium in the drip tests, and about the same in the flow through tests. The variation in release of technetium with respect to test method may be a function of the ability of the specific alteration product to incorporate technetium in the structure. Neptunium was less than uranium in the drip tests and more than uranium in the batch tests. It was not measured in the flow through tests. The effects of available water may have contributed to the variation in neptunium releases because of its low solubility, though releases were larger in the low drip rate tests than in the high drip rate. Strontium was equivalent to uranium in the flow through tests and the drip tests (no measurements were made in the batch tests). Table 5-10 summarizes the relationships between radionuclides for the different test methods.

Uranium was released into solution from the flow through and drip tests at comparable rates, roughly 0.1 $mg/m^2/d$ for most conditions. However, the rate was less than 2×10^{-5} from the batch tests. Static batch tests were designed to increase the reaction rate, which obviously did not happen. It appears that static conditions either decrease the susceptibility to degrade or increase the tendency for alteration products to retain radionuclides.

A comparison between the test results with MOX fuel and LWR fuel was made earlier in the sections on individual experimental methods. In general, MOX fuel degrades more slowly than UO_2 fuel. Molybdenum and iodine were also released faster from the MOX fuel. This may be due to the redistribution of mobile radionuclides during the irradiation process. Section 5.1 discusses the extensive changes in the material structure of the MOX fuel from the steep temperature gradient.

A graph was prepared (Figure 5-32) with the measured uranium release rates from several flow through tests of MOX and LWR fuels. For comparison, Equations (5-5) and (5-8) are included in the figure to show the YMP model for UO_2 fuel and the literature model for PuO_2. It was assumed the pH was above 7, the carbonate concentration was 0.002 M (similar to J-13 water), and atmospheric oxygen levels were available. Most of the values are between the UO_2 and PuO_2 equations at the bottom of the graph. However, two data points are above the upper YMP curve. Both of these are for UO_2 fuel at high carbonate concentrations. It is clear that the YMP model for UO_2 fuels is adequate to model uranium releases from MOX fuel, even when the configuration is small pieces. The plutonium model may be a more realistic model, but it will not be conservative.

Table 5-10. Radionuclide releases compared to uranium for different test methods.

Radionuclide	Flow Through	Drip	Batch
Cesium	$^{137}Cs > {}^{235}U$	$^{137}Cs > {}^{238}U$	$^{137}Cs > {}^{235}U$
Iodine	NA	$^{129}I > {}^{238}U$	NA
Plutonium	$^{238}Pu = {}^{235}U$ $^{239/240}Pu < {}^{235}U$	$^{239}Pu < {}^{238}U$	$^{239}Pu < {}^{235}U$
Technetium	$^{99}Tc = {}^{235}U$	$^{99}Tc > {}^{238}U$	$^{99}Tc < {}^{235}U$
Neptunium	NA	$^{237}Np < {}^{238}U$	$^{237}Np > {}^{238}U$
Strontium	$^{90}Sr = {}^{235}U$	$^{90}Sr = {}^{238}U$	NA

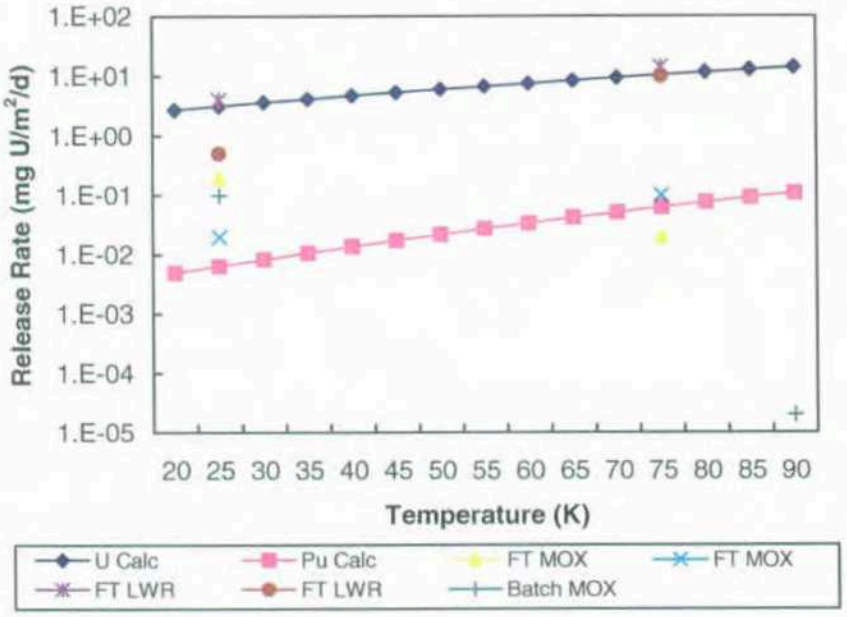

Figure 5-32. Mixed oxide release rate data compared to the UO_2 and PuO_2 predictive models. FT is flow through.

In summary, Equation (5-5) used in the YMP Analysis and Model Report for degradation of UO_2 fuel will be a conservative representation of the DOE-owned MOX fuel. However, a multiplication factor is recommended when evaluating specific radionuclides. Technetium and iodine releases were as much as two orders of magnitude higher from MOX fuel than from the UO_2 fuel. In addition, cesium, iodine, technetium, and neptunium were released at rates higher than uranium from the MOX fuel in at least one test. The increase is dependent on the test methods and the nuclide, but all would be conservatively bounded by two orders of magnitude.

5.6 References

1. M. M. Goldberg, "Activity Plan for Spent Nuclear Fuel Program Mixed Oxide Fuels," SNF-3A-001, Revision 0, April 8, 1998.

2. R. V. Strain, "Report: Characterization of Mixed-oxide fuel pins UW02010 and UW08036," Argonne National Laboratory Intra-Laboratory Memo, October 4, 2000.

3. K. N. Grimm, Argonne National Laboratory, ORIGEN code calculation.

4. W. J. Gray, "Test Plan for Dissolution Rate Testing of Mixed Oxide Spent Nuclear Fuel," NP/PNNL-MOX, Revision 0, January 1999.

5. J. Abrehaf, W. J. Gray, and C. V. Shelton-Davis, "Initial Results On Flowthrough Dissolution Rate of MOX Spent Fuel," PNL-xx, TBI.

6. L. H. Johnson and D. W. Shoesmith, "Spent Fuel," *Radioactive Waste Forms for the Future*, W. Lutze and R. C. Ewing, eds., Chapter 11, North-Holland Publishers, New York, 1988.

7. W. J. Gray, "Inventories of Iodine-129 and Cesium-137 in the Gaps and Grain Boundaries of LWR Spent Fuels." *Sci. Basis for Nucl. Waste Management XXII*, D. J. Wronkiewicz and J. H. Lee, eds., Vol. 556, pp. 487–494, Materials Research Society, Pittsburgh, Pennsylvania, 1999.

8. W. J. Gray and C. N. Wilson, *Spent Fuel Dissolution Studies: FY 1991 to 1994*, PNL-10540, Pacific Northwest Laboratory, Richland, Washington, 1995.

9. L. E. Thomas and R. J. Guenther, "Characterization of Low-Gas-Release LWR Fuels by Transmission Electron Microscopy," *Sci. Basis for Nucl. Waste Management XII*, W. Lutze and R. C. Ewing, eds., Vol. 127, Materials Research Society, Pittsburgh, Pennsylvania, 1988, pp. 293-300.

10. S. Brunauer, P. Emmett, and E. Teller, "Adsorption of Gases in Multimolecular Layers," *J. Am Chem. Soc.*, Vol. 60, 1938, pp. 309–319.

11. W. J. Gray, "Spent Fuel Dissolution Rates as a Function of Burnup and Water Chemistry," PNNL-11895, Pacific Northwest National Laboratory, Richland, Washington, 1998.

12. U.S. Department of Energy Environmental Management, *DOE Spent Nuclear Fuel Information in Support of TSPA – SR*, DOE/SNF/REP-0047, Rev. 0, August 1999.

13. W. J. Gray and R. E. Einziger, *Initial Results from Dissolution Rate Testing of N-Reactor Spent Fuel Over a Range of Potential Geologic Repository Aqueous Conditions*, DOE/SNF/REP-022, PNNL-11894, UC-802, Revised April 1998.

14. V. J. Tennery and T.G. Godfrey, "Oxidation Properties of (U, Pu)O_2 Solid Solutions," *J. Am .Chem. Soc.*, 56,129, 1973.

15. D. M. Gruen, "Valence Stabilization in Crystals," *J. Chem. Phys.*, 21, 2083, 1953.

16. P. A. Finn, "Test Plan for Reactions between Irradiated MOX Fuel and J-13 Well Water under Unsaturated Conditions," SNF-3A-003, Revision 1, Argonne National Laboratory, February 1, 1999.

17. P. A. Finn, R. V. Strain, Y. Tsai, and M. M. Goldberg, "^{129}I Release in Unsaturated Tests with Fast-Flux Mixed Oxide Fuels," 9th International High-Level Radioactive Waste Management Conference, May 2001.

18. C. V. Shelton-Davis, INEEL, to Distribution, "NSNFP Release Rate Test Meeting Minutes from November 14, 2001," P. A. Finn Presentation, December 19, 2001.

19. C. V. Shelton-Davis, INEEL, to Distribution, "Meeting Minutes from NSNFP Release Rate Test Program Held on May 3, 2001," P. A. Finn Presentation, June 7, 2001.

20. C. V. Shelton-Davis, INEEL, to Distribution, "May 11, 2000, Release Rate Test Review Meeting Minutes," M. M. Goldberg Presentation, August 10, 2000.

21. M. M. Goldberg, "Test Plan for Batch Testing of Irradiated MOX Fuel," SNF-3A-002, Revision 0, Argonne National Laboratory, April 8, 1998.

22. C. V. Shelton-Davis, INEEL, to Distribution, "Meeting Minutes from NSNFP Release Rate Test Program Held on May 3, 2001," J. A. Fortner Presentation, June 7, 2001.

23. C. V. Shelton-Davis, INEEL, to Distribution, "NSNFP Release Rate Test Meeting Minutes from November 14, 2001," J. A. Fortner Presentation, December 19, 2001.

24. C. V. Shelton-Davis, INEEL, to Distribution, "May 11, 2000, Release Rate Test Review Meeting Minutes," J. A. Fortner Presentation, August 10, 2000.

25. R. B. Stout and H. R. Leider, LLNL, "Waste Form Characteristics Report," Version 1.3, UCRL-ID-132375, April 4, 1997.

26. M. A. Ebner, "Review of Oxidation Rates of DOE Spent Nuclear Fuel, Part 2. Nonmetallic Fuel," DOE/SNF/REP-068, July 2003.

27. S. A. Stewart, "CSNF Waste Form Degradation: Summary Abstract," ANL-EBS-MD-000015, Revision 00, January 2000.

28. D. L. Fillmore, "Parameter Selection for Department of Energy Spent Nuclear Fuel to be Used in the Yucca Mountain License Application," INEEL/EXT-98-00666, May 2003.

6. THORIUM/URANIUM CARBIDE FUEL

The thorium/uranium carbide fuel group consists primarily of Fort St. Vrain (about 90%) and Peach Bottom fuels. Carbide particles coated with layers of pyrolytic carbon (and silicon carbide in the Fort St. Vrain fuel) are bonded together in a carbon matrix. The particles are either thorium and ~93% enriched uranium (fissile) or pure thorium (fertile). Peach Bottom fuel elements are from two core assemblies, Core 1 and Core 2. Core 1 particles had only a pyrolytic coating and as much as 60% were damaged during irradiation. Core 2 particles included a second, inner low density pyrolytic carbon layer, which improved the durability. Addition of a third layer, a silicon carbide coating, made the Fort St. Vrain fuel highly resistant to degradation.[1] The particles are bonded in a carbon matrix and formed into a cylindrical shape called a compact. A small amount of Core 2 particles had the silicon carbide layer. Compacts are then arranged on top of each other within a fuel element.

For the release rate test program, Peach Bottom Core 2 was chosen as a representative that would bound most of the fuel in this group (Fort St. Vrain and Peach Bottom Core 2), but would be more robust than Core 1 fuel. The plan was to crush one compact and test the broken particles, which would adequately simulate the damaged Core 1 fuel. An activity plan discusses the purpose of testing thorium/uranium carbide fuel, potential sample selections, and the planned experiments.[2] Three test methods were outline in the plan; characterization, static batch tests, and flow through tests. Fuel samples were identified and retrieved from storage. However, the release rate project was terminated prior to any test initiation, thus no experimental data are available for the thorium/uranium carbide group. This discussion is on the identification and retrieval of the fuel samples, which have since been returned to storage.

6.1 Uranium/Thorium Carbide Fuel Sample Recovery

Oak Ridge National Laboratory possessed Peach Bottom fuel in their dry storage facilities and planned to repackage and ship the fuel to INEEL. Thus, access to a fuel sample would be possible for a minimal cost. To optimize the bounding characteristics of the selected fuel samples, elements were reviewed based on high fluence, power level, burnup, and temperature history. Based on these criteria, driver elements from radial rows 8 through 14, with preference to compacts from axial positions 10 through 20, were selected for retrieval. The test plan provides details on sample selection and the approach for retrieval and identification.[3] In addition, one compact was to be deconsolidated to remove the graphite matrix and leave the coated particles undamaged. Two elements were in storage at ORNL that would meet these criteria, E14-01 (radial row 14, circumferential position 1) and E11-07. Unfortunately, they were packed with element E06-01 into two storage containers. Both containers would potentially need to be retrieved, and the contents would need to be examined.

6.1.1 SNF Package ATN-1616 Recovery

The first package retrieved from dry storage was labeled ATN-1616, and it contained two aluminum tubes closed with rubber stoppers and about ½ liter of water.[4] Below are the markings found on the two tubes:

A E11-07 2 9 13 16 18 20 21 24 25 26 27 28

B E14-01 2 9 17 18 20 21 22 23 24 25 26 27 28 29 30

Tube E11-07 contents were found to be dry, but tube E14-01 was moist inside. A stainless steel 'snuff can' recovered from the bottom of the latter tube was found to have a fuel piece and ~5 mL of

water. Compacts from tube E14-01 were placed in plastic bags, which indicated fog and water drops on the inside of the bags after one day (see Reference 4).

Most of the compacts recovered from ATN-1616 were incomplete. Some were broken, but most had been sectioned for previous post-irradiation examination. The numbers on the outside of the tubes correspond to post-irradiation examination records, although they were not in order within the tubes. Due to the damage from exposure to water and post-irradiation examination, it was concluded none of this material would be acceptable for release rate experiments (see Reference 4).

6.1.2 SNF Package STN-1272 Recovery

Because no useable material was found in ATN-1616, SNF package ATN-1272 was recovered. Four aluminum tubes with rubber stoppers were found inside with no indications of water leakage. Figure 6.1 shows the tubes still inside the fuel storage canister. As verification of dryness, a compact was removed from each tube and placed in a plastic bag. Subsequent examination revealed no condensation as was found with compacts from ATN-1616. The tubes were labeled as follows:

E06-01 Fuel Compacts Nos. 2–6 and 8–16, also 18

E06-01 Fuel Compacts Nos. 19–25 and 27–32

E11-07 Fuel Compacts Nos. 1, 3, 4, 5, 6, 7, 10, 11, 12, 14, 15, 19, 22, 23, 30

E14-01 Fuel Compacts Nos. 1, 3, 4, 5, 6, 7, 8, 10, 11, 12, 13

A preliminary view down the inside of the tubes indicated that only E14-01 contained all intact compacts. These compacts are of primary interest for the release rate test project, because they received the highest burnup of the three available elements. The compacts were removed from the tube and placed in cans with a label designating the order of removal (starting with A). None had been used for post-irradiation examination and only two were broken (designated D and J). Compact E1401-D also had a circumferential groove near one end, which proved valuable in verifying the identity. All others appeared to be in relatively good condition and could potentially be used for release rate experiments.

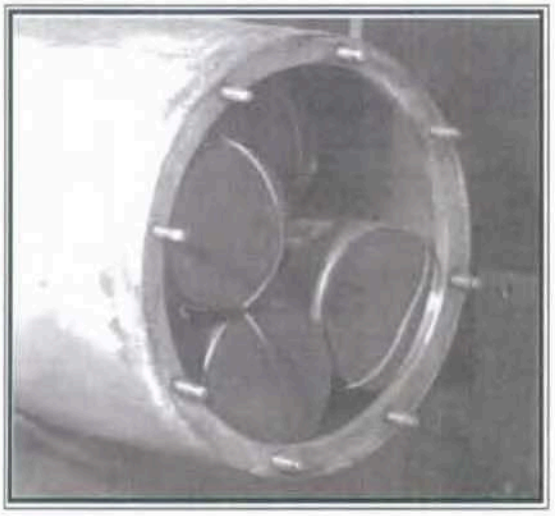

Figure 6-1. Spent nuclear fuel package ATN-1272 with four aluminum tubes.

6.1.3 Sample Identification

Positive identification of the compacts was necessary for traceability prior to selecting samples for testing. Initial identification was simplified by the labeling information written on the sides of the aluminum tubes found within package ATN-1272. Each tube was clearly marked as to the fuel element identification and the compacts it contained. What was missing in the documentation was the order of the compacts in the tube and hopefully some corroborating evidence to help establish the unique identity of each compact.

A gamma scan was made of each compact for comparison with archived documentation to assist with identifying the material. The only significant gamma-rays emitted by the compacts arise from ^{137}Cs. It decays by beta emission to ^{137}Ba, which has a half life of 2.5 minutes and produces a 661.6 KeV gamma-ray. Gamma scans, therefore, produce a relative measure of the ^{137}Cs inventory of each compact. Figure 6-2 is a photograph and an example of the resulting scan for compact ATN-1272, E1401-G. Reference 5 presents the scanning results and photographs for every compact measured.

It was determined from the gamma-scan that the ^{137}Cs activity of the recovered compacts generally decreased from E1401-A to E1401-K. Therefore, if the compacts had been placed in the aluminum tube in the order given, recovered compacts "–A" would correspond to compact 13, recovered "–B" would correspond to compact 12, and so on with recovered compact "–K" corresponding to compact 1. This is because compacts in the center of an element (compacts 10 through 20) would have the highest activities while those at the ends of an element (compacts 1 and 30) would have the lowest activities. To further quantify this comparison, the relative ^{137}Cs activities determined from the gamma-scans were compared with the ^{137}Cs reported in the original post-irradiation examination report.[6] This comparison is shown graphically in Figure 6-3. In the figure, the historic data have been normalized at compact 13, and the gamma-scan data have been scaled by a constant factor to minimize the square of the deviations between the current and historic ^{137}Cs measurements. Agreement between the two sets of data taken 25 years apart is very good with only two comparisons noticeably outside the error bars of the original measurements. These two comparisons are from the two compacts that were broken into two matching pieces. It is possible that the breaks in the compacts had an adverse effect on the gamma-scans because signal response was very sensitive to vertical positioning of the compact.

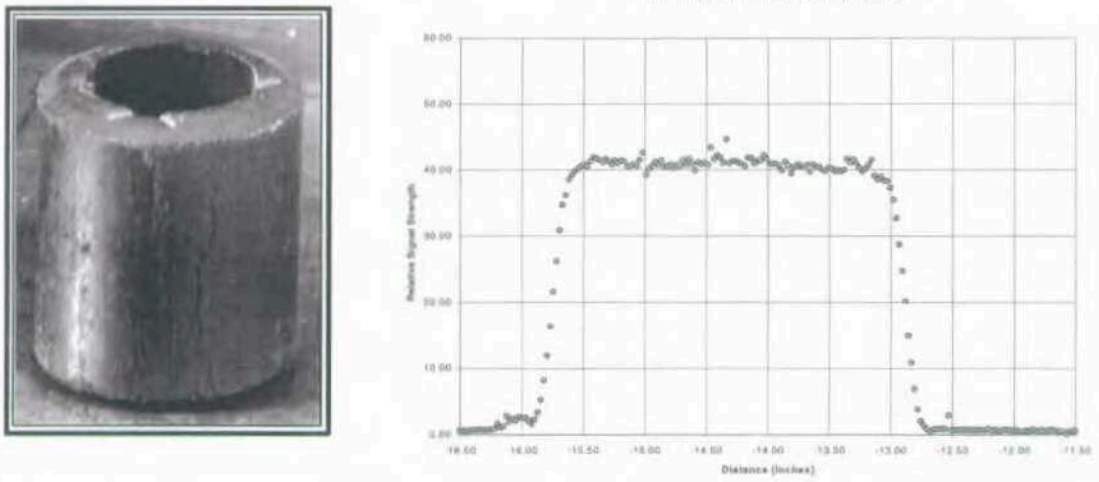

Figure 6-2. Photograph and gamma scan results of compact ATN-1272, E1401-G.

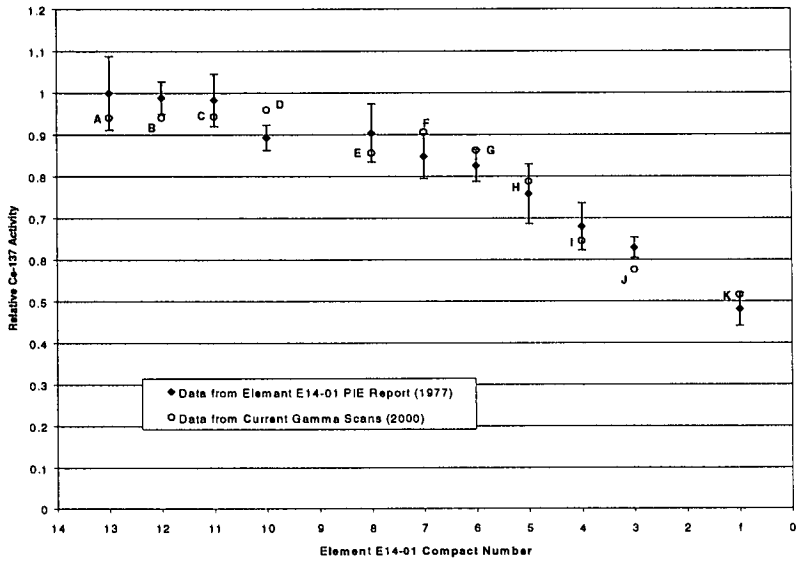

Figure 6-3. Comparison of relative ^{137}Cs from compact gamma-scans with archived documentation.

As a final check, photographs from the original post-irradiation examination report were reviewed to look for any features that might be unique to a given compact. One such feature was found on compact 10. Figure 6-4, a photograph of compact 10 taken during the early 1970s, clearly shows a thin circumferential groove cut near the end of the compact. A comparison was made with recovered compact E1401-D, which is thought to be compact 10, and the circumferential groove is indeed present as shown in Figure 6-5. Based on these three pieces of evidence, it was concluded that the compacts are indeed numbered sequentially as originally postulated. Table 6-1 lists the verified compact number with the corresponding storage container identification.

6.1.4 Compact Sample Selection

As stated in Section 6-1, three compacts of Peach Bottom Core 2 fuel with a high amount of irradiation history were requested for release rate testing. Driver elements from radial rows 8 through 14, with preference to compacts from axial positions 10 through 20, were selected as optimum. Storage container ATN-1272 was retrieved, and eleven compacts from fuel element E14-01 were removed and identified. The obvious choice-based irradiation history is compact E1401-13. However, it was rejected because it appeared to have been exposed to water at some time in the past. Compacts E1401 12, 11, and 10 were selected for use for release rate experiments. ORNL planned to perform a deconsolidation on compact E1401-11 and the resulting particles will be used in flow through tests at PNNL. Compact E1401-12 was also scheduled flow through experiments as a whole compact. Static batch tests and colloid studies would be performed at ANL-E with compact E1401-10, which would be crushed prior to testing. The crack and groove in compact E1401-10 should not be a hindrance to the experiments because it was to be crushed anyway. All compacts were returned to storage once the project was terminated, and all testing with graphite fuel was cancelled.

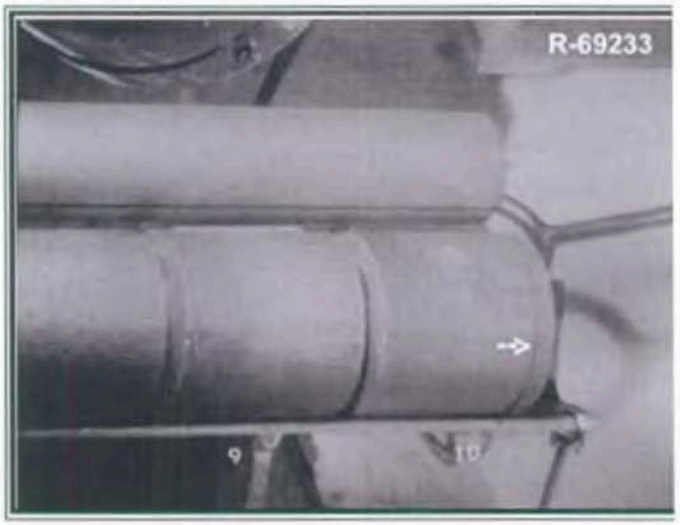

Figure 6-4. Archived photograph of E1401-10 showing groove at one end.

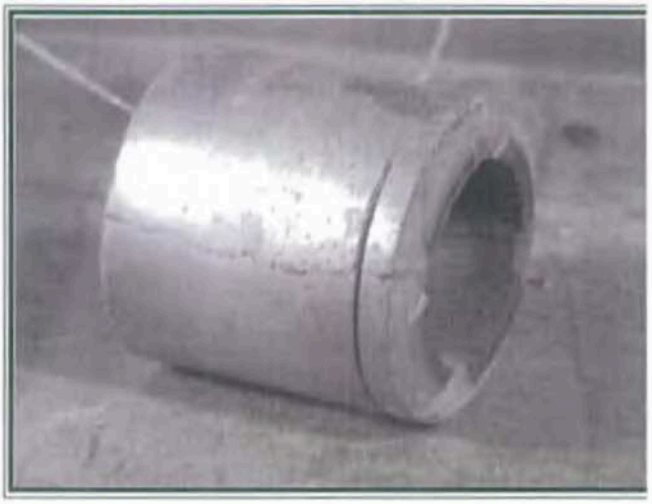

Figure 6-5. Photograph of ATN-1272, E1401-D showing characteristic groove.

Table 6-1. Fuel element E14-01 compact numbers and corresponding storage identification numbers.

Compact Number	Storage Container ID
Element E14-01 compact 01	ATN-1271, E1401-K
Element E14-01 compact 03	ATN-1271, E1401-J
Element E14-01 compact 04	ATN-1271, E1401-I
Element E14-01 compact 05	ATN-1271, E1401-H
Element E14-01 compact 06	ATN-1271, E1401-G
Element E14-01 compact 07	ATN-1271, E1401-F
Element E14-01 compact 08	ATN-1271, E1401-E
Element E14-01 compact 10	ATN-1271, E1401-D
Element E14-01 compact 11	ATN-1271, E1401-C
Element E14-01 compact 12	ATN-1271, E1401-B
Element E14-01 compact 13	ATN-1271, E1401-A

6.2 References

1. S. C. Marschmann, F. M. Berting, R. G. Clemmer, E. R. Gilbert, R. J. Guenther, W. C. Morgan, P. Sliva, "Characterization Plan for Fort St. Vrain and Peach Bottom Graphite Fuels," PNL-xxx, draft, September 1993.

2. M. Ebner, "Activity Plan for Release Rate Testing of Graphite Spent Nuclear Fuel," DOE/NSNF/PP-013, Revision 0, November 1998.

3. R. Morris, "Test Plan for Retrieval, Identification and Preparation of Peach Bottom Graphite Fuel Samples for Repository Release Rate Testing," MET-FE-TP/PB2-01/R0, March 1999.

4. C. A. Baldwin, "Recovery and Examination of Peach Bottom Fuel Compacts from ATN-1616," Oak Ridge National Laboratory, July 1999.

5. C. A. Baldwin, "Recovery and Examination of Peach Bottom Fuel Compacts from ATN-1272," Oak Ridge National Laboratory, March 2000.

6. R. P. Wichner, F. F. Dyer, W. J. Martin and L. L. Fairchild, *Distribution of Fission Products in Peach Bottom HTGR Fuel Element E14-01*, ORNL/TM-5730, Oak Ridge National Laboratory, August 1977, Table 4.2-1, pg. 50.

7. CONCLUSIONS

Current plans dictate that DOE-owned SNF will be disposed of in a geological repository proposed at the YMP site in Nevada. In support of the performance assessment, experiments were performed to evaluate the potential for radionuclides to be released to the environment during fuel degradation. The project was terminated prematurely, but several years worth of results were generated. In parallel to the laboratory research, a review of literature data that could be applied to specific DOE fuel types was completed. A general model that encompassed all relevant published data was generated. Finally, a comparison between the literature model and the experimental results was presented with recommendations for describing the expected fuel performance in a repository.

The release rate test project included three fuel groups (uranium metal, aluminum-based, and MOX) used in three experimental methods. Graphite fuel was originally planned for study, but the project was terminated prior to any experimentation. Flow through tests were designed to evaluate the forward dissolution rate with no back reactions. Results should give the maximum release rate and the dependence on individual solution components. Unsaturated drip tests simulated the expected repository conditions to more closely estimate the actual release rates. An evaluation of alteration product generation and composition could also be made from these tests. Static batch tests were originally developed to accelerate the drip test conditions and to provide information on the solution composition at the fuel surface. This test method was also used to support the anoxic/oxic studies with uranium metal fuel. In addition, some colloid generation and stability tests were performed with each fuel type. The colloid studies were the most extensive with uranium metal fuel.

7.1 Uranium Metal Fuel

Uranium reacts rapidly in water, as was seen with every test method. The samples showed significant alteration after only a few days of exposure. In fact, a 1-gram sample completely reacted in less than 90 days during a drip test. Other test methods resulted in degraded samples with increased surface roughness and large amounts of alteration products. Some of the flow through tests produced a sludge and increased reaction rates. A faster flow rate and smaller sample size delayed the onset of accelerated reaction, but did not eliminate it. Analyses showed the reaction products for all three test methods were primarily uraninite, schoepite, and metaschoepite; although a variety of other uranium oxyhydroxides were identified.

Release rates of uranium ranged from 4 to 44,000 $mg/m^2/d$, depending on the environmental conditions (temperature, solution chemistry, pH, test method). In general, higher temperatures increased the reaction rate and J-13 well water was more aggressive than solutions of individual components. SNF rates were about an order of magnitude larger than the results with unirradiated uranium metal fuel. However, the most significant effect appears to be the change from oxic to anoxic conditions. This may be the reason for the unusual results from the flow through tests (generation of a sludge and faster reaction rates).

Limited data were collected on isotopic distribution from uranium SNF degradation. Plutonium was found primarily in the alteration products, and what was released to the environment was in the form of colloids. About half of the technetium was found in the reaction products and half in solution. No analysis for technetium colloids was performed. Only a small amount of the cesium was entrained in the reaction products and none appeared as colloids; most of it was dissolved in solution.

A large percentage of the uranium released early in the degradation process appears as colloid sized particles. They were present as spherical UO_2 and entrained in clay colloids. Size distributions of about 10 nm and 200 nm represent the two types of colloids. Over time, the particles agglomerated, and

the percentage of uranium released as colloids dropped to nearly zero. Literature documents report a similar phenomenon. The amount of plutonium released as colloids varied in the literature, but was often high. Results from the release rate tests indicated plutonium colloids were near 90%. No other isotope evaluated in the experiments showed a tendency toward colloid formation.

The literature review indicated all uranium degradation systems eventually reach the faster anoxic state, and the resulting equation was based on oxygen deprived systems. Plotting the experimental data for comparison with the literature equation indicated the model is an adequate conservative estimate of uranium degradation. All data points were less than the predictive expression except those believed to be anoxic, and they were essentially on the line. The equation derived from the literature data under anoxic conditions is recommended for use in the performance assessment to describe uranium metal fuel degradation:[1]

$$K = 5.03 \times 10^{9} \exp[-66.4/RT] \text{ mg/m}^2\text{/d}$$

A series of experiments designed to study the generation and stability of colloids from uranium metal in individual solution components was initiated but not completed. Some conclusions were made based on the data collected, however. In silicate solution, only about 3% of the uranium released were colloidal, increasing to about 15% in EJ-13 and to 50% or more in the iron, carbonate, and deionized water. Laboratory tests and literature results indicated an initially large release of uranium colloids that decreased over time. Agglomeration of the particles has been seen by TEM analysis, which could account for the decrease in colloid concentration. Increases in pH in the colloid tests indicated larger sized particles.

7.2 Aluminum-Based Fuel

Aluminum-based fuels are more resistant to degradation than uranium metal and the reaction mechanisms are different. Typical of aluminum metal, degradation in many of the experiments showed preferential attack. Pitting of the aluminum matrix was identified in the flow through and static tests. Aluminum corroded preferentially to the uranium-aluminum particles in all the experiments, possibly indicating a galvanic effect. In the drip tests, an aluminum tri-hydroxide (as boehmite) gel formed on the surface that controlled the release of uranium. Other uranyl oxyhydroxides were seen with aluminum, calcium, and silicon. Stable colloids of aluminum and silicate measuring 10 and 300 nm were identified in the drip tests, but no uranium was associated with the particles.

Four fuel types were evaluated in the flow through tests resulting in similar uranium release rates except with the alloy fuels, which were more reactive. Fabrication method and alloy composition were varied in the static tests at SRS. Wrought material appeared to be more resistant to degradation than castings except in high pH solutions. The amount of uranium in the alloy did not have a significant effect of the release rates. Raising the temperature increased the uranium releases for all conditions. Likewise, changing the pH in either direction increased the degradation rate. Significant differences between carbonate, nitric acid, or high chloride solutions were not seen, but simulated J-13 well water was definitely the least corrosive to the aluminum-based fuel.

Only flow through experiments were completed with irradiated fuel, and thus isotopic analyses were restricted to that test method. Plutonium releases were less than uranium regardless of the fuel type or the solution chemistry. Cesium and strontium rates were typically larger than uranium. Technetium to uranium ratios varied depending on the solution, being greater than one in bicarbonate and less than one in nitric acid (with one exception).

Release rates of uranium from aluminum-based fuel ranged from 0.1 to 298 mg/m^2/d at 25°C and 0.2 to 420 mg/m^2/d at 90°C. The literature review derived an equation for uranium-aluminum alloy fuels shown below. The Analysis and Model Report prepared for YMP chose numerical values rather than an expression for bounding the aluminum-based fuels, also shown below. In fact, none of these predictions bound all of the test data generated from this experimental project. The regression model results in values at about the median of all experiments and bounds the SNF tests in J-13 well water. This may serve as a best estimate prediction. Most of the data are bounded by the selected conservative model, particularly at the higher temperature. A value of 360 mg/m^2/d for all temperatures would capture a greater portion of the data. Alternatively, a value of 300 mg/m^2/d for 25°C and 450 mg/m^2/d for 90°C would include the experimental results (see References 1 and 2).

$K = 1.0 \times 10^6 \exp[-32.8/RT]$ mg U/m^2/d

Conservative model: 36 mg U/m^2/d @ 25°C

360 mg U/m^2/d @ 90°C

Best estimate model: 0.22 mg U/m^2/d @ 25°C

2.20 mg U/m^2/d @ 90°C

7.3 MOX Fuel

MOX fuel is similar to UO_2 commercial fuel except it contains PuO_2, about 25% in the fuel tested. However, the large temperature gradient across the surface of the fuel during irradiation has caused extensive redistribution within the fuel element. It is much more resistant to degradation than either uranium metal or aluminum-based fuels. Little reaction was seen after 3 years of exposure, and no analysis of the alteration products was completed. Based on color and morphology, it was assumed most of the products were uranyl oxyhydroxide compounds. Experiments using MOX fuel were exposed for the longest time, but the least amount of reaction had taken place.

Radionuclide releases were evaluated in the drip, batch, and flow through tests. Cesium and iodine releases were greater than uranium, regardless of the test method. Plutonium releases were less than uranium in every sample, but most of the particles were sorbed onto the vessel walls. Essentially all of the released plutonium was sorbed at the 1 and 2.5-year samples. Technetium and neptunium releases were not consistent, and their behavior compared to uranium is not clear. The variation in release with respect to test type may be a function of the ability of the specific alteration product to incorporate the radionuclide in the structure. The effects of available water may have contributed to the release of neptunium because of its low solubility. Strontium releases were about the same as uranium.

Uranium was released into solution from the flow through and drip tests at comparable rates, roughly about 0.1 mg/m^2/d for most conditions. However, the rate was less than 2×10^{-5} from the batch tests. Static batch tests were designed to increase the reaction rate, which obviously did not happen. It appears that static conditions either decrease the susceptibility to degrade or increase the tendency for alteration products to retain radionuclides. Flow through tests evaluated the dissolution rates from fragments compared to grain-sized particles. The larger fragments resulted in higher reaction rates in both carbonate solutions and in J-13 well water, by about two orders of magnitude. Redistribution of the radionuclides during irradiation may have resulted in an accumulation of elements in the grain boundaries that are preferentially exposed in the fragments.

Dissolution or oxidation expressions of mixed oxides are not reported in the literature. However, rates of individual oxides (uranium and plutonium) are discussed. A condensation of the available UO_2 data and the resulting expressions were prepared for the Analysis and Model Report. Two equations are shown below to differentiate the reaction rates in acidic versus caustic solutions. An expression was also derived from the literature for PuO_2 oxidation. MOX fuel degradation should be represented by some combination of these expressions. A graphical comparison was made of the UO_2 regression for solutions above 7, the PuO_2 regression, and the MOX fuel degradation data. Most of experimental results were between the two curves. The more conservative model for UO_2 bounded all the data but two points, which were from concentrated carbonate solutions.[3.a]

For basic conditions (pH > 7):

$$K = 4.9 \times 10^4 [CO_3]^{0.12} [O_2]^{0.32} \exp[-20.8 \text{ kJ/mol/RT}] \text{ mg } UO_2/m^2/d$$

For acidic conditions (pH ≤ 7):

$$K = 1.35 \times 10^7 [H^+]^{0.41} [O_2]^{0.32} \exp[-20.8 \text{ kJ/mol/RT}] \text{ mg } UO_2/m^2/d$$

$$K = 4.46 \times 10^4 \exp[-39 \pm 3 \text{ kJ/mol/RT}] \text{ mg } PuO_2/m^2/d$$

7.4 Conclusions

Three fuel groups were evaluated in the release rate experimental program, and the results were compared to a literature review. A regression of published uranium oxidation rates bounded the uranium metal fuel release rates and is the recommended model. Colloid formation is only significant in the early stages of degradation. Agglomeration appears to quickly dominate the generation discounting long-term effects. However, these experiments were in a stagnant condition. If flow rates are significant enough to prevent agglomeration, then the initial generation rates may dominate. Aluminum-based fuels vary considerably depending on fuel type and environmental conditions. Currently, the repository model uses fixed values to bound uranium release. Based on the experimental data from this project, these estimates are low. New conservative values are presented that include all the available data. MOX fuel is the least reactive of those evaluated. Literature reports indicate PuO_2 is more resistant than UO_2, and that seems to hold true with the experimental results. The repository model for commercial UO_2 fuel adequately bounds the experimental data.

Release of radionuclides is not congruent from SNF. Cesium and iodine rates are consistently higher than uranium. These two elements may migrate to the grain boundaries and fuel edges during irradiation. In addition, they will not be readily entrained into the alteration products. Initial releases will be high, as much as four orders of magnitude above the uranium rates. Plutonium will be released at a slower rate than uranium. It is incorporated into alteration products and readily sorbs onto materials. A significant fraction of the released plutonium may be as colloids, but the concentrations are very low. Uranium release rates should bound the plutonium releases, including the colloid fraction. Neptunium, technetium, and strontium releases varied based on fuel material, test method, and environmental conditions. Some will be entrained in the alteration products, but the amount is not consistent. A conservative bounding value would be the same used for cesium and iodine, four orders of magnitude.

---

a. M. A. Ebner, "Review of Oxidation Rates of DOE Spent Nuclear Fuel, Part 2. Nonmetallic Fuel," DOE/SNF/REP-068, to be issued.

7.5 References

1. B. A. Hilton, *Review of Oxidation Rates of DOE Spent Nuclear Fuel, Part 1: Metallic Fuel*, DOE/SNF/REP-054, Revision 0, September 2000.

2. T. A. Thorton, "DSNF and Other Waste Form Degradation Abstraction," ANL-WIS-MD-000004, Rev. 0, February 2000.

3. S. A. Stewart, "CSNF Waste Form Degradation: Summary Abstract," ANL-EBS-MD-000015, Revision 0, January 2000.